NASA CONTRACTOR REPORT

NASA CR-1157

NASA CR-1157

STUDY, FABRICATION AND TESTING OF A FOIL-BEARING ROTOR SUPPORT SYSTEM

by L. Licht and A. Eshel

Prepared by

AMPEX CORPORATION

Redwood City, Calif.

for

NATIONAL AERONAUTICS AND SPACE ADMINISTRATION • WASHINGTON, D. C. • NOVEMBER 1968

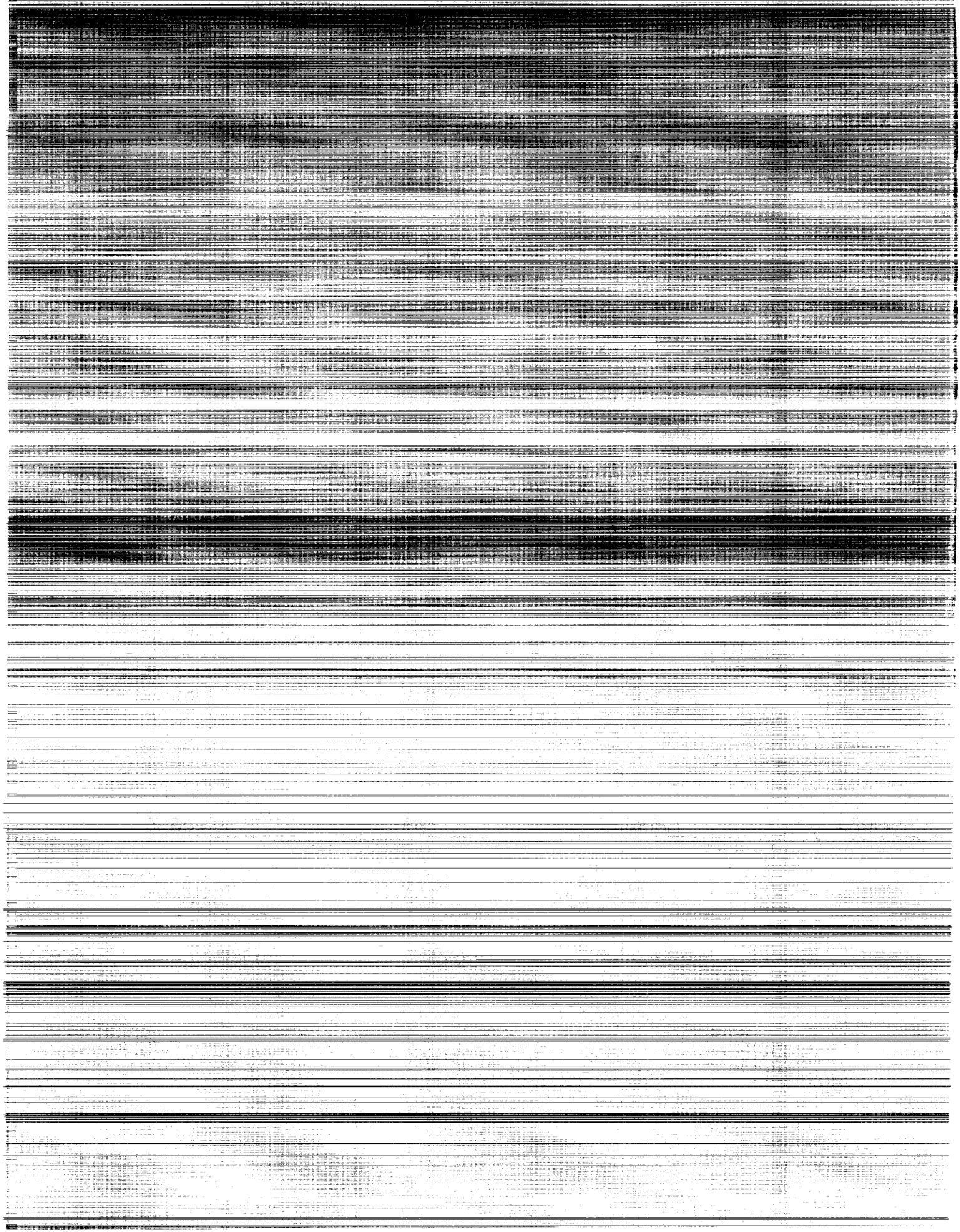

NASA CR-1157

STUDY, FABRICATION AND TESTING OF A FOIL-BEARING ROTOR SUPPORT SYSTEM

By L. Licht and A. Eshel

Issued by Originator as Report No. RR 68-2

Prepared under Contract No. NASw-1456 by
AMPEX CORPORATION
Redwood City, Calif.

for

NATIONAL AERONAUTICS AND SPACE ADMINISTRATION

For sale by the Clearinghouse for Federal Scientific and Technical Information
Springfield, Virginia 22151 – CFSTI price $3.00

ACKNOWLEDGEMENTS

The authors gratefully acknowledge the support received from Mr. Joseph Maltz and Mr. Herbert Rochen; National Aeronautics and Space Administration, Washington D. C., who displayed keen interest in the progress of this investigation.

Mr. William J. Anderson, Bearings Branch, Fluid Systems Component Division, Lewis Research Center, monitored the project and offered constructive criticism and suggestions.

This study was conducted in the Mechanics Section of the Research Department. Mr. Manfred Wildmann, Section Manager, has been largely responsible for the smooth progress of this investigation and has been instrumental in the solution of many technical problems.

The following personnel of the Ampex Corporation, listed in alphabetical order, contributed to the success of this undertaking:

Edward Barlow	- Comments on theoretical formulations
Arthur Caponera	- Manufacture of rotors and of thrust bearings
Alan Huckabay	- Assistance in the initial phase of the investigation
Helmut Kayan	- Manufacture of components
Joseph Kral	- Design of components of experimental apparatus and preparation of an excellent set of engineering drawings.
Robert Lawson	- Instrumentation, calibration of transducers, balancing of rotors, preparation and mounting of foils. Construction, modification and repair of components of test apparatus. Data taking, photography and active participation in all phases of this investigation.

Ralph Lauterborn - Manufacture of rotors.

Howard Menche - Operation of vibrator, instrumentation, calibration of accelerometers and numerous useful suggestions offered in the course of vibration experiments.

Fred Schneider - Manufacture, assembly and modifications of experimental apparatus. Construction of special fixtures and auxiliary mechanical components. Useful suggestions and ideas relevant to design modifications. Supervision of manufacture of the entire test apparatus.

Robert Schumacher Manufacture of capacitance probes.

Tene Woo - Assistance in programming and numerical calculations.

ABSTRACT

A high speed rotor is supported by means of an air-lubricated foil bearing and operated in both the vertical and horizontal attitudes, in excess of rated speed, 60,000 rpm. The foil bearing is stable and free from "half-frequency whirl" encountered in conventional gas-lubricated journal bearings. External pressurization is applied briefly to separate the foil surfaces from the journal during the initial and final stages of rotation only, with adequate self-acting support and foil separation established at approximately 6000 rpm.

In the first part of the experimental investigation, the response of the foil-rotor system to residual unbalance and to impact is studied. The gap width at the center of the foil wrap is determined, and the temperature rise of the foil above ambient is measured at several locations. Ultraharmonic resonances are observed and studied when the system is operated in the pressurized mode, in the low speed range. The theoretical prediction that disturbances propagate along the foil at half the speed of rotation is verified.

In the second part of the experimental investigation, the housing of the foil-rotor assembly is mounted on a vibrator and subjected to excitation normal to the axis of rotation. The in-line and transverse responses of the rotor are determined, and the relative motion of the foil and of the rotor are studied. In addition, the response of the rotor is determined at various g-levels of excitation, both at resonance and at frequencies of excitation equal to half the rotational speed.

Comparisons are made between measured gap widths and results predicted by theory, in which an attempt is made to account for the effects of inertia and compressibility of the fluid, of extensibility and temperature increase of the foil, and of friction at the foil supports. Comparisons are also made between theoretically predicted values of resonant frequencies, based on a simplified representation of foil-rotor dynamics, and results obtained from vibration and impact tests.

The potential and practicality of gas-lubricated foil bearings for high-speed turbomachines is demonstrated, wherein the main advantages appear to be:

(a) Stability (freedom from "half-frequency whirl);

(b) Tolerance of distortion and misalignment, coupled with excellent wipe-wear characteristics;

(c) Ability to accommodate excursions of journals exceeding by an order of magnitude the clearance of rigid-surface gas bearings.

CONTENTS

CONTENTS (Cont)

LIST OF FIGURES

LIST OF FIGURES (Cont)

LIST OF FIGURES (Cont)

LIST OF FIGURES (Cont)

LIST OF FIGURES (Cont)

LIST OF FIGURES (Cont)

LIST OF TABLES

LIST OF TABLES (Cont)

NOMENCLATURE

a	Distance between rotor center "O" and line connecting points of tangency with the guides
$a_{1,2}$	Amplitudes of foil excursion
A_k	Constant, related to length of foil segment (Eq. 5.16c)
$2A_{1,2}$	Maximum amplitudes of rotor orbit (peak-to-peak)
$2A_{x,y}$	Transverse and in-line amplitude of rotor (peak-to-peak)
b	Distance between points of tangency of foil guides (Fig. 5.3)
B	Distance between bearings (Fig. 5.11)
c	Thrust-bearing clearance
C_k	Compressibility parameter of k^{th} foil sector, $C_k = p_a/(T_k/r_o)$
E	Young's modulus
f	Friction coefficient
f_e	Frequency of excitation
f_n	"Natural frequency" of foil-rotor system
$F_{x,y}$	Components of resultant force of foil-support system on the rotor
F_i	Displacement of foil at center of foil segment, $i = 1, 2, 3$ (Fig. 4.29)
g	Gravitational acceleration
$G_{x,y}$	Amplitudes of transverse and in-line excitation (in g's)

h	Foil-bearing clearance
h_i	Foil-bearing clearance at center of segment, $i = 1, 2, 3$
$h_k(\theta, \tau)$	Clearance distribution of the k^{th} foil segment
h_{ik}	Distance of foil asymptote to rotor at the inlet of the k^{th} foil
h_{ek}	Distance of foil asymptote to rotor at the exit of the k^{th} foil
h^*_k	Clearance in uniformity region of k^{th} foil sector
$\bar{h}$	Effective surface-film heat transfer coefficient
H_k	Dimensionless clearance, $H_k = h_k/r_o\,(6\mu U/T)^{2/3}$
H^*_k	Dimensionless clearance in uniformity region of k^{th} foil sector
I_k	Inertia parameter of k^{th} foil sector, $I_k = 1/2\rho_a U^2/(T_k/r_o)$
i, k	Sequential number of foil-bearing segment, $i = 1, 2, 3 \ldots n$
k	Bearing stiffness per unit width
k	Thermal conductivity of foil material
k_{xx}, k_{yy}, k_{yx}	Components of stiffness matrix of foil bearing
L	Foil width
ℓ_k	Foil length between points of tangency with foil guides
ℓ_o	Initial foil length between points of tangency with foil guides
ℓ_{ik}, ℓ_{ek}	Length, defined in Fig. 5.3
m	Fin parameter, $m = (2\bar{h}/kt)^{1/2}$
n	Number of foil sectors of multisector foil bearing
n	Number of ultraharmonic (Figs. 4.20 through 4.23)
N	Rotational speed ($N = \omega/2\pi$; ω = angular velocity)
O	Position of rotor center at zero speed and no radial load

p_a	Ambient pressure, absolute
p_b	Thrust-bearing supply pressure, gauge
p_ℓ	Foil-lift supply pressure, gauge
P_k	Radial force of k^{th} foil sector on rotor
P_o	Radial force of foil sector on centered rotor at zero speed
P_u	Speed parameter
P_r	Radius parameter
P_e	Extension parameter
P_{T_o}	Initial tension parameter
P_t	Thermal expansion parameter
P_s	Slack parameter
P_h	Dimensionless gap
P_k	Dimensionless stiffness per unit width
Q_k	Tangential force of k^{th} foil sector on rotor
Q_o	Tangential force of foil sector on centered rotor at zero speed
r_o	Radius of rotor
r_p	Polar radius of gyration of rotor
r_t	Transverse radius of gyration of rotor
s	Distance from point of tangency (Fig. 5.5)

t	Foil thickness
t_a	Ambient temperature
t_f	Temperature of foil in region of wrap
t_{av}	Average foil temperature outside the region of wrap
T	Tension per unit width of foil
T_o	Initial tension per unit width of foil
T_k	Tension per unit width of k^{th} foil segment
T_1	Tension per unit width at guide clamp of anchoring post (Fig. 5.4)
T_{REF}	Steady state tension per unit width of foil
u	Residual rotor unbalance
U	Surface velocity of rotor
V	Velocity of propagation of disturbance along a foil (Fig. 4.47)
W	Rotor weight
x, y	Component of displacement of rotor center (Fig. 5.2)
x_k, y_k	Components of displacement of rotor center in the k^{th} auxiliary coordinate system (Fig. 5.2)
$(XY)_{1,2}$	Components of displacement of rotor in two monitoring planes [$(XY)_2$ displaced by 30° from $(XY)_1$ in the sense of rotation]
Z_i	Displacement of rotor along bisectors of foil segments, $i = 1, 2, 3$
α	Coefficient of thermal expansion of foil
α_k	Angle, defined in Fig. 5.3
β_k	Angle, defined in Fig. 5.3
γ_k	Angular position of k^{th} foil referred to foil $k = 1$

δ	Operator denoting a small deviation of magnitude of a quantity
$(\Delta\ell_p)_k$	Increase of ℓ_k due to effects other than tension, $\Delta\ell_p = \Delta\ell_t + \Delta\ell_s$
$(\Delta\ell_s)_k$	Increase of ℓ_k due to foil length supplied across lines of tangency with guides
$(\Delta\ell_t)_k$	Increase of ℓ_k due to thermal effects
ΔT_k	Difference in tension between the inlet and exit branches of k^{th} foil sector due to fluid friction
$\Delta\theta$	Temperature increase above ambient (Fig. 4.38)
ϵ	Foil bearing number, $\epsilon = 6\mu U/T$
θ	Angular polar coordinate
Θ	Angle of wrap
Θ_g	Total angle of wrap of guides, $\Theta_g = \Theta_{g1} + \Theta_{g2}$ (Fig. 5.4)
μ	Viscosity
φ	Arbitrary angle at which solution of foil-bearing equation is matched with a straight-line approximation (Fig. 5.3)
ρ_a	Density of lubricating fluid at ambient pressure
τ	Time
ξ	"Stretched" coordinate $\xi = \theta/(6\mu U/T_{REF})^{1/3}$

1. INTRODUCTION

The tacit assumption generally made in the conventional theory of lubrication is that bearings and journals are perfectly rigid. Results based on this idealization are valid for a wide range of practical bearing applications. On the other hand, it is self-evident that an adverse combination of intense loading and insufficient structural and material rigidity will result in deformations and corresponding changes of bearing performance. The effect of geometrical distoriton may be equally important as the variation of fluid properties of the lubricant. From this point of view, therefore, the difference in the generation of an oil film in a railroad-car journal bearing, and of an air film between a moving web of aluminum foil and a cylindrical guide, is one of degree rather than of kind.

At one extremity of the wide spectrum of elasto-hydrodynamic lubrication is the foil bearing, the existence of which, though generally unrecognized, is at least as old as the continuous manufacture of foil, film, and fabric. Despite the ubiquity of the foil bearing, the first theoretical and experimental study [1]* of its characteristics is only fifteen years old. The subject, with a few exceptions [2], attracted little attention until the advent of electronic data processing machines, when the study of foil bearings received an impetus from problems arising in magnetic tape drives [3, 4, 5, 6] and in recording on flexible media in general [7, 8, 9]. Numerous analytical [10 through 20] and a number of experimental investigations [21, 22, 23, 24] have followed during recent years.

*Numbers in brackets designate references in bibliography.

The focal point of these investigations has remained in the area of mechanics associated with digital and analog recording. The digital computer has furnished means for the numerical solution of high-order nonlinear differential equations and the analysis of experimental data has been facilitated by the availability of magnetic recorders. The results contributed in turn toward the development of sophisticated methods of tape guidance and support.

With the exception of peripheral applications as loading devices in experimental gas-bearing research and, possibly, as a method of stabilization of very long and flexible shafts [25], no serious attempts have been made in the past to utilize foil bearings as a means of rotor support in high-speed turbomachines. Recently, however, in the course of a feasibility study which preceded the present investigation, rotational speeds of order 350,000 rpm were attained with a small, one inch diameter rotor, mounted vertically and supported laterally by very flexible foil bearings [26]. Subsequent experience, accumulated in the course of the present investigation, has demonstrated that the concept of foil-bearing support for high-speed rotors is not only feasible, but also practical. Also, as a by-product of this study, considerable knowledge has been gained of the operational characteristics and of certain physical phenomena associated with this type of suspension.

A multi-function experimental apparatus has been designed, manufactured, and instrumented, which accommodates air-turbine driven 2" x 3" rotors of variable mass and inertia, supported radially by a single, 3-sector foil bearing and constrained axially by pressurized thrust bearings. A method of starting and stopping with the aid of an external pressure source has proved most effective and also economical in terms of air consumption. The response to residual unbalance, in both the self-acting and pressurized modes, has been determined, as well as response to impact and unidirectional excitation by means of a vibrator. A number of experiments involved

rotors which differed in mass and mass distribution and foils of various rigidities and material properties. It has thus been possible to study the influence of several variables on the dynamic response of the foil-rotor system and to assess, at the same time, the wipe-wear characteristics of various foil materials. In addition to measurements of the absolute displacement of the rotor under steady-state and dynamic conditions, the width of the air gap between the rotor and the foil has been determined under various operating conditions. The theoretical prediction that disturbances propagate along the foil at approximately one-half of the rotor surface speed [17, 18] has been verified experimentally. The relative motion of the rotor and of the foil, responding to a sinusoidal excitation of a vibrator, has also been studied.

In order to assess the importance of relaxation of tension, the temperature rise of the foil above ambient has been measured by means of thermocouples at various speeds and locations. Important information has also been gained from experiments, wherein the turbine air supply was suddenly cut off at rated speed and the displacement of the decelerating rotor and the gap width were monitored in the absence of cooling by turbine air. The motion of rotors has also been studied in the pressurized mode of operation, which is characterized by sharply defined, ultraharmonic resonances. The latter occur at rotational speeds which are related by nearly exact fractions to frequencies of synchronous resonance. In the self-acting mode, on the other hand, the foil-rotor system appears to be characterized essentially by a single, dominant resonance, the frequency of which varies but slightly with the intensity of excitation.

Among many rather remarkable characteristics of the foil bearing is the very apparent absence of instability, frequently referred to as "half-frequency" or "fractional frequency" whirl, which invariably imposes a severe restriction on the maximum safe speed of gas-bearing

supported rotors. Nor is excitation at a frequency equal to one-half the rotational speed associated with a condition of large-amplitude resonance, which characterizes other types of fluid-film bearings. Finally, the self-aligning and distortion-accommodating properties of the foil bearing, coupled with excellent wipe-wear characteristics and tolerance of foreign particles, indicate that it may provide solutions for many problems arising in the operation of high-speed and high-temperature turbomachines.

2. EXPERIMENTAL APPARATUS

The main components of the experimental foil-bearing apparatus are indicated in the assembly drawings, Fig. 2.1 and Fig. 2.2. A two-inch diameter, three-inch long steel rotor (1)* is supported radially by a single, one-inch wide foil (2) along three equally spaced and equal regions of wrap, each extending over an angle of sixty degrees. Axial and pitching constraint for the rotor is furnished by two externally pressurized air bearings (3). Two rows of thirty-two impulse buckets are milled close to each end of the rotor to form turbine wheels (4), supplied with compressed air through two sets of nozzles (5). The rotor also contains two rows of twenty-four orifices of 0.020 inch diameter (6), equally spaced at 0.125 inches from the edges of the foil. Compressed air is supplied to the interior of the rotor (7) and to the orifices to separate the preloaded foil from the rotor during initial and final stages of rotation. A rotating seal (8) for this supply is formed by the annulus between the rotor and the central area of the thrust bearing, which is separated from the actual thrust pads by venting grooves. The thrust-bearing air supply (9) is maintained at all times, and the foil-lift supply is discontinued as soon as adequate support and foil separation are established by self-acting effects.

The foil bearing consists of a single foil strip, looped around the rotor and through an array of symmetrically spaced, cylindrical guides and anchoring posts (10), (11), (12). The guide posts are press-fitted into the lower housing plate (13), which contains also three sturdy spacers (14) for the alignment and bolting of the upper housing plate (15),

*Numbers in parentheses designate components of apparatus in Figs. 2.1 and 2.2.

following insertion, preloading, and locking of the foil. The preload (initial tension) is applied at the extremities of the foil which protrude beyond two externally pressurized guides (11), adjacent to the foil lock (16).

The procedure followed in applying an initial tension is the following. The foil is separated from the surface of the rotor and from the surface of the cylindrical air-bearing guides (11) by external pressurization, so that tension applied by means of a simple pulley-and-weight arrangement (not shown) is unaffected by friction.* With the rotor floated on the lower thrust pad, the foil-lift pressure is gradually reduced, until normal contact is reestablished at the rotor and air-bearing guides. A sensibly uniform preload tension having thus been applied in each of the foil-bearing sectors, the foil is locked (16) and also secured at the anchoring posts (12), in order to prevent slippage under operating conditions.

The motion of the rotor can be monitored in two planes by means of capacitance probes (17) and Wayne Kerr DM 100 Displacement Meters, the output of which can be observed on oscilloscopes and recorded simultaneously on magnetic tape by means of an Ampex Model FR 600 Instrumentation Recorder. Provision is also made for mounting probes opposite the center of each of the three foil sectors for the measurement of foil displacement. By applying the outputs of the rotor and of the foil monitoring probes to the terminals of a differential-input amplifier, the width of the air gap can be measured directly. Capacitance probes can also be mounted by means of auxiliary fixtures at various stations along the arc of wrap for the simultaneous measurement of foil displacement at several angular positions.

Details of the rotor, thrust bearings, and of the lower housing assembly are shown in the photograph of Fig. 2.3 and in the

*The friction moment of the ball-bearing mounted pulley is negligible.

schematic diagram of Fig. 2.4. The method of foil mounting is illustrated in the photograph of Fig. 2.5, in which - with the upper housing plate removed - the rotor, the foil, the foil guides, and the foil lock are clearly discernible. The entire foil bearing apparatus and the supporting frame are shown in the photograph of Fig. 2.6, in which the assembly is mounted horizontally and the foil bearing supports a radial load equal to the weight of the rotor. The photographs of Fig. 2.7 and Fig. 2.8 show the rotor, supported on air bearings, in a fixture mounted on the bridge of a Schenck Balancing Machine, Model RS1-b.

The experimental apparatus, the vibrator table, the exciter, the control consoles and panels, and an array of various instruments and transducers used in the course of dynamic experiments are shown in fig. 2.9 and Fig. 2.10.

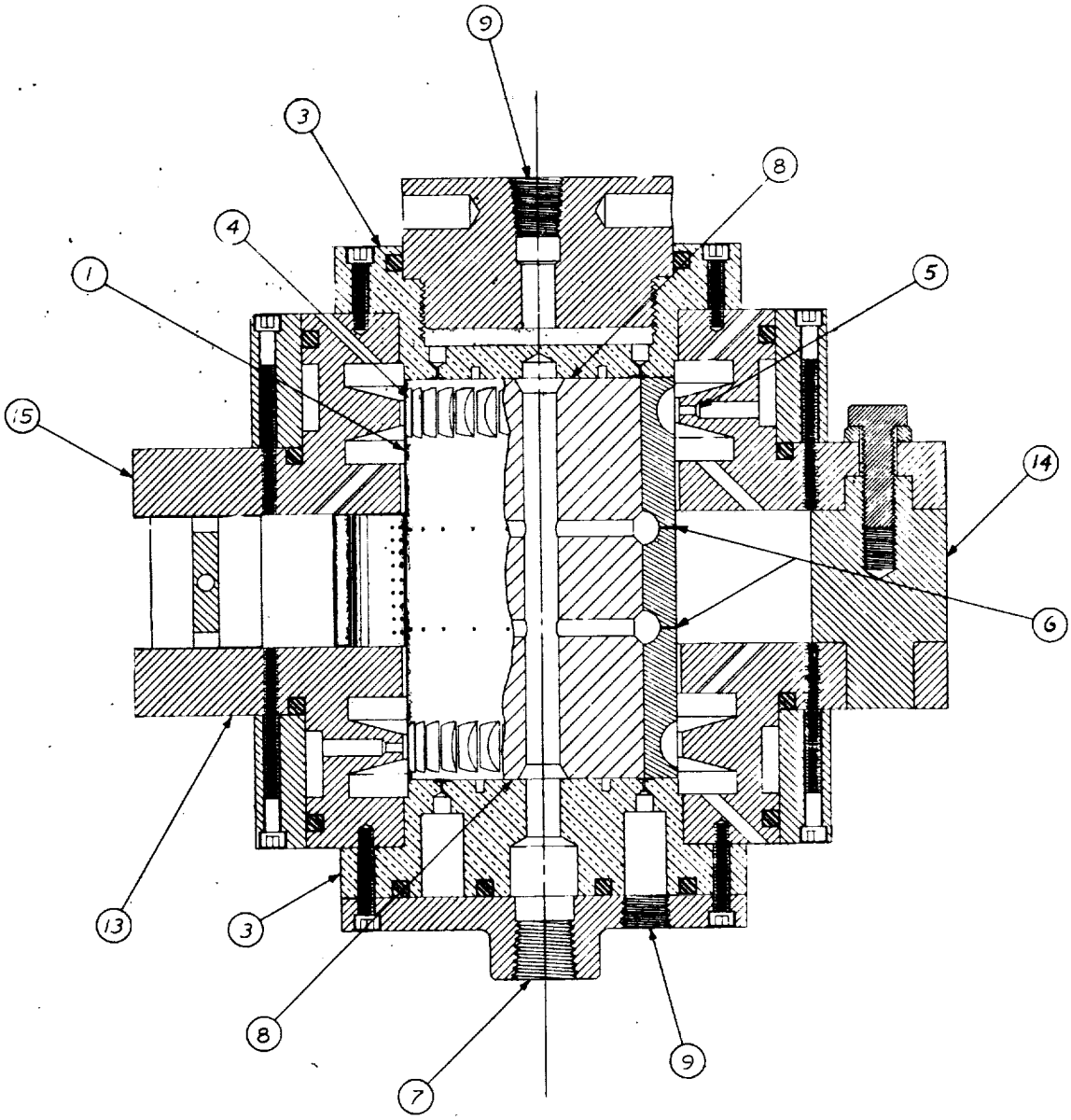

ITEM	DESCRIPTION
1	ROTOR
2	FOIL
3	THRUST BEARINGS
4	TURBINE
5	NOZZLE
6	ORIFICES
7	FOIL-LIFT AIR SUPPLY
8	SEALING ANNULUS
9	THRUST BEARING AIR SUPPLY

ITEM	DESCRIPTION
10	FOIL GUIDE
11	PRESSURIZED FOIL GUIDE
12	FOIL ANCHORING POST
13	LOWER HOUSING PLATE
14	SPACER
15	UPPER HOUSING PLATE
16	FOIL LOCK
17	CAPACITANCE PROBE

Fig. 2. 1 Section View of Experimental Apparatus

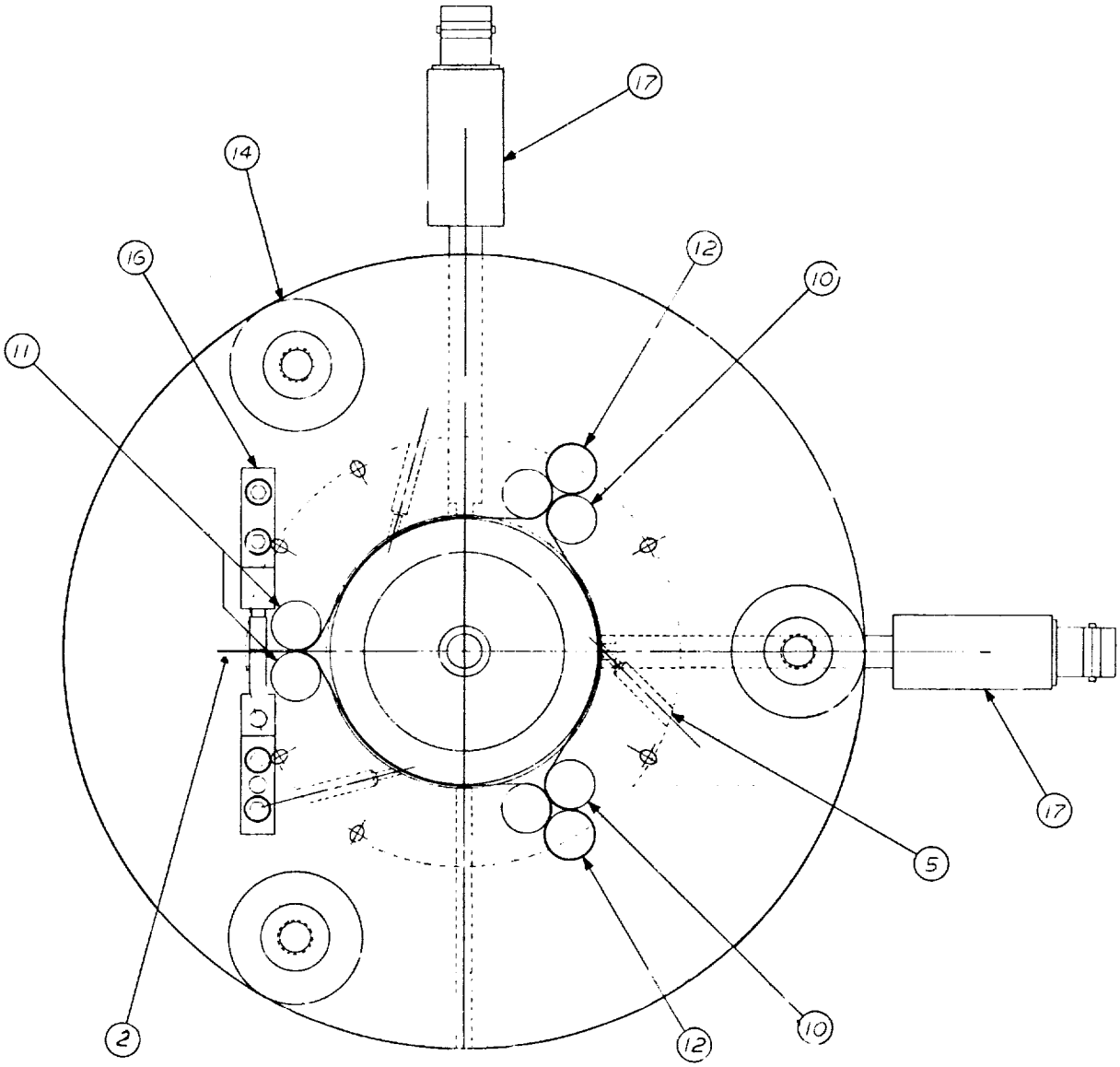

ITEM	DESCRIPTION
1	ROTOR
2	FOIL
3	THRUST BEARINGS
4	TURBINE
5	NOZZLE
6	ORIFICES
7	FOIL-LIFT AIR SUPPLY
8	SEALING ANNULUS
9	THRUST BEARING AIR SUPPLY

ITEM	DESCRIPTION
10	FOIL GUIDE
11	PRESSURIZED FOIL GUIDE
12	FOIL ANCHORING POST
13	LOWER HOUSING PLATE
14	SPACER
15	UPPER HOUSING PLATE
16	FOIL LOCK
17	CAPACITANCE PROBE

Fig. 2.2 Plan View of Experimental Apparatus

Thrust Bearing
Lower Housing Plate
Rotor
Probe

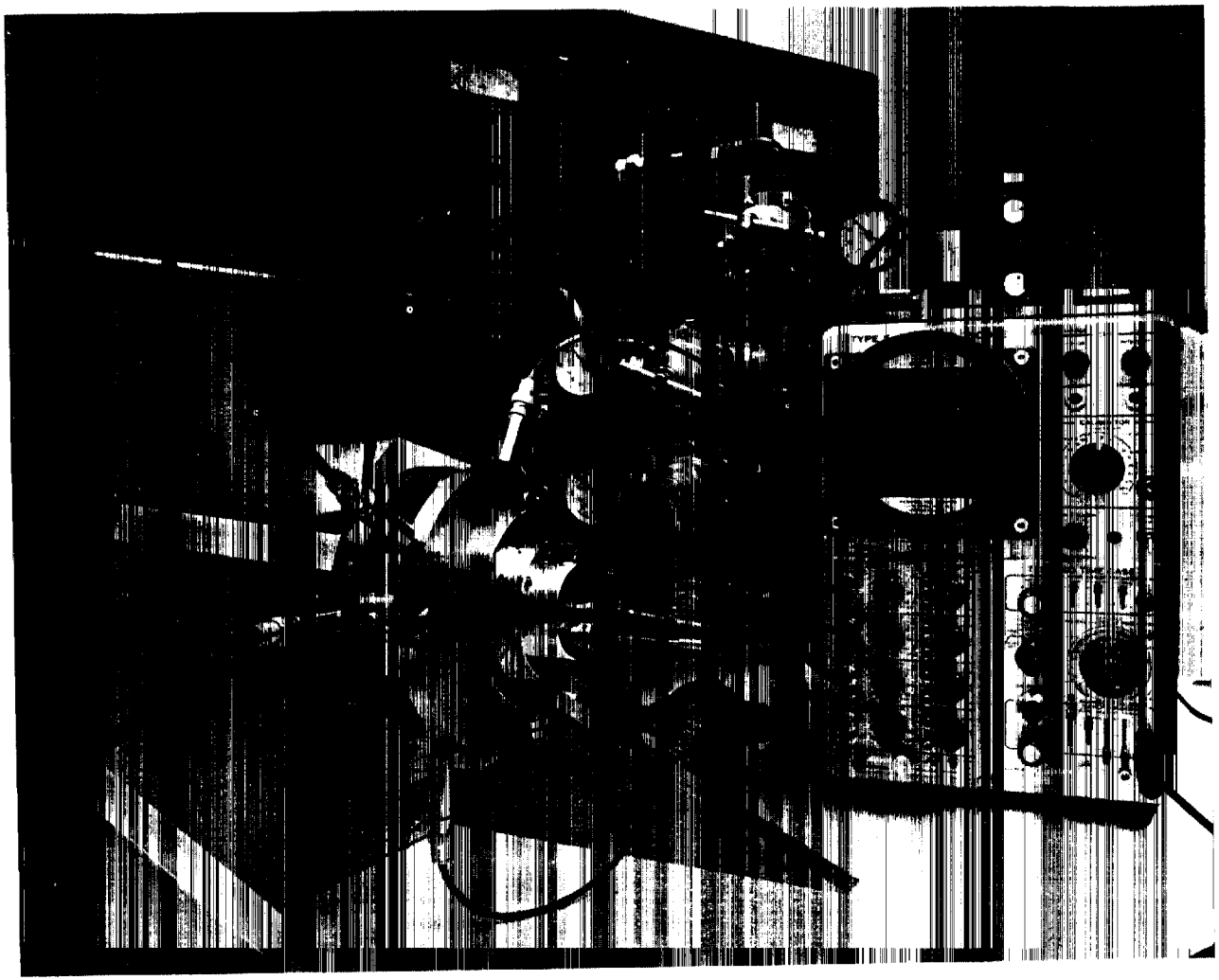

Fig. 2.6 View of Experimental Apparatus in Horizontal Attitude

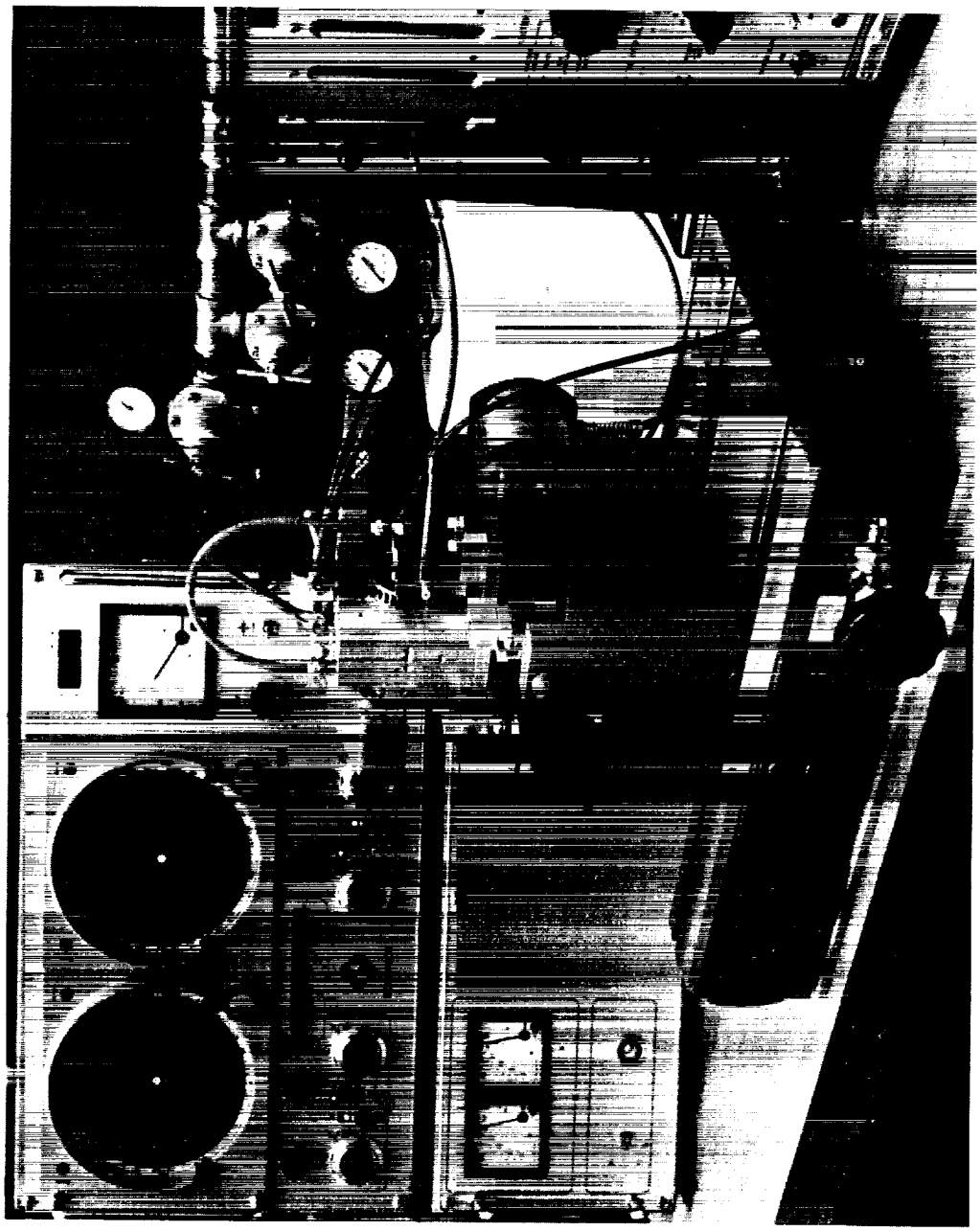

Fig. 2.7 View of Rotor and Balancing Machine

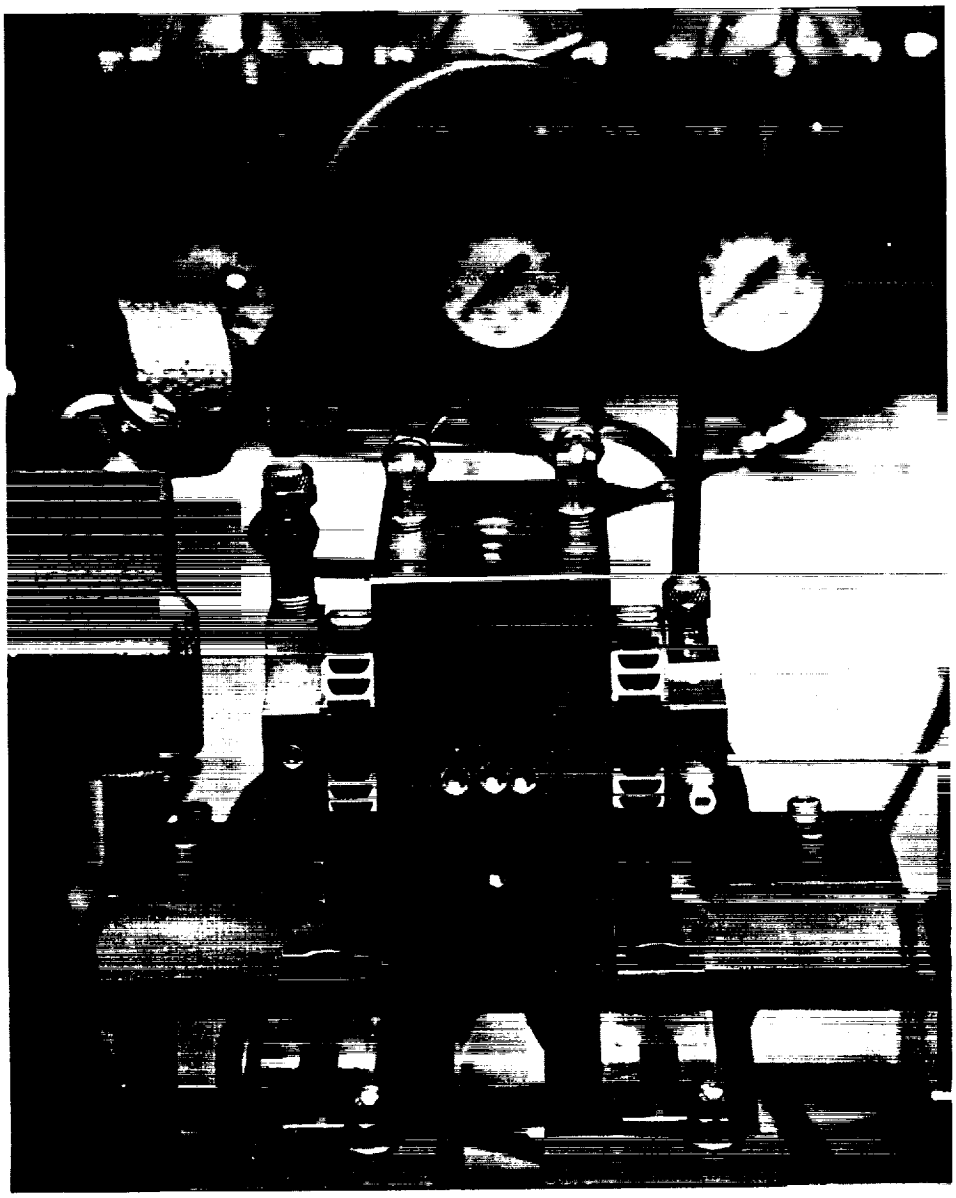

Fig. 2.8 View of Rotor and Auxiliary Air Bearing on Pedestal of Balancing Machine

Fig. 2.9 View of Experimental Apparatus and Vibrator

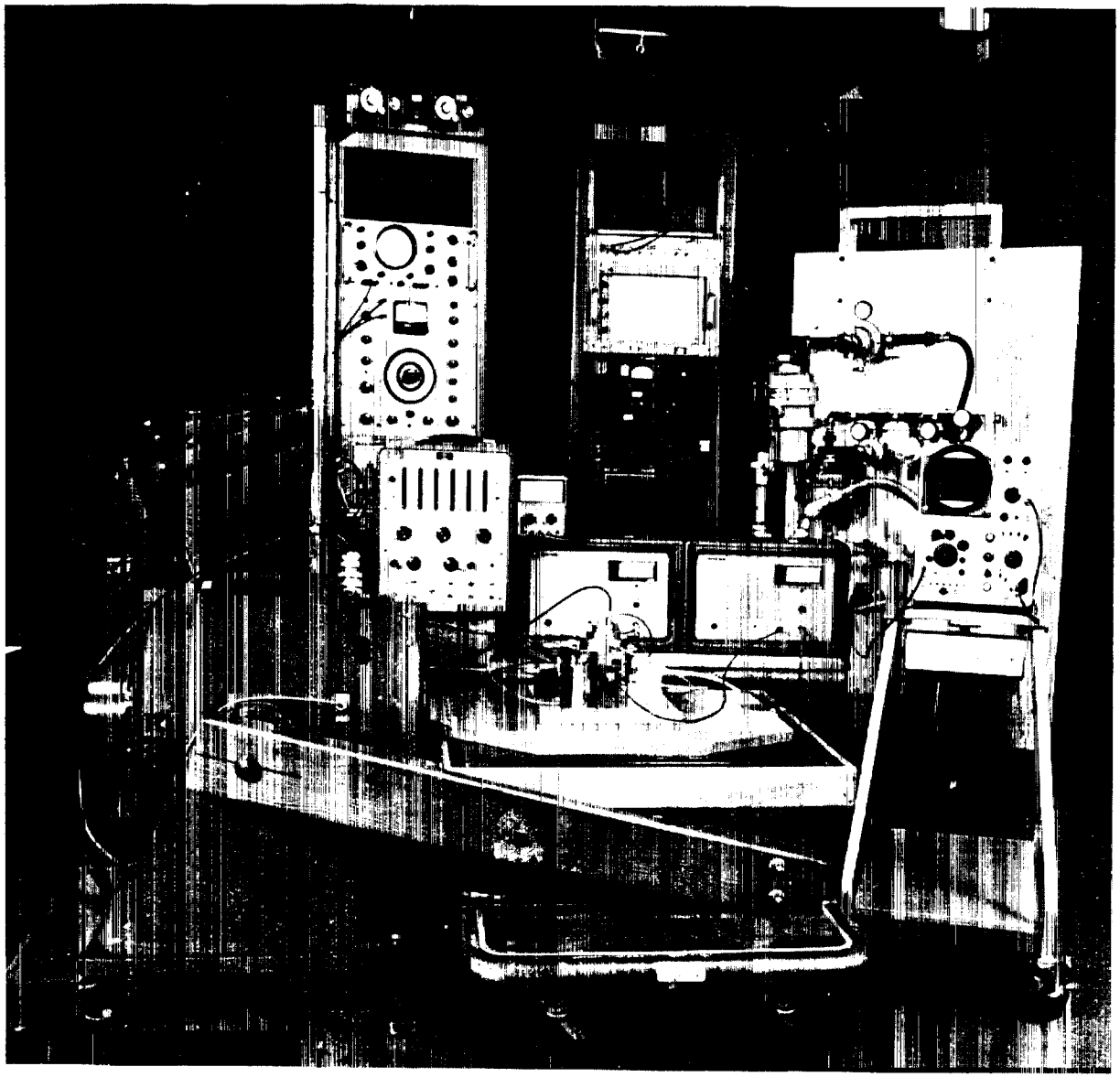

Fig. 2. 10 General View of Experimental Apparatus, Vibrator and Instruments

3. INSTRUMENTATION AND AUXILIARY APPARATUS

The displacement of the rotor and of the foil has been measured by means of capacitance probes and Wayne Kerr DM 100 Displacement Meters. Six probes, of nominal diameter 0.1 inches, have been constructed to a degree of uniformity corresponding to a maximum deviation from their average sensitivity of ±3%. The probe characteristics were sensibly linear. At a nominal offset of approximately 0.004 inches, the mean sinsitivity was 180 mv/1000 μin. Excursions of ±0.002 inches from this position correspond to a variation of sensitivity of approximately +3%. The scale factors of all oscilloscope photographs, therefore, involve a maximum possible error of ±6%. The probes have been calibrated by means of precision gauge blocks and a ground, 2.0 inch dia cylinder. The calibration has been carried out in 16 increments of 0.0005 inches. Three calibration runs have been made for each of the six probes. The frequency response of the displacement meters, inclusive of output filters, has been found to be flat to at least 2.5 kc and, therefore, quite adequate in the range of experimental speeds of rotation and frequencies of excitation.

The speed of rotation was measured by means of an optical probe and on an MTI KD-38 Fotonic Sensor, using a Hewlett-Packard Model 523B Electronic Counter. The speed could be maintained and measured with an accuracy better than ±1%. The thrust bearing and foil-lift supply pressures have been recorded by means of bourdon-tube type pressure gauges, accurate to ±2% of full scale deflection.

With regard to measurement of temperature rise of the foil above ambient, it is difficult to assess the local influence of thermocouples

on the temperature field. The thermocouples were of 3 mil copper-constantan wire, with welded, quasi-spherical junctions, approximately 6 to 10 mils in diameter. The latter were held in contact with the foil surface, while a minute droplet of fast-drying strain-gauge cement was applied under a microscope in the immediate vicinity of the contact point. The reference junction was situated sensibly far from the foil-rotor assembly, at a location where the ambient room temperature varied by less than $\pm 1.5^{\circ}$F. An Astrodata Nanovoltmeter, Model TDA-121, has been used, the accuracy of which is specified as ±3% of full scale deflection in all ranges and the drift of which is less than 0.03% of full scale per day.

The vibrator (MB, Model C-10 Exciter) used in the experiments is capable of transmitting a maximum force of 1200 lb within a frequency range 5 to 3000 cps. A maximum displacement of 1.0 inch and a maximum velocity of 70 in/sec can be realized. With a movable mass, consisting of an oil-floated plate and the foil-rotor assembly, peak acceleration up to 15 g could be maintained. Three Endevco crystal type accelerometers have been mounted on the compact rotor housing, along axes corresponding to the direction of excitation, the transverse axis, and the vertical axis parallel to the axis of the rotor. The accelerometer outputs were amplified by Glemite amplifiers, having a flat frequency response 5 c to 35 kc. Since high-frequency components of excitation, such as multiples of the rotational speed corresponding to the number of turbine buckets (32), the number of pressurization orifices (24) and other spurious, high-frequency disturbances could be sensed by the accelerometers; the amplified outputs of the latter were passed through SKL variable bandwidth filters to eliminate frequency components above 6000 cps. This arrangement resulted in proper control of motion of the vibrator by the in-line accelerometer and in nearly sinusoidal vibration input to the housing, except at a number of isolated structural resonances.

A number of experiments involved the determination of the phase between the in-line motion of the housing (accelerometer) and the in-line response of the rotor (capacitance probe) in the neighborhood of resonance. Since the outputs of corresponding transducers have been amplified and filtered by different systems, the relative phase difference of these systems was determined by mounting the accelerometer directly on the exciter and monitoring the sinusoidal motion of the unloaded exciter with a capacitance probe. A comparison of outputs of the accelerometer and of the capacitance-probe systems, in a frequency band centered at the resonant frequency of the foil-rotor system, has indicated that the outputs of the monitoring systems were almost exactly in phase. The determination, therefore, of the phase angle between the in-line motion of the housing and of the rotor required no correction within the limits of experimental accuracy.

Three 2" x 3" rotors, of 1.0, 2.414, and 2.390 lb weight respectively, have been used in the course of the present investigation. The light rotor was hollow, and the two heavier rotors were largely solid. Balancing of the 1.0 lb and the 2.414 lb rotors has been performed in a fixture, the essential components of which were two 0.5-inch wide pressurized gas bearings, located inboard of the turbine buckets. The motion of the rotor was monitored in two planes, while plane separation has been achieved, approximately, in the following manner. The supply pressure of one journal bearing was increased to constrain the motion of the rotor in one plane, and the supply pressure of the second journal bearing was lowered substantially to induce relatively large rotor excursions in the second plane, i.e., in the balancing plane. With the foregoing procedure reversed, balancing in the first plane was performed next. With these simple means, the unbalance of the 1.0 lb rotor has been reduced to less than 200 μ in-oz and that of the 2.414 lb rotor to less than 800 μ in-oz. The balancing of the 2.390 lb rotor has been performed

on a Schenck Model RS-1B Balancing Machine (Fig. 2.7), and the residual unbalance was less than 20 μ in-oz.

4. EXPERIMENTS

A. General Remarks and Summary of Experiments and Experimental Results

The design of the experimental apparatus described in Section 2 of this report has been aimed at fulfilling several important functions. The main objective has been the construction of a simple and realistic foil bearing support, by means of which it would be possible to study the planar motion of a rotor under steady running conditions, and also the response to impact and to sinusoidal excitation by means of a vibrator (shake-table). Other important objectives of the present investigation have been to develop a practical method of starting and stopping the rotor; to determine the effects of rotor mass and mass distribution, of preload tension, and of the extensional rigidity of the foil; and to assess at the same time the wipe-wear characteristics of various foil materials under operating conditions. The construction of a prototype of size and weight corresponding to an actual turbomachine would have presented an undertaking for which the present state of the art could furnish no design data and no reservoir of previous experience. On the other hand, the purpose of the present investigation has been to construct and to analyze a practical foil bearing, which would support a rotor in both the vertical and the horizontal attitudes and furnish a degree of constraint commensurate with the requirements of a real machine. The constraint of the operation of a high-speed rotor between two narrowly spaced thrust bearings ($C \approx 0.0008"$) and by means of a <u>single</u> foil-bearing support imposed more severe limitations than would be encountered in an actual application. The fact that it has been at all possible to support a high-speed rotor in

this manner and to accommodate resonances in the pitching mode is most encouraging, especially if one considers that in the course of nearly 300 hours of operation the foil-rotor system has been subjected to appreciable impact and a high level of excitation.

Before embarking on a detailed description and discussion of the experimental work, a brief outline of experiments and of experimental results is appended hereto. We begin with the description of the motion of the rotor in the self-acting mode, under the influence of residual unbalance, which is characterized by quasi-cylindrical resonances,* related to the foil bearing, and conical resonances, influenced mainly by the thrust bearings. Rotational speeds up to and in excess of 60,000 rpm are attained in both the vertical and horizontal (gravity load) modes of operation. The motion is stable and free from "half-frequency" or "fractional frequency" whirl. The report continues with the description of the rather complex motion in the pressurized mode of operation, characterized by the occurrence of ultra-harmonic resonances at angular velocities, which are related to speeds of synchronous resonance by nearly integral numbers. It is concluded that rotation in pressurized foil bearings is not only practical, and economical in terms of air consumption, but that it offers an excellent transition to and from the self-acting mode of operation.

The next topic deals with the determination of the average gap width at the center of the region of wrap, as well as with the displacement of the rotor axis with speed from its initial position. It is observed that the gap width is generally greater than the clearance initially

*The quasi-cylindrical resonances occurred at relatively low speeds of rotation and have been reported whenever operation in the self-acting mode could be maintained in the lower speed range.

predicted by theory. The subsequent inclusion of several, hitherto disregarded, effects in the theoretical model yields a considerably better agreement between theory and experiments. It is also found that residual dissymetries of the foil-bearing sectors result in the displacement of the rotor axis, with speed, from its initial position. The rotor is then operated in the horizontal attitude, and the gap width is determined at one of the foil segments, when the latter is either unloaded or subjected to a radial gravity load. It is demonstrated that foil-bearing supported rotors can be operated in the presence and in the absence of radial loads, and that adequate separation can probably be maintained with gravity loads of order 2 to 3 pounds per square inch of projected bearing area.

Other experiments performed in the course of the present investigation include the determination of the temperature rise of the foil as a function of the rotational speed. A complementary experiment involves the measurement of gap width and of rotational speed when the rotor is decelerated in the absence of cooling air from the turbine discharge. The foregoing experiments indicate that the temperature increase is sensibly uniform in the region of wrap and comparatively insignificant wherever the foil is not in the immediate proximity of the journal. When the turbine air is cut off at 60,000 rpm, the temperature rise above ambient is nearly doubled, and an additional 10% increase of gap width can actually be observed during the initial period of deceleration! No essential differences, however, are noted in the behavior of the rotor during acceleration and coastdown.

The latter part of this chapter deals with the transient and steady-state response of the foil-rotor system. The theoretical prediction that disturbances along the foil propagate at approximately one-half the surface velocity of the rotor is verified for the first time. The response of the rotor-foil system to impact is studied, in order to determine the

"natural frequencies" at various speeds and for various foils and rotors. A fairly good correlation is obtained between theory and experiment. The determination of the "natural frequencies" is followed by the study of the response to sinusoidal excitation by means of a vibrator (shake-table). These experiments concern the determination of resonant frequencies, amplitudes, and phase relations, with rotor speed and mass as variable parameters. In addition, several experiments involve excitation at variable g-level, both at resonance and at frequencies of excitation equal to one-half the rotational speed. The results of these experiments are most encouraging. It appears that in the range of excitation, 0 - 2000 cps, the system behaves essentially as a simple, damped oscillator. Furthermore, in contrast to other fluid-film bearings, excitation at frequency equal to half the rotational speed does not produce large amplitudes of motion.

Finally, the continuous study of wipe-wear characteristics of foils confirms the "forgiving" nature of the foil bearing and its particle and distortion-accommodating capability.

B. Response to Residual Unbalance

The main objective of this investigation has been focussed on the study of rotor-foil interactions. An ideal experimental apparatus for this purpose would have insured a purely planar motion, so that all points on the rotor axis described identical paths. This degree of perfection, however, can never be achieved, even with simple, rigid rotors supported symmetrically by nearly identical journal and thrust bearings. A quasi-cylindrical motion can, at best, be approximated, and then only at speeds which do not excite large amplitudes of angular (conical) motion. Furthermore, it is seldom possible to eliminate the coupling between the journal and thrust bearings.

The advantages of experimenting with a single foil bearing, rather than with a tandem support, are self-evident. The price which had

to be paid for this advantage has been the necessity to rely entirely on the thrust bearings to limit angular excursions and to accommodate within the axial clearance the resonant amplitudes of pitching motion. The constraints imposed on the motion of a high-speed rotor supported in this manner have been much more severe than in the case of a rotor mounted on two journal bearings. The fact that rotors supported in this manner could be operated over prolonged periods of time, in both the vertical and horizontal running positions, and frequently in the presence of severe dynamic loads, has been heartening.

Since the motion of the rotor in the entire speed range has been influenced in varying degrees by both the foil bearing and by the thrust bearings, the response of the entire system has been determined for parametric variations of rotor inertia, foil rigidity and material, and preload tension. Initial attempts to operate with largely unbalanced rotors and relatively compliant thrust pads were unsuccessful and resulted in several thrust bearing failures at relatively low speeds. The experimental rotors have subsequently been balanced by methods described in Chapter 3, and the thrust bearing geometry has been modified to correspond to the configuration illustrated in the right hand side of Fig. 2.4. As a result of these changes and of reduction of remanent unbalance, no subsequent difficulties have been experienced in passing through resonances and in attaining rotational speeds in excess of 60,000 rpm.

Transitions from the pressurized mode of operation occurred frequently above the speeds of cylindrical resonances of the self-acting system, so that the latter have only been recorded whenever sufficient self-acting support could be maintained for adequately long periods of time at low speeds. On the other hand, the speeds and amplitudes of conical resonances, while extremely sensitive to changes of thrust bearing supply pressure and clearance, remained practically unaffected by the torsional stiffness of the foil bearing.

The response of the system to synchronous excitation by residual unbalance* has been determined by monitoring the motion in two planes, 1.375 inches apart and equidistant from the midplane of the rotor. The data is presented in Figs. 4.1 through 4.19 and in Tables 4.1 through 4.5. The maximum double amplitudes of motion in each plane are plotted against the speed of rotation, for both the vertical and horizontal modes of rotor support. To each graph and set of tabulated data corresponds an array of oscilloscope photographs of rotor orbits. A number of photographs are also included in each array, in which the outputs of corresponding probes in two monitoring planes** are displayed against a time base. The "phase" relation of these outputs is indicative of whether a resonance is predominately "conical" or "cylindrical," and whether the motion is governed essentially by the thrust bearings or by the foil bearing. Each set of data contains information pertinent to rotor mass and inertia, preload tension, foil and foil material, thrust bearing supply pressure and clearance, and the approximate magnitude of remanent unbalance. The reader's attention is drawn to the fact that, despite the relative paucity of experimental points, the response curves have been faired in correctly. The procedure followed has been to scan the response throughout the entire speed range and to locate as accurately as possible all maxima and minima. The oscilloscope displays corresponding to these stationary and to a number of intermediate points have then been photographed and the maximum amplitude recorded. The reader should also consider the seemingly large orbits in terms of appended sensitivity scale factors and note that the maximum double amplitudes of conical resonances did not exceed 500 μin.

---

*Other sources of periodic excitation, of lower intensity than the residual unbalance may have also been present.

**The X_1 and Y_1 probes in the "upper" monitoring plane were displaced by 30° in the opposite sense of rotation from the corresponding X_2 and Y_2 probes in the "lower" monitoring plane.

In examining the pitching motion of the rotor, it becomes immediately apparent that resonances occurred generally at more than one speed, regardless of whether the rotor has been operated in the vertical or in the horizontal position. The response curves present a picture of several peaks and valleys, grouped rather closely within a relatively narrow speed range. The response curves of Fig. 4.15, for example, are characterized by as many as four resonant peaks, while Fig. 4.10 displays a single peak only. One of the resonances is always dominant, and the rotational speed at which the latter occurs appears to be sensibly independent of the rigidity of the foil, the preload tension, and the attitude of the rotor. On the other hand, the interval of rotational speeds, in which conical resonances occur, can be translated by changing the inertia of the rotor, and even more effectively by varying the thrust bearing supply pressure and clearance. The nature of conical resonances is probably influenced by both the nonlinearities and the dissymetries of the system. The fact that as many as four pitching resonances could be observed can be related to four possible degrees of freedom of motion,* or a lesser number, depending on the extent of symmetry.

The effect of changing the thrust bearing supply pressure is illustrated in Fig. 4.9. The first photograph of Fig. 4.9 shows two orbits in the conical mode of motion. The outer orbit has been obtained at resonance and at a thrust bearing supply pressure of 40 psig. The inner orbit in the same photograph has been obtained by increasing the supply pressure to 85 psig. The second photograph of Fig. 4.9 illustrates an analogous situation, wherein the resonant orbit at 85 psig has been decreased by reducing the thrust bearing supply pressure to 40 psig, without altering the speed. On contrast, the third photograph, which corresponds to a

*Neglecting rotation about the rotor axis and translation parallel to the axis.

cylindrical resonance of the foil-rotor system, indicates that changes of the thrust bearing supply pressure had no appreciable effect on the motion of the rotor. Finally, the fourth photograph in Fig. 4.9 illustrates a spiralling orbit of a low-inertia rotor, rapidly approaching the dominant pitching resonance at relatively high speed and thrust bearing supply pressure. In this case, the motion may have also been influenced by a relatively rigid foil and increased preload tension. Had the investigators attempted to run through this resonance at approximately 700 rps and 85 psig supply pressure, the result would have been disastrous. The thrust bearing supply pressure has subsequently been decreased to 45 psig, which reduced the resonant speed to approximately 480 rps. The resonant double amplitude at this speed was of order 300 μin, as illustrated by the response curve in Fig. 4.14. With a thrust bearing clearance of approximately 800 μin, the resonant amplitude of conical motion resulted, in this case, in a tolerable reduction of the parallel clearance by 27.5% at the outer thrust-bearing perimeter.

The occurrence of quasi-cylindrical resonances of the rotor and of the foil bearing has been observed and recorded whenever adequate self-acting support could be generated in the lower speed range. Referring to Fig. 4.5 and Fig. 4.6, it is noted that a dominant and minor quasi-cylindrical resonance occur respectively in the neighborhood of 155 rps and 209 rps. The dominant resonance corresponds to the orbits and to the timebase display, denoted by the ordering number 2 in Fig. 4.7. The timebase display represents the outputs of the X_1 and X_2 capacitance probes, which were in phase (allowing for an included angle of 30° between probes). The mean size of the corresponding orbits is indicative of the extent of "cylindricity" of motion. The rotational frequency of the dominant resonance is in fairly good agreement with data obtained from impact and vibration tests reported in the following sections of this chapter. The reason for the existence of two closely spaced resonances,

rather than one, is undoubtedly a consequence of dissymmetry, augmented by nonlinearities and cross-coupling effects at large amplitudes of motion. The foil bearing, therefore, displays directional properties which vary generally with the position and motion of the rotor.

In drawing an analogy with the lightly damped, linear system, the orientation of corresponding pairs of resonant orbits 2 and 4 in Fig. 4.7 can be considered approximately along the "principal axes" of bearing compliance. An analogous situation is depicted in the photographs of Fig. 4.8, denoted by the ordering numbers 1, 2, and 3. In this case, the rotor has been operated in the horizontal attitude and the dissymmetry has been accentuated by the gravity load. The orbits 1 and 2 corresponded to speeds which were slightly below and above the resonant speed. The reader will note that the orbits 1 and 2 in the $(XY)_2$-plane are nearly symmetrical about the vertical axis, which reflects a change of phase of nearly 180° in passing through the first resonance. The orientation of orbits in 1 and 2 is nearly orthogonal to the corresponding orbits in 3. Allowing for the 30° angle between respective probes in the two monitoring planes, it can be seen that the orbits in 1 and 2 correspond to a transverse resonance, while the orbits in 3 correspond to a resonance along the load line. Similar observations can also be made with reference to data presented in Fig. 4.18 and Fig. 4.19.

After passing through a series of cylindrical and conical resonances, the motion of the rotor upward of approximately 40,000 rpm has been characterized by orbits of representative size less than 100 μin. Random excitation of very small amplitude could be observed at higher speeds, and this accounts for the blurred appearance of orbits at 750 rps and 1000 rps in most oscilloscope photographs. Overharmonic components of motion have also been observed at higher rotational speeds, despite the smallness of the orbital motion. A good example of overharmonic

motion is presented in the photographs of Fig. 4.19, denoted by the ordering numbers 15, 16, and 17. The timebase displays of probes X_1 and X_2 indicate the presence of the third overharmonic, which is reflected in a corresponding number of small loops and cusps in the orbital path of the rotor.

C. Rotation in Pressurized Foil Bearing; Ultraharmonic Resonances

During the initial and final stages of rotation, external pressurization is applied through the interior of the rotor, in order to overcome the initial tension and to insure adequate separation between the journal and the foil. The external pressure source is disconnected when sufficient self-acting support can be generated. The lower speed limit of transition from the pressurized to the self-acting mode of operation (and vice versa) and the minimum foil-lift pressure depend on the extensional rigidity (Et) of the foil and on the preload tension (T_o). Typical safe cut-off speeds and representative lift-off supply pressures have been of order 5,000 to 10,000 rpm and 20 to 35 psig. The external air supply can be reduced gradually with increasing speed, or discontinued instantaneously at a predetermined speed; both methods are satisfactory. It is estimated that the air consumption per start/stop may be of order 0.01 lb of air per bearing, so that sufficient compressed gas can be stored for this purpose within a sensibly small volume.

Since acceleration and deceleration from rated speed involved pressurization of the foil bearing during the initial and final stages of rotation, the behavior of the rotor in that mode of operation has been studied in some detail. It has been found that the motion of the rotor in the pressurized foil bearing is very dissimilar from the motion which has been observed in the self-acting mode of operation. Specifically, the response is characterized by a series of sharply defined, ultraharmonic

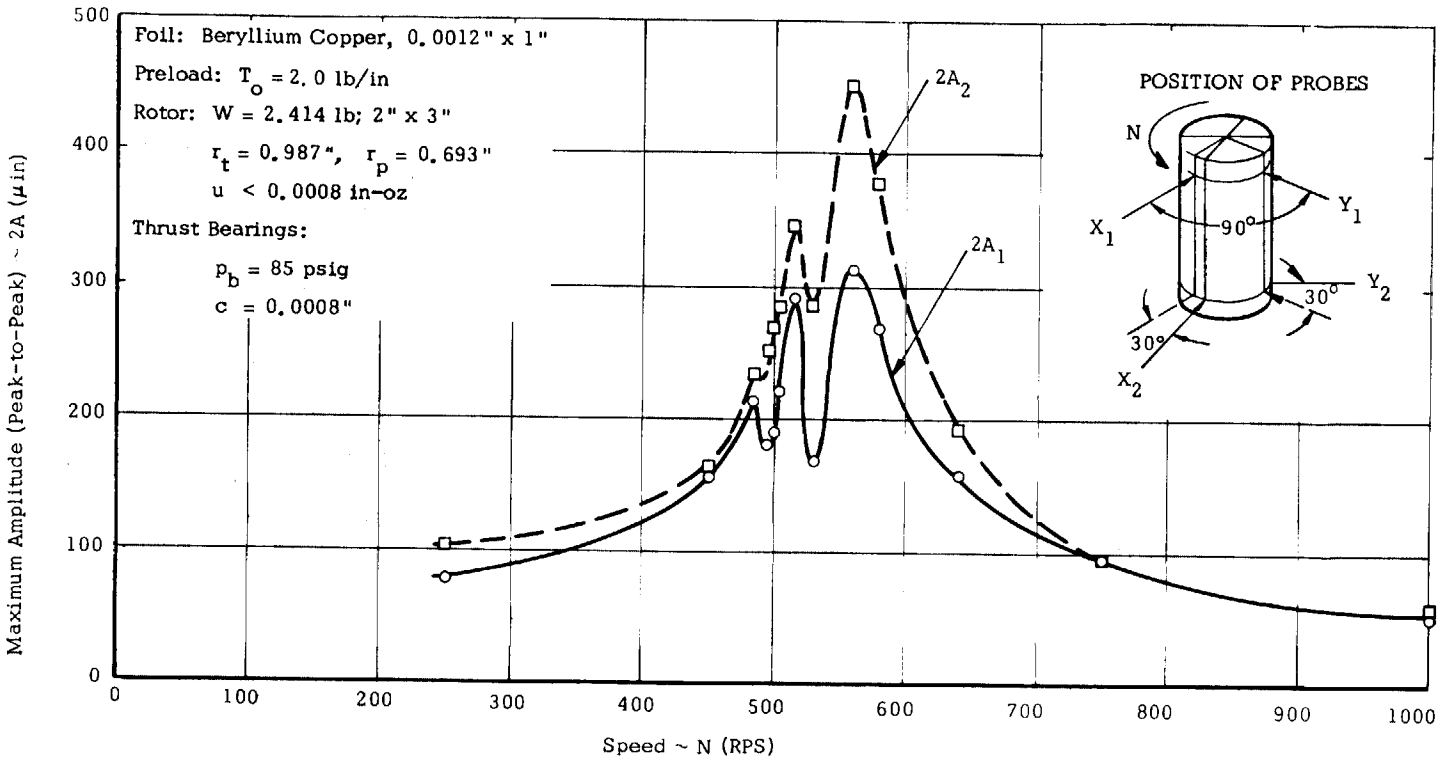

Fig. 4.1 Response to Excitation by Residual Unbalance (Rotor Axis Vertical)

Table 4. 1 Response to Excitation by Residual Unbalance

	Axis Vertical			Axis Horizontal	
Speed	$2A_1$	$2A_2$	Speed	$2A_1$	$2A_2$
RPS	μin	μin	RPS	μin	μin
250	78	103	250	100	111
450	155	162	440	155	155
485	212	233	475	233	244
495	178	250	485	133	206
500	188	269	495	144	244
505	219	283	500	167	250
515	288	344	508	194	311
530	166	283	518	155	272
560	310	450	550	300	400
580	266	378	570	388	490
640	155	190	600	258	302
750	72	72	750	72	75
1000	55	55	1000	55	45

$2A_{1,2}$ = Maximum Peak-to-Peak Amplitude in Plane of Probes

Foil: Beryllium - Copper 0.0012" x 1"

Preload: T_o = 2.0 lb/in

Rotor: W = 2.414 lb, 2" x 3"

r_t = 0.987 in

r_p = 0.693 in

u < 0.0008 in - oz

Thrust Bearings:

p_b = 85 psig

C = 0.0008 in

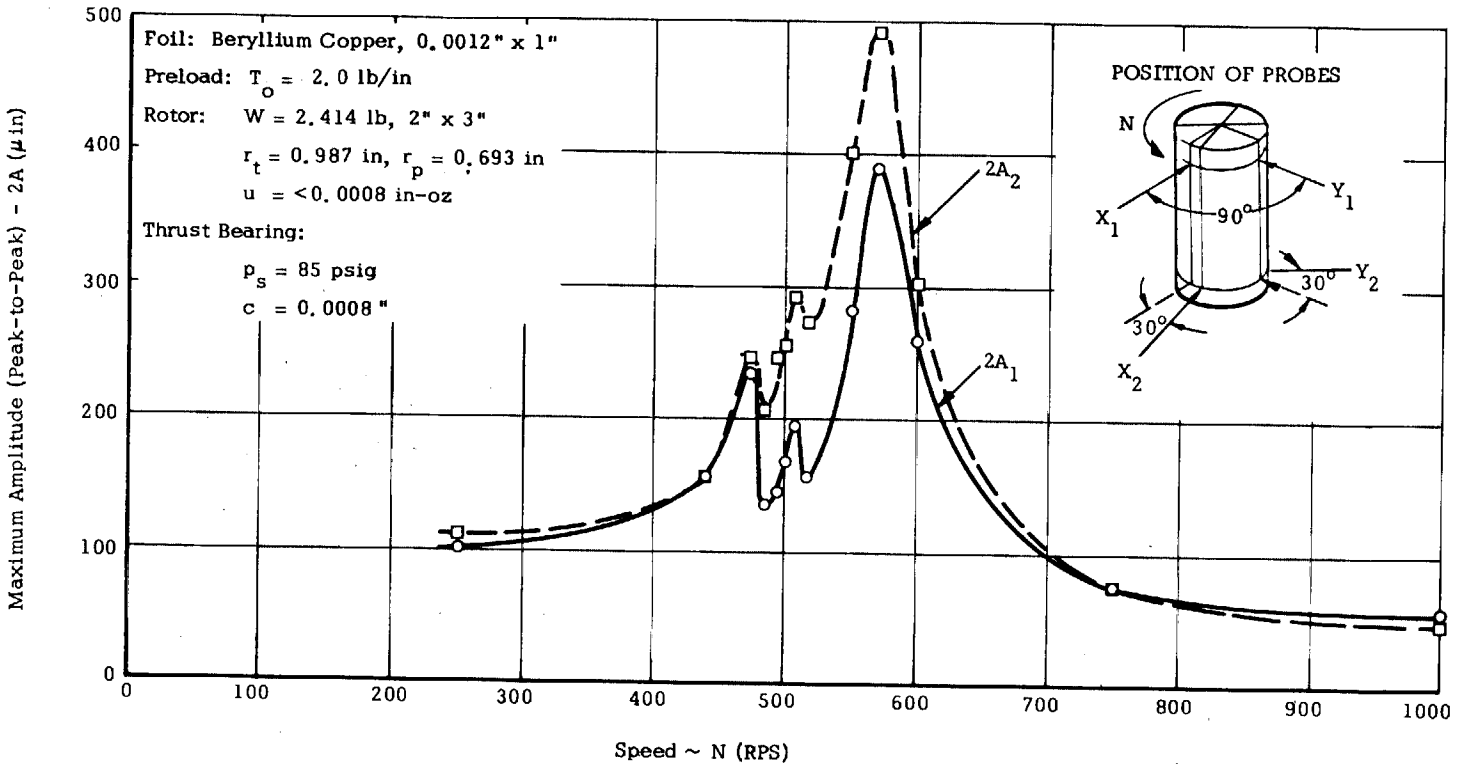

Fig. 4.2 Response to Excitation by Residual Unbalance (Rotor Axis Horizontal)

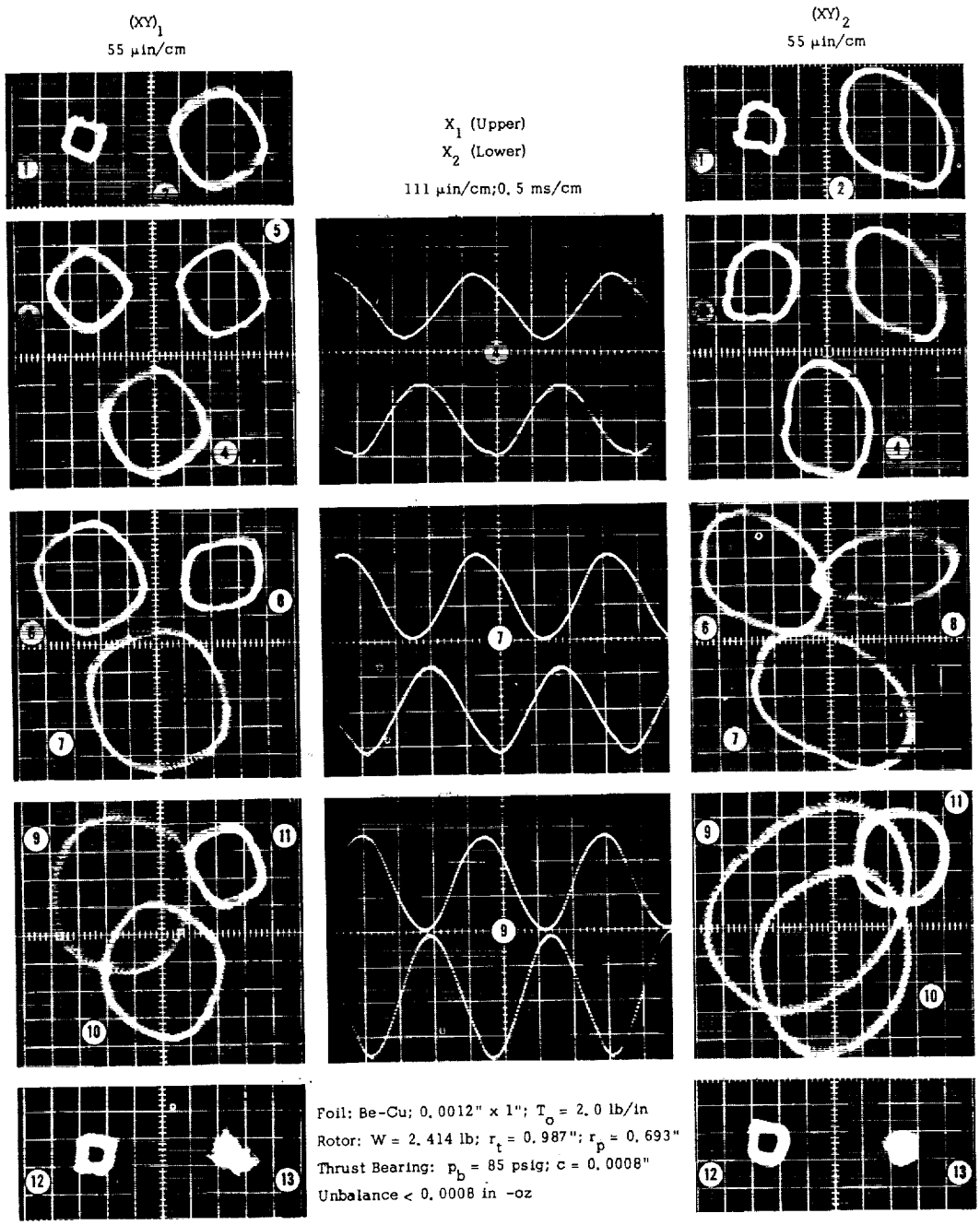

Fig. 4.3 Orbital Motion of Rotor with Residual Unbalance (Rotor Axis Vertical)

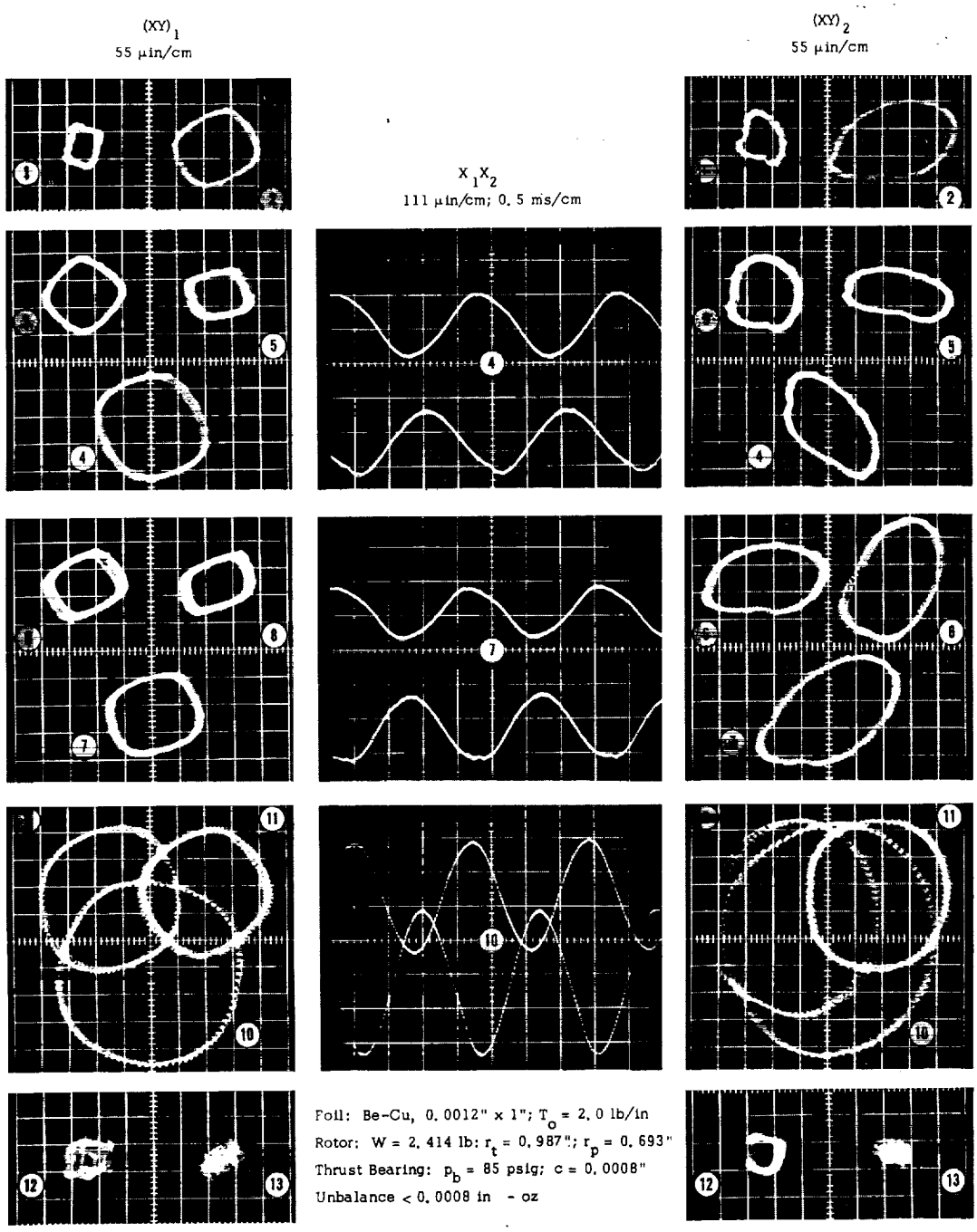

The Speeds (RPS) for Orbits 1-13 are: 250, 500, 440, 475, 485, 495, 508, 518, 550, 570, 600, 750, 1000

Fig. 4.4 Orbital Motion of Rotor with Residual Unbalance (Rotor Axis Horizontal)

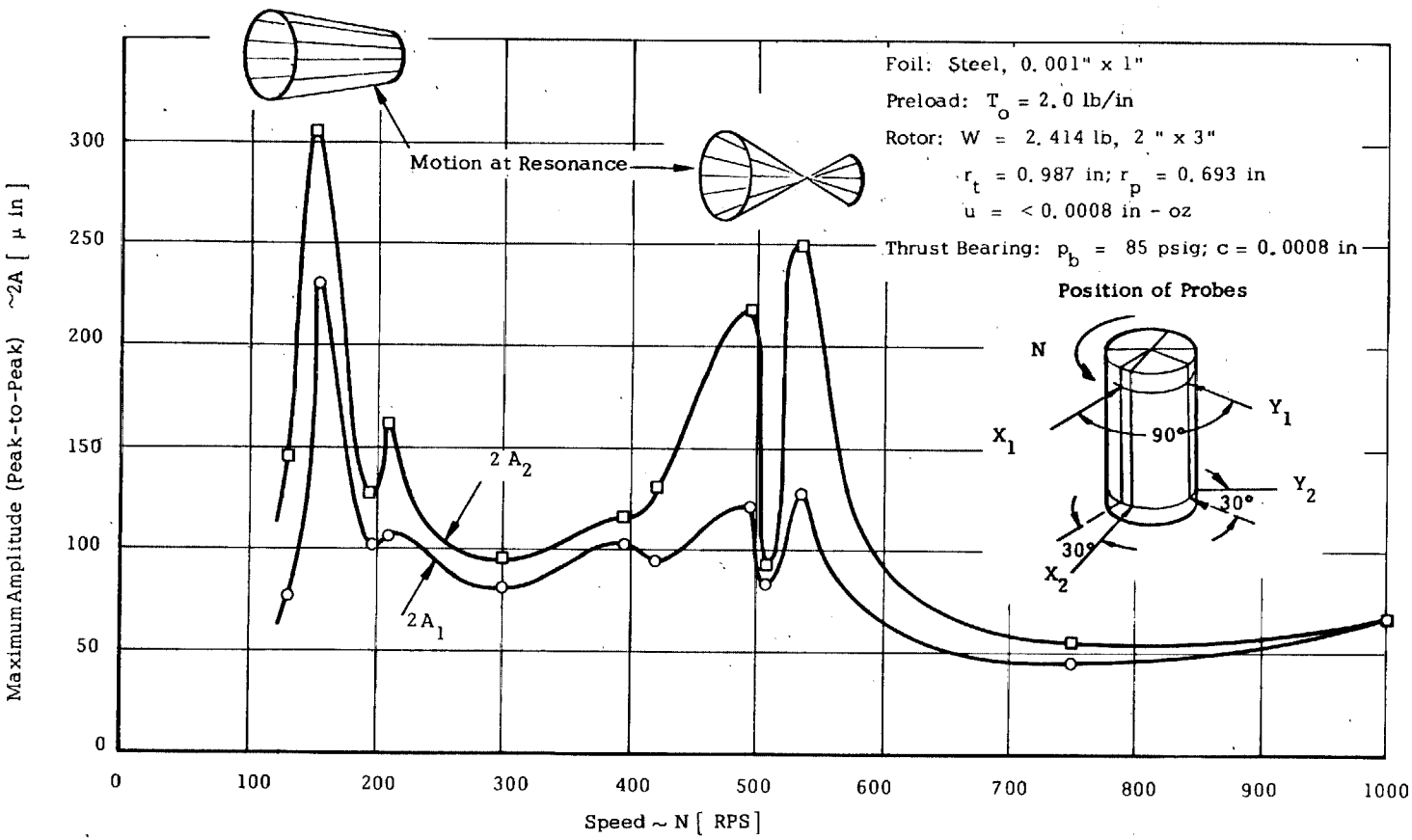

Fig. 4.5 Response to Excitation by Residual Unbalance (Rotor Axis Vertical)

Table 4. 2 Response to Excitation by Residual Unbalance

	Axis Vertical			Axis Horizontal	
Speed	$2A_1$	$2A_2$	Speed	$2A_1$	$2A_2$
RPS	μin	μin	RPS	μin	μin
130	76	144	135	156	250
155	230	304	146	166	247
196	101	126	212	200	278
209	106	161	300	86	104
300	81	95	420	117	147
396	102	116	433	78	150
420	94	131	460	125	195
495	121	218	472	93	192
507	83	89	532	150	250
536	128	248	625	71	117
750	45	55	750	45	55
1000	67	67	1000	61	61

$2A_{1,2}$ = Maximum Peak-to-Peak Amplitude in Plane of Probes

Foil: Steel, 0.001" x 1"

Preload: T_o = 2.0 lb/in

Rotor: W = 2.414 lb, 2" x 3"

r_t = 0.987 in

r_p = 0.693 in

$u < 0.0008$ in - oz

Thrust Bearing:

p_b = 85 psig

C = 0.0008 in

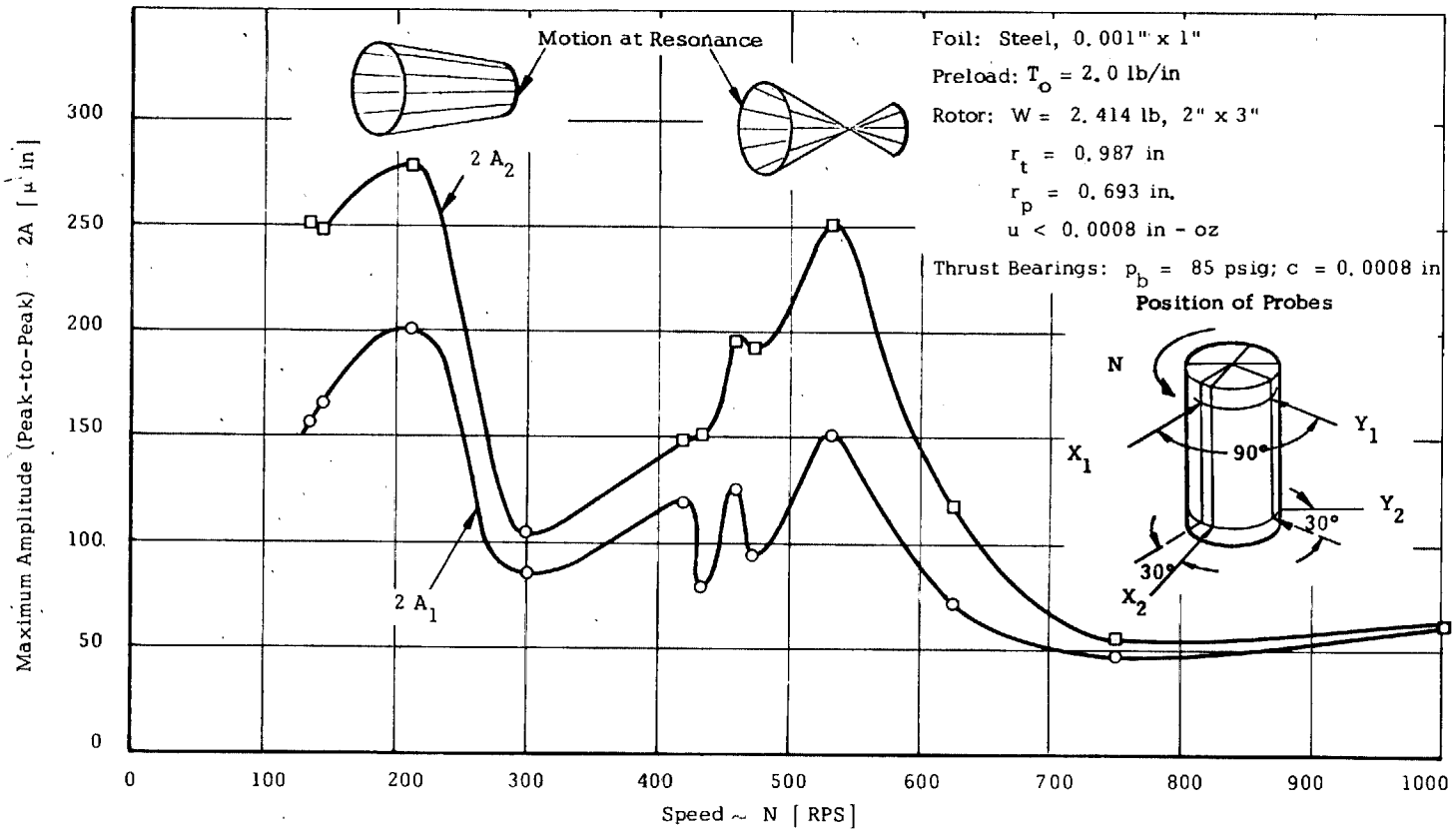

Fig. 4.6 Response to Excitation by Residual Unbalance (Rotor Axis Horizontal)

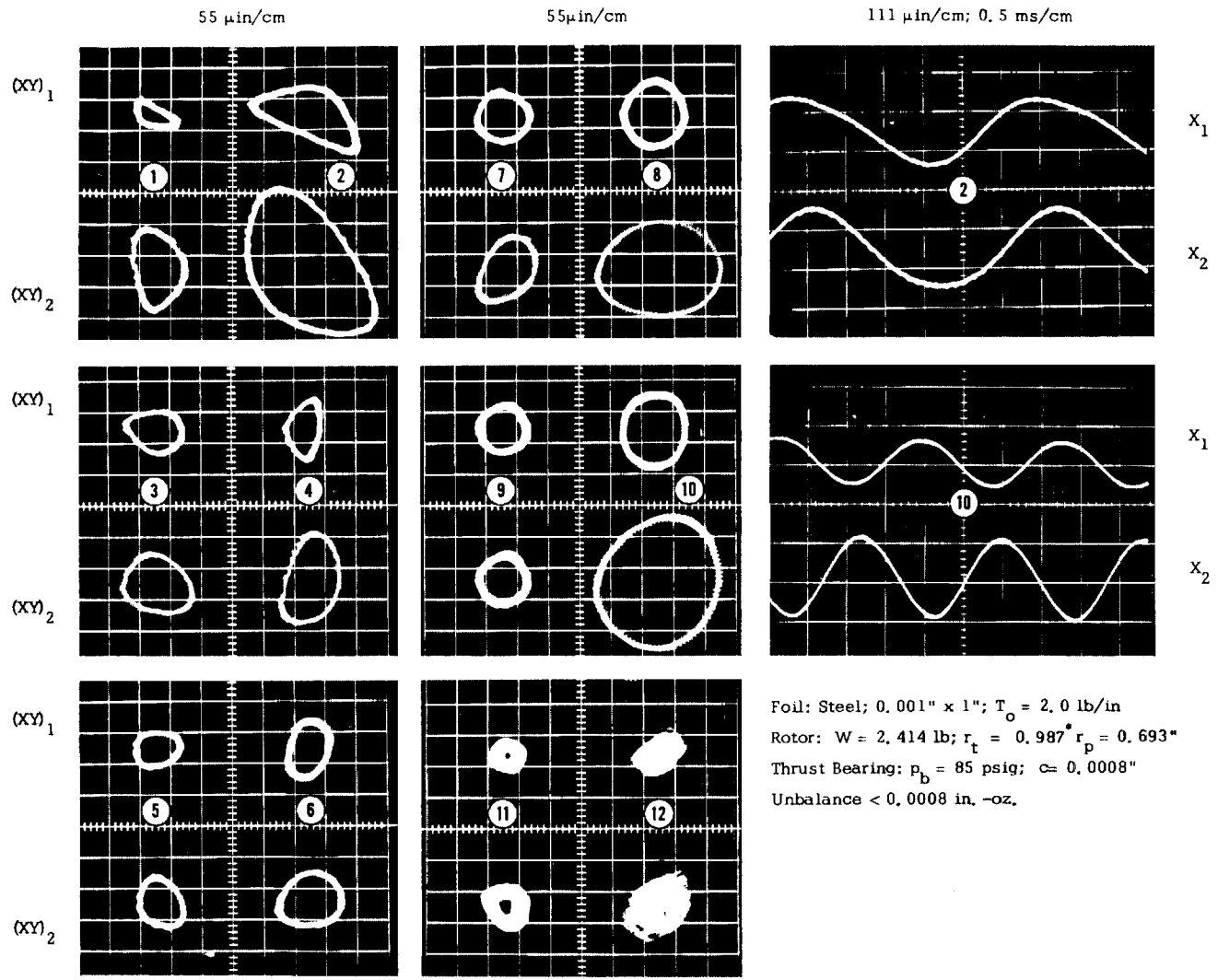

The Speeds (RPS) for Orbits 1-12 are: 130, 155, 196, 209, 300, 396, 420, 495, 507, 536, 750, 1000

Response to Excitation by Residual Unbalance (Rotor Axis Vertical)

Fig. 4.7 Orbital Motion of Rotor with Residual Unbalance (Rotor Axis Vertical)

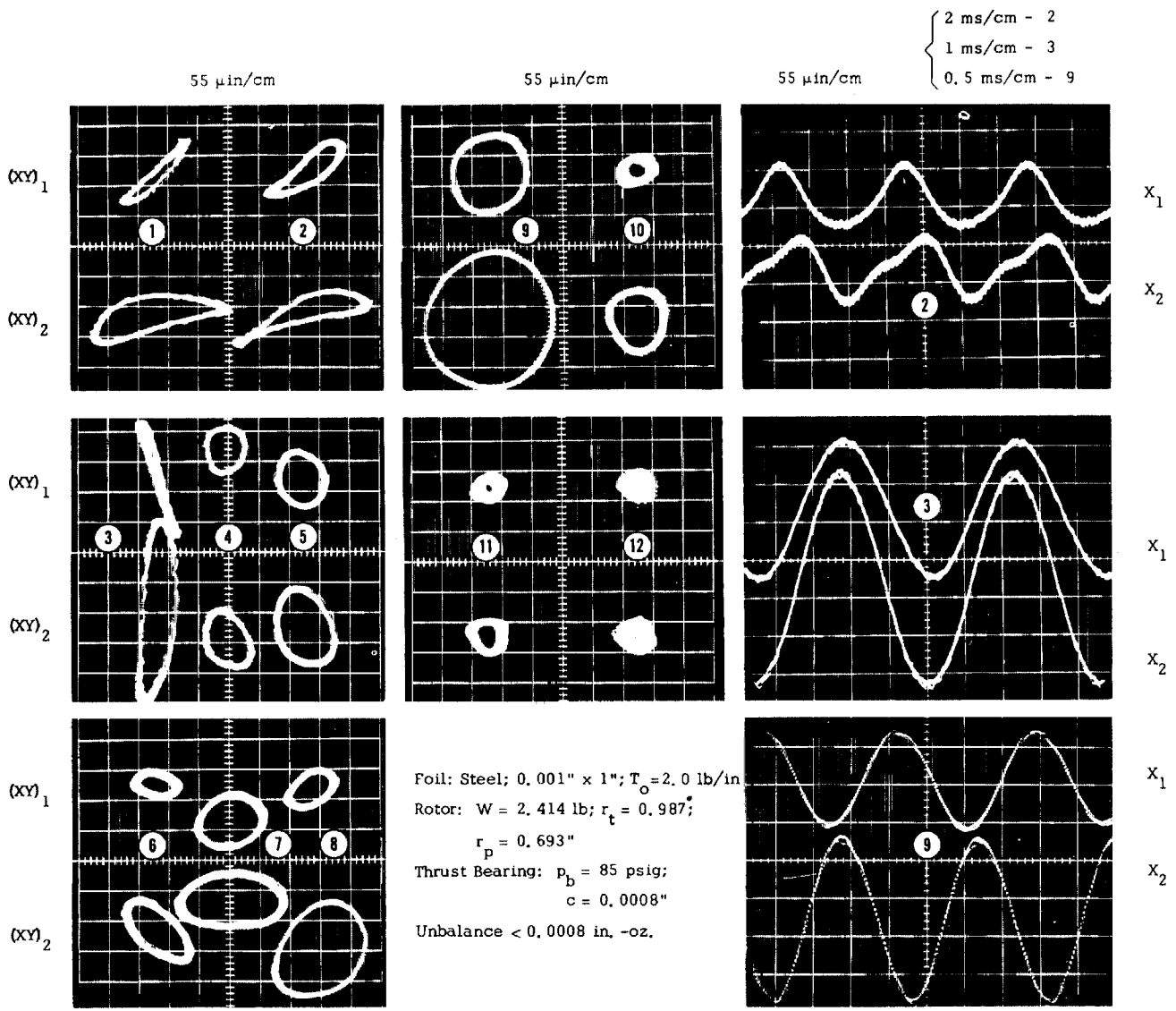

The Speeds (KPS) for Orbits 1-12 are: 135, 146, 212, 300, 420, 433, 460, 472, 532, 625, 750, 1000

Response to Excitation by Residual Unbalance (Rotor Axis Horizontal)

Fig. 4.8 Oribital Motion of Rotor with Residual Unbalance (Rotor Axis Horizontal)

Probe Plane $(XY)_2$ - 55 μin/cm

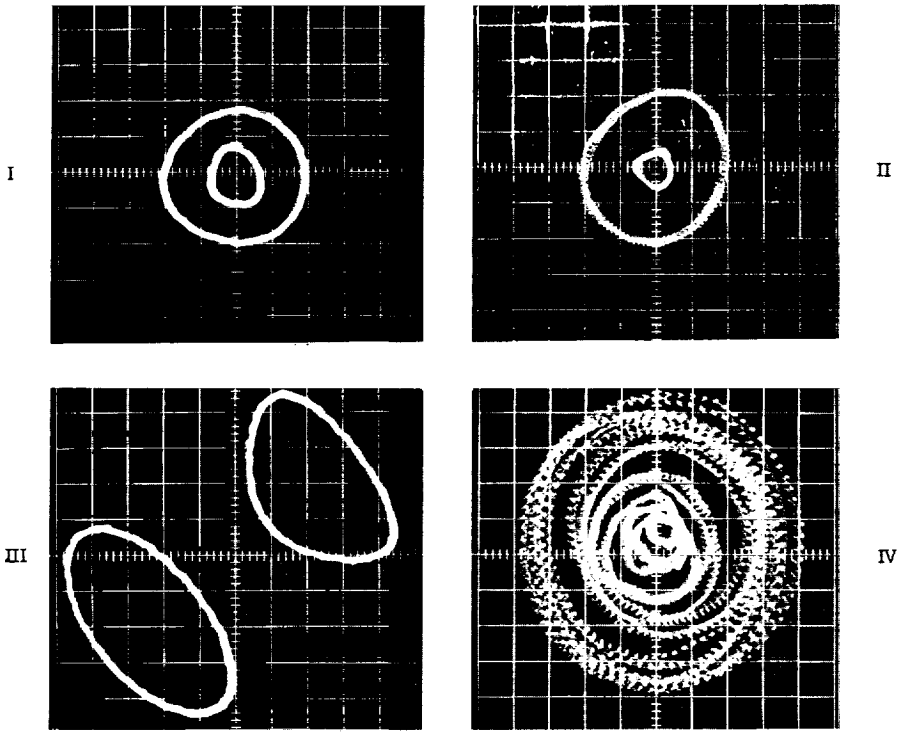

	Orbit	p_b	N	Remarks	Foil	T_o	W	r_t	r_p
		Psig	Rps		Mils	lb/in	lb	in	in
I	Outer	40	287	Conical Resonance	1.0	2.0	2.414	0.987	0.693
	Inner	85		———					
II	Outer	85	536	Conical Resonance	1.0	2.0	2.414	0.987	0.693
	Inner	40							
III	Lower Left	40	155	Quasi-Cylindrical (Foil) Resonance	1.0	2.0	2.414	0.987	0.693
	Upper Right	85							
IV	———	85	687		2.0	3.0	1.0	1.197	0.807

*Thrust Bearing Clearance 0.0008"

Effect of Thrust Bearing Pressure on Motion of Rotor (Rotor Axis Vertical)

Fig. 4.9 Effect of Thrust Bearing Supply Pressure on Rotor Response

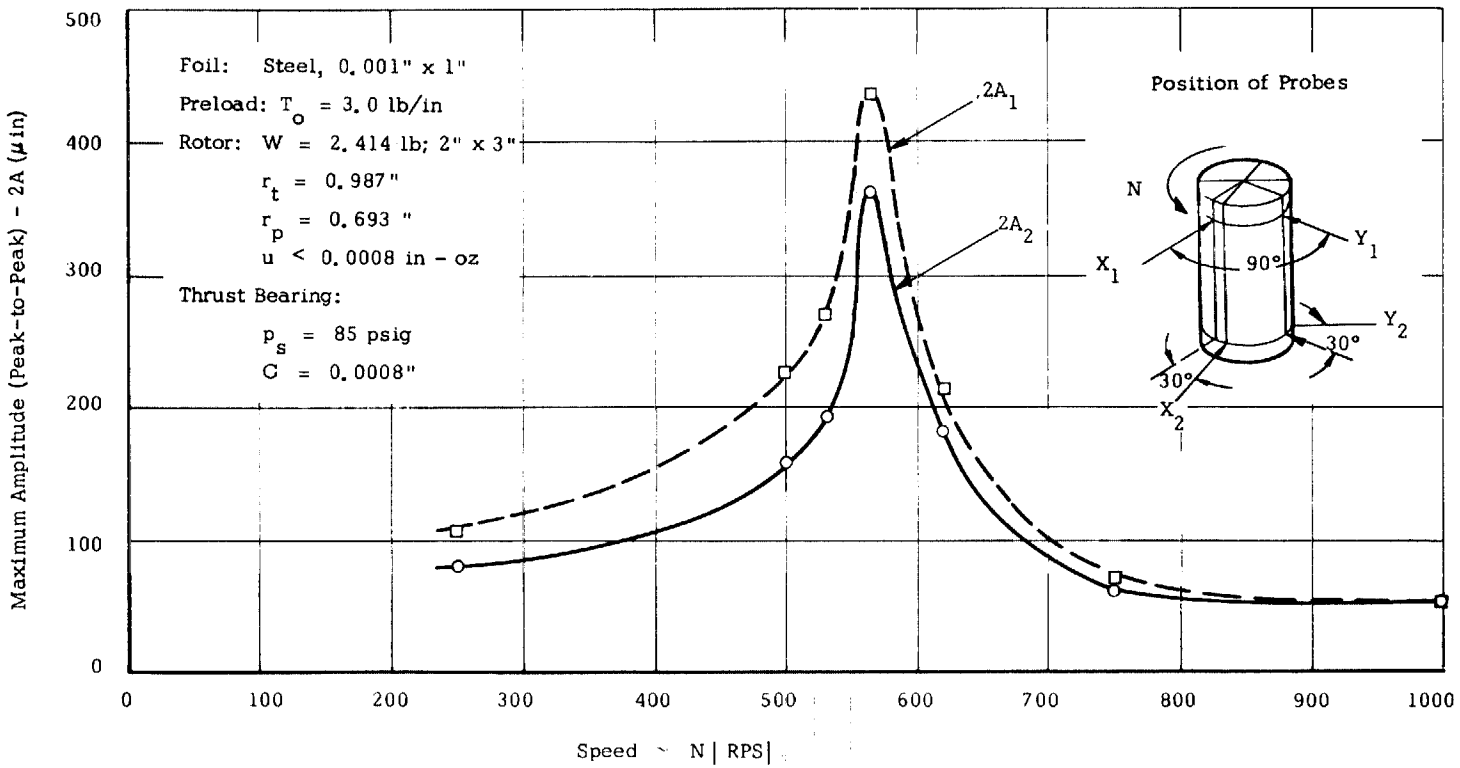

Fig. 4.10 Response to Excitation by Residual Unbalance (Rotor Axis Vertical)

Table 4.3 Response to Excitation by Residual Unbalance

Axis Vertical			Axis Horizontal		
Speed	$2A_1$	$2A_2$	Speed	$2A_1$	$2A_2$
RPS	μin	μin	RPS	μin	μin
250	78	106	250	92	136
500	156	225	500	181	219
530	189	268	510	222	268
565	361	434	525	244	344
620	180	211	535	183	278
750	58	67	540	161	261
1000	50	50	550	178	280
			575	306	453
			620	173	244
			750	67	78
			1000	61	60

Foil: Steel, 0.001" x 1"

Preload: T_o = 3.0 lb/in

Rotor: W = 2.414 lb; 2" x 3"

r_t = 0.987 in

r_p = 0.693 in

u < 0.0008 in - oz

Thrust Bearings:

p_b = 85 psig

C = 0.0008 in

$2A_{1,2}$ = Maximum Peak-to-Peak Amplitude in Plane of Probes

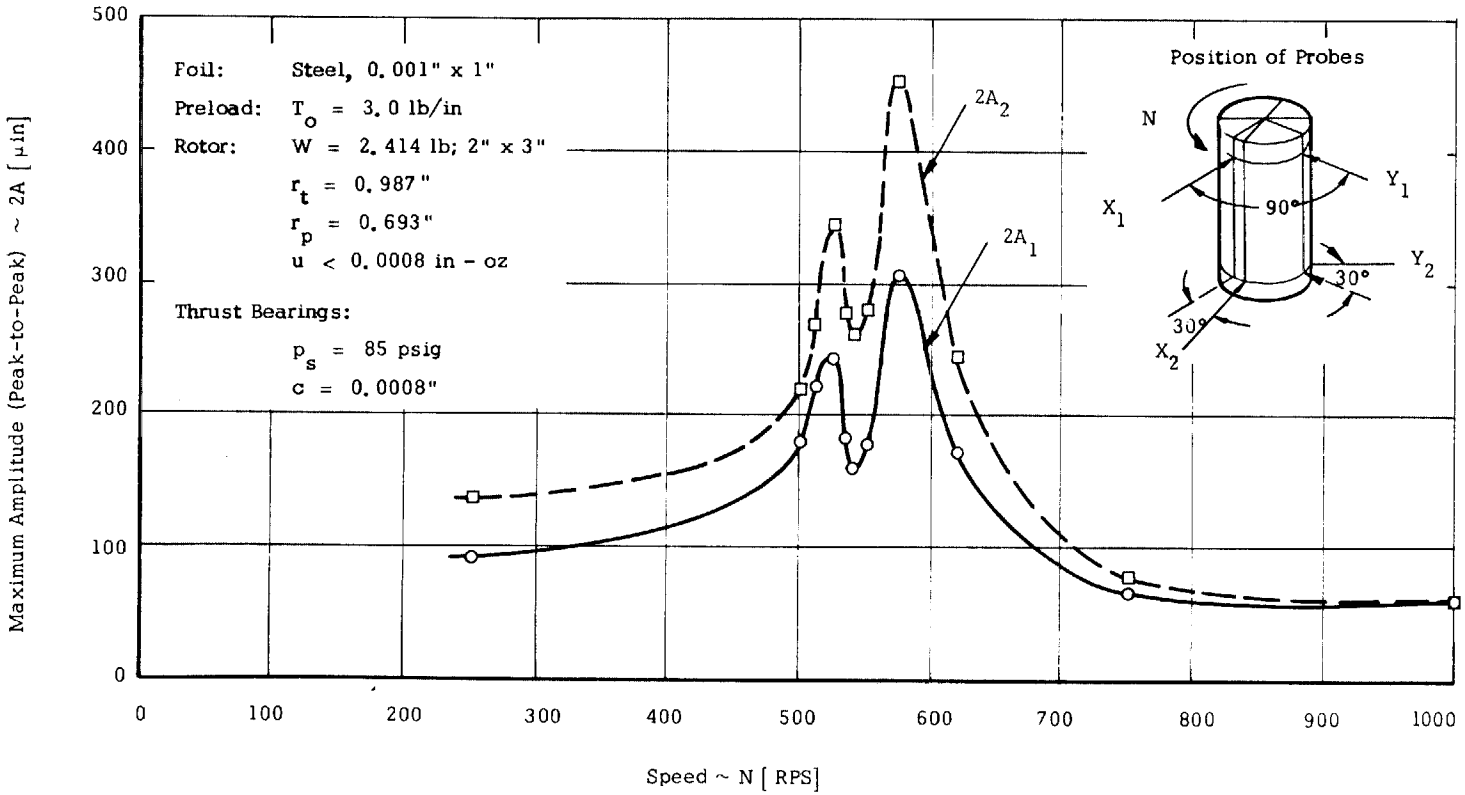

Fig. 4.11 Response to Excitation by Residual Unbalance (Rotor Axis Horizontal)

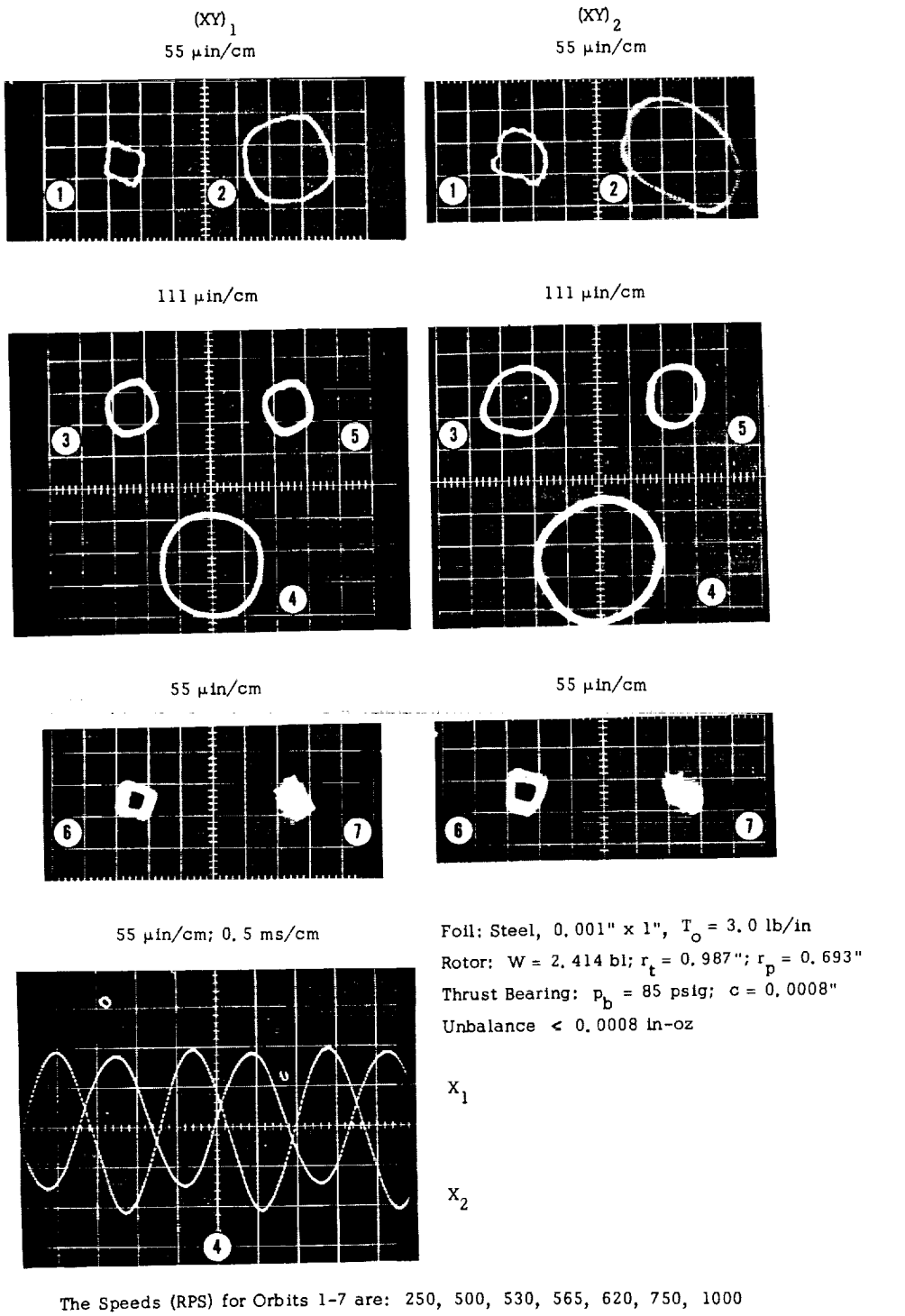

The Speeds (RPS) for Orbits 1-7 are: 250, 500, 530, 565, 620, 750, 1000

Fig. 4.12 Orbital Motion of Rotor with Residual Unbalance (Rotor Axis Vertical)

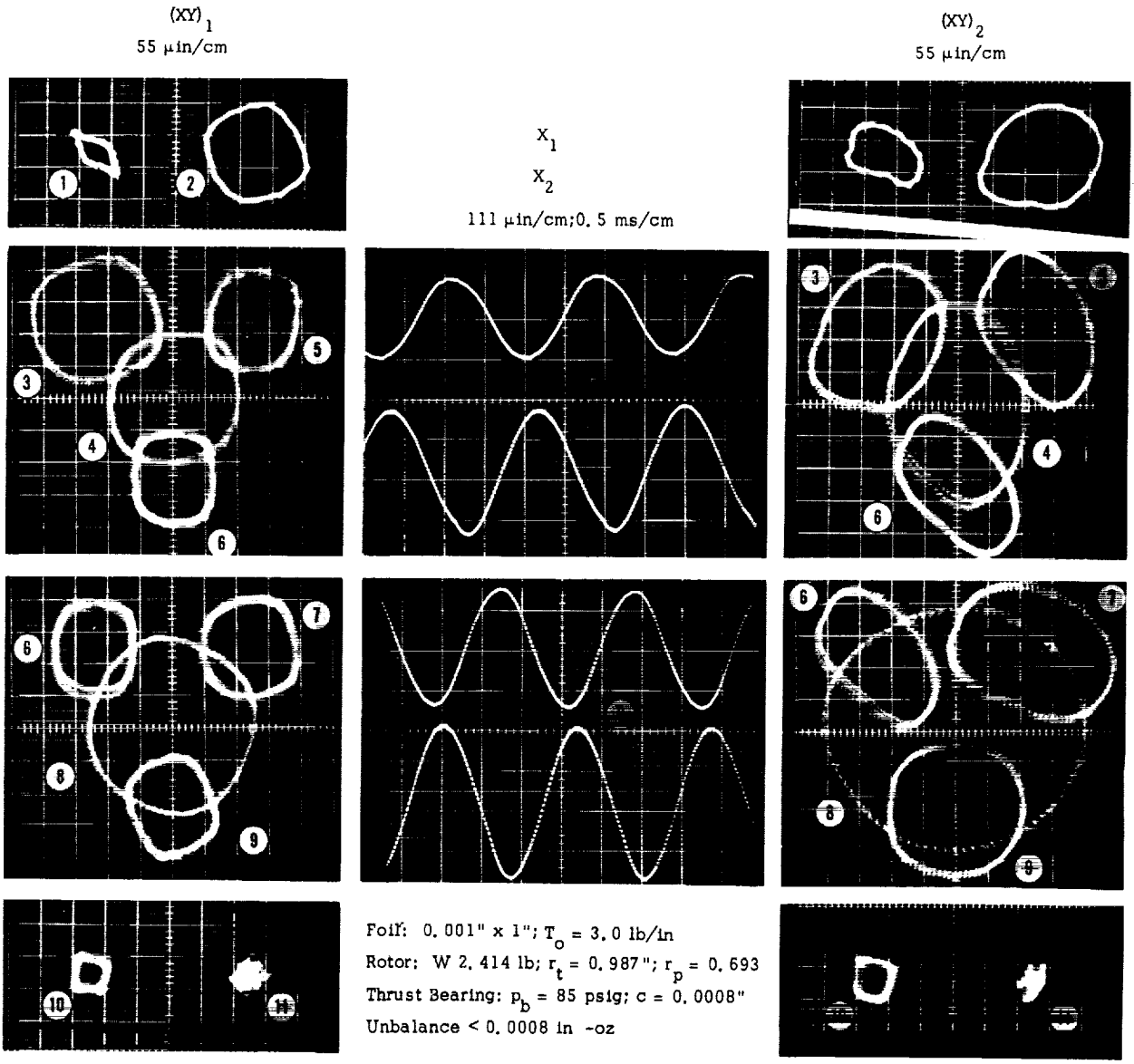

The Speeds (RPS) for Orbits 1-11 are: 250, 500, 510, 525, 535, 540, 550, 575, 620, 750, 1000

Fig. 4.13 Orbital Motion of Rotor with Residual Unbalance (Rotor Axis Horizontal)

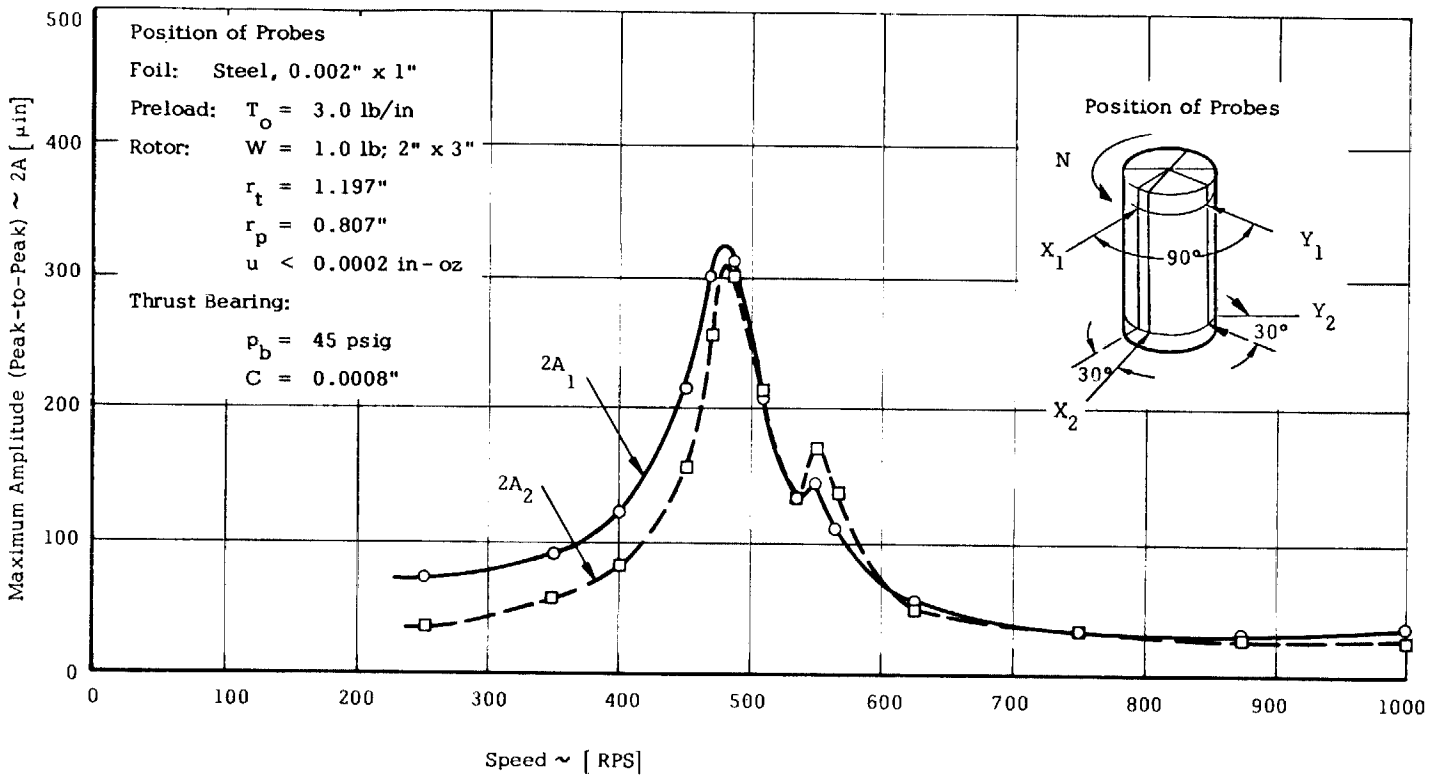

Fig. 4. 14 Response to Excitation by Residual Unbalance (Rotor Axis Vertical)

Table 4. 4 Response to Excitation by Residual Unbalance

Axis Vertical			Axis Horizontal		
Speed	$2A_1$	$2A_1$	Speed	$2A_1$	$2A_2$
RPS	μin	μin	RPS	μin	μin
250	72	34	250	78	42
350	89	55	350	92	55
400	122	81	450	258	170
450	216	158	463	300	217
470	300	255	474	210	150
488	311	300	485	206	231
510	211	214	495	272	289
535	134	134	500	255	255
550	144	169	509	142	156
565	111	136	521	164	230
625	55	47	530	152	175
750	33	33	537	144	133
875	28	23	547	156	150
1000	33	23	560	120	122
			750	45	50
			1000	55	55

$2A_{1,2}$ = Maximum Peak-to-Peak Amplitude in plane of probes

Foil: Steel 0. 002" x 1"

Preload: T_o = 3. 0 lb/in

Rotor: W = 1. 0 lb, 2" x 3"

r_t = 1. 147 in

r_p = 0. 807 in

u < 0. 0002 in - oz

Thrust Bearings:

p_b = 45 psig

C = 0.0008 in

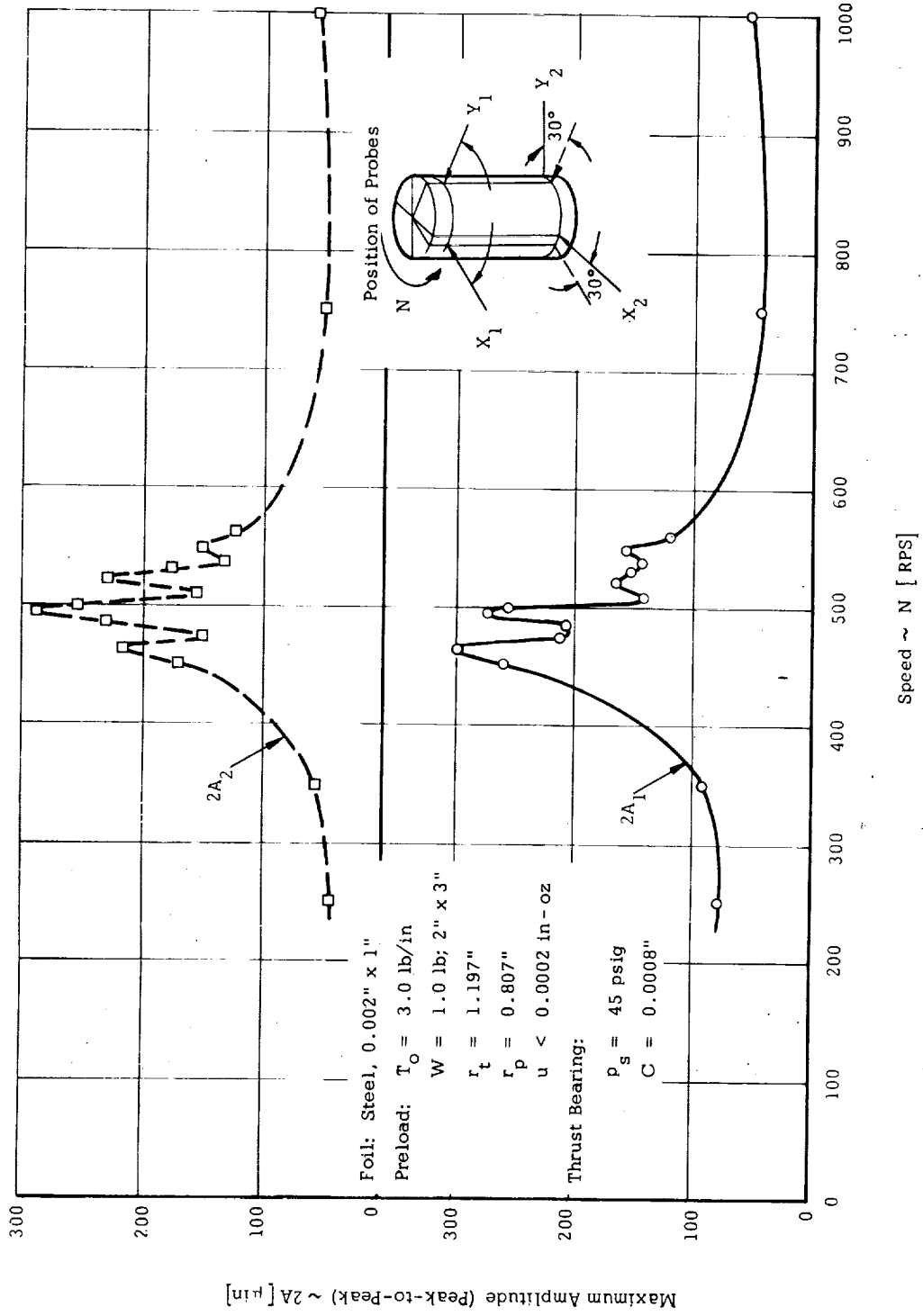

Fig. 4.15 Response to Excitation by Residual Unbalance (Rotor Axis Horizontal)

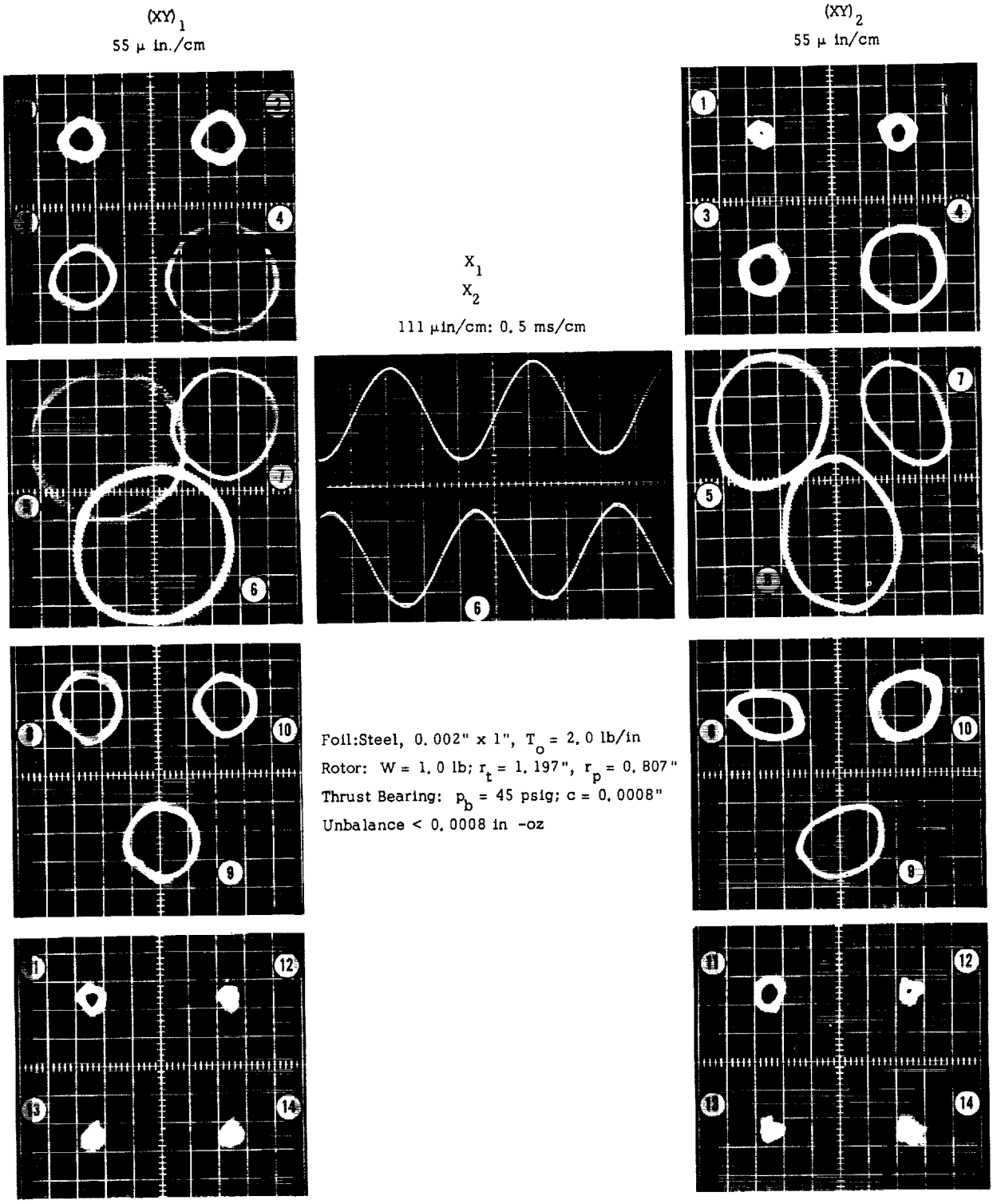

The Speeds (RPS) for Orbits 1-14 are: 250, 350, 400, 450, 470, 488, 510, 535, 550, 565, 625, 750, 875, 1000

Fig. 4.16 Orbital Motion of Rotor with Residual Unbalance (Rotor Axis Vertical)

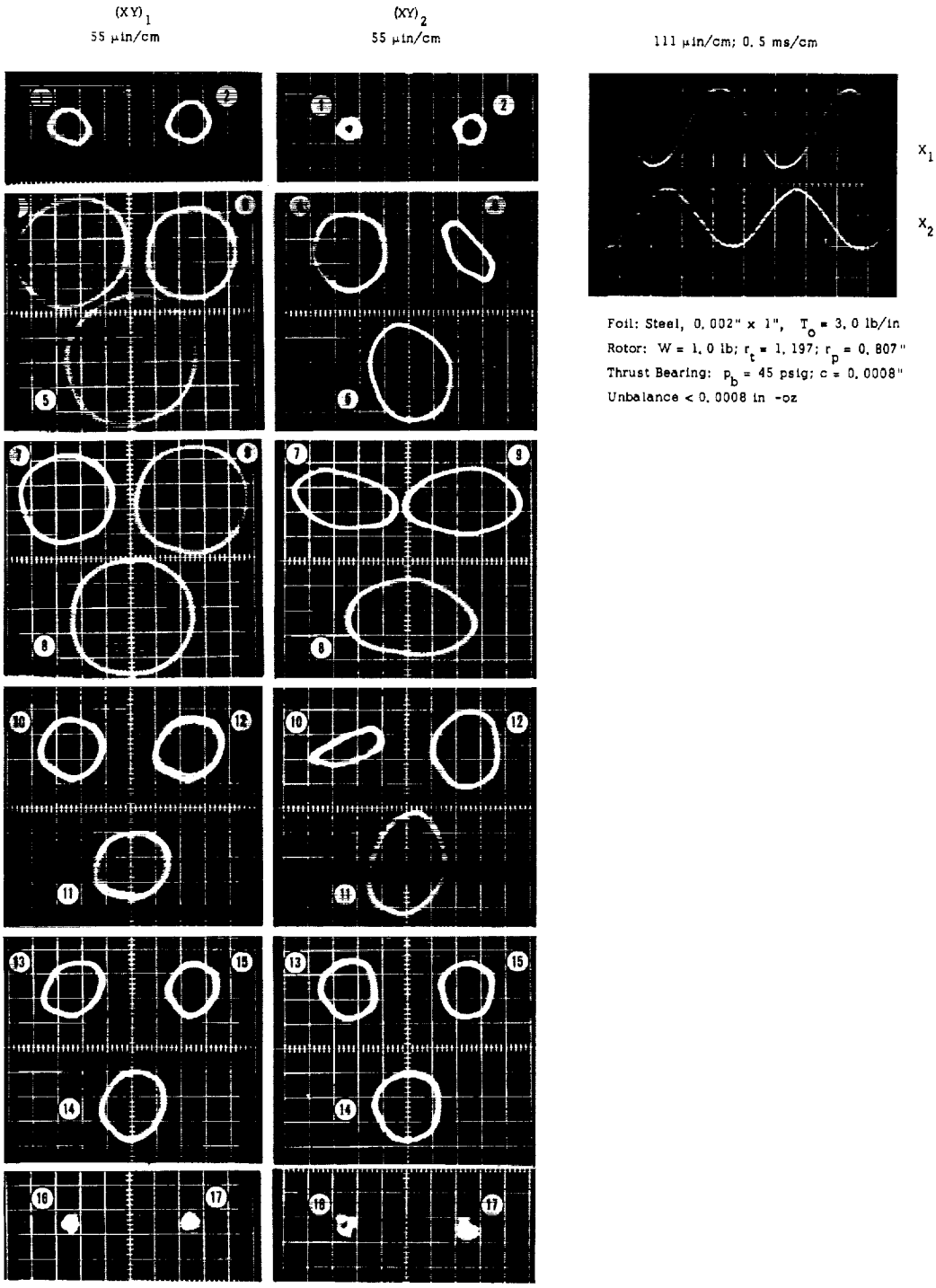

Fig. 4.17 Orbital Motion of Rotor with Residual Unbalance (Rotor Axis Horizontal)

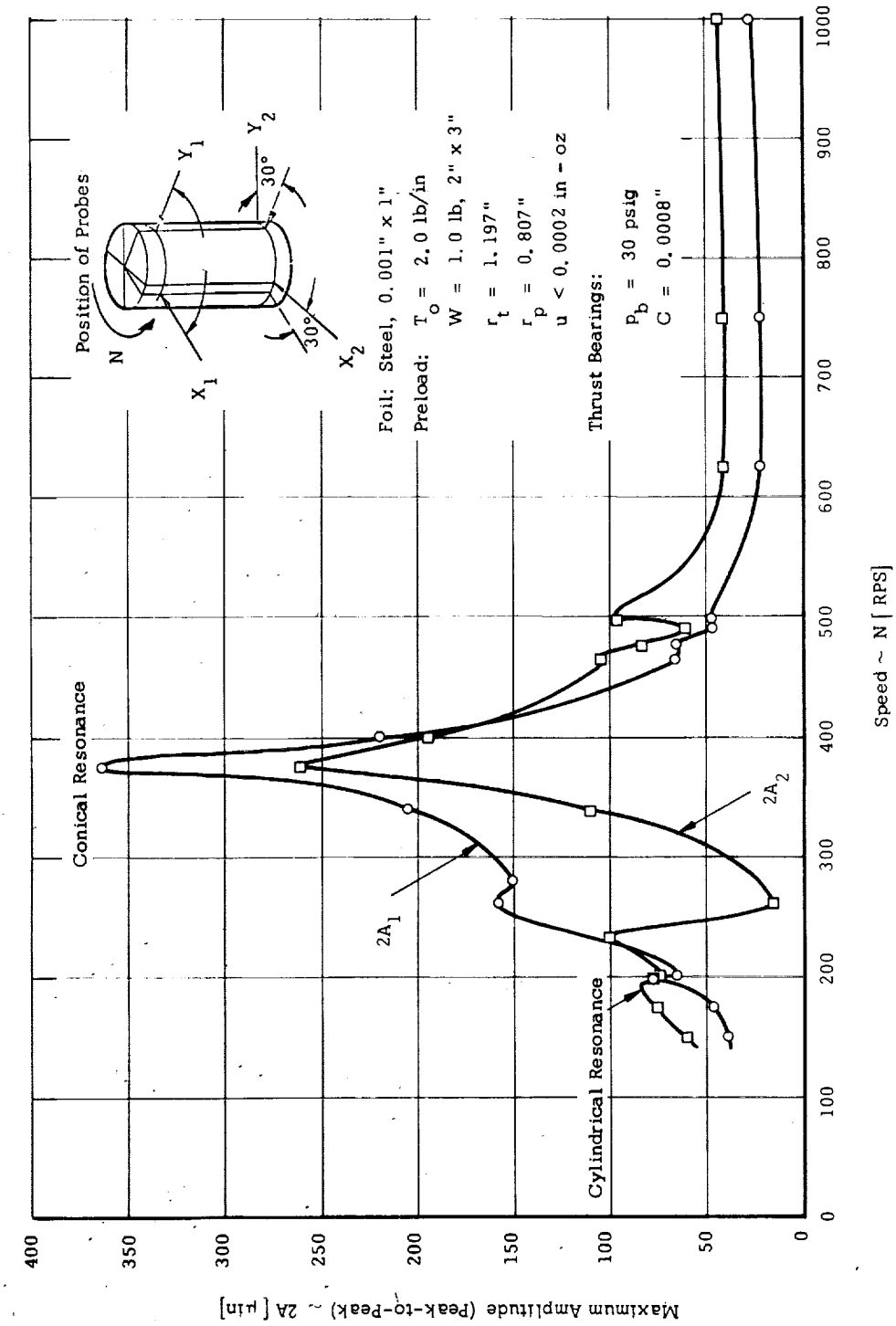

Fig. 4.18 Response to Excitation by Residual Unbalance (Rotor Axis Vertical)

Table 4.5 Response to Excitation by Residual Unbalance

Speed	$2A_1$	$2A_2$
RPS	μin	μin
150	39	61
175	47	75
198	78	78
200	67	75
234	-	100
262	158	-
280	150	16
340	205	111
377	366	261
400	219	194
465	67	105
477	67	83
490	46	61
497	47	97
625	22	41
750	22	40
1000	25	42

$2A_{1,2}$ = Maximum, Peak-to-Peak Amplitude in Plane of Probes

Foil: Steel; 0.001" x 1"

Preload: T_o = 2.0 lb/in

Rotor: W = 1.0 lb; 2" x 3"

r_t = 1.197 in

r_p = 0.807 in

$u < 0.0002$ in - oz

Thrust Bearing:

p_b = 30 psig

C = 0.0008 in

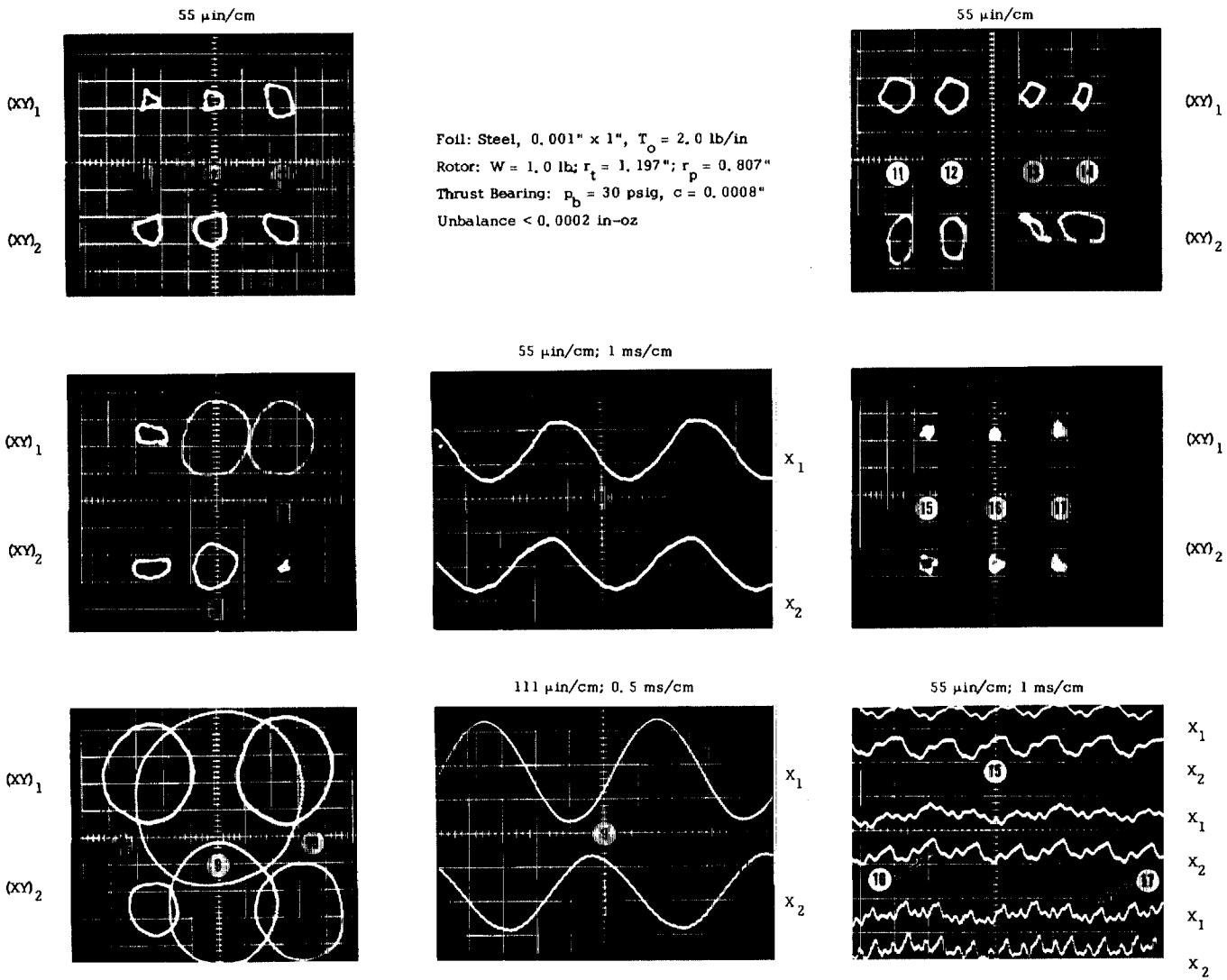

The Speeds (RPS) for Orbits 1-17 are: 150, 175, 198, 200, 234, 262, 280, 340, 377, 400, 465, 477, 490, 497, 625, 750, 1000

Fig. 4.19 Orbital Motion of Rotor with Residual Unbalance (Rotor Axis Vertical)

resonances, which occur at frequencies of rotation spaced at relatively close intervals, and which appear to bear a very definite relation to one another.

It has been observed that there exist at least one, and generally two, frequencies at which the resonance of the foil-rotor system is synchronous and the axis of the rotor describes a simple, quasi-elliptical orbit. The products of all other resonant frequencies and of corresponding ultraharmonic numbers are then nearly equal in magnitude to one of the frequencies of synchronous resonance. The foregoing relation is illustrated graphically in Fig. 4.20 and Fig. 4.22 and is substantiated by corresponding sets of oscilloscope photographs in Fig. 4.21 and Fig. 4.23. Numerical data pertaining to the foregoing figures is contained in Tables 4.6 and 4.7. Referring to Fig. 4.20, it will be noted that the product of resonant frequency and corresponding number of ultraharmonic decreases slightly with increasing speed and gap width. It may be inferred that the increase of gap width with speed, due to self-acting effects, results in a slower rate of rotor response* and in a progressive lowering of frequencies of ultraharmonic resonances at higher angular velocities. The motion of the rotor at successive resonant speeds is illustrated rather poignantly in the series of oscilloscope photographs of Fig. 4.21. The left column of photographs contains rotor orbits, while the corresponding time displays of capacitance-probe outputs are presented in parallel in the right column of photographs. The resonances correspond to ultraharmonics of order 24, 11, 7, 5, 4, and 2 and are related to the two synchronous resonances in a manner described in the foregoing. The number of each ultraharmonic can be ascertained from the number of orbit loops, but a more positive identification can be obtained from the timebase displays. Ultraharmonic

*Smaller "stiffness."

resonances of order 3 and 6 have been conspicuously absent, and no ultraharmonic resonances of measurable amplitude, other than those listed in Fig. 4.21, have been observed. All resonances have been sharply defined within very narrow frequency intervals. The motion of the rotor in the pressurized mode has been nearly planar, and the largest double amplitudes of motion at synchronous resonance has seldom exceeded 600 μin.

Operation in the pressurized mode involves an important source of excitation other than the rotating unbalance, namely the successive impacts and reactions of jets, emerging from 24 pairs of orifices. This effect is clearly discernible in a number of oscilloscope photographs, which display outputs of foil-monitoring capacitance probes, Fig. 4.29 for example.* Despite the complexity of rotor orbits in Fig. 4.21 and Fig. 4.23, it can be observed that at resonance there is a tendency of the loops to orient themselves consecutively along the 45°, 90°, and 135° lines, which is indicative of the phase between the X and Y components of motion. Between resonances, the axis of the rotor moves along very symmetrical, multi-loop orbits of rather striking appearance, a number of which are illustrated in the oscilloscope photographs of Fig. 4.24.

Although components of excitation higher than the rotational speed may have been involved, no simple explanation of the multiplicity of ultraharmonic resonances can be given beyond the well known fact that the latter, as well as subharmonic resonances, frequently occur in nonlinear systems. From the point of view of analysis, the problem is sufficiently complex to defy even formulation. This fact notwithstanding, starting, stopping, and rotation in externally pressurized foil bearings are not only practical, but offer one of the very few feasible methods of transition to and from the self-acting mode of operation.

---

*One of the 24 ripples in the uppermost trace of Fig. 4.29 displays an amplitude larger than the remaining oscillations. This is due to the irregular shape of one of the orifices, following removal of a broken drill.

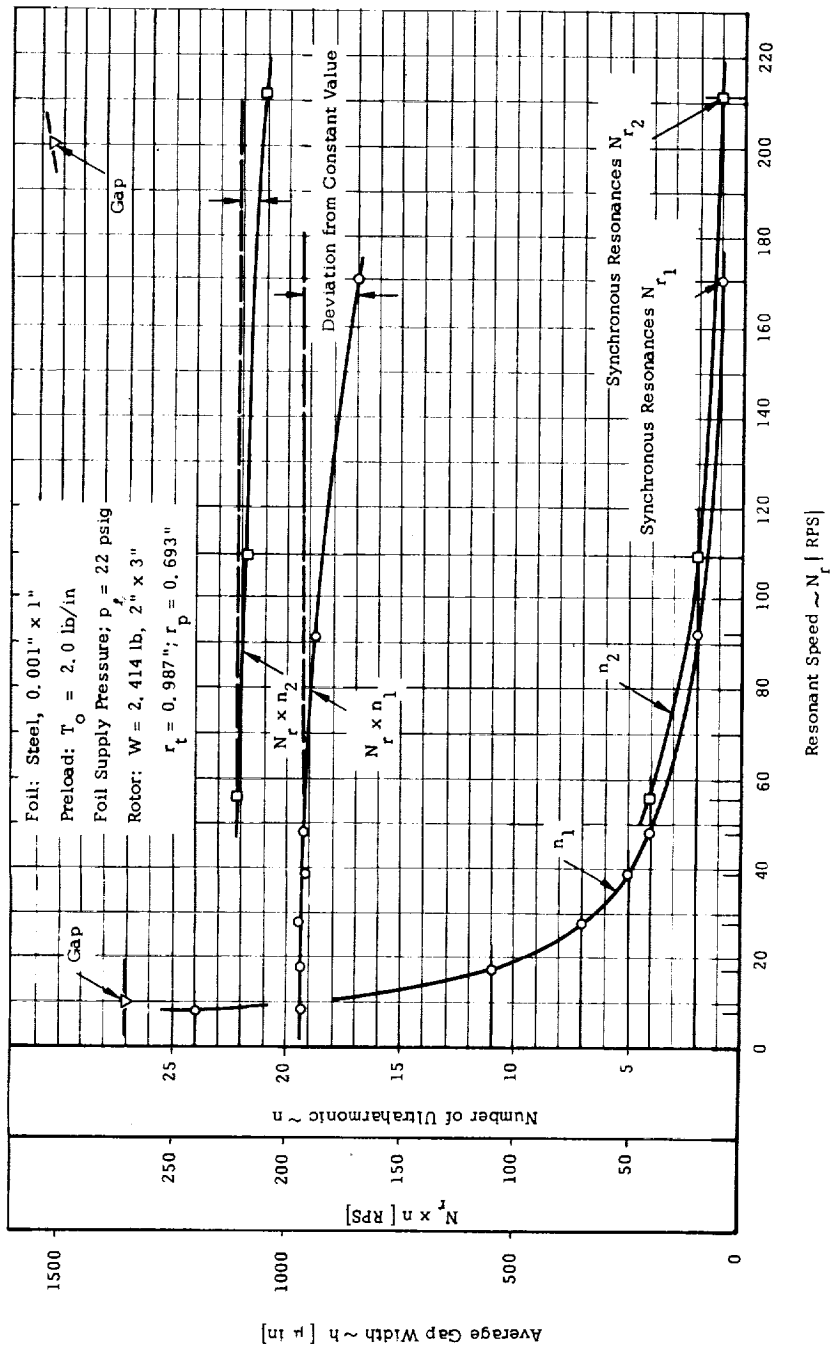

Fig. 4.20 Ultraharmonic Resonances of Rotor and Pressurized Foil-Bearing

Table 4.6 Ultraharmonic Resonances of Rotor and Pressurized Foil Bearing

N_R	n	$N_R \times n$	Remarks
RPS	-	RPS	-
8.07	24	194	
17.6	11	194	
27.8	7	195	
38.4	5	192	
47.8	4	195	
92.0	2	184	
170.0	1	170	Synchronous Resonance
55.5	4	222	
109.0	2	218	
211.0	1	211	Synchronous Resonance

N_R = Resonant Speed

n = Number of Ultraharmonics/Rev

Foil: Steel; 0.001" x 1"

Preload: T_o = 2.0 lb/in

Rotor: W = 2.414 lb, 2" x 3"; r_t = 0.987 in; r_p = 0.693 in.

Foil Supply Pressure; p_ℓ = 22 psig

Gap Width:

h = 1356 μin at 10 RPS
h = 1525 μin at 200 RPS
} Average Values

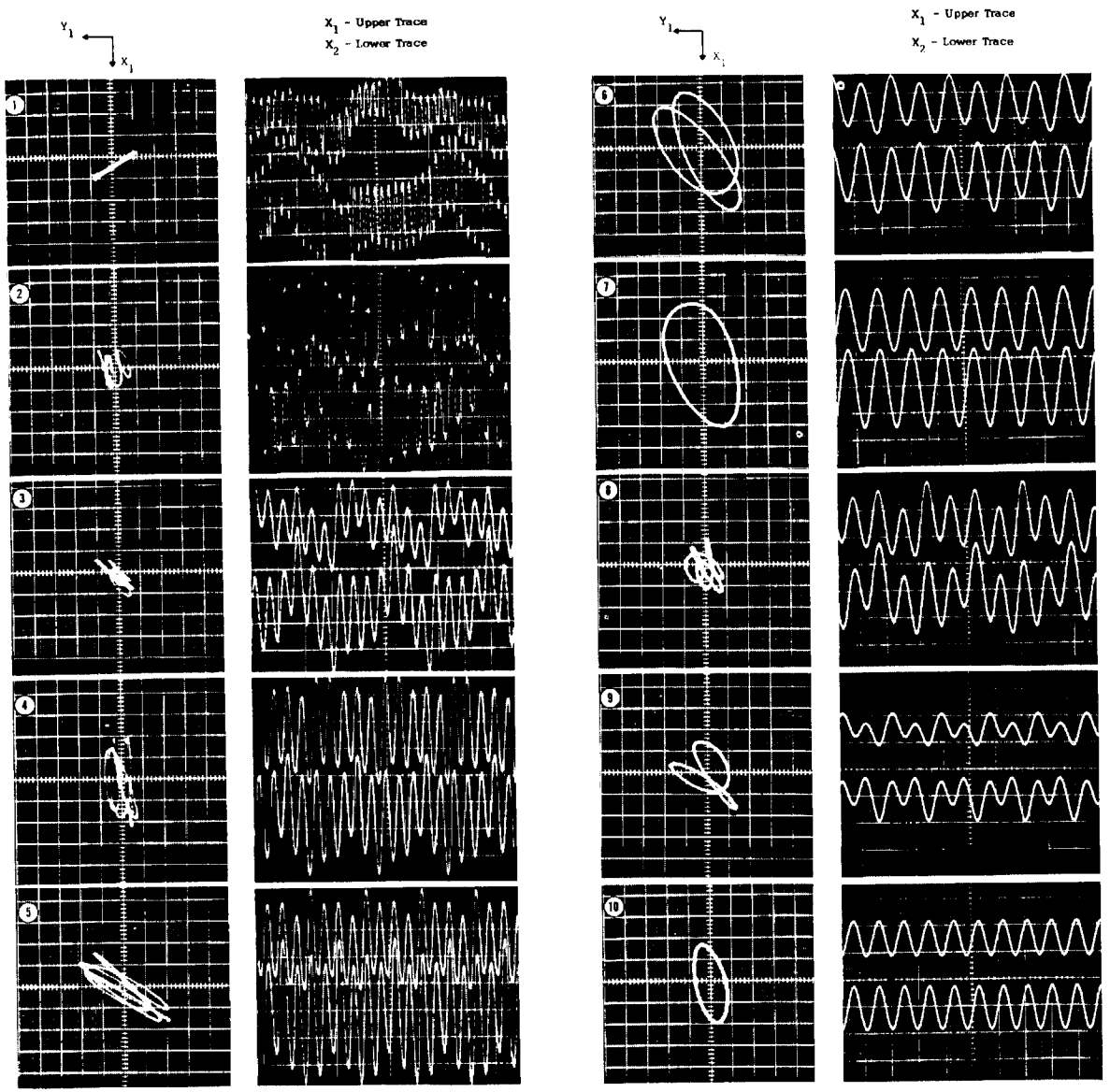

Ultraharmonic Resonances (Pressurized Foil Bearing; Rotor Axis Vertical)

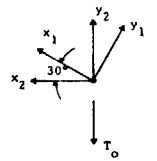

	N	n	N x n	$(XY)_1$	X_1 X_2
	RPS	-	RPS	μin/cm	μin/cm	ms/cm
1	8.07	24	194	111	55	20
2	17.6	11	194	111	55	10
3	27.8	7	195	111	55	10
4	38.4	5	192	111	111	10
5	47.8	4	191	111	111	10
6	92.0	2	184	111	278	5
7	170.0	1	171	111	278	5
8	55.5	4	222	111	111	5
9	109.0	2	218	111	278	5
10	211.0	1	211	111	278	5

Foil: Steel, 0.001" x 1"; T_o = 2lb/in;
p_t = 22 psig
Rotor: W = 2.414 lb; r_t = 0.987 in;
r_p = 0.693 in
Unbalance < 0.0008 in. -oz.
Thrust Bearing: P_b = 85 psig; c = 0.0008 in.

N = Rotor Speed (RPS)
n = Number of Ultraharmonic

Fig. 4.21 Orbital Motion at Ultraharmonic Resonances; - Pressurized Foil Bearing

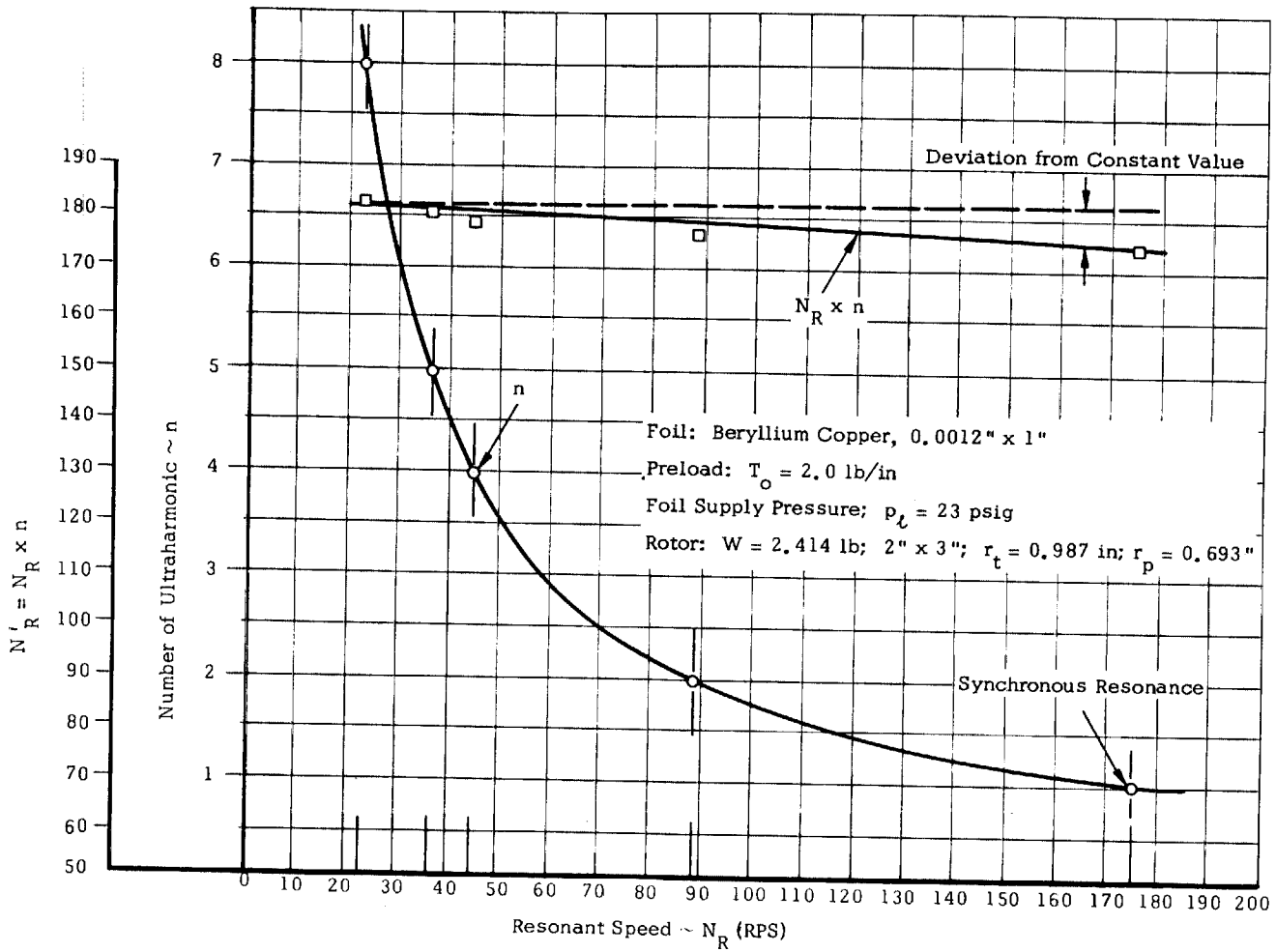

Fig. 4.22 Ultraharmonic Resonances of Rotor and Pressurized Foil-Bearing

Table 4.7 Ultraharmonic Resonances of Rotor and Pressurized Foil Bearing

N_R = Resonant Speed

n = Number of Ultraharmonics/Rev.

N_R	n	N_R x n	Remarks
RPS	-	RPS	-
22.9	8	183	
36.2	5	181	
44.7	4	179	
88.3	2	177	
175	1	175	Synchronous Resonance

Foil: Beryllium Copper, 0.001" x 1"

Preload: T_o = 2.0 lb/in

Rotor: W = 2.414 lb, 2" x 3", r_t = 0.987 in; r_p = 0.693 in

Foil supply pressure: 23 psig

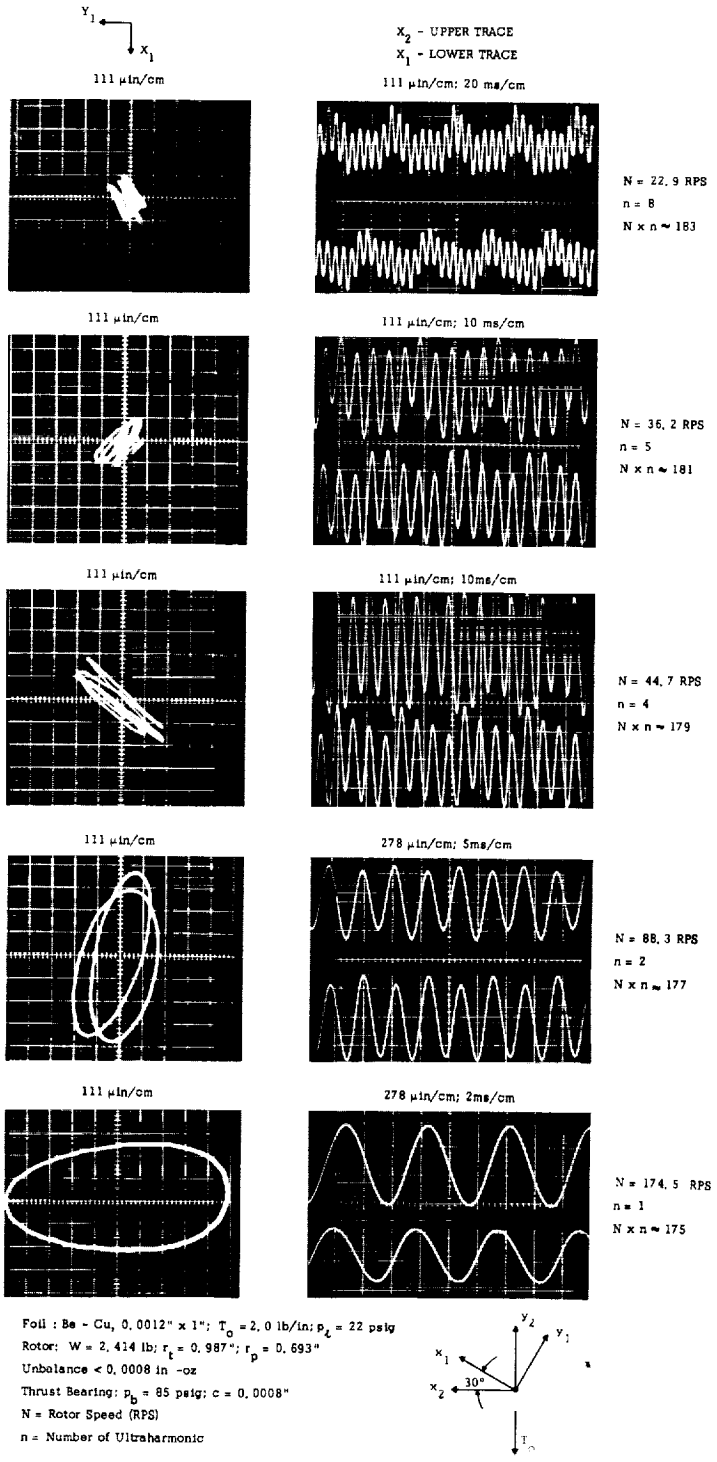

Fig. 4.23 Orbital Motion at Ultraharmonic Resonances;
- Pressurized Foil Bearing

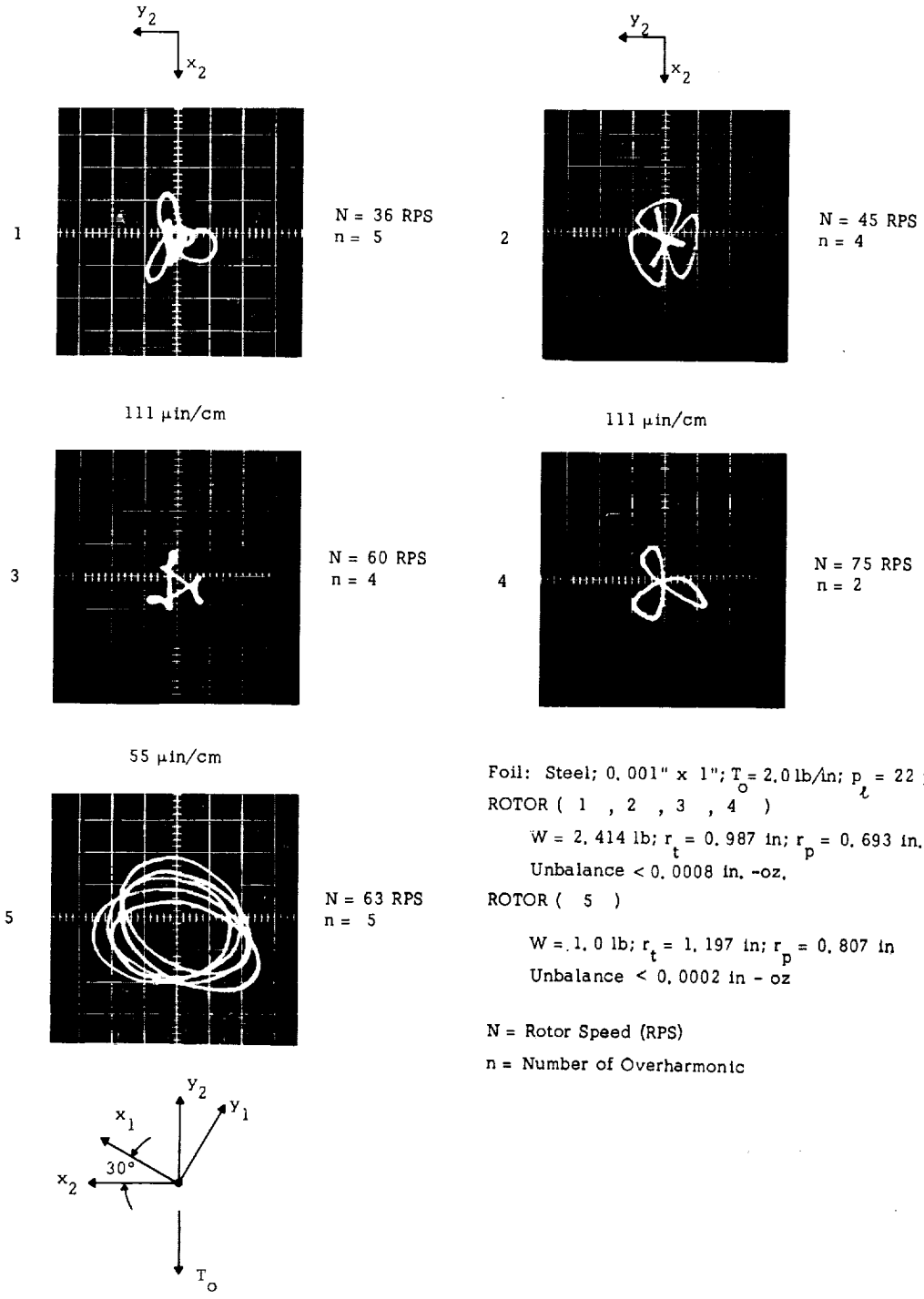

Foil: Steel; 0.001" x 1"; T_o = 2.0 lb/in; p_ℓ = 22 psig

ROTOR (1 , 2 , 3 , 4)

W = 2.414 lb; r_t = 0.987 in; r_p = 0.693 in.

Unbalance < 0.0008 in. -oz.

ROTOR (5)

W = 1.0 lb; r_t = 1.197 in; r_p = 0.807 in

Unbalance < 0.0002 in - oz

N = Rotor Speed (RPS)

n = Number of Overharmonic

Typical Orbits (Pressurized Foil Bearing, Rotor Axis Vertical)

Fig. 4.24 Typical Rotor Orbits in Pressurized Mode of Operation

D. Measurement of Average Gap Width and Position of Rotor at Variable Speed

It is an established fact that the gap width of foil bearings is sensibly constant throughout the region of wrap, except in relatively narrow transitions in the entrance and exit zones and along the edges of the foil [13, 14]. The foregoing statement applies to foil bearings of commensurate length and width and to small foil-bearing numbers $\epsilon = 6\mu U/T$. There is no direct analogy between the clearance of a rigid-surface bearing and the gap width of a foil bearing. The gap width of the foil bearing combines the roles played by both the clearance and the eccentricity in a rigid-surface, fluid-film bearing. In the latter, maximum excursions of the journal are limited by the size of the clearance circle, whereas the foil bearing can accommodate appreciably greater excursions of the journal without necessarily decreasing the gap width beyond a tolerable limit. The foregoing considerations reflect one of the important advantages of foil bearings, particularly with respect to conventional gas bearings, provided adequate constraint is embodied in the design to prevent excessively large displacements of the rotor.

The procedure followed in the determination of the average gap width has been the following. A capacitance probe was inserted in the spacer opposite the foil lock; and a second probe, in the same vertical plane as the first probe, was inserted in the lower housing plate (Fig. 2.2). The first probe faced the midpoint of the foil segment opposite the pressurized foil guides, and the second probe faced the rotor 0.187 inch from the edge of the foil. The outputs of the probes could be recorded individually with the aid of a dual-trace amplifier unit, the difference of outputs being proportional to the gap width. Alternatively, the outputs could be fed into a differential-input amplifier, in which case the gap width could be determined directly from a single oscilloscope trace.

The gap width has also been measured when the rotor was operated in the horizontal attitude. Since rotation of the housing presented no difficulty, gap measurements were made for two positions of the same foil segment: (a) when unloaded and bisected by the load line; and (b) when radially loaded, following rotation of the housing by 120^{o}. The relative positions of the foil sector and of the monitoring probes are illustrated schematically in several figures, e.g. Fig. 4.25.

In designing the foil mounting and in the manufacture of the experimental apparatus a great deal of attention has been devoted to insuring a maximum degree of symmetry of the foil bearing with respect to radial lines, spaced at 120^{o}. The investigators have recognized, however, that relatively small dissymmetries could induce appreciable differences of gap width in the three foil-bearing sectors. When measurements of gap width at one of the foil arcs had been completed, it was decided to embark on a careful determination of the gap width at all three foil-bearing sectors, with the rotor operated in the vertical attitude. This experiment has been performed in the following manner: Capacitance probes were inserted in three spacers, facing the midpoints of foil arcs in the directions of the bisectors. The absolute displacement of each foil segment with speed was then determined using, as a reference, the position of the preloaded foil in contact with the stationary rotor. The absolute displacement of the rotor axis with speed was measured simultaneously in two monitoring planes. The gap width at the midpoint of each foil segment could thus be determined by subtracting from the absolute displacement of the foil the component of rotor displacement in the direction of the bisector of the foil arc.

The experimental results of measurements described in the preceding paragraphs are presented graphically and in the form of oscilloscope photographs in Figs. 4.25 through 4.37, and numerically in Tables 4.8 through 4.12. The point of departure in the discussion which follows

is the simultaneous determination of gap widths at the midpoints of three foil arcs. Referring to Fig. 4.27, it becomes immediately apparent that the magnitudes of gap widths differed very appreciably. The ratios of experimentally determined gap widths at the midpoints of three foil-bearing sectors were, approximately:

$$h_1 : h_2 : h_3 = \begin{cases} 0.80 : 1.0 : 1.2 & \text{at 1000 rps} \\ 0.96 : 1.0 : 1.3 & \text{at 600 rps} \\ 1.1 : 1.0 : 1.3 & \text{at 300 rps} \end{cases}$$

The "average" of three gap widths at 1000 rps has been 1000 μin, but this value cannot be interpreted as the magnitude which may have resulted under conditions of perfect symmetry. The foregoing measurements have been repeatable within limits of experimental accuracy, and the same trend has been observed with various foils, so that the variance must be attributed to inherent dissymmetries, the effect of which is amplified with speed.

Two theoretical curves are also presented in Fig. 4.27. The lowermost curve, referred to as "Theoretical I," has been obtained on the assumptions of viscous, incompressible flow and of constant foil temperature at all speeds. It involved also a geometrical simplification, wherein each foil segment was assumed to be clamped at the lines of tangency with the guides (Fig. 2.2). The analysis which followed (Chapter 5) included the extension of the additional foil length in frictional contact with the guides, the influence of fluid inertia and compressibility, and the effect of temperature rise on the relaxation of tension and increase of clearance. The combined effect of the foregoing contributions is reflected in the uppermost curve, referred to as "Theoretical II" in Fig. 4.27. The intermediate curves reflect consecutively the compounded contributions of additional foil length, of fluid inertia and compressibility, and of thermal

extension. The analytical research has been precipitated by a large divergence of the initially predicted and the experimentally determined gap widths. The experimental determinations of friction at the guides and of variation of temperature of the foil with speed, in the presence of appreciable heat convection, furnished the ingredients for the semi-empirical method of accounting for the foregoing effects in the analysis. The net result has been a considerable improvement in correlation between the measured gap widths and the numerical data based on the analysis presented in Chapter 5. The measurement of clearance in three-foil-bearing sectors involved the determination of the displacement of the rotor from the initial reference position with increasing speed. The locus of the rotor center is shown in Fig. 4.28 and represents the average of displacements recorded in two probe planes, equidistant from the center of the rotor. Since the coordinate axes of probes in the two monitoring planes were inclined at 30° to one another, the notation $(XY)_2^1$ in Fig. 4.28 is simply an indication that the points in plane $(XY)_1$ have been referred to plane $(XY)_2$ by rotation through an angle of 30°. The position of points on the rotor axis in the two probe planes are denoted by circles and by squares. A common reference point for both sets of probes has been established with the preloaded foil in contact with the stationary rotor. It can be noted that the axis of the rotor does not translate parallel to itself, but that its inclination increases with the speed of rotation. Corresponding experimental points, surrounded respectively by circles and by squares, are joined by straight lines. The midpoints of these lines (large circles) locate the center of the rotor within the limits of experimental error, and the smooth curve faired in between these points represents a very probable locus of the rotor center for speeds up to 1000 rps. The line joining the origin and the point corresponding to a speed of 1000 rps is inclined to the Y-axis at an angle of approximately 30°.

The reader will note the points in Fig. 4.28, joined to the origin by a dashed line and representing the position of the rotor in the externally pressurized bearing in the speed range 10 to 200 rps. It is rather remarkable that the direction of the displacement of the rotor supported by the pressurized bearing is nearly perpendicular to the direction of displacement in the self-acting mode of operation, and that the axis of the rotor translates essentially parallel to itself with no apparent change in position in the speed range 10 to 200 cps. It follows that the effects of inherent dissymmetry and misalignment are quite different in the pressurized and in the self-acting modes of operation.

The oscilloscope photographs relevant to data presented in Fig. 4.27, Fig. 4.28, and Table 4.9 are contained in Fig. 4.29 and Fig. 4.30. The absolute displacements of the foil-bearing arcs have been determined from the photographs of Fig. 4.29. The undulations of the traces reflect the orbital motion of the rotor, and also the impingement of air jets in the pressurized mode of operation. The absolute displacement of the rotor with speed has been determined from the photographs of Fig. 4.30. The foregoing determinations apply to a steel foil, 0.001 inch thick, preloaded to an initial tension of 2.0 lb/in, and supporting a 2.414 lb rotor in the vertical position.

An even more drastic example of differences in gap width at three foil-bearing arcs and of displacement of the rotor with speed is illustrated in Fig. 4.37. The data pertains to a steel foil, 0.002 inch thick, preloaded to an initial tension of 3.0 lb/in and supporting a hollow 1.0 lb rotor in the vertical position. Not only have the differences between the three gap widths been more pronounced in this case, but both gap width and rotor displacement have been larger than those which have previously been measured, using a less rigid foil and a lower preload tension. In the case of the less rigid foil and lower initial tension, and

at a speed of rotation 1000 rps, the rotor has been displaced by 260 μin, at an angle of 30° from the positive direction of the Y-axis (Fig. 4.28). The "average" of three gap widths was 1000 μin, and their respective ratios were 0.80 : 1.0 : 1.2. In the case of greater foil rigidity and higher preload tension, and at 1000 rps, the rotor displaced approximately 1170 μin, at an angle of 22° with the positive direction of the Y-axis (Fig. 4.37). The "average" of three gap widths was approximately 1800 μin, and the gap widths were in the ratio 0.53 : 1.0 : 1.56.

The reader will note that in both cases the directions of rotor displacement did not differ greatly and that the rate of displacement increased with speed. At 500 rps, for example, the rotors displaced approximately only one-third of the maximum excursion attained at 1000 rps. It is reasonable to attribute the phenomenon described in the preceding paragraphs to the residual dissymmetries of the foil-bearing suspension, both inherent and due to small misalignments. The mechanism by which these dissymmetries are amplified with speed is not known. At any rate, the latter have had no adverse effect on the operation of the system and have not resulted in excessively large rotor excursions.

The displacement of the rotor with reference to the initial position, when in contact with the preloaded foil, has been determined under the following conditions and in the following sequence: A 2.414 lb rotor has been mounted vertically and held in contact with a 0.001 inch thick steel foil, preloaded to 2.0 lb/in. The foil bearing was then pressurized and the new position of the rotor recorded at negligibly small rotation. The rotor was subsequently returned to the initial position (bearing depressurized) and rotated with the entire assembly into the horizontal attitude. The displacement under gravity was then recorded; following which the bearing was pressurized again and the change in position of the rotor determined. Finally, with the rotor remaining in the horizontal

attitude, the bearing was depressurized again and the last position of the rotor recorded.

The sequence outlined in the preceding paragraph is illustrated graphically in Fig. 4.31, and by means of oscilloscope photographs in Fig. 4.32. It can be seen that the displacement in the vertical attitude, following pressurization, was only 100 μin, at 45° to the Y-axis (Position B). The displacement relative to Position A, following rotation of the housing into the horizontal attitude, was approximately 425 μin, and nearly along the load-line (Position C). The rotor was lifted in the pressurized foil bearing (Position D) and sagged to approximately 1100 μin (position E) following depressurization. When the bearing was pressurized again, the rotor returned invariably, and almost exactly, to Position D. A major part of the maximum displacement has been attributed to slippage, rather than to foil extension. When the preload tension was increased from 2.0 lb/in to 3.0 lb/in, the maximum displacement in position E was very nearly identical with that of Position C. The most important position, of course, is one from which rotation commences in the horizontal attitude, that is Position D.

In the course of experiments concerning the measurement of gap width at three foil-bearing arcs, it has been found that the least gap width corresponded invariably to sector 1, that is the sector opposite the pressurized foil guides and the foil lock, and opposite the point at which the preload tension has been applied (Fig. 2.2). A certain amount of dissymmetry between this sector and the remaining sectors has been inherent in the geometry of the foil-bearing configuration. In addition, other contributing factors must have been present, since the gap widths have <u>not</u> been equal <u>in all three</u> foil-bearing sectors, and since the rotor center did not displace exactly along the bisector of arc No. 1.

In order to asses, at least relatively, the effect of various foil rigidities, loads and preloads, measurements of gap width at sector No. 1 have been performed in both the vertical and horizontal attitude and in the entire self-acting speed range. The procedure followed has been outlined in the first part of this section, and the results are presented graphically and numerically in Figs. 4.25, 4.33, and 4.35 and in Tables 4.8, 4.11, and 4.12. Corresponding sets of oscilloscope photographs, from which the foregoing data have been obtained, are contained in Figs. 4.26, 4.34, and 4.36. The results of these measurements have been rather surprising, since, contrary to what may have been anticipated, the effects of varying the rigidity of the foil and the preload tension produced no drastic changes in gap width. Furthermore, at least in one case, the trend was partly reversed.* The following summary shows the approximate magnitudes of gap width determined at foil sector No. 1 at 60,000 rpm and with the rotor in the vertical attitude:

CASE No.	FOIL MATERIAL Metal	ELASTIC MODULUS lb/in^2	FOIL THICKNESS Mils	PRELOAD TENSION lb/in	GAP WIDTH μ in
1	Beryllium -Copper	$\sim 17 \times 10^6$	1.2	2.0	$\sim$ 800
2	Steel	$\sim 30 \times 10^6$	1.0	2.0	$\sim$ 800
3	Steel	$\sim 30 \times 10^6$	1.0	3.0	$\sim$ 770
4	Steel	$\sim 30 \times 10^6$	2.0	3.0	$\sim$ 1070

It can be seen that the gap widths in the first two cases were nearly equal, despite the difference of approximately 47% in

*Case 4 in above table.

extensional rigidities of beryllium-copper and of steel foils. In the third case listed in the foregoing tabulation, an increase of preload tension resulted in a slight decrease of gap width - an anticipated effect. In the fourth case, however, a combined increase of both rigidity and preload tension produced the unexpected result of an appreciable increase, rather than a reduction, of measured gap width. (It will be recalled that, in the course of the latter experiment, an appreciable displacement of the rotor from the initial reference position has been observed, Fig. 4.37.) In the horizontal mode of operation, the difference in gap width between loaded and unloaded foil sectors decreases with rigidity and preload tension and increases with the rotor weight, which is physically plausible.

In discussing the apparent differences of measured gap widths in three foil-bearing sectors, the investigators attributed this inequality to the inherent dissymmetries of the system and imperfections of alignment. This conclusion, though undoubdedly true, requires additional qualification. The deviations from the 120° symmetry and perpendicularity of the supporting guides could not have exceeded 0.02°. In addition, the contribution to angular dissymmetry, due to a slight displacement of the rotor from the geometric center of the system, has been equally small. Assuming a sensibly uniform pressure distribution in the region of wrap, it follows that the resultant forces acting through the midpoints of the foil arcs formed a nearly equilateral triangle and that, consequently, the tensions in the three foil-bearing sectors remained sensibly constant.

Now, in the region of uniformity, the gap width is given by the relation $h^*/r_o = H^*(6\mu U/T)^{2/3}$, in which H^* is generally a complex function of foil and fluid parameters and of the boundary conditions of the probelm.* Since at any given speed and for a constant viscosity,

*In the simplest form of the foil-bearing equation, H^* = constant [6, 10].

$h^*_1/h^*_2 = (H^*_1/H^*_2)(T_2/T_1)^{2/3}$, and since the possibility of appreciable variance of tension is unlikely, the differences in measured gap widths appear to be associated with the effects of dissymmetries on H*.

Dissymmetries and imperfections will always be present in any realistic foil-rotor system. The encouraging and rather surprising aspect of the entire operation has been that the system behaved very well and remained largely insensitive to nonuniformities which could not be tolerated by conventional gas bearings. The progress of this study has been favorably influenced by the interaction of theory and experiment. The search for a better correlation between experimental and analytical data led to the inclusion in the formulation of the problem of several important, but hitherto disregarded, effects. Among the latter has been the relaxation of tension with increasing temperature of the foil at high rotational speeds. A brief description of the determination of the temperature rise of the foil with speed is contained in the following section.

E. Determination of the Temperature Increase of the Foil with Speed; Coastdown of the Rotor from Rated Speed

The air-driven rotor and the foil have been thoroughly cooled by the discharge from the nozzles and two rows of turbine buckets. The prime mechanism, therefore, for the transfer of heat generated in the foil-bearing film has been through forced convection.

Since the foils have been relatively thin, a large portion of the generated heat has been convected directly from the outer foil surface in the region of the wrap. The rotor also furnished a good heat sink for the energy dissipated in shearing the fluid film. Only one-half of the cylindrical surface matching the width of the foil corresponded to the <u>total</u> foil wrap at any instant of time. The other half and the remainder of the rotor surface have been continuously swept by the turbine-air discharge. It is reasonable to suppose that the temperatures at the rotor

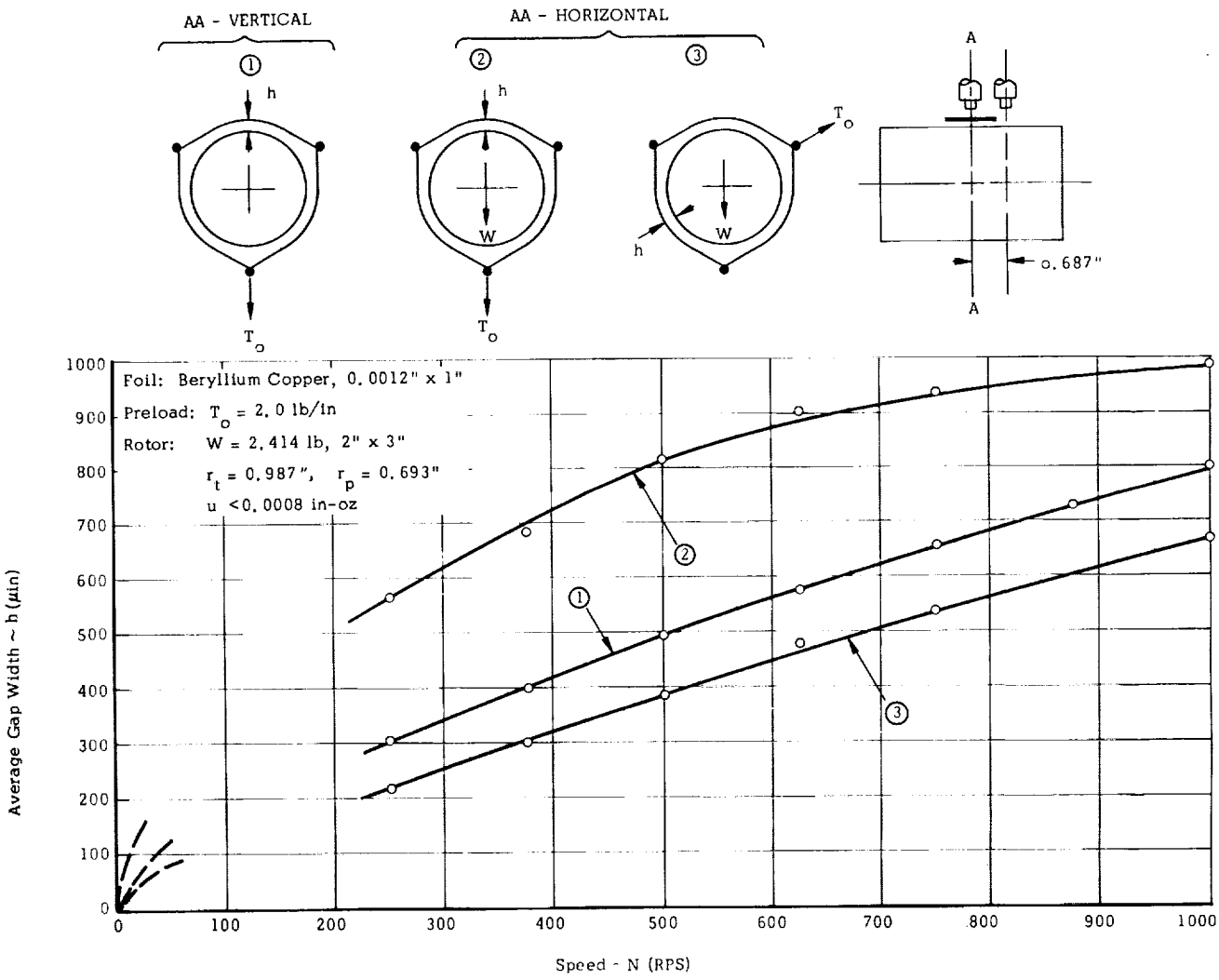

Fig. 4.25 Average Gap Width as a Function of Speed

Table 4. 8 Average Gap Width as a Function of Speed

Speed	h - (1)	h - (2)	h - (3)
RPS	μin	μin	μin
250	305	566	216
375	400	683	300
500	494	815	384
625	576	900	477
750	655	933	538
875	727	-	-
1000	800	984	666

(1) - Vertical Position

(2) - Horizontal Position, Foil Unloaded

(3) - Horizontal Position, Foil Loaded

Foil: Beryllium Copper, 0. 0012" x 1"

Preload: T_o = 2. 0 lb/in

Rotor: W = 2. 414 lb

r_t = 0. 987 in; r_p = 0. 693 in

u < 0. 0008 in - oz

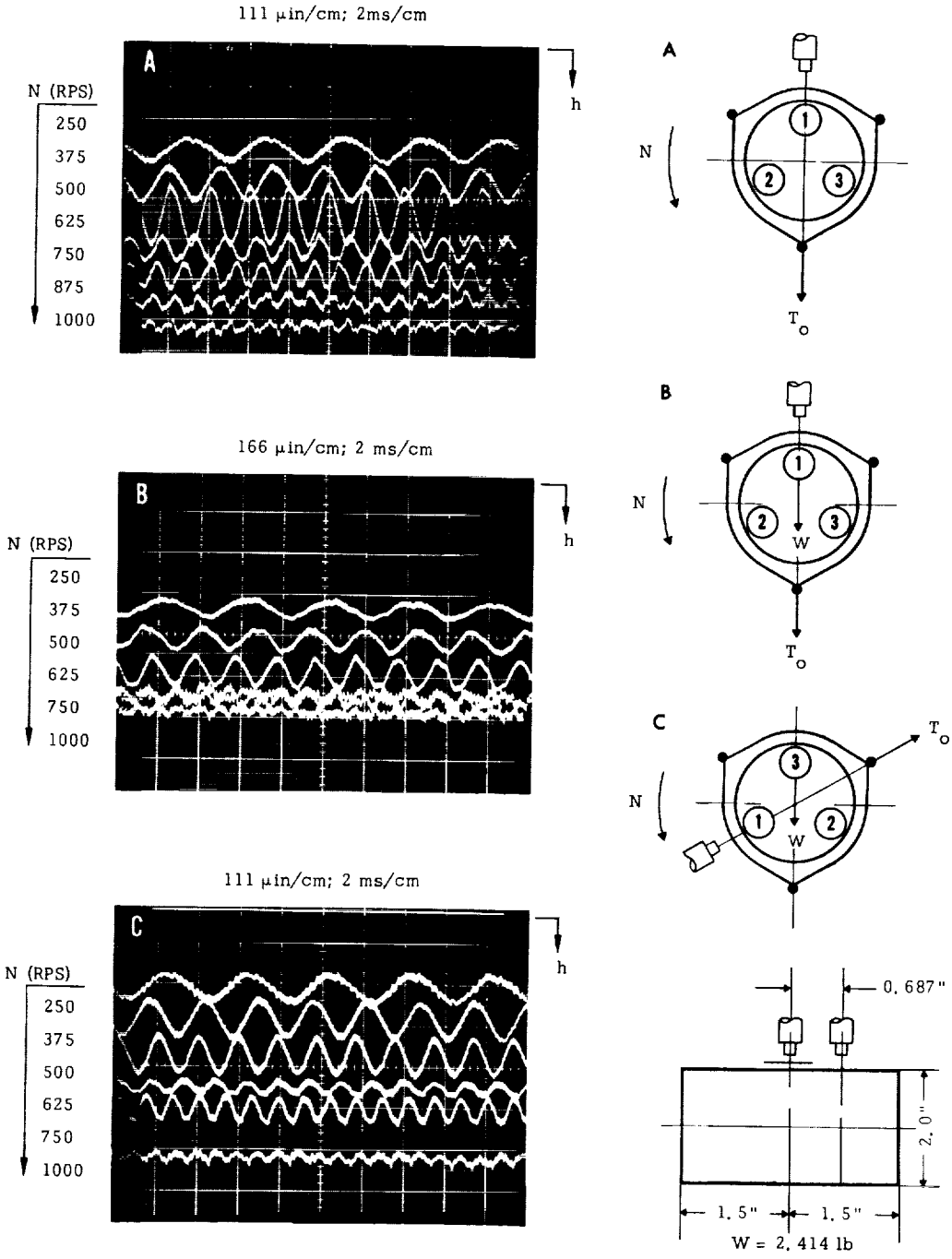

Fig. 4.26 Determination of Average Gap Width

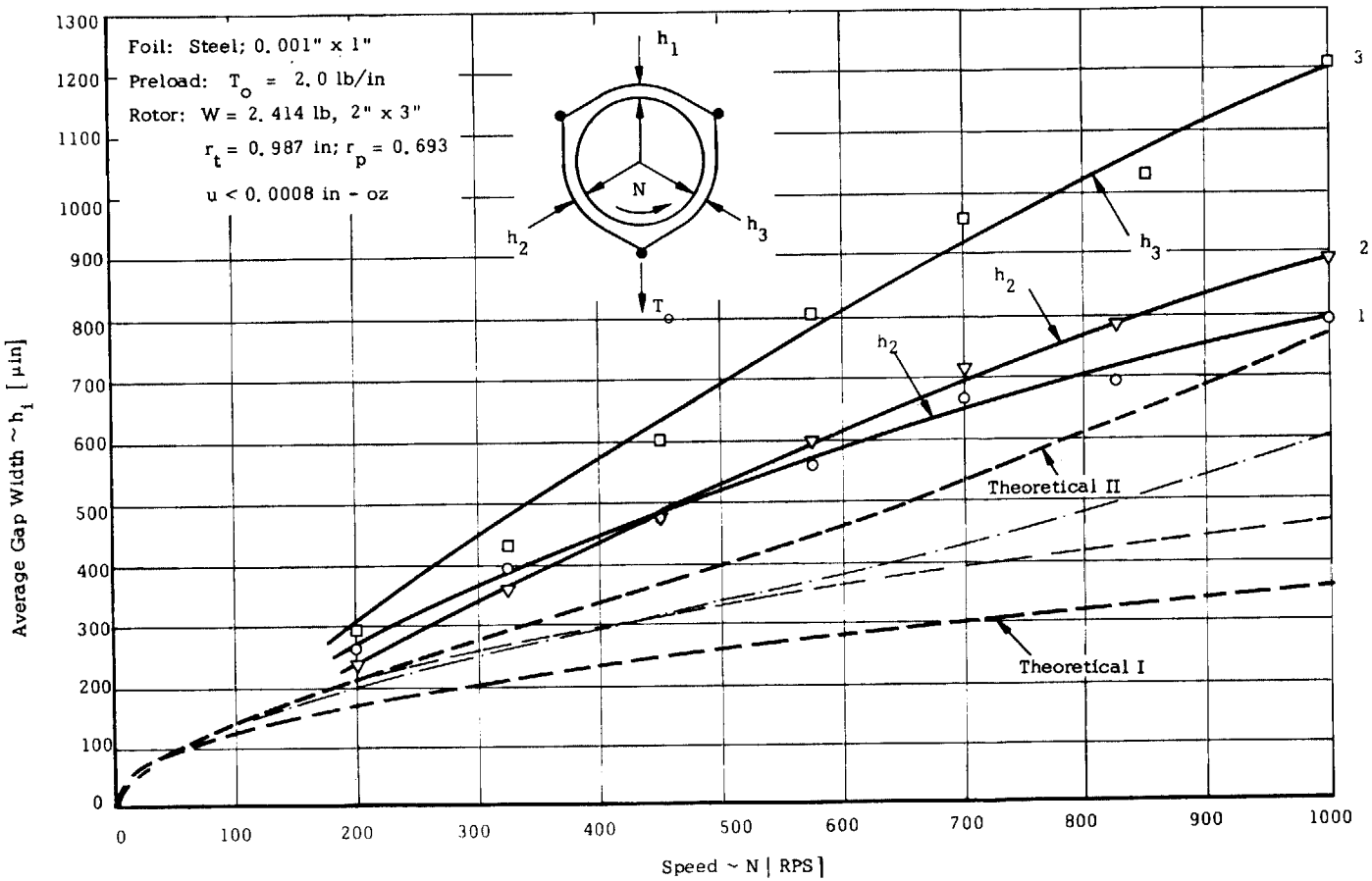

Fig. 4.27 Variation of Gap Width with Speed at 3 Foil-Bearing Segments

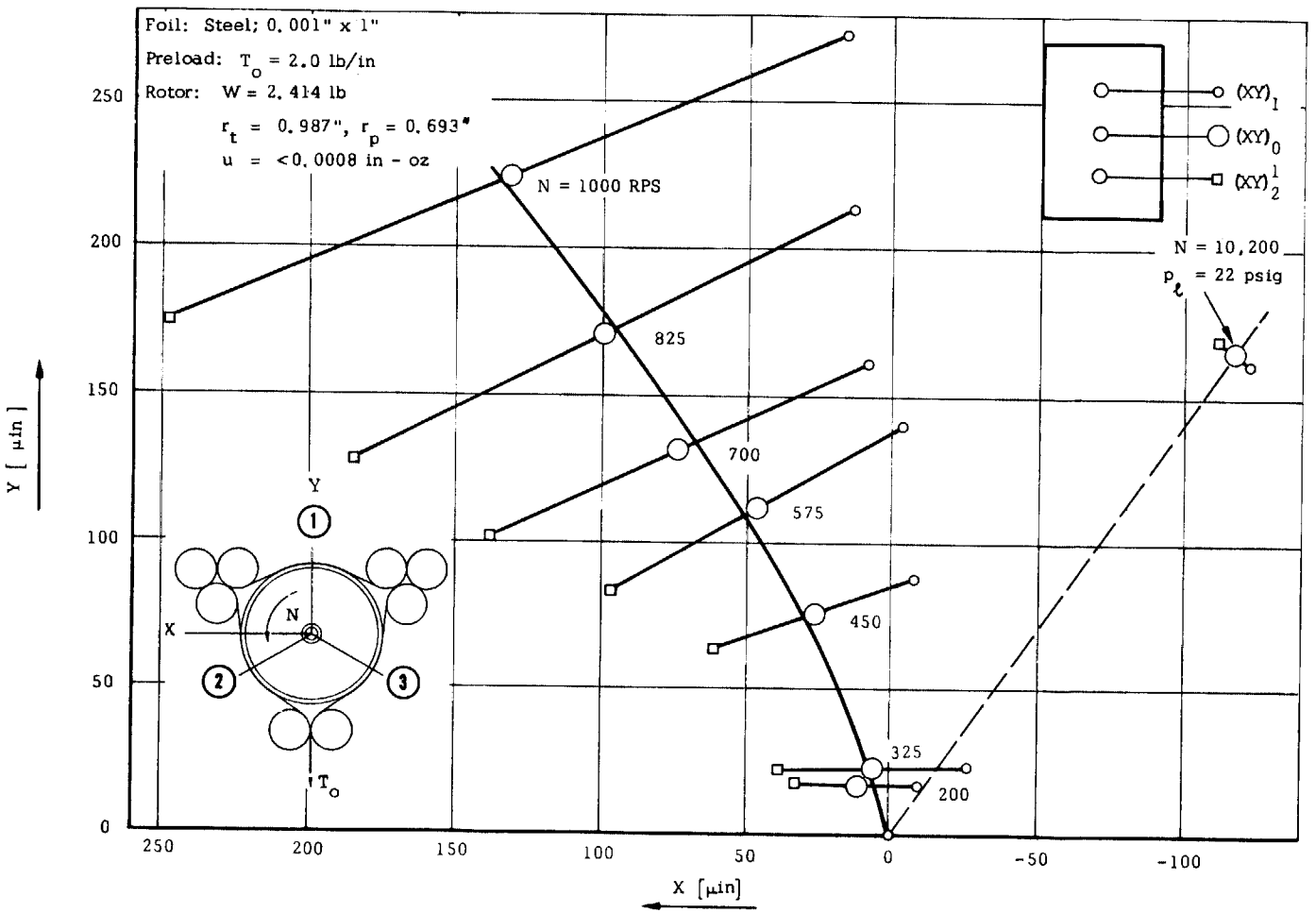

Fig. 4.28 Displacement of Rotor Center as a Function of Speed

Table 4.9 Determination of Gap Widths at 3 Foil-Bearing Segments

Foil: Steel, 0.001" x 1"

Preload: T_o = 2 lb/in

Rotor: W = 2.414 lb; r_t = 0.987 in; r_p = 0.693 in

u < 0.0008 in - oz

Speed N	X_2	Y_2	X_2^1	Y_2^1	X_o	Y_o	F_1	Z_1	h_1	F_2	Z_2	h_2	F_3	Z_3	h_3
RPS	μin														
Pressurized Foil Bearing (p_ℓ = 22 psig)															
10	-111	167	-122	161	-117	165	1445	165	1280	1195	-188	1383	1420	14	1406
200	-111	167	-122	161	-117	165	1670	165	1505	1335	-188	1523	1560	14	1546
Self-Acting Foil Bearing															
200	33	17	-10	17	7	18	280	18	262	239	4	235	278	-15	293
325	39	22	-26	23	8	21	413	21	392	355	-5	360	411	-15	426
450	61	63	-8	88	29	73	545	73	472	466	-12	478	541	-62	603
575	97	83	-3	139	50	108	666	108	558	588	-11	599	710	-97	807
700	139	101	9	161	69	135	800	135	665	710	-8	718	833	-127	960
825	185	128	14	213	97	172	863	172	691	780	-2	782	860	-170	1030
1000	248	175	17	273	134	222	1015	222	793	1000	5	995	986	-227	1213

$(XY)_2$; $(XY)_2^1$ = Displacement of rotor center in lower and upper plane of probes

$(XY)_o$ = Displacement of rotor center in midplane

F_j = Displacement of foil at midpoint of region of wrap, j = 1, 2, 3

Z_j = Displacement of rotor center in midplane in the direction of F_j

$h_j = F_j - Z_j$ = Gap width at midpoint of region of wrap

Note:

The upper probes $(XY)_1$ are displaced from the lower probes $(XY)_2$ by $\alpha = 30°$ in a sense opposite to the direction of rotation. The following relations apply:

$X_2^1 = X_1 \cos\alpha - Y_1 \sin\alpha$; $Y_2^1 = X_1 \sin\alpha + Y_1 \cos\alpha$ $\quad Z_1 = Y_o$; $Z_2 = X_o \cos\alpha - Y_o \sin\alpha$; $Z_3 = -X_o \cos\alpha - Y_o \sin\alpha$

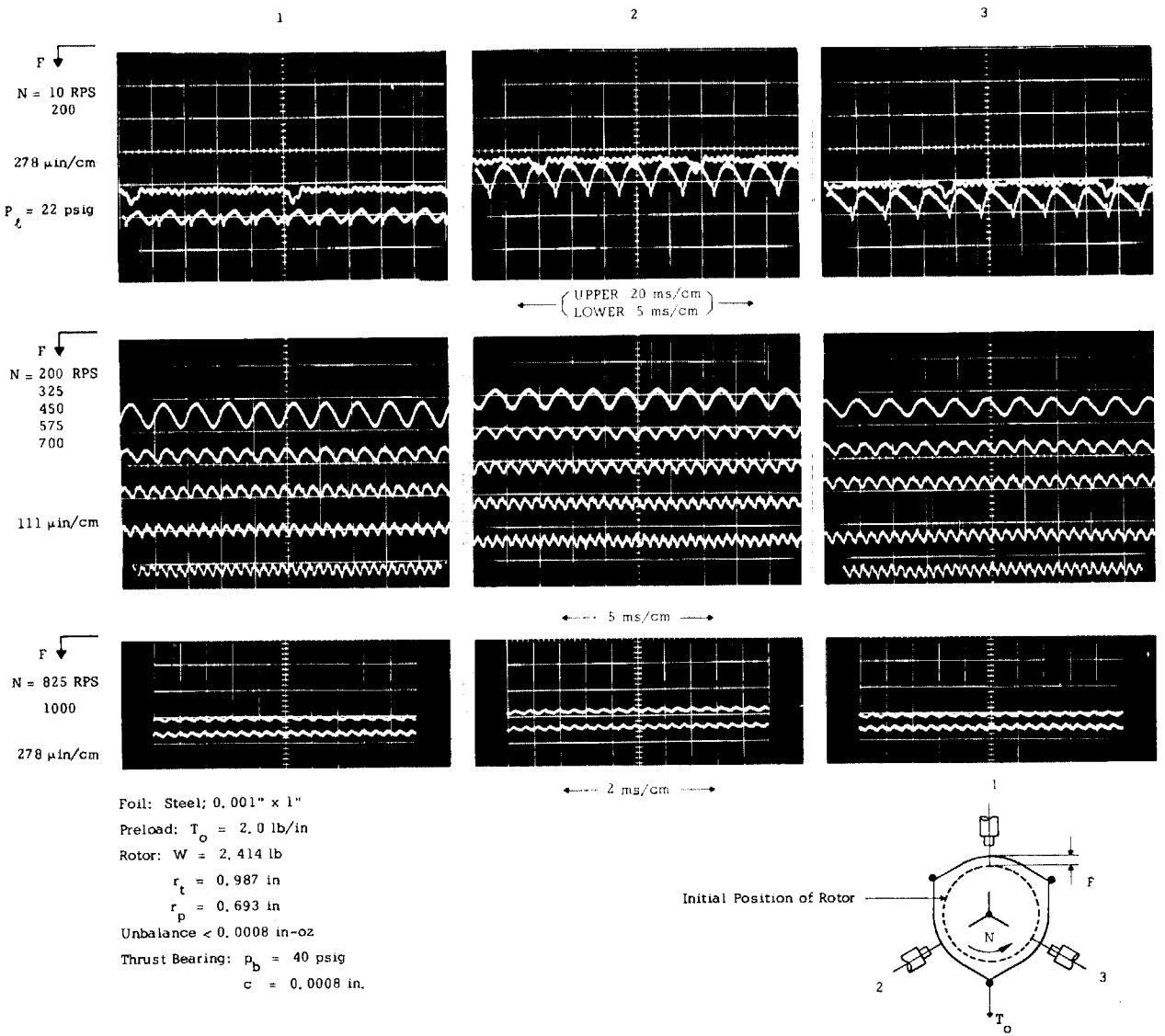

Displacement of Foil-Bearing Sectors at Center of Wrap with Speed

Fig. 4.29 Displacement of 3 Foil-Bearing Arcs as a Function of Speed

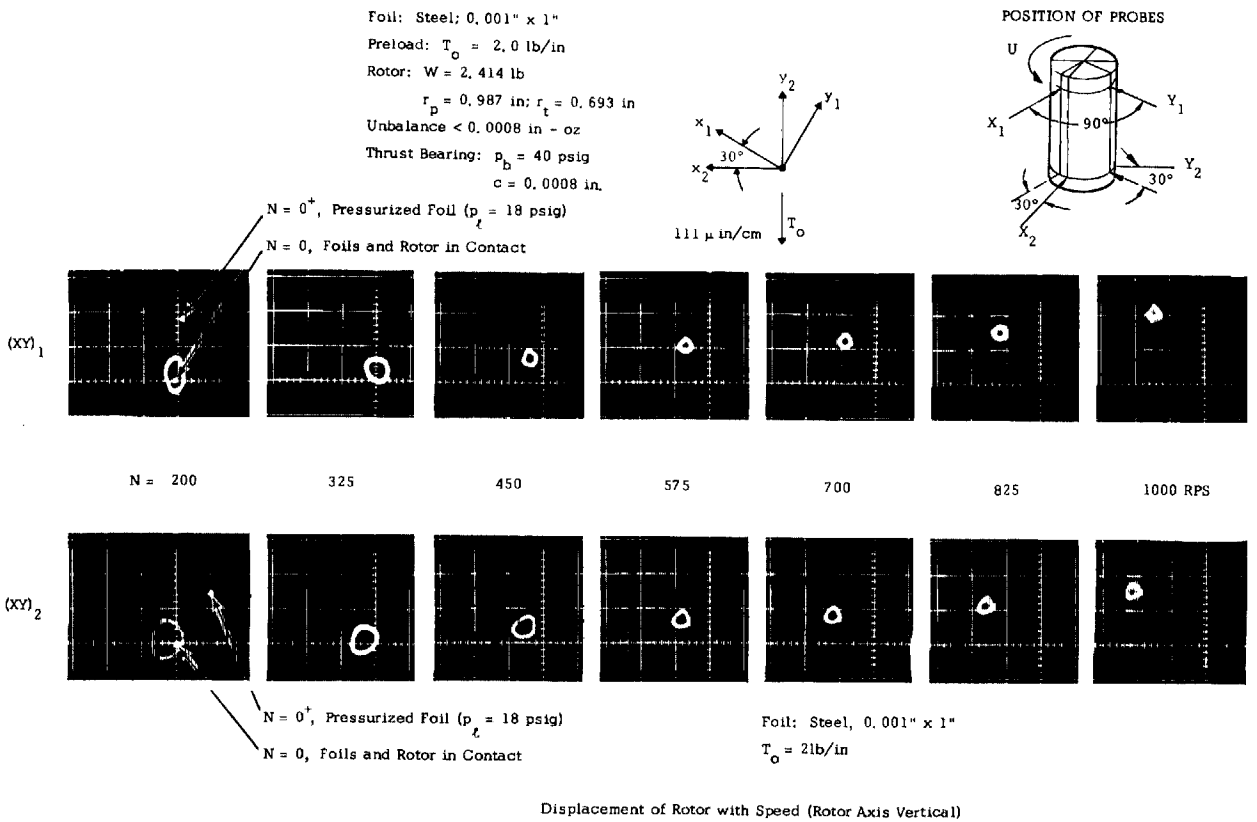

Fig. 4.30 Determination of Displacement of Rotor Center with Speed

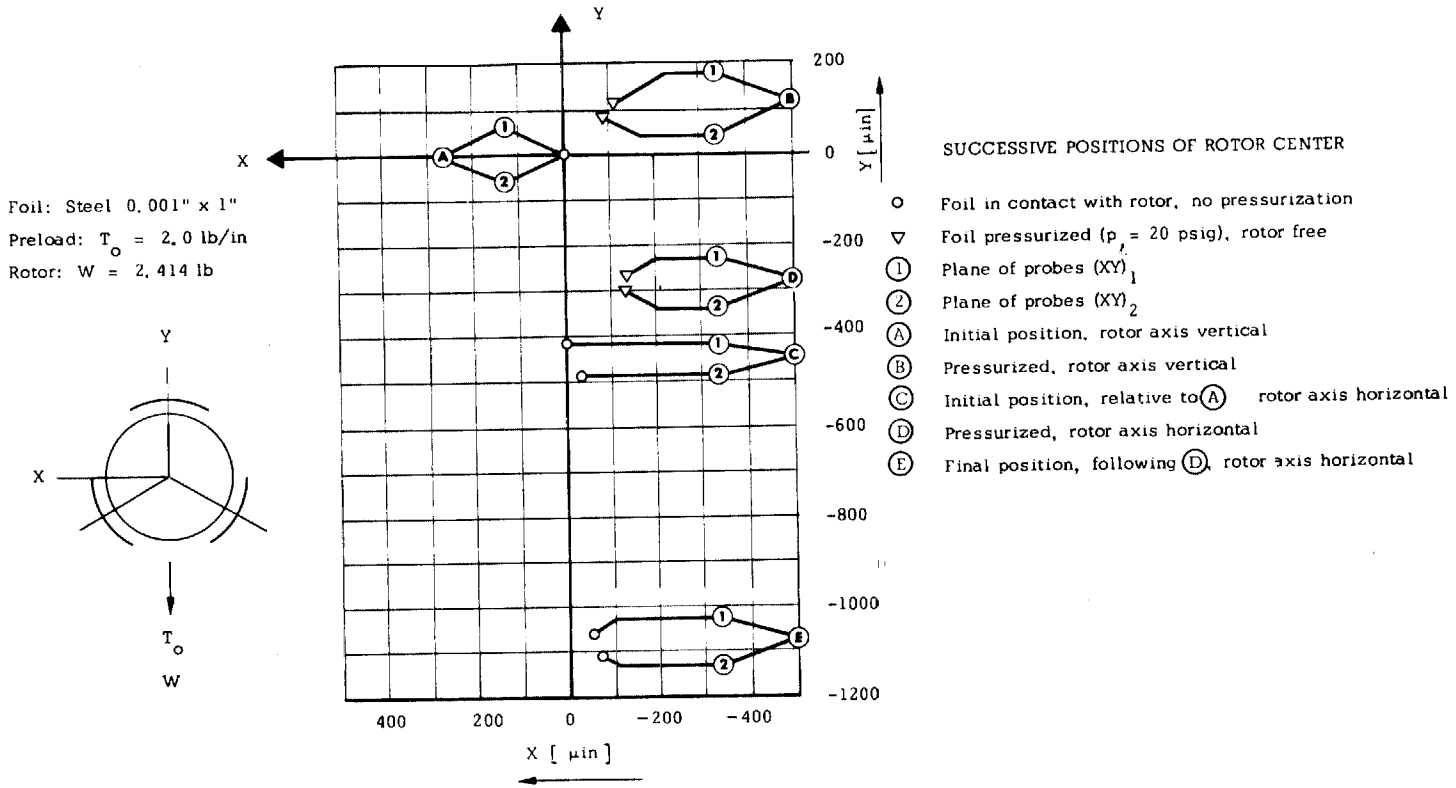

Fig. 4.31 Successive Positions of Rotor in Pressurized Foil Bearing

Table 4. 10 Successive Positions of Rotor in Pressurized Foil Bearing

	Sequential Position	Rotor Axis	Foil - Rotor	X_2	Y_2	X_2'	Y_2'
	-			μ in.	μ in.	μ in.	μ in.
	A	Vertical	In Contact	0	0	0	0
	B	Vertical	Pressurized	-84	84	-111	117
	A	Vertical	In Contact	0	0	0	0
*	C	Horizontal	In Contact	-28	-495	0	-420
	D	Horizontal	Pressurized	-125	-300	-134	-270
	E	Horizontal	In Contact	-70	-1110	-50	-1060

*Following (A) and due to change of rotor attitude from vertical to horizontal only.

Foil: Steel; 0. 001" x 1"

Preload: T_o = 2. 0 lb/in

Rotor: W = 2. 414 lb

Foil supply pressure; p_ℓ = 20 psig

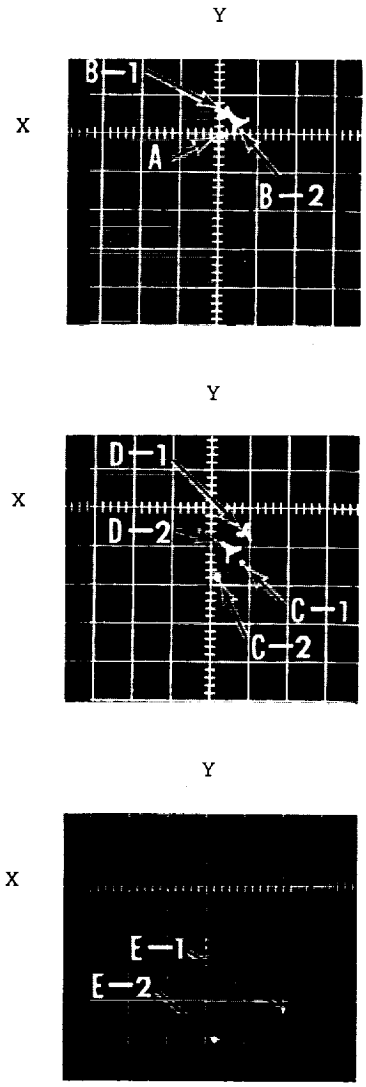

Foil: Steel; 0.001" x 1"

1 - Plane of Probes $(XY)_1$

2 - Plane of Probes $(XY)_2$

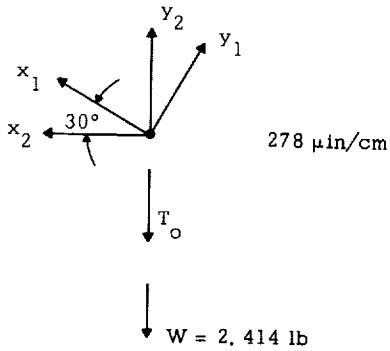

A - Rotor Axis Vertical, Initial Position, Foils Contact Rotor

B - Rotor Axis Vertical, Foils Pressurized (p_ℓ = 20 psig)

C - Rotor Axis Horizontal, Foils Contact Rotor

D - Rotor Axis Horizontal, Foils Pressurized (p_ℓ = 20 psig)

E - Rotor Axis Horizontal, Foils Contact Rotor

The Sequence is as Follows:

A → B → C → D → E

Rotor revolves at 2 - 3 RPS when foils are pressurized

NOTE: In Fig. 4.31 , the displacements in $(XY)_1$ are referred to the $(XY)_2$ - plane

Fig. 4.32 Determination of Successive Positions of Rotor in Pressurized Foil Bearing

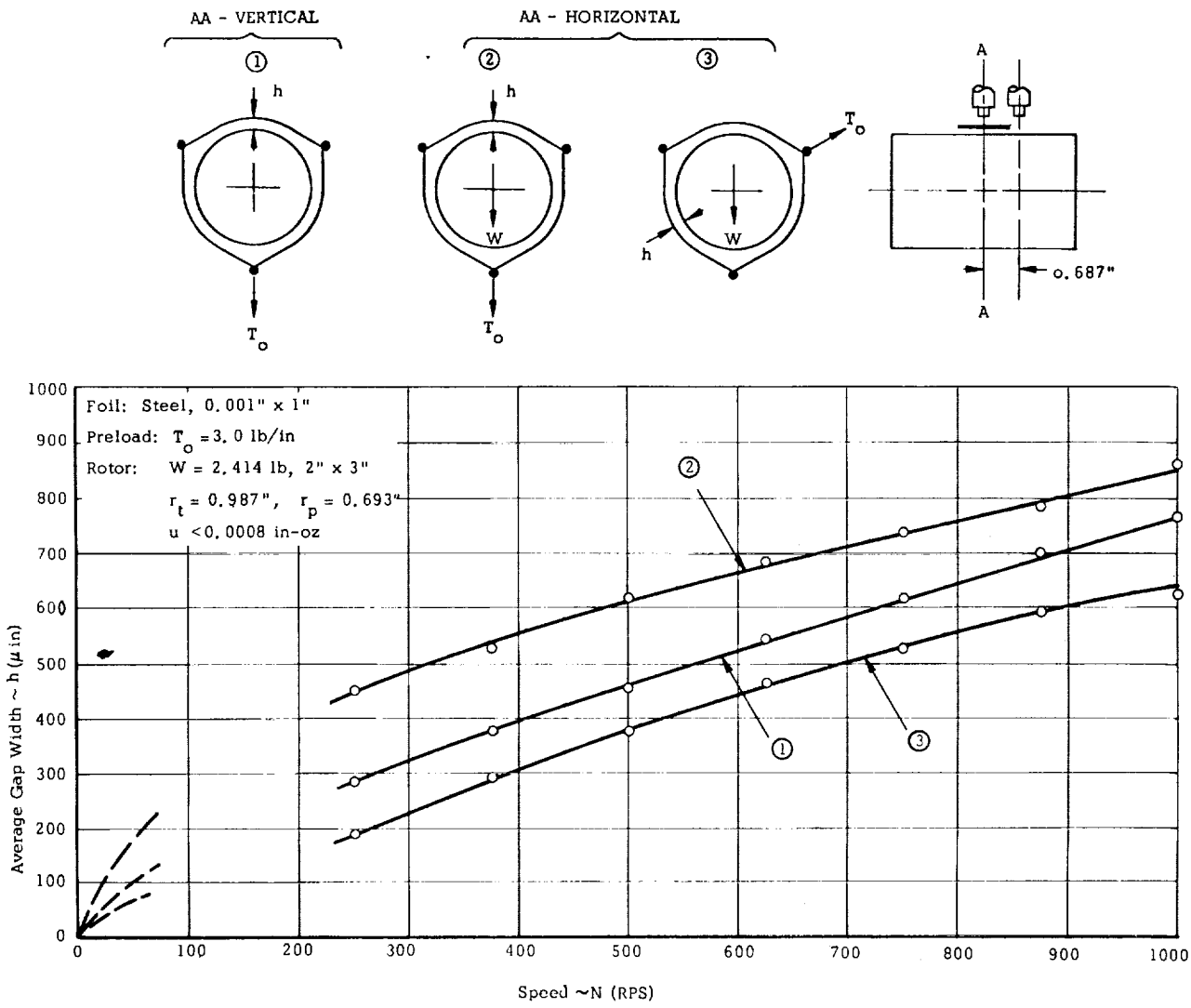

Fig. 4.33 Average Gap Width as a Function of Speed

Table 4.11 Average Gap Width as a Function of Speed

Speed	h-(1)	h- (2)	h - (3)
RPS	μin	μ in	μin
250	284	450	189
375	375	528	295
500	455	619	372
625	535	682	462
750	616	737	527
875	700	785	594
1000	768	860	623

(1) - Vertical position

(2) - Horizontal position, Foil unloaded

(3) - Horizontal position, Foil loaded

Foil: Steel, 0.001" x 1"

Preload: T_o = 3.0 lb/in

Rotor: W = 2.414 lb

r_t = 0.987 in, r_p = 0.693 in

u < 0.0008 in-oz

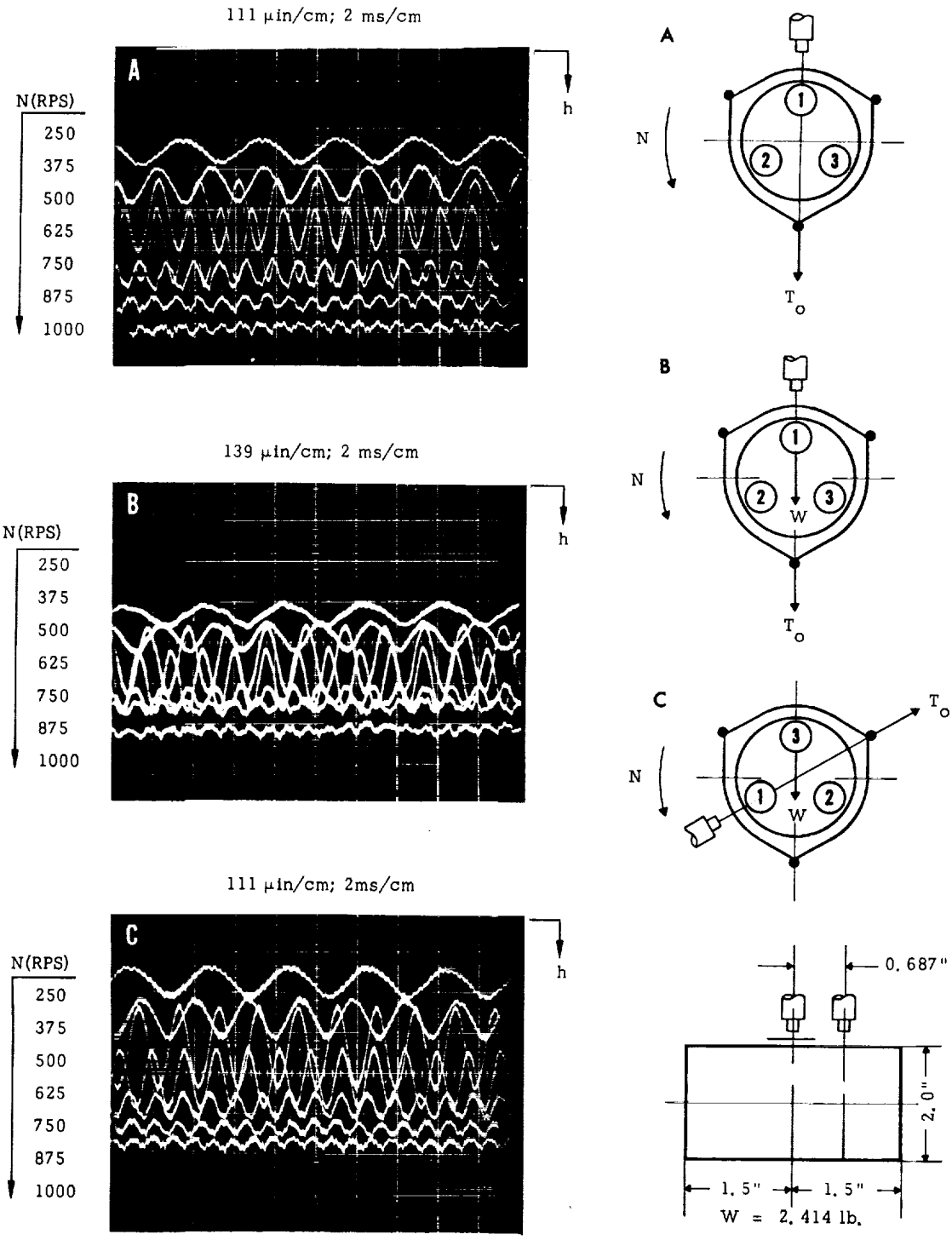

A - Rotor Axis Vertical Foil: Steel, 0.001" x 1"

B, C - Rotor Axis Horizontal T_o = 3.0 lb/in

Fig. 4.34 Determination of Average Gap Width

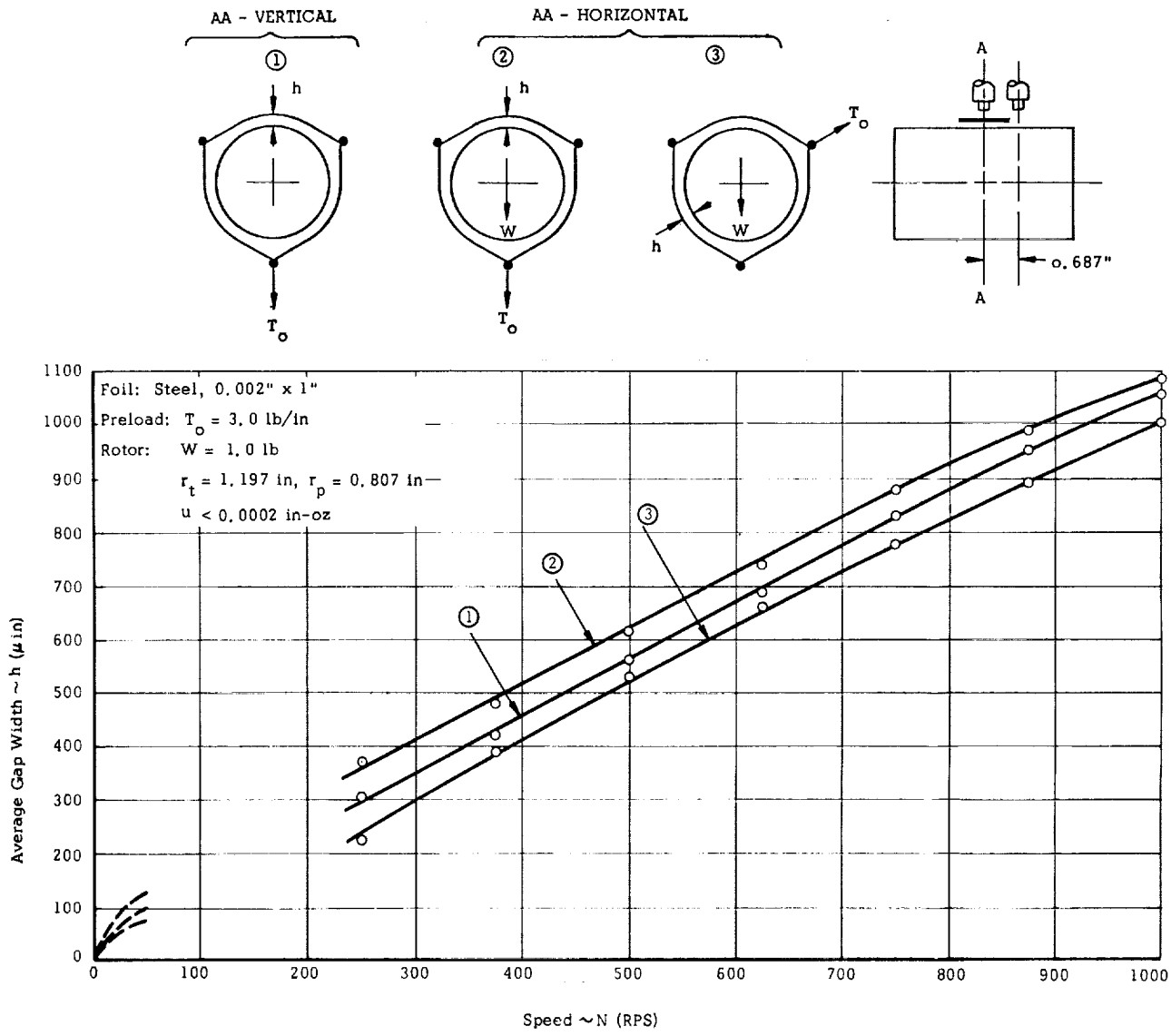

Fig. 4.35 Average Gap Width as a Function of Speed

Table 4. 12 Average Gap Width as a Function of Speed

Speed	h - (1)	h - (2)	h - (3)
RPS	μin	μin	μin
250	305	370	326
375	420	480	390
500	560	612	528
625	685	737	660
750	830	878	778
875	950	986	890
1000	1055	1085	1000

(1) - Vertical Position

(2) - Horizontal Position, Foil Unloaded

(3) - Horizontal Position, Foil Loaded

Foil: Steel 0. 002" x 1"

Preload: T_o = 3. 0 lb/in

Rotor: W = 1. 0 lb

r_t = 1. 147 in; r_p = 0. 807 in

u < 0. 0002 in - oz

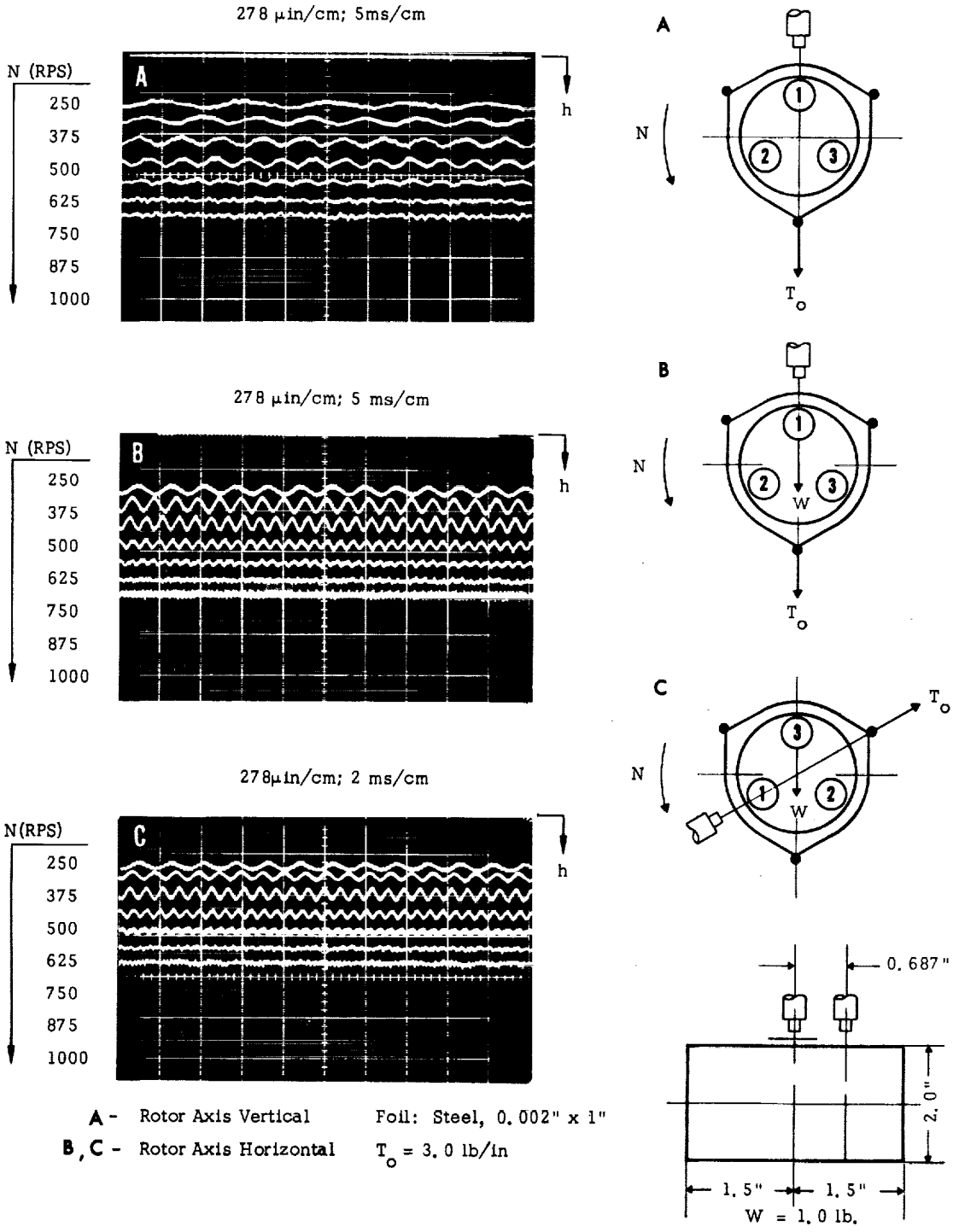

Fig. 4.36 Determination of Average Gap Width

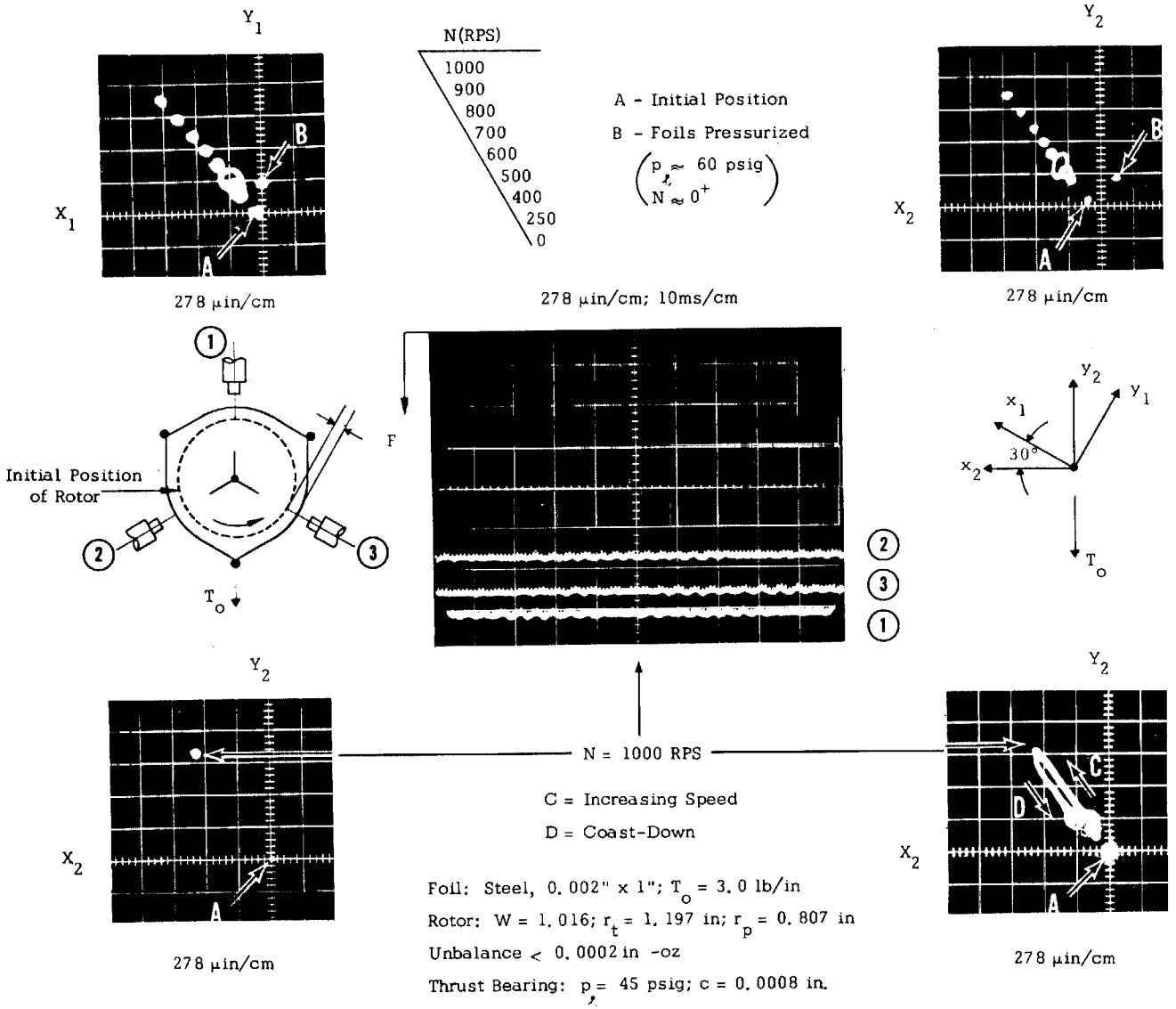

Fig. 4.37 Determination of Average Gap Width

surface and in the interior of the rotor did not differ appreciably from ambient.

As a precursor to temperature measurements, the following test has been performed. The turbine air supply was cut off at 60,000 rpm and the rotor was allowed to coast down in the absence of cooling air discharge. The photograph in the lower right hand side of Fig. 4.37, for example, shows the paths corresponding to the locus of the rotor with increasing speed and during coastdown which are nearly parallel and only slightly displaced from one another. On two occasions, following a reduction of the initial thrust-bearing clearance from 0.0008 in to approximately 0.0005 in, failure occurred during coastdown, in the neighborhood of a pitching resonance. The axial clearance had apparently been decreased because of axial expansion of the rotor, so that the amplitude pitching resonance could no longer be accommodated within limits of reduced clearance.

The upper and lower oscilloscope traces in the photographs of Fig. 4.39 correspond respectively to the positions of the rotor and of the foil, as monitored by parallel capacitance probes, in line with the bisector of foil arc No. 1. The distance between the traces is proportional to the gap width, which is plotted in the same figure as a function of time, together with the speed curve. Following cutoff of turbine air at 1000 rps, the initial gap width of 836 μ in increased with decreasing speed, attaining within approximately 5 sec a maximum of 885 μ in at 950 rps. This corresponds to an increase of gap width of order 6%, accompanied by a 5% reduction of speed. The reader will note, from the photograph of Fig. 4.39, that the increase of gap width due to temperature rise of the foil has not been paralleled by thermal growth of rotor diameter and that the rotor appears to displace very slowly in the direction of the monitoring probe.

A beryllium-copper foil, 0.0012 inch thick and preloaded to 2.0 lb/in, has been used in the determination of variation of foil temperature with speed. The experimental results are presented in Fig. 4.38, in which the location of thermocouples is indicated by means of a schematic diagram. It is apparent that the temperatures at the quarter points of the angle of wrap remained practically identical and that the temperature rise at the approximate midspan between the lines of tangency of the foil to the rotor and to the guides was of order 25% of the increase in the central zone. At 1000 rps, for example, the respective temperature readings have been 31°F and 7.5°F above ambient. It is reasonable to assume that the temperature remained sensibly uniform in the region of wrap and that rapid transitions to nearly ambient temperatures occurred in the vicinity of entrance and exit zones. The relatively small amount of heat conducted along the foil from the central region has been rapidly convected from both surfaces of the foil by cooling air currents.

Although no attempt has been made to record the temperature during coastdown of the rotor, a nearly two-fold increase of temperature has been recorded by the thermocouple nanovoltmeter, within a few seconds following the cutoff of turbine air (approximately 70° F above ambient in the centeral zone). The thermal conductivity of metal foils has probably very little effect on the temperature distribution, since the heat flux normal to the narrow cross-sectional area must be commensurately small. The heat-transfer model used in the analysis is discussed in Chapter 5 of the present report; at this point it suffices to mention that the average value of the surface heat-transfer coefficient used in obtaining numerical data has been based on the temperature measurements described in this section.

The information gathered from temperature measurements and the observed increase of gap width in the initial stages of deceleration

leads to the conclusion that the relaxation of tension with increasing temperature may have contributed an estimated 10% of the difference between the measured and the initially predicted gap widths. The appreciable divergence, therefore, had to be attributed to a number of other effects. On the other hand, the investigators have observed no deterioration in foil-bearing performance in decelerating the rotor in the absence of forced convection.

F. Response to Impact - Determination of "Natural Frequencies" of Foil-Bearing Supported Rotors

The experiments described in the preceding sections concerned principally the evaluation of the overall response of the system as a function of speed and under the influence of residual unbalance. These experiments involved, necessarily, both the foil bearing and the thrust bearings. In addition, the effects of several parameters on the performance of the foil-rotor system have been studied under quasi-steady conditions.

The present section concerns the determination of "natural frequencies,"* from the motion of the rotor following impact, for various speeds and foil preload-rotor mass combinations. Impact to the housing has been imparted along the bisector of one of the foil arcs and in the midplane of the rotor. A quarter-inch diameter rod was threaded into one of the spacers between the upper and the lower housing plates (Fig. 2.2). The protruding end of the rod was inserted into a blind hole in a cylindrical slide, the impact of which was transmitted to the housing. Since the

*The subject of this investigation is a highly complex, nonlinear system. The motion following impact is probably aperiodic, and the term "natural frequency" should be interpreted here as the reciprocal of the average time between the occurrence of an arbitrary number of maximum excursions of the decaying oscillation.

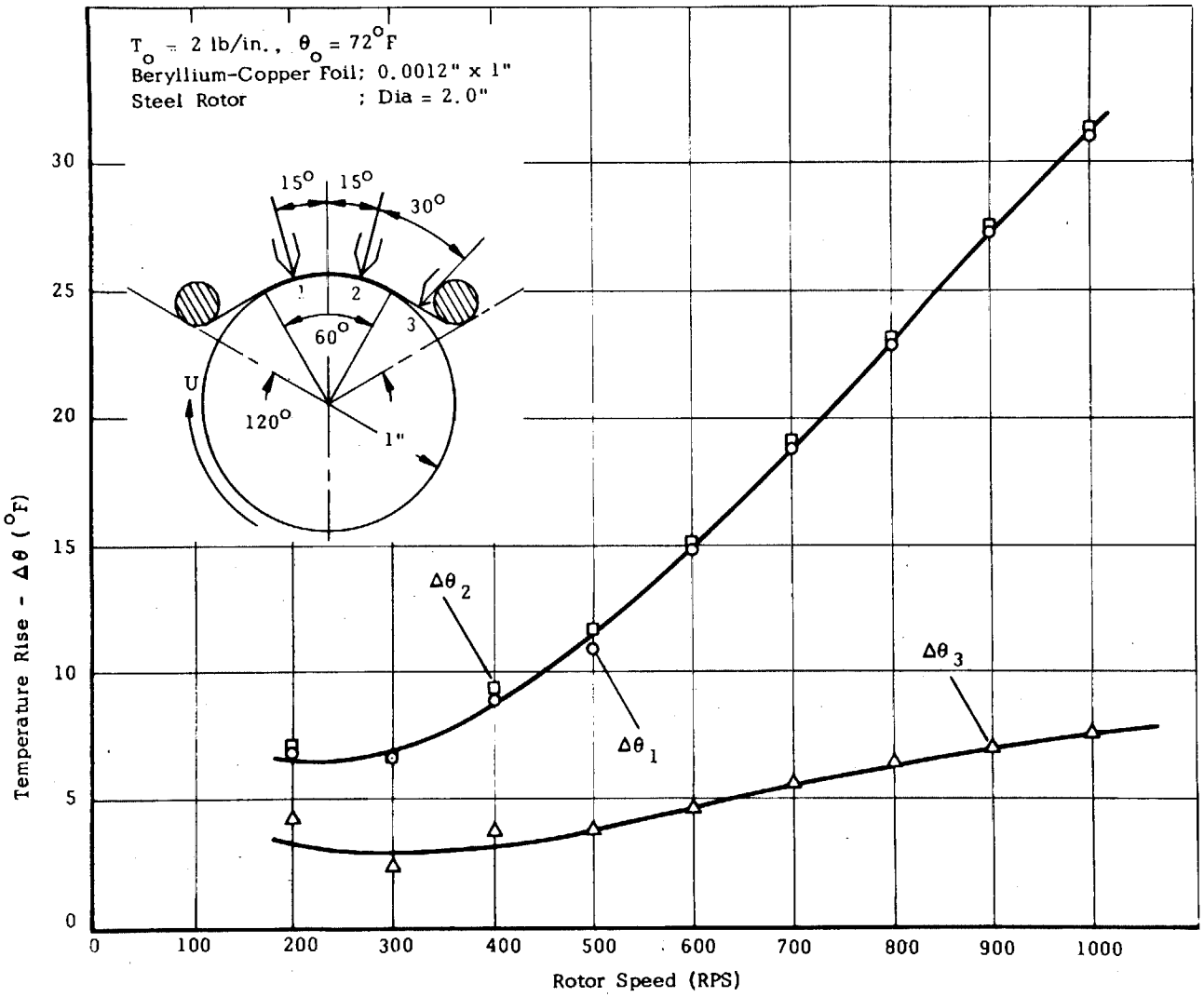

Fig. 4.38 Variation of Foil Temperature with Speed

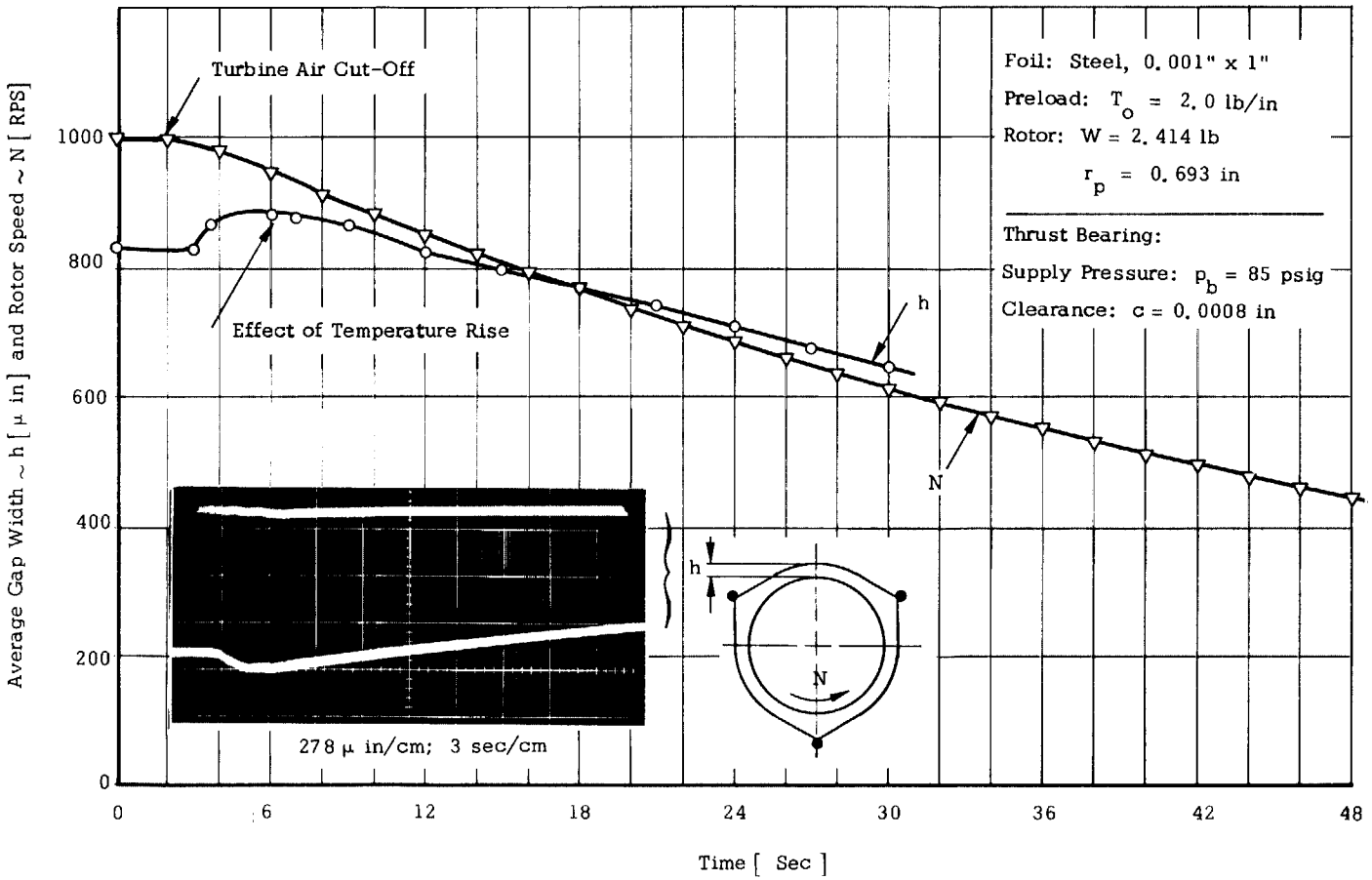

Coast - Down of Rotor: - Average Gap Width and Rotor Speed Versus Time

Fig. 4.39 Coastdown of Rotor; - Variation of Gap Width and Speed with Time

Table 4. 13 Coastdown of Rotor; - Variation of Gap Width and Speed with Time

Time	Speed	Time	Gap
Sec	RPS	Sec	μ in
0	1000	0	836
2	999	3	825
4	983	3. 6	857
6	951	6	885
8	916	6. 9	875
10	883	9	857
12	851	12	825
14	820	15	800
16	791	18	770
18	763	21	745
20	736	24	707
22	710	27	675
24	684	30	645
26	660		
28	634		
30	614		
32	592		
34	572		
36	551		
38	532		
40	513		
42	495		
44	477		
46	461		
48	445		
50	429		

Foil: Steel; 0. 001" x 1"

Preload: T_o = 2. 0 lb/in

Rotor: W = 2. 414 lb

r_p = 0. 693 in

Thrust Bearings:

Supply Pressure: p_s = 85 psig

Clearance: C = 0. 0008 in

investigators have been concerned mainly with with determinations of frequency, rather than with the magnitude of ensuing excursions, no attempt has been made to control the impacts, other than to insure sensibly equal excursions of the rotor and to minimize pitching components of motion.

The experimental results are presented graphically in Fig. 4.40 and numerically in Table 4.14. The corresponding oscilloscope traces of response are illustrated in Figs. 4.42 through 4.46. A comparison between a number of experimental and theoretical results is also made in Fig. 4.40 and Fig. 4.41. The positions of foil-bearing sectors and of monitoring probes, relative to the direction of impact, is indicated in the majority of figures by means of a schematic diagram.

Referring to Fig. 4.40, it will be noted that the "natural frequencies" have been nearly independent of the rotational speed, regardless of magnitudes of preload tension, of foil rigidity, and of rotor mass. Furthermore, it is apparent that an increase of both the rigidity of the foil (Et) and of the preload tension (T_o) produced no appreciable effect on the "natural frequency" of the foil-rotor system. Specifically, an increase of 100% in preload tension and of approximately 47% in extensional rigidity resulted in an average increase of frequency of order 12% in the speed range 200 - 1000 rps (experimental curves A and C). A comparison of experimental curves D and E in Fig. 4.40 indicates an even smaller variation of frequency - of order 1.5% - when the extensional rigidity and and the preload tension have been increased respectively by factors of 100% and 33%. On the other hand, it would appear that the effect of rotor mass on the natural frequency is exactly the same as in the case of a simple oscillator. Comparing the frequency and mass ratios corresponding to curves B and E, for which the rigidity and preload have been identical, one finds that $(f_n)_E / (f_n)_B \approx (W_B / W_E)^{1/2} \approx 1.55$.

The irregular shape of waveforms in the oscilloscope photographs of Figs. 4.42 through 4.46 reflects the superposition of several components of motion. Although the conical component of motion has been minimized by translating the resonance* of this mode to a region sensibly far removed from the speed at which the response to impact has been determined, the impact itself induced a moderate degree of pitching and other spurious components of motion. In addition, because of directional properties of compliance (due to inequality of clearance of the three foil-bearing sectors, as well as to nonlinear and coupling effects associated with large rotor excursion), the ensuing motion of the rotor has been only approximately colinear with the direction of impact. The determination of "natural frequencies," therefore, involved a certain degree of arbitrariness. Errors, however, have been minimized by basing the average values on the largest possible number of the dominant undulations discernible in any given oscilloscope photograph.

In studying the response to residual unbalance, the investigators have observed quasi-cylindrical resonances occurring in a relatively narrow speed interval, one of which was always dominant. These dominant resonances (Figs. 4.5 and 4.18) have been observed to occur approximately at 155 rps and 240 rps. The corresponding values of "natural frequencies" obtained from impact tests have been 135 and 210 cps, as illustrated by the experimental curves B and D in Fig. 4.40.

A comparison of experimental and theoretical data in Fig. 4.40 indicates that the correlation of curves A, B, and C is remarkably good, considering the complexity of the problem. The frequency values of the theoretical curves B and E differ only by a factor involving the square root of the rotor mass, since the calculated stiffness has been

*By increasing, or by decreasing the thrust bearing supply pressure.

identical in both cases. The decrease of "natural frequency" with increasing speed of rotation has not generally been observed in the course of the present experiments. The theoretical curves indicate that the "natural frequency" is a slowly varying function of speed, except at low speeds. In this region, it has been difficult to maintain self-acting support and to obtain experimental data.

An appreciable difference between numerical and experimental results exists in the case of curves D in Fig. 4.40, which corresponds to a foil of relatively high extensional rigidity Et. A plausible explanation of this divergence is the following. The bending rigidity of the foil, $Et^3/12(1-\nu^2)$, which has not been considered in the analysis, has the effect of extending the transition zones between the flat section of the foil and the nearly cylindrical sectors adjacent to the journal and to the foil guides. The smaller the radii of the journal and of the guides, the more pronounced is the effect of bending, especially whenever the distance between the lines of tangency of the foil is commensurately small. The approximate shape of the foil between the journal and the guide is illustrated in the appended diagram, in which the curvature has been purposely exaggerated.

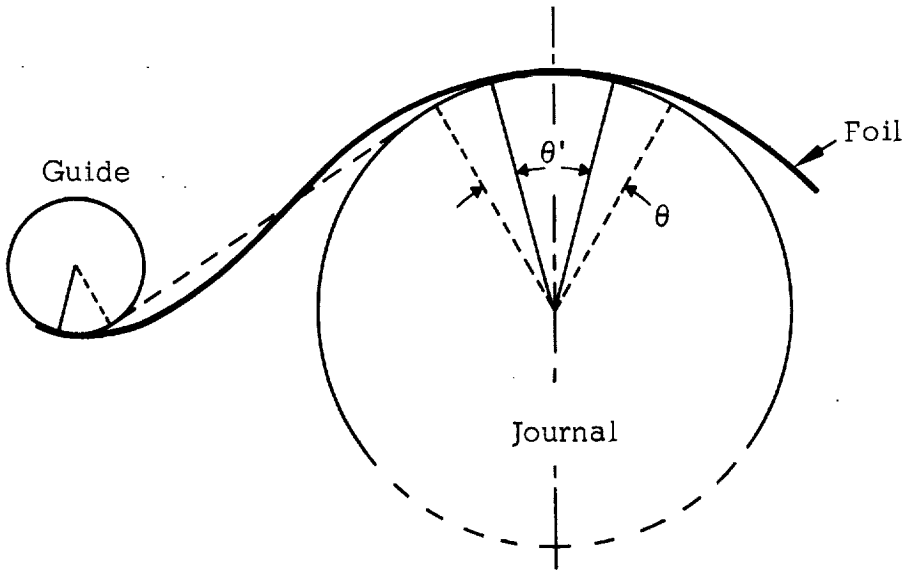

In the case of less flexible foils, the effect of initial curvature is to increase the effective foil length. This additional length, or "slack," is reflected in the magnitude of the clearance, which has been found, paradoxically, to be greater than the gap width obtained with a more flexible foil under identical speed and preload conditions. Since the overall "stiffness" of the foil bearing decreases with increasing thickness of the air film and decreasing thickness of the foil, the cancelling of the foregoing effects may have manifested itself in an apparent insensitivity of the foil bearing to the extensibility of the foil.

The curves in Fig. 4.41 illustrate sequentially the transition from the numerical results based on an early formulation of the problem to those based on the analysis presented in Chapter 5. The four theoretical plots of natural frequency versus rotational speed, starting with the uppermost curve, correspond to the following cases: (a) The flow is purely viscous and incompressible, and the foil segments are clamped along the lines of tangency with the guides (Fig. 2.2). (b) The extension of the foil sector between the lines of tangency with the guides is augmented by an additional foil length in frictional contact with the guides. (c) The effects of fluid inertia and compressibility are included in the fluid-flow equations. (d) The relaxation of tension due to temperature increase with speed is taken into account. The relative contributions of the foregoing effects in lowering the rate of rotor response can be assessed from the displacements of successive curves.

The exerimental foil-bearing parameters and rotor mass, applicable to Fig. 4.41, correspond to curve B of Fig. 4.40, which is reproduced here for the purpose of comparison. In addition, four experimental points, obtained in the course of vibration tests described in the last section of this chapter, have been included in Fig. 4.41. Two values, 150 cps and 173 cps at zero speed, have been recorded with the rotor in

contact with the preloaded foil.* Two other points, 132 cps at 666 rps and 129 cps at 800 rps, correspond to unidirectional, sinusoidal excitation of amplitude $G_y = 0.5\,g$. Finally, the fifth point, at 155 rps, corresponds to the major resonance observed in determining the response to residual unbalance (Fig. 4.5).

G. Response to Sinusoidal Excitation

This section deals with the determination of the response of the foil-rotor system to unidirectional, sinusoidal excitation by means of a vibrator (shake table). The instrumentation and auxiliary apparatus relevant to these experiments have been described in the preceding chapters. Pictorial views of the test apparatus and of the vibrator are presented in Fig. 2.9 and Fig. 2.10.

The foil-rotor assembly was supported in a rigid frame, securely attached to a sturdy magnesium plate. The plate was floated hydrostatically on a massive granite table and a thin film of oil and was firmly bolted to the exciter head. All experiments were conducted with rotors mounted in the vertical attitude. The direction of excitation was normal to the rotor axis and along the bisector of the bearing segment opposite the foil lock (Fig. 2.2). Two rotors, of 1.0 lb and 2.390 lb weight** respectively, have been used in the vibration experiments. A stainless steel foil, 0.001" x 1.0", preloaded to 2.0 lb/in, has been used with both rotors.

All capacitance probes were rigidly secured by means of special adaptors, in order to prevent relative motion between the probes

---

*Discontinuities of amplitude, characteristic of "softening" springs, have been observed at 150 cps and 173 cps.

**The difference in weight between this rotor and the rotor used in previous experiments was 1%.

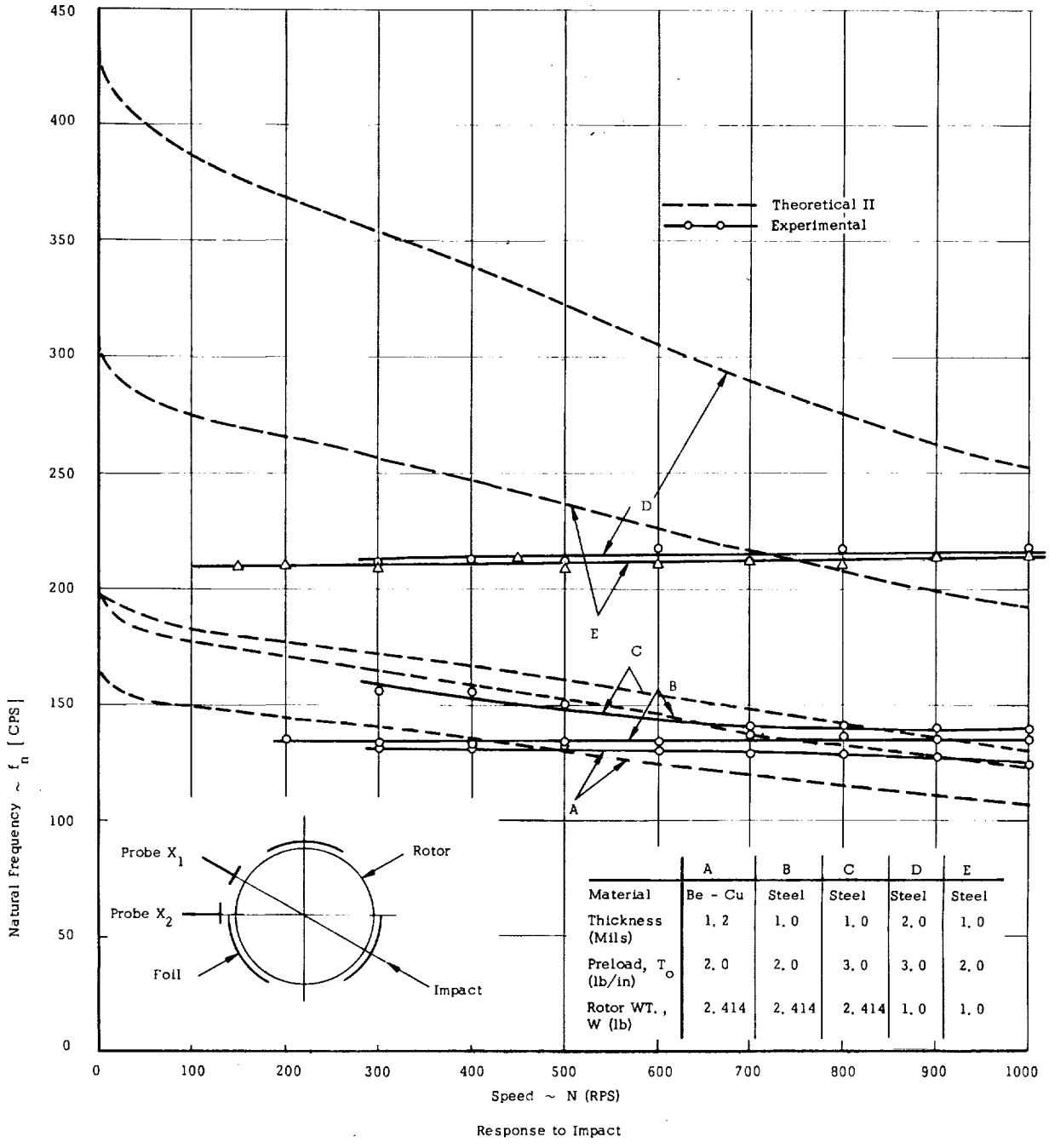

Fig. 4.40 "Natural Frequencies" of Foil-Bearing Supported Rotors as a Function of Speed

Table 4. 14 "Natural Frequencies" of Foil-Bearing Supported Rotors as a Function of Speed

A		B		C		D		E	
Foil: Be - Cu; 0. 0012" x 1" Preload: T_o = 2. 0 lb/in Rotor: W = 2. 414 lb		Foil: Steel; 0. 001" x 1" Preload: T_o = 2. 0 lb/in Rotor: W = 2. 414 lb		Foil: Steel; 0. 001" x 1" Preload: T_o = 3. 0 lb/in Rotor: W = 2. 414 lb		Foil: Steel; 0. 002" x 1" Preload: T_o = 3. 0 lb Rotor: W = 1. 0 lb		Foil: Steel; 0. 001" x 1" Preload: T_o = 2. 0 lb/in Rotor: W = 1. 0 lb	
Speed	f_n	Speed	f_n	Speed	f_n	Speed	f_n	Speed	f_n
RPS	CPS	RPS	CPS	RPS	CPS	RPS	CPS	RPS	CPS
300	131	200	135	300	156	300	211	150	209
400	131	300	133	400	155	400	212	200	210
500	132	400	132	500	150	500	211	300	209
600	130	500	133	600	-	600	216	450	213
700	128	600	133	700	140	700	211	500	209
800	128	700	136	800	140	800	216	600	210
900	126	800	135	900	139	900	213	700	212
1000	123	900	134	1000	138	1000	216	800	210
		1000	134					900	212
								1000	213

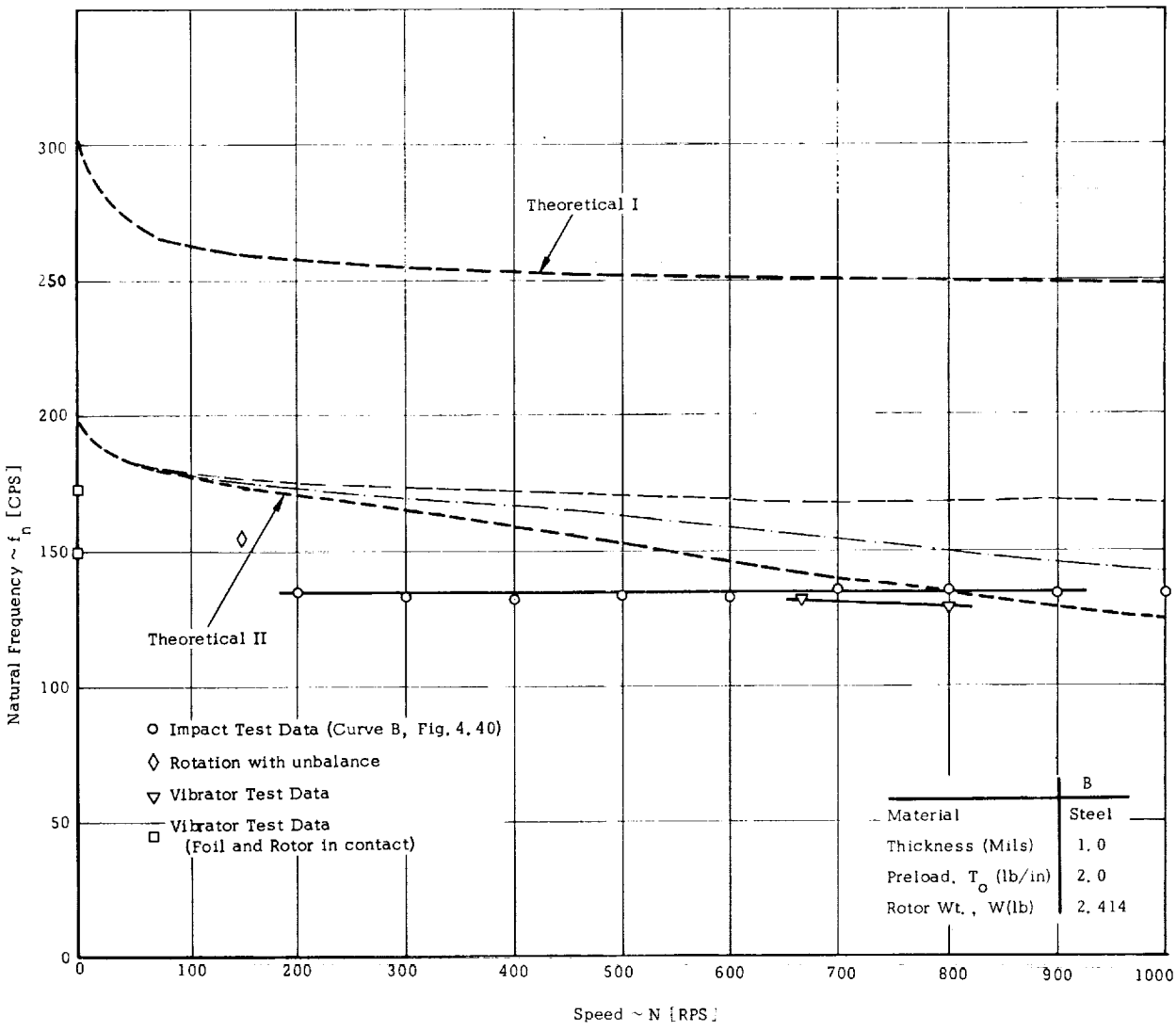

Fig. 4.41 "Natural Frequencies" of Foil-Bearing Supported Rotor; - Comparison with Theory

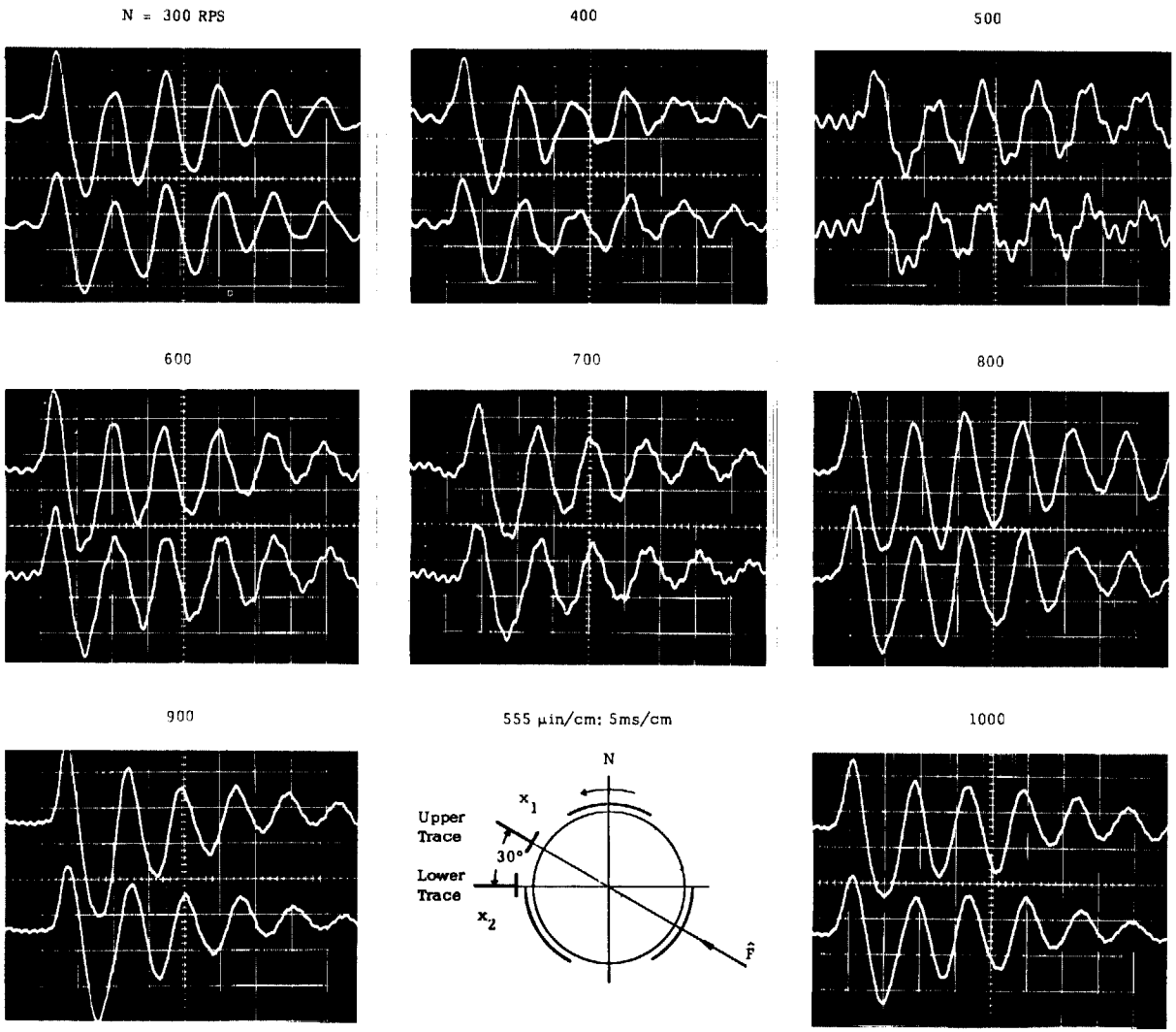

Foil: Be - Cu: 0.0012" x 1"; T_o = 2.0 lb/in

Rotor: W = 2.414 lb

N = Rotor Speed (RPS)

$\hat{F}$ = Impact to Housing (Center of Rotor and along X_1)

Fig. 4.42 Response to Impact at Various Rotor Speeds

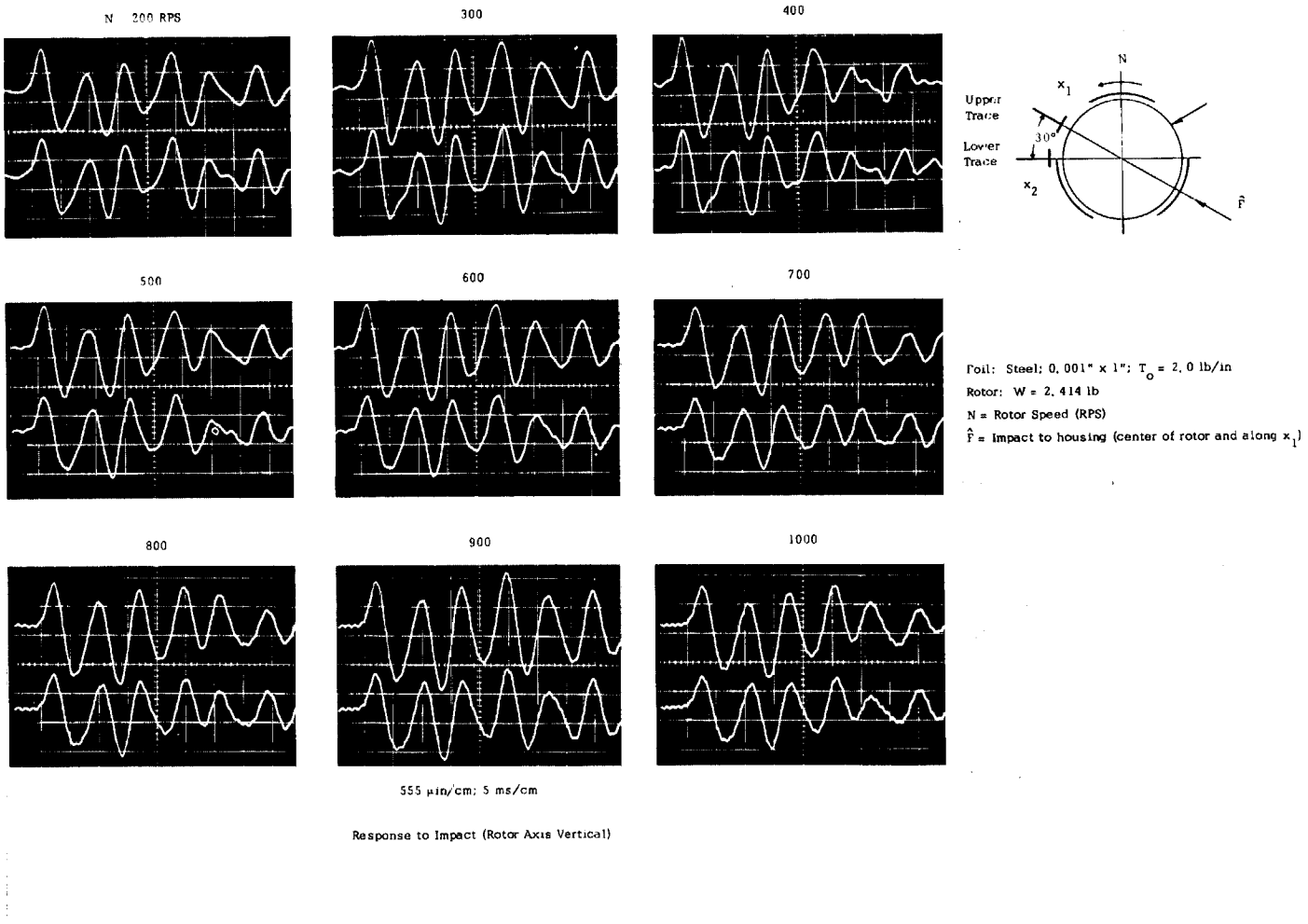

Fig. 4.43 Response to Impact at Various Rotor Speeds

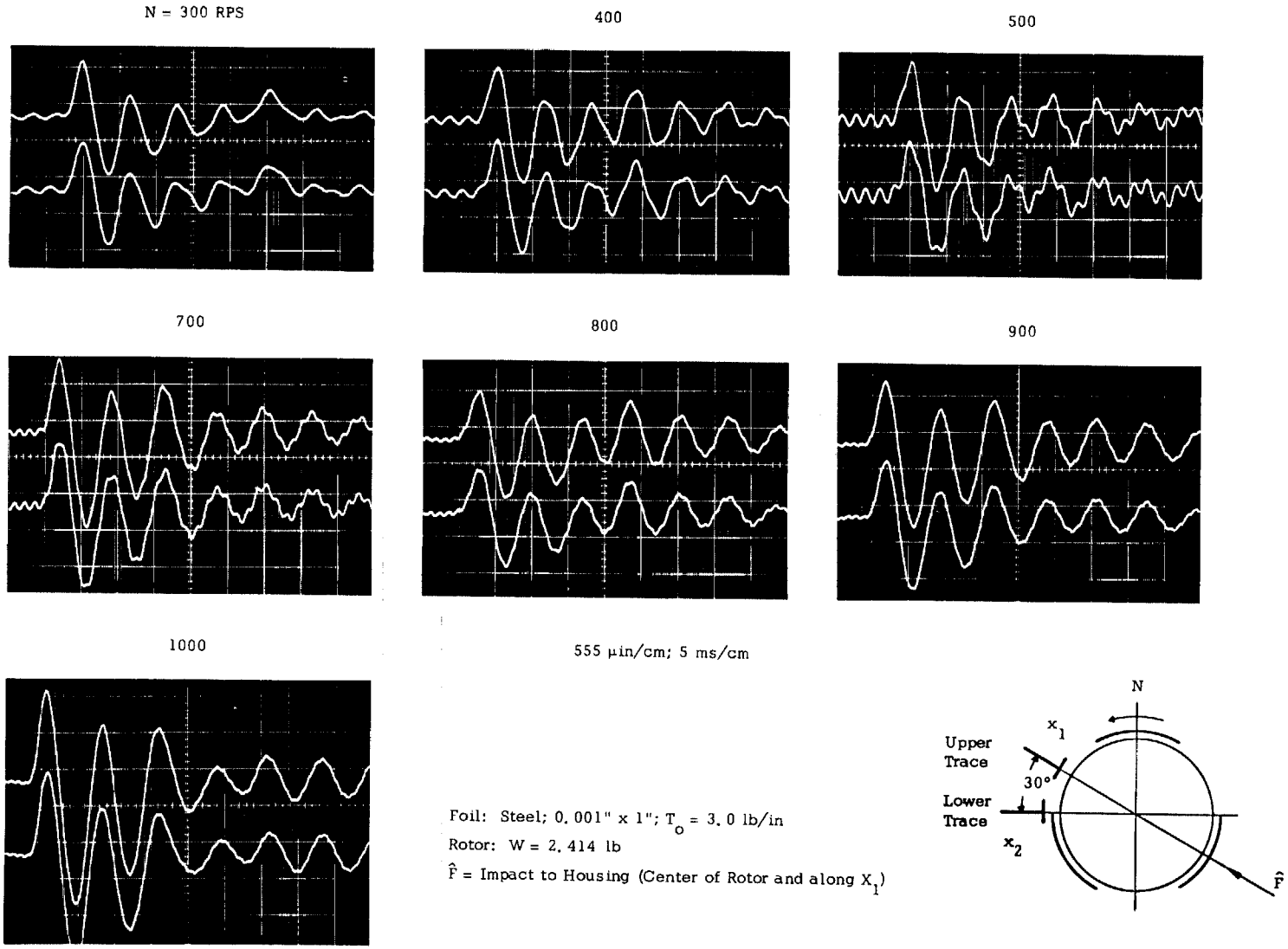

Fig. 4.44 Response to Impact at Various Rotor Speeds

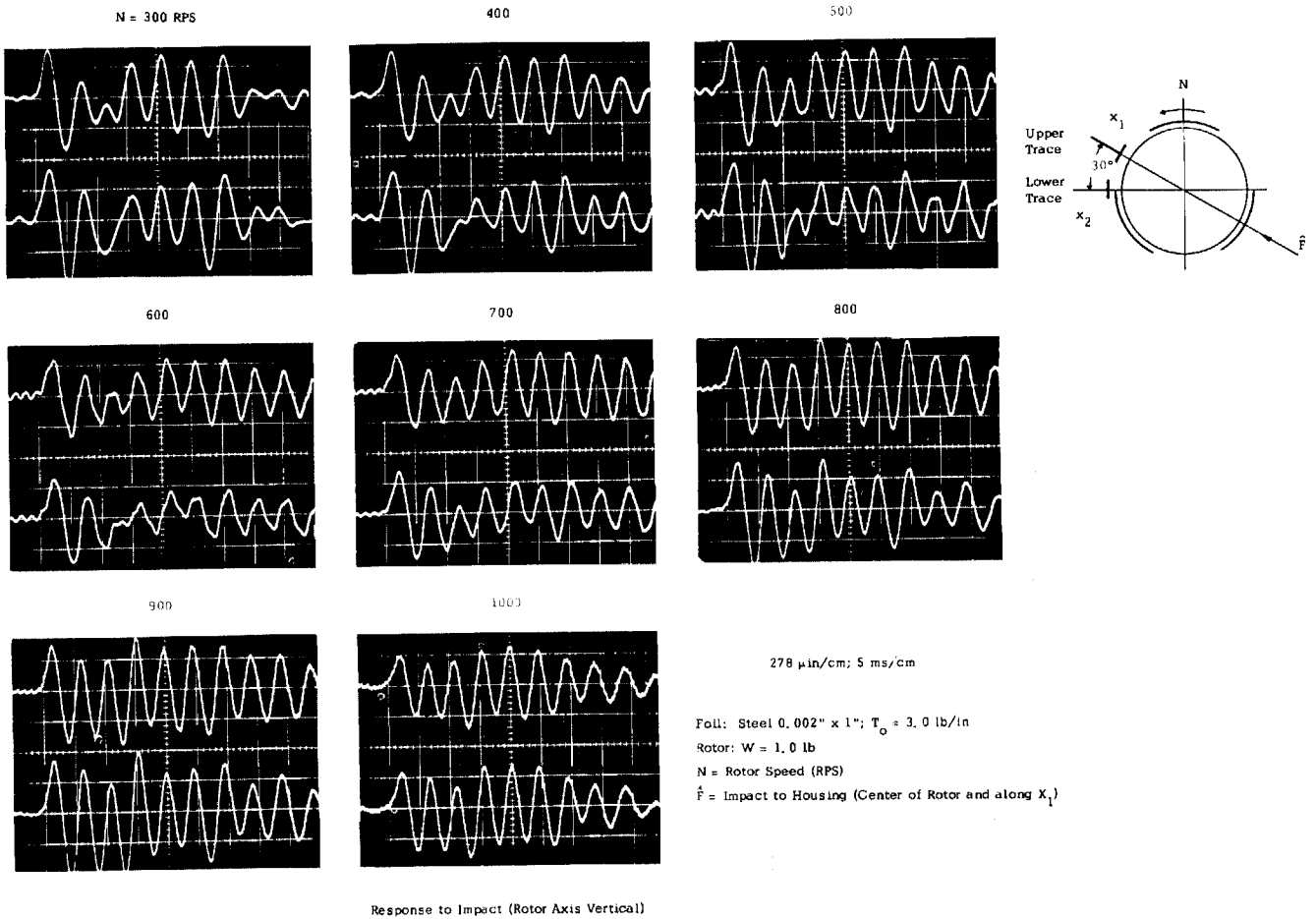

Fig. 4.45 Response to Impact at Various Rotor Speeds

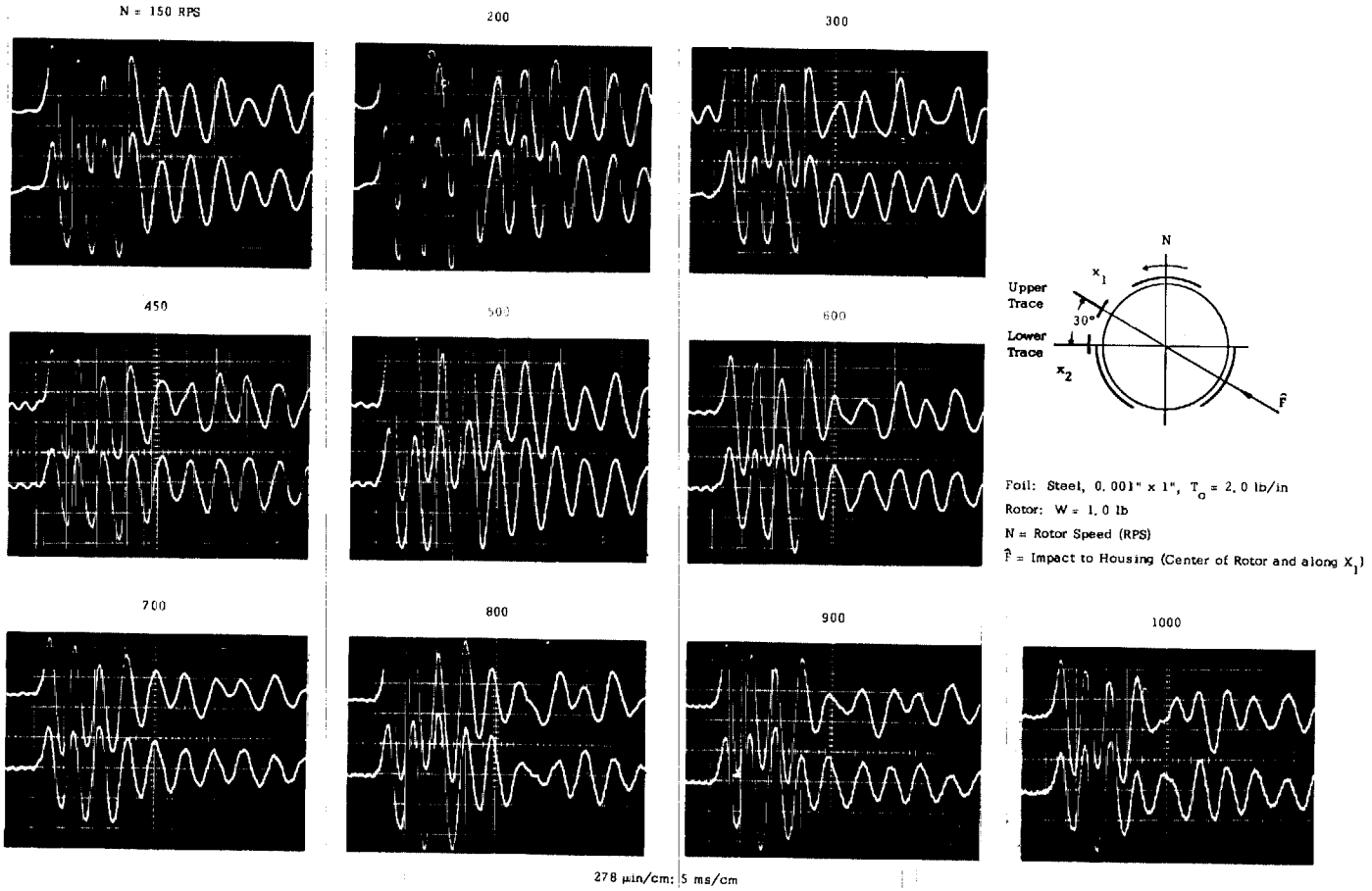

Fig. 4.46 Response to Impact at Various Rotor Speeds

and the housing. Preliminary tests have been conducted to ascertain the extent of angular motion of the rotor, when excited by the vibrator. No measurable degree of pitching, however, has been detected, even at frequencies of excitation corresponding to previously established resonances in the conical mode. The in-line motion of the vibrator was controlled by the output of the in-line accelerometer, but no control could be exercised with respect to spurious, transverse and vertical components of motion. The outputs of three accelerometers, mounted orthogonally on the rotor housing, indicated that the motion in the direction of the oil-floated plate was negligible at all frequencies of excitation. The transverse component of motion was also negligible for frequencies of excitation lower than 425 cps. At higher frequencies of excitation, the motion was characterized by a series of transverse resonances. Between these resonant peaks, the ratio of transverse to in-line excitation was generally of order 0.05 to 0.15. With the exception of measurements of the response by continuous scanning of the frequency range, the amplitudes of motion have been determined at discrete points corresponding to the minima of transverse excitation.

The definition, "Response to Sinusoidal Excitation," requires additional qualification, since it implies a purely sinusoidal motion of single amplitude and frequency of the entire housing. The vibrator and the entire assembly constituted a complex, distributed-parameter system, which received two inputs - one from the exciter, and the other from the turbine-driven rotor. The latter imparted to the housing a relatively high level of excitation, the main components of which could be related to multiples of the rotational speed, such as the number of turbine buckets (32), pressurization orifices (24 pairs), nozzles (6), and several others. In order to gain satisfactory feedback control of the exciter through the output of the in-line accelerometer, and in order to "separate" the input of the vibrator from the high-frequency, low-amplitude components

of excitation transmitted to the housing by the rotor, the outputs of the accelerometers has been filtered to a low-pass bandwidth, 6000 cps.* Since the objective was to control and to monitor the g-input at points closest to the foil supports, the accelerometers were mounted directly on the housing, rather than at other locations of the vibrated assembly. The filtered accelerometer outputs remained largely undistorted, except, and unavoidably, in the vicinity of foil-rotor resonance.

The vibrator (shake-table) tests involved three types of experiments: (a) the determination of the frequency response of rotors at 40,000 rpm and 60,000 rpm; (b) the determination of the response at resonance and at variable level of excitation; and (c) the determination of the response at variable level of excitation and frequency equal half the rotational speed. The motivation of experiments (a) and (b) is self-evident. Experiments (c) have been performed in order to ascertain that excitation of foil-bearing supported rotors at frequencies $f_e = N/2$ did not produce large amplitudes of motion, a condition invariably associated with other types of fluid-film bearings. In addition to the foregoing experiments, the response of a stationary rotor has been studied when supported in a pressurized foil bearing and when in contact with a preloaded foil.

It has been convenient to study the response of rotors by means of slow (250 sec) logarithmic scans of the experimental frequency bandwidth. The results are presented in the oscilloscopes of Figs. 4.52, 4.60, and 4.61. Each of the foregoing oscillograms contains traces of outputs of in-line and transverse capacitance probes and of corresponding accelerometers. The positions of foil-bearing sectors, probes, and accelerometers relative to the vibrator are illustrated in the schematic diagram appended to each figure. The response of the 1.0 lb rotor, subjected

*The experimental frequency range of excitation was 50 - 2000 cps.

to an excitation $G_y = 1.0\,g$ at N = 1000 rps, is presented in Fig. 4.52. The in-line and transverse resonances occurred within a narrow frequency bandwidth centered approximately at 235 cps. The maximum in-line excursion of the rotor was approximately 1500 μin, as compared with a maximum of 610 μin in the transverse direction. The reader will note that the G_x trace reflects a series of structural resonances in the range $425 < f_e < 2000$ cps. The effect of the latter on the controlling accelerometer G_y has been relatively small, indicating that the exciter responded satisfactorily in maintaining a sensibly constant in-line input to the housing. The effect of rotor resonance is also reflected in the traces of accelerometer outputs. The combined electro-mechanical noise level has been taken into account in scaling the amplitudes of motion and of excitation from the oscillograms.

A similar oscillogram, presented in Fig. 4.60, refers to a 2.390 lb rotor, subjected to an excitation $G_y = 0.5\,g$ at N = 1000 rps. Closely spaced resonances occurred in the vicinity of $f_e \approx 130$ cps, and the maximum in-line and transverse amplitudes were of order 2550 μin and 1550 μin. A minor resonance at one-half the frequency of the major resonance can also be discerned in Fig. 4.60 and, to a lesser extent, in Fig. 4.52.* The physical parameters and test conditions relevant to the oscillograms of Fig. 4.60 and 4.61 were identical, except that a lower rotational speed, N = 666 rps, corresponded to the last figure. Referring to Figs. 4.60 and 4.61, it can be seen that resonances occurred at nearly identical frequencies of excitation ($f_e \approx 130$ cps), but that the resonant amplitudes were smaller by approximately 20% at the lower speed of rotation. The response at N = 666 rps was also characterized by a minor resonance at one-half the frequency of the major resonance. All traces

*The orbit of the minor resonance is characterized by a loop, which corresponds to a second ultraharmonic. This ultraharmonic resonance is similar to the behavior observed in the pressurized mode of operation (see Sec. C).

of in-line response in the foregoing scans display a secondary peak in the region of resonance, and the transverse resonance appears to decay almost discontinuously with increasing frequency. The in-line and transverse resonances occur at nearly the same frequency and the interaction of the two modes of motion is appreciable. The gross character of the response is similar to that of a damped, linear oscillator with two degrees of freedom.

The study of response by means of slow logarithmic scans, and at discrete frequencies of excitation, has also been applied in the case of rotors supported in an externally pressurized foil bearing, in the absence of rotation. An analogous experiment concerned the determination of the response of rotors when in contact with a preloaded foil. Fig. 4.57 contains oscilloscope photographs of a rotor orbit and of the complementary timebase displays of monitoring probes. The case corresponds to the resonance of a 1.0 lb rotor at zero speed when supported in a pressurized foil bearing and excited at $G_y = 0.5g$. Pressurization at 24 psig produces a gap width commensurate with that generated by self-acting effects at N = 1000 rps. A comparison of resonant frequencies for N = 1000 rps (self-acting) and N = 0 (pressurized) shows the latter to be greater by nearly 25%. The reader will note in Fig. 4.57 that the X-component of motion is small compared with the in-line component. The quasi-elliptical orbit is oriented in the direction of excitation and the phase between the in-line motion of the housing and of the rotor in passing through the resonance is nearly 90^{o}.

The response of the 2.390 lb rotor, supported under identical conditions in a pressurized foil bearing, is presented in Fig. 4.62. The resonant peak corresponds to a frequency of excitation $f_e = 178$ cps, which is approximately 35% greater than the resonant frequency of the self-acting system at N = 1000 rps. In the immediate vicinity of the

resonant peak, the orbit oscillated very slowly between the extreme positions shown in the photograph of Fig. 4.62. The reader will observe a very rapid increase of amplitude in approaching the resonant peak from the left and the comparatively gentle subsidence of amplitude to the right of the resonant peak. The oscillogram in Fig. 4.62 is similar in this respect to a response curve of a nonlinear oscillator characterized by a "softening spring." This trend is even more pronounced in the oscillogram presented in Fig. 4.63. In this case, the 2.390 lb rotor remained in contact with the preloaded foil. A characteristic "jump" phenomenon has, indeed, been observed in this test. Increasing the frequency of excitation, the amplitude changed in a discontinuous manner from a low value to approximately 910 μin at f_e = 173 cps. Decreasing the frequency, an amplitude of nearly 1160 μin was attained at f_e = 150 cps, following which a sudden drop to a low value was observed.

The response to residual unbalance (Section B) has been characterized by a multiplicity of conical and cylindrical resonances, which involved interactions of thrust and foil bearings. The study of the response to unidirectional excitation at various rotor speeds revealed that the foil-rotor system was characterized essentially by a single resonance in the low frequency range and that no other resonances occurred up to 2000 cps. In order to examine the motion of the foil-rotor system in greater detail, the 1.0 lb rotor has been subjected to excitation at discrete frequency intervals, in the range 50 to 1000 cps. The experiments have been carried out at two speeds of rotation, 40,000 and 60,000 rpm, and at a 0.5 g amplitude of excitation. The measurements involved a determination of the in-line and transverse amplitudes of the rotor and of phase between the in-line motion of the rotor and of the housing. The results are presented graphically in Fig. 4.48 and Fig. 4.50, and numerically in Table 4.15. The measurements have been obtained from the oscilloscope records in Fig. 4.49 and Fig. 4.51. Two sets of photographs

are presented in each of the foregoing figures. The first set of photographs contains traces of outputs of the in-line and transverse capacitance probes and the output of the in-line accelerometer. The second set of photographs illustrates the orbital motion of the rotor at various frequencies of excitation, including the frequency of in-line resonance, which is nearly coincident with the transverse resonance of the system.

It can be seen that the rotor describes an orbit only in the vicinity of the resonant frequency, and then only at the higher of the two rotational speeds (1000 rps). In all other cases, the motion is nearly colinear with the direction of excitation. A slight change of the inclination of the quasi-rectilinear path can be discerned before and after resonance. The reader will note the 180° phase shift between the timebase displays of the in-line capacitance probe and of the accelerometer. The modulating ripple of capacitance-probe outputs reflect the small, orbital motion of the rotor and reveals, upon closer examination, the presence of several subharmonics. Although components of excitation of frequency higher than 6000 cps have been filtered in the accelerometer output, the lower frequency components, transmitted by the turbine-driven rotor to the housing, are reflected in the waveform of the accelerometer trace. The excitation frequencies in the interval $400 < f_e < 1000$ cps have been selected to correspond to the minima of transverse acceleration, i.e., to small G_x/G_y ratios.

The response curves presented in Fig. 4.48 and Fig. 4.50 indicate that the maximum amplitudes of motion at N = 1000 rps and N = 666 rps did not differ appreciably, although the transverse component of motion at resonance appears to have been greater at 1000 rps than at 666 rps. Both figures contain complementary graphs of the variation of phase in the frequency bandwidth centered about the resonance. The phase angle is nearly 90° when A_y is maximum.

The resonant frequencies of the self-acting system appeared to have been influenced by the rotor mass, rather than by the speed of rotation. The vibration experiments have been considerably involved and difficult, and it has not been possible to include additional variations of parameters in the study of response of foil-bearing supported rotors. The rigidity of the foil has not been varied, and its effect in a given bearing configuration is not yet fully understood. In the case of the 0.001" x 1.0" steel foil used in the vibration test, the correlation of the predicted resonant frequencies, both theoretical and based on impact test, with those obtained in the course of the present experiments has been satisfactory. In the speed range $666 < N < 1000$ ips, the deviations of the theoretical results from the mean value of experimental determination are in the order 4% to 9%.

It is instructive to assess the influence of mass and of damping in analogy to a linear system. The question posed is the following: Given two rotors of unequal mass, supported in identical foil bearings and subjected to equal g-levels of excitation at their respective resonant frequencies, what is the ratio of resonant amplitudes? In the case of simple, damped oscillators, the amplitude ratio is given by $Y_R = M^{3/2}/K^{1/2}C$, in which M, K, and C are respectively the mass, stiffness, and damping ratios. Assuming that the last two parameters are identical for both systems, the amplitudes stand in the ratio $M^{3/2}$. The critical damping ratio of a simple oscillator is given by $C/C_c = G_y/8\pi^2 f^2 y_r$, in which G_y, f_r, and y_r are the amplitude of excitation, the resonant frequency and the resonant amplitude. Forming the ratio of resonant amplitudes A_y (Fig. 4.48 and Fig. 4.60) and comparing it to the mass ratio raised to the power 3/2, it is found that the amplitudes stand in the ratio of approximately 3, as compared with $(M)^{2/3} = 3.7$. Also, if the data presented in Fig. 4.48 and Fig. 4.60 were to apply to a linear system, the critical damping ratio in both cases would be of order 0.06. Comparisons of this kind may be useful,

inasmuch as they provide at least a crude measure in estimating the influence of various physical parameters, but the analogy should not be construed as a literal interpretation of foil-bearing behavior. It is not suggested here that the foil-rotor system is either simple or linear. Even if it were possible to represent the periodic motion in terms of a second order differential equation, the dependence of "stiffness" and "damping" on displacement and on velocity would have to be taken into consideration.

The complexity of motion is illustrated in Fig. 4.54 and Fig. 4.65. The latter contains oscilloscope photographs of orbital motion of the 1.0 lb rotor and of the 2.390 lb rotor when subjected to increasing amplitudes of excitation at resonance. The procedure followed in this series of experiments has been the following: A constant level of in-line excitation was maintained and the excitation frequency was increased until the in-line amplitude of motion was maximum. The amplitude of in-line excitation was then increased and the experiment repeated. The maximum amplitudes of excitation, G_y, applied to the 1.0 lb rotor and to the 2.390 lb rotor have been 1.0 g and 0.5 g. The frequency of in-line resonance has been recorded for each run.

The in-line and transverse resonances do not occur at exactly the same frequency, although both are located within a very narrow frequency bandwidth. The maximum transverse amplitude, therefore, does not coincide exactly with the frequency of in-line resonance. The strong interaction of the two modes of motion and the ensuing phase changes in a narrow frequency bandwidth were reflected in large changes of orbit size and attitude for small frequency increments. Also, the frequency of in-line resonance varied slightly with the amplitude of excitation.

The reader will undoubtedly note the unusual form of orbits, particularly of the 2.390 lb rotor (Fig. 4.65). In this case, the paths bear no resemblance at all to elliptical orbits of harmonic motion. The experiments

have been carried out at two speeds of rotation, N = 666 rps and N = 800 rps, and larger amplitudes of motion have been observed at the lower of the two speeds. The manner in which the orbits vary with increasing level of excitation has been very similar at both speeds, and the progressive elongation, widening, and curvature increase of the "Joukowski airfoil"-like orbits has been quite consistent. The timebase displays of outputs of the in-line accelerometer are shown in the right hand side of Fig. 4.65. It can be seen that, at resonance, the excitation of the housing by the vibrator was augmented by higher frequency components of excitation. The latter subsided in parallel with the amplitude of the rotor on both sides of the resonant frequency bandwidth. The unavoidable interaction of vibrator and rotor inputs to the housing is complex and varies with the level of excitation.

An analogous set of photographs is presented in Fig. 4.54 for the 1.0 lb rotor. The experimental runs correspond to rotational speeds of N = 666 rps and N = 1000 rps.* The maximum amplitude of excitation applied to the 1.0 lb rotor was 1.0 g, as compared with 0.5 g for the 2.390 lb rotor. As anticipated, the decrease of rotor mass resulted in an appreciable reduction of resonant amplitudes of motion at equal amplitudes of excitation. In addition, the motion of the 1.0 lb rotor differed qualitatively from the motion which has been observed with the 2.390 lb rotor. At N = 666 rps, for example, the path of the 1.0 lb rotor remained nearly colinear with the direction of excitation up to G_y = 0.9 g. A transition occurred above 0.8 g, but the orbits at 0.9 g and 1.0 g differed in inclination, curvature, and symmetry from the corresponding orbits at N = 1000 rps. Furthermore, at N = 1000 rps, the motion of the 1.0 lb rotor along elongated orbits could be observed at all levels of excitation and did not degenerate to rectilinear motion along the line of excitation. From qualitative point of view, the motion of both rotors has been similar at all speeds, with

*The reason for using a lower speed, N = 800 rps, in the case of the 2.390 lb rotor is due to an inadvertent miscalculation. Both rotors, however, have been subjected to variable excitation at N = 666 rps.

the exception of the characteristics displayed by the motion of the 1.0 lb rotor at N = 666 rps.

It has been pointed out in Section D of this chapter that the foil-rotor system was only approximately symmetrical with respect to the line along which the excitation G_y has been applied. In addition, small spurious components of transverse excitation have also been present, as by-products of inputs stemming from both the vibrator and the air-driven rotor. But neither initial dissymmetries nor relatively small components of transverse excitation could possibly account for the modes of motion depicted in Fig. 4.54 and Fig. 4.65. It is more likely that the orbital motion which has been observed was a consequence of strong coupling between the in-line and transverse motions and that the effect of nonlinearities have become particularly pronounced at resonance, when the excursions of the rotors have been large.

The data pertinent to Figs. 4.54 and 4.65 is presented graphically in Figs. 4.53 and 4.64 and numerically in Tables 4.16 and 4.19. The reader should take note that, of the two peak-to-peak amplitudes, $2A_y$ and $2A_x$, only the in-line amplitude $2A_y$ is maximum, since the resonance of the transverse motion occurred at a slightly higher frequency than the in-line resonance. It can be seen that the rate of increase of $2A_y$ with G_y diminished perceptibly at higher g-levels of excitation and that the deviation of resonant frequency from a constant value was very small. In the case of the 1.0 lb rotor, the amplitudes of motion appear to have undergone a discontinuous change between $G_y = 0.4\,g$ and $G_y = 0.5\,g$. At N = 666 rps, the transverse motion of the 1.0 lb rotor remained negligibly small in comparison with the in-line component below $G_y \approx 0.7\,g$, but at N = 1000 rps the transverse motion was pronounced at all levels of excitation. Equal excitations G_y resulted in nearly equal excursions $2A_y$ of the 1.0 lb rotor at both speeds. In the case of the 2.390 lb rotor, the in-line amplitude of motion $2A_y$ at N = 666 rps exceeded in magnitude the corresponding amplitudes at N = 800 rps by approximately 20% to 30%. The ratios of transverse and in-line components of motion of the 2.390 lb rotor have been found to be appreciably greater than those of the 1.0 lb rotor.

It is of interest to assess again the effect of rotor mass on the magnitude of resonant amplitudes. Both rotors have been supported in identical foil bearings and both have been subjected to variable excitation at resonance at a speed of rotation N = 666 rps. Referring to Figs. 4.53 and 4.64, it will be noted that the ratio of resonant amplitudes $2A_y$ increases from approximately 3, at $G_y = 0.5\,g$, to approximately 4, at $G_y = 0.2\,g$. It will be recalled that, in an analogous linear system, the amplitude ratio varies as the mass ratio to the power 3/2. For the case at hand, this gives a resonant amplitude ratio of 3.7. It would appear, therefore, that nonlinearities could be helpful in limiting excursions of heavier rotors at resonance.

Under steady-state conditions and at 666 rps, the foil-bearing clearance was of order 750 μin. At resonance and at excitation $G_y = 0.5\,g$, the maximum amplitude attained by the 2.390 lb rotor has been 2500 μin, or 3.3 times the steady-state gap width. It is rather remarkable that the foil-rotor system suffered no adverse effects under prolonged excitation and that it continued to operate satisfactorily.

It is well known that large amplitudes of motion invariably occur when rotors supported in rigid-surface, fluid-film bearings are excited at frequency equal one-half the rotational speed. This phenomenon has been theoretically predicted and experimentally confirmed by many investigators. It has been observed with self-acting bearings, liquid and gas lubricated journal bearings of various configurations: plane, herringbone grooved, floating sleeve type, and many others. In the course of the present experiments, the investigators have observed neither the type of instability commonly referred to in literature as "half-frequency" or "fractional-frequency" whirl nor the occurrence of large amplitudes of oscillation at frequencies of excitation equal to half the speed of rotation. The logarithmic frequency scans, for example, uncovered no resonances

other than those which have been observed at relatively low frequencies of excitation. The "half-frequency taboos," however, have been so firmly rooted and universally respected in the world of hydrodynamic lubrication that it has been difficult at first to conceive of the foil-bearing as being an exception to the rule.

In order to lend additional support to the contention that excitation at frequency equal half the speed of rotation would not produce the much feared effect, it was decided to subject the 1.0 lb and 2.390 lb rotors to in-line excitation of variable amplitude G_y and of frequency equal exactly to one-half the speed of rotation. The experiments have been performed with both rotors at N = 666 rps and f_e = 333 cps, and at N = 800 rps and f_e = 400 cps. The maximum amplitude of excitation applied in the foregoing experiments has been G_y = 10.0 g, with the exception of the first run attempted with the 1.0 lb rotor at N = 666 rps, in which the maximum amplitude of excitation did not exceed G = 8.0 g.* The results are depicted in the oscilloscope photographs in Figs. 4.56 and 4.67, presented graphically in Figs. 4.55 and 4.66, and tabulated in Tables 4.17 and 4.20.

Referring to Fig. 4.56 and Fig. 4.57, it can be seen that the motion of rotors has been invariably rectilinear and nearly colinear with the direction of excitation. (The photographs in Fig. 4.67 were recorded at higher sensitivity and reflect mainly small, synchronous orbits due to rotating unbalance.) In the case of the 1.0 lb rotor, the speed of rotation had very little effect on the amplitude of motion (Fig. 4.55). In the case of the 2.390 lb rotor, the excursions at equal excitation were 1.6 times greater at N = 666 rps than at N = 800 rps. The amplitudes of motion

---

*The reason for selecting N = 800 rps, rather than N = 1000 rps, has been a more favorable "cross-talk" ratio G_x/G_y at 800 rps. The reason for not exceeding G_y = 8.0 g during the first run was dictated by caution.

increased nearly linearly with the amplitudes of excitation. The same trend has been observed at frequencies other than half the speed of rotation; so, in this respect, the ratio $f_e/N = 1/2$ has no particular significance with regard to foil-bearing supported rotors, regardless of amplitude of excitation.* The amplitude ratios of the two rotors were of order 0.55 at N = 666 rps and of order 0.35 at N = 800 rps.

Although the experiments, wherein the foil-rotor system has been subjected to variable excitation both at resonance and at $f_e = N/2$ are not directly related, it is instructive to contrast the intricacy of motion at resonance (Figs. 4.54 and 4.65) with the simplicity of motion in a frequency interval sensibly far removed from the resonances of the system (Figs. 4.56 and 4.67). The intensity of excitation at resonance has necessarily been reduced, but the amplitudes of motion in both experiments have been commensurately large compared to the steady-state gap width. One is immediately impressed by the complexity and "nonellipticity" of the resonant orbits, undoubtedly due to the nonlinearities of the system, and the nearly exact colinearity of force and displacement at frequencies other than resonant.

H. Velocity of Propagation of a Disturbance Along a Foil

The experiments described in the preceding sections dealt largely with the overall steady-state and dynamic characteristics of the foil-rotor system. Also, because of the complexity of the problem, the theory developed in Chapter 5 has been based on numerous simplifications, including the neglect of time-dependent terms in the fluid-film equations. A number of experiments have, nevertheless, been directed toward a better understanding of some of the more fundamental aspects of foil-bearing dynamics.

---

*In Section H it will be shown that the perennial fraction 1/2 reappears in the foil bearing as the approximate ratio of the velocity of propagation of a disturbance along the foil and the surface speed of the rotor.

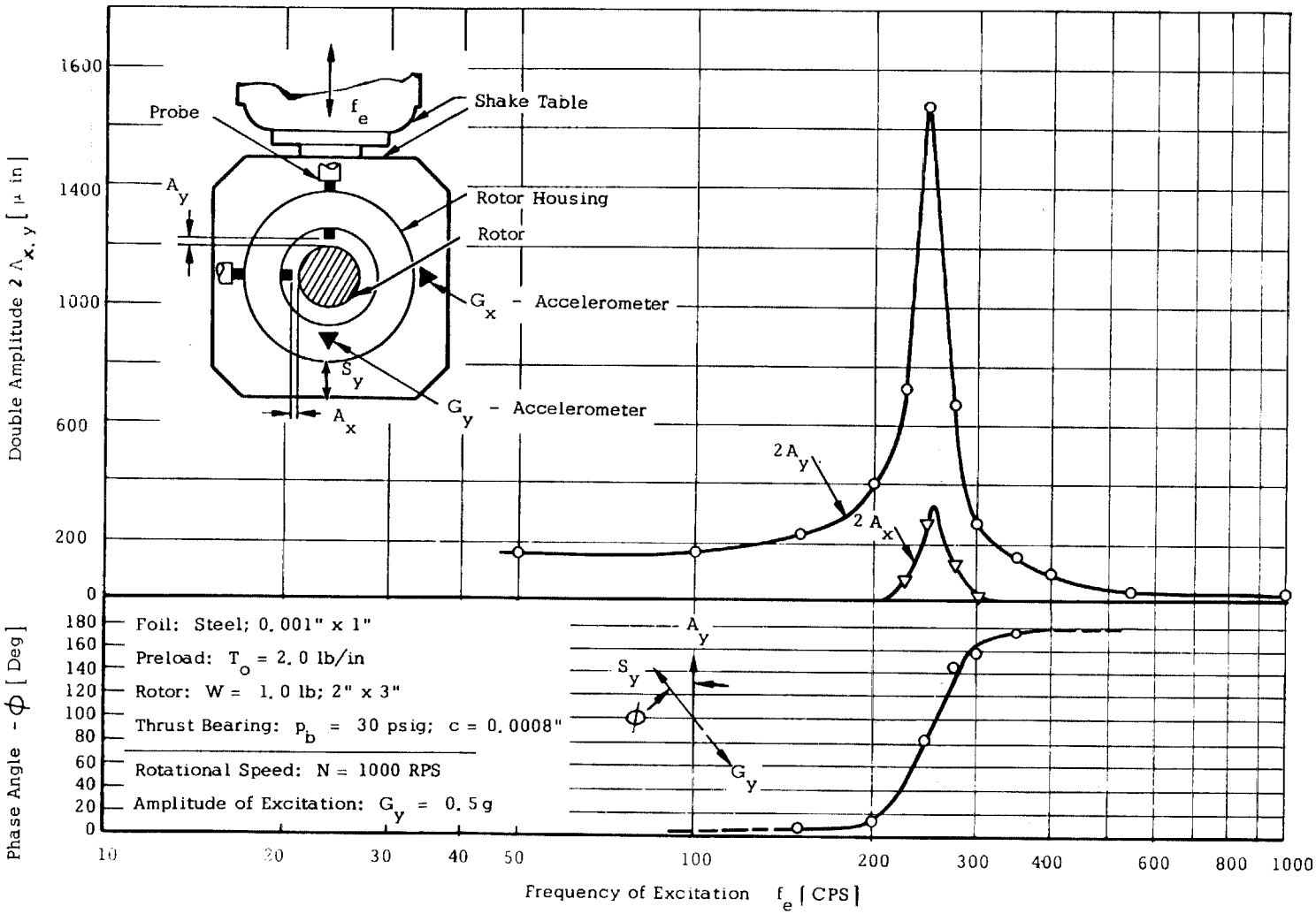

Fig. 4.48 In-Line and Transverse Response of 1.0 lb Rotor to Sinusoidal Excitation (N = 1000 rps)

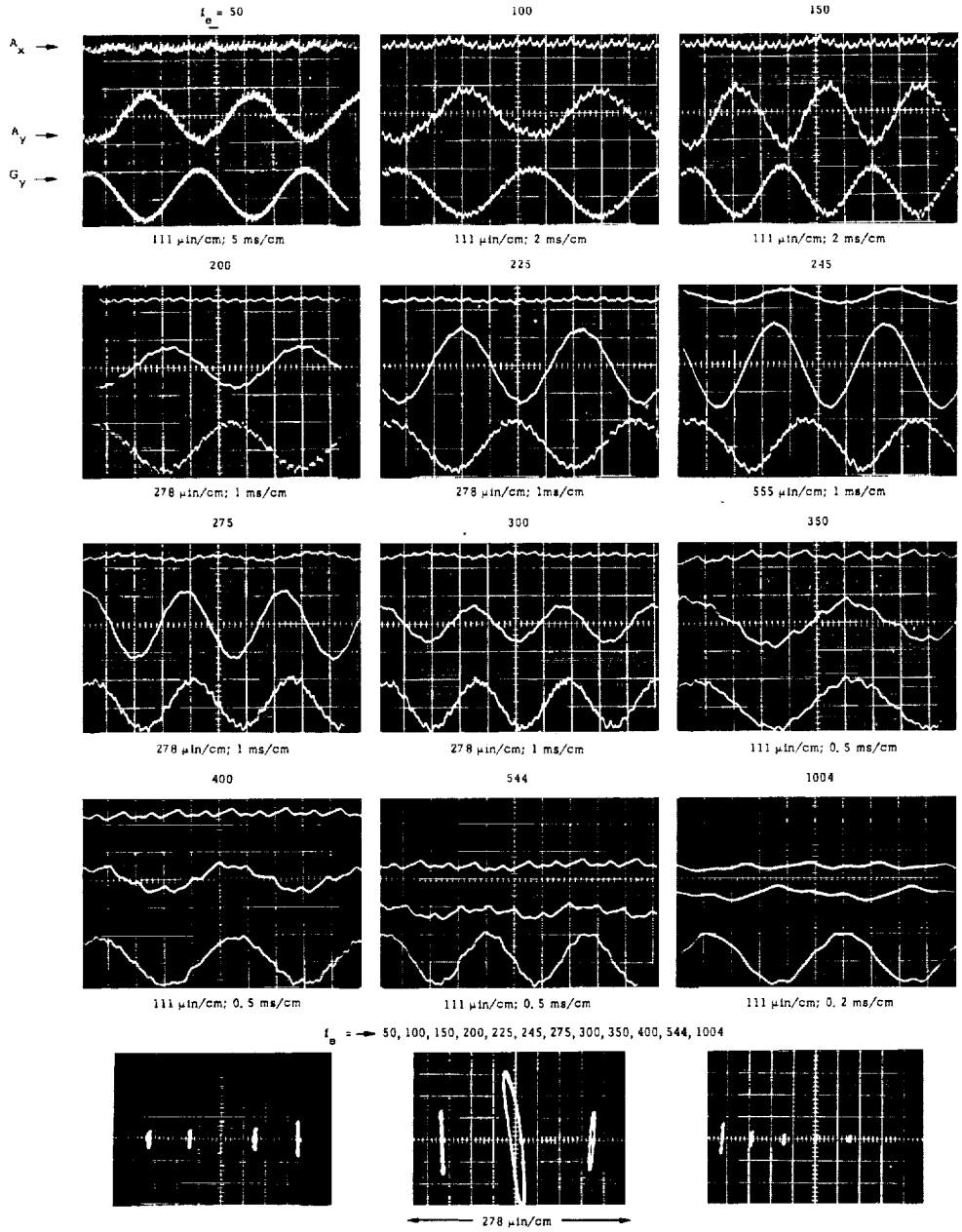

Foil: Steel: 0.001" x 1"
Preload: T_o = 2.0 lb/in
Rotor: W = 1.0 lb; 2" x 3"
Rotational Speed: N = 1000 RPS
Thrust Bearing: p_b = 30 psig; c = 0.0008"
Amplitude of Excitation: G_y = 0.5g

In-Line and Transverse Response of Foil-Bearing Supported Rotor

Fig. 4.49 Motion of 1.0 lb Rotor Induced by Sinusoidal Excitation (N = 1000 rps)

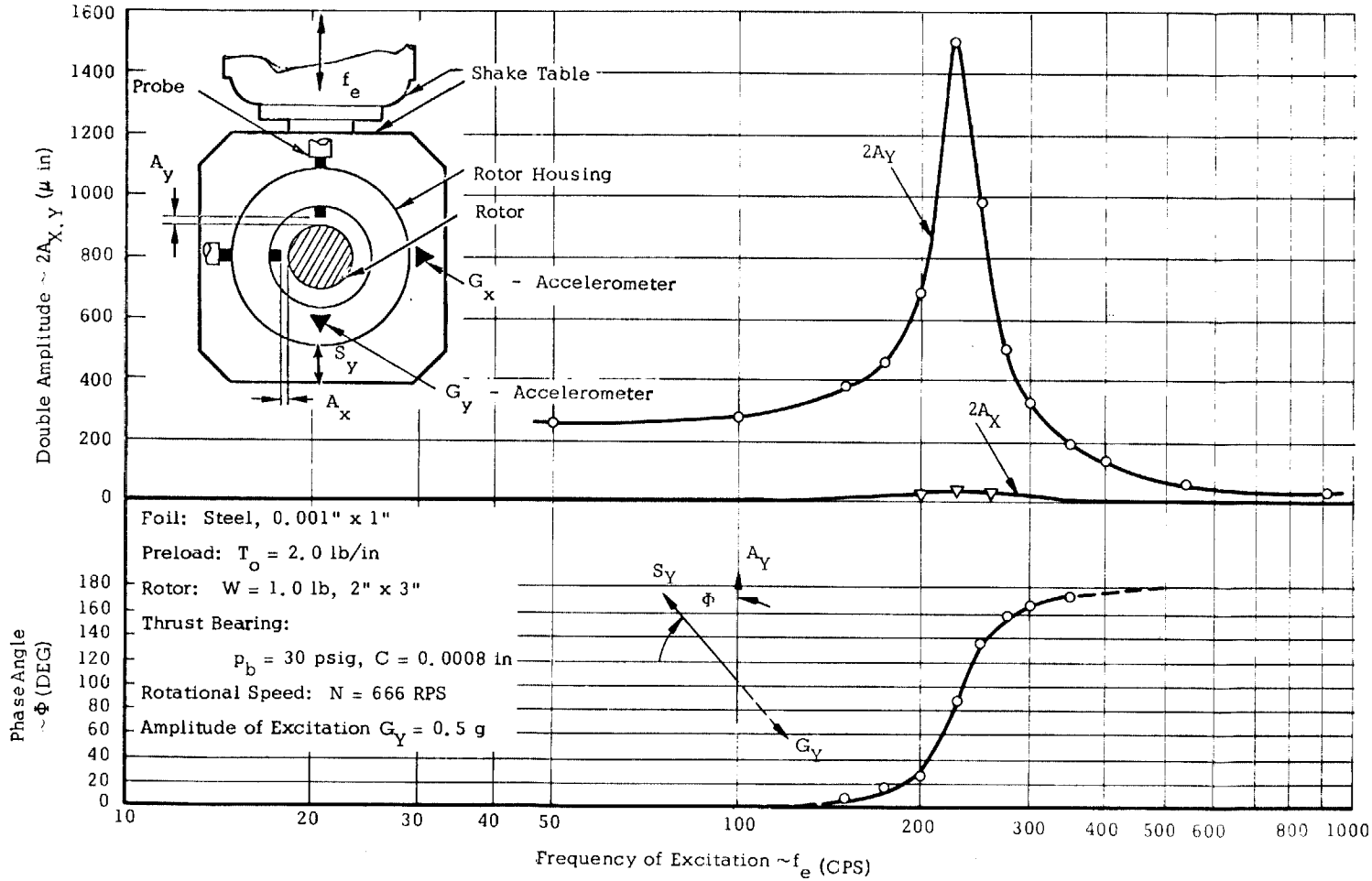

Fig. 4.50 In-Line and Transverse Response of 1.0 lb Rotor to Sinusoidal Excitation (N = 666 rps)

Table 4. 15 In-Line and Transverse Response of 1. 0 lb Rotor to Sinusoidal Excitation

N = 1000 RPS; G_y = 0. 5g

f_e	CPS	50	100	150	200	225	245	275	300	350	400	544*	1004*
$2A_x$	μin	-	-	-	-	70	264	125	14	-	-	-	-
$2A_y$	μin	178	183	233	398	725	1670	670	362	178	100	40	40
Φ	Deg	-	-	8	13	17	81	144	158	176	-	-	-

N = 666 RPS; G_y = 0. 5g

f_e	CPS	50	100	150	175	200	227	250	275	300	350	400	538*	914*	1014*
$2A_x$	μin	-	-	-	-	15	30	15	-	-	-	-	-	-	-
$2A_y$	μin	255	270	360	445	680	1490	970	490	310	178	123	45	25	65
Φ	Deg	-	-	6	13	25	86	131	154	163	170	-	-	-	-

N = Rotational Speed

G_x = Transverse Amplitude of Excitation; A_x = Transverse Amplitude of Rotor Response

G_y = In-Line Amplitude of Excitation; A_y = In-Line Amplitude of Rotor Response

Φ; Phase Angle between Y-Amplitudes of Motion of Housing and of Rotor

Foil: Steel; 0. 001" x 1"

Preload: T_o = 2. 0lb/in

Rotor: W = 1. 0 lb; 2" x 3"

Thrust Bearing: p_b = 30 psig; C = 0. 0008 in

Note: G_y controlled; $G_x \approx 0$ for $f_e < 400$ CPS; A speeds denoted by (*) $0.15 < \frac{G_x}{G_y} < 0.25$

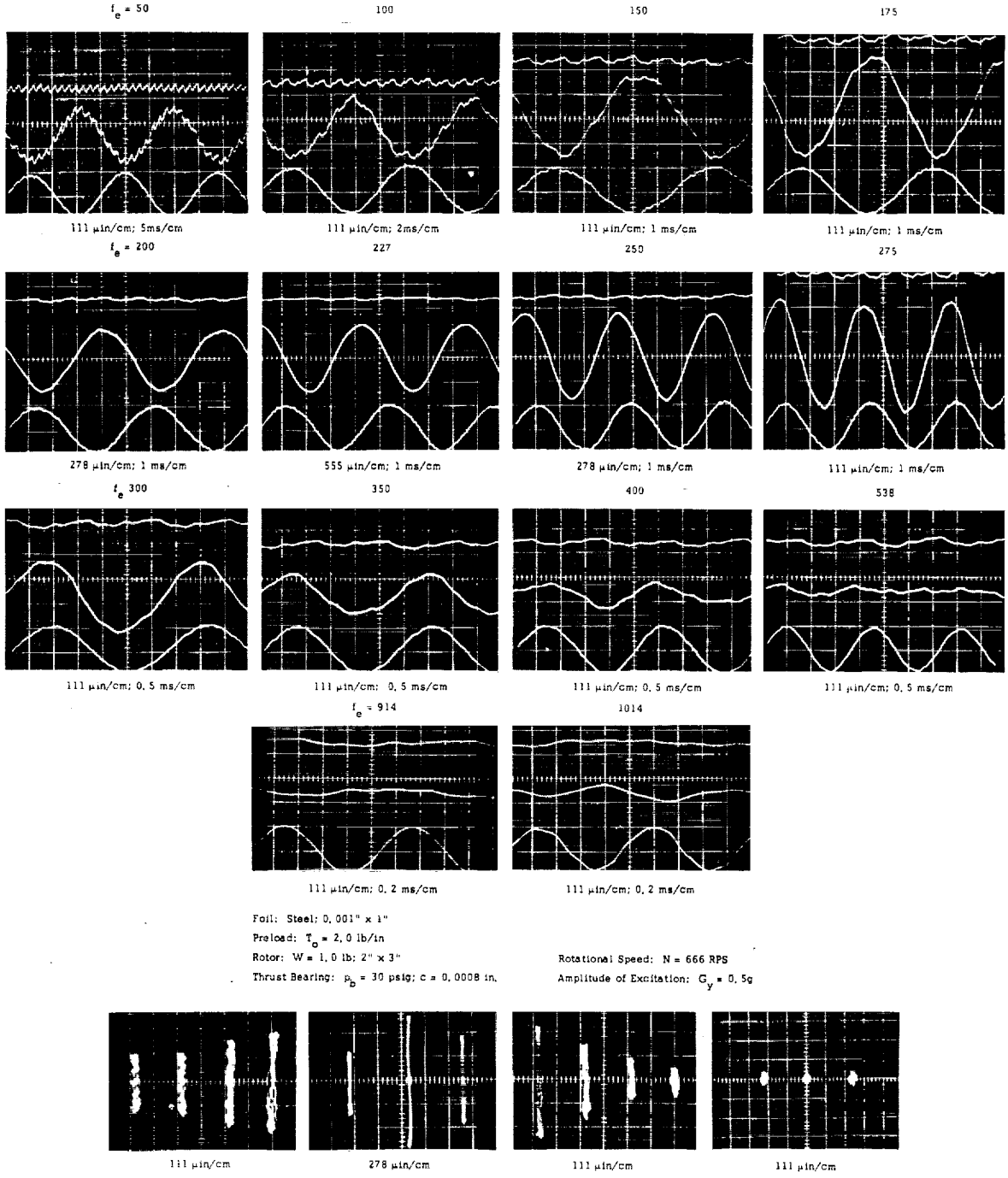

Fig. 4. 51 Motion of 1. 0 lb Rotor Induced by Sinusoidal Excitation (N = 666 rps)

Table 4. 16 Response of 1. 0 lb Rotor to Sinusoidal Excitation of Variable Amplitude at Resonance

N = 1000 RPS

G_y	$(f_e)_{RES}$	$2A_x$	$2A_y$
g	CPS	μin	μin
0. 1	249	55	280
0. 2	248	110	720
0. 3	247	165	1050
0. 4	246	220	1290
0. 5	245	390	1860
0. 6	244	445	2140
0. 7	243	610	2380
0. 8	241	585	2680
0. 9	237	750	2910
1. 0	235	785	3180

N = 666 RPS

G_y	$(f_e)_{RES}$	$2A_x$	$2A_y$
g	CPS	μin	μin
0. 1	-	-	-
0. 2	232	0^+	665
0. 3	231	0^+	1000
0. 4	230	0^+	1275
0. 5	229	0^+	1665
0. 6	229	20	2000
0. 7	228	70	2280
0. 8	227	170	2610
0. 9	227	555	2880
1. 0	226	880	3110

Foil: Steel; 0.001" x 1"

Preload: T_o = 2. 0 lb/in

Rotor: W = 1. 0 lb; 2" x 3"

Thrust Bearing:

p_b = 30 psig

C = 0. 0008 in.

N = Rotational Speed

G_y = In-line amplitude of excitation

$(f_e)_{RES}$ = Resonant frequency of Excitation

A_x = Amplitude of transverse response of rotor

A_y = Amplitude of in-line response of rotor

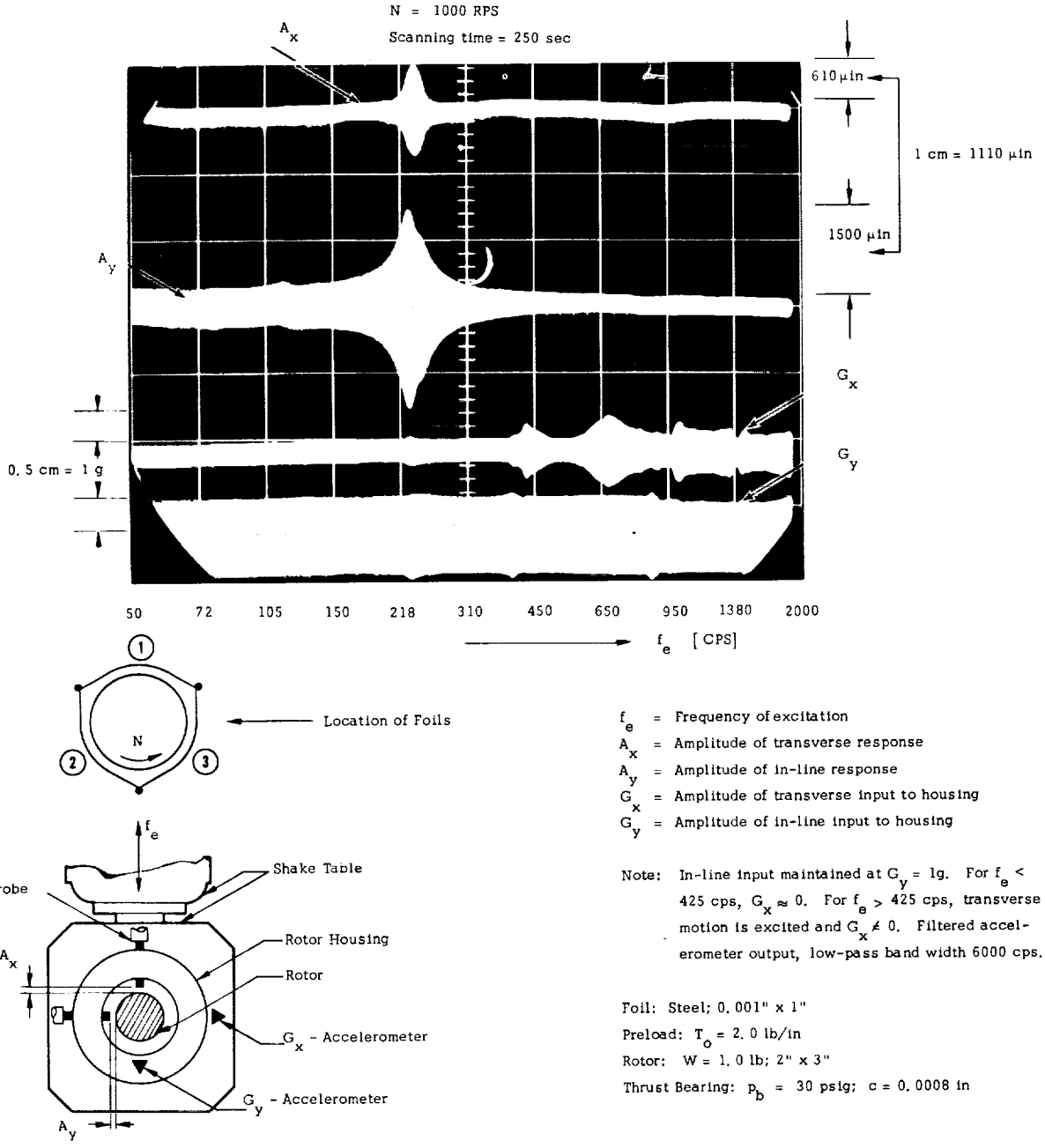

Frequency - Response of Foil-Bearing Supported Rotor

Fig. 4.52 In-line and Transverse Response of 1.0 lb Rotor to Sinusoidal Excitation (250 sec Scan 50 - 2000 cps, at N = 1000 rps and G_y = 1.0g)

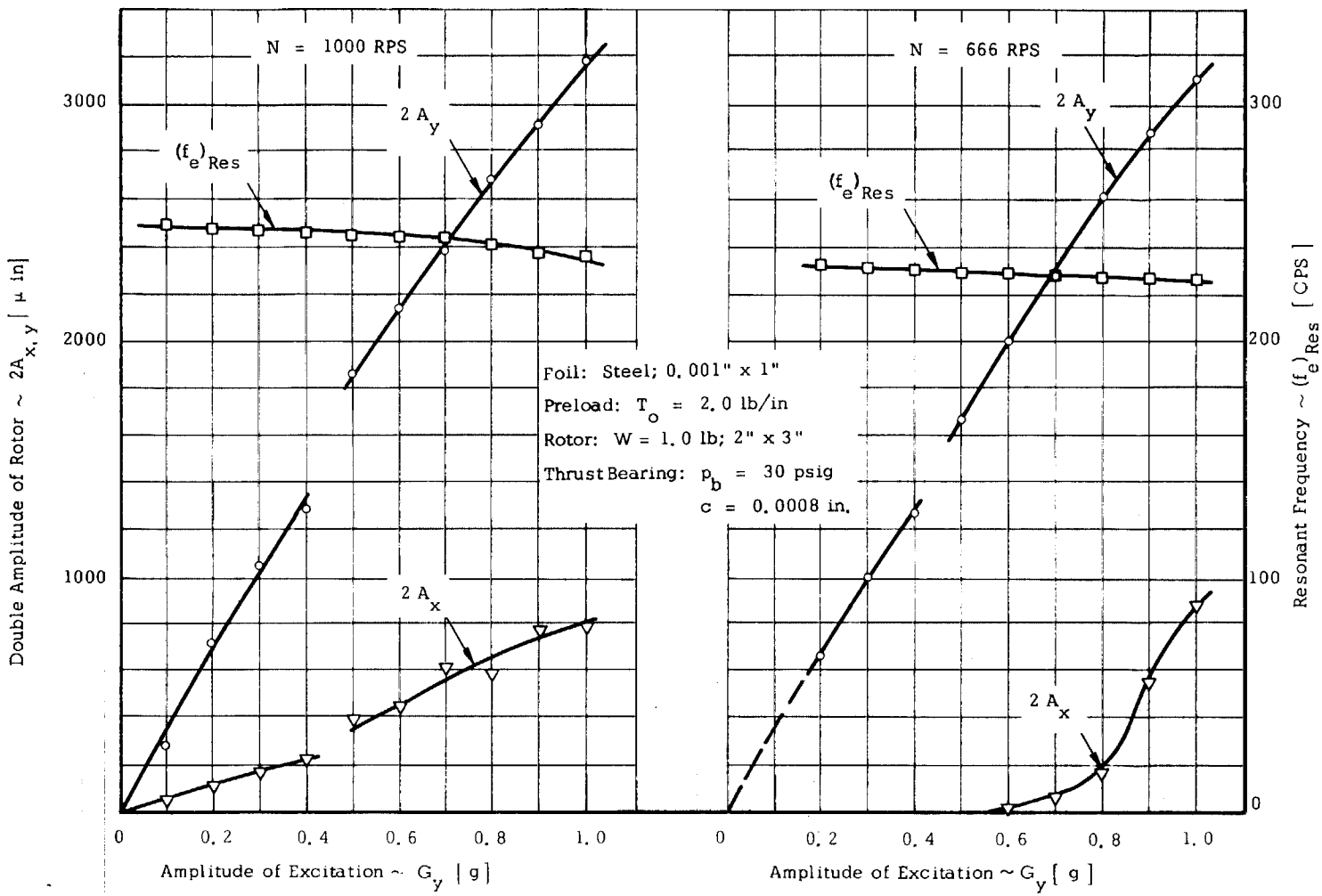

Fig. 4.53 Response of 1.0 lb Rotor at Resonance and Variable Amplitude of Sinusoidal Excitation

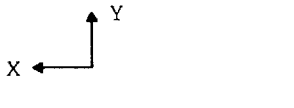

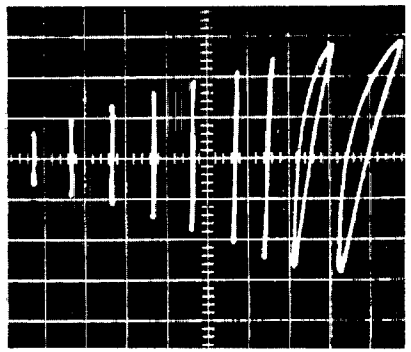

N = 666 RPS

G_y = 0.2 → 1.0g (ΔG_y = 0.1g)

555 μin/cm

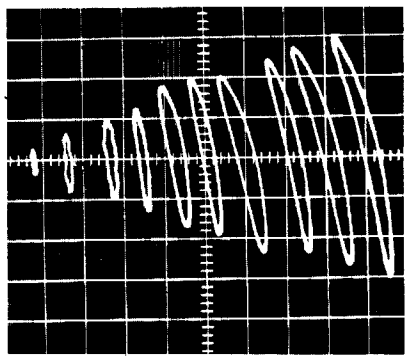

N = 1000 RPS

G_y = 0.1 → 1.0g (ΔG_y = 0.1g)

555 μin/cm

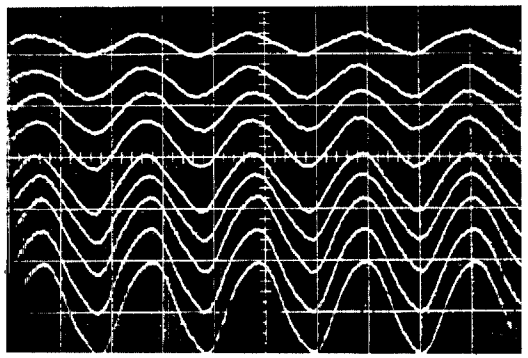

G_y = 0.2g

1.0g

1 g = 2 cm

2 ms/cm

Foil: Steel; 0.001" x 1"

Preload: T_o = 2.0 lb/in

Rotor: W = 1.0 lb; 2" x 3"

Thrust Bearing: p_b = 30 psig; c = 0.0008 in.

Response of Foil-Bearing Supported Rotor at Resonance and Variable Level of Excitation

Fig. 4.54 Motion of 1.0 lb at Resonance and Variable Amplitude of Sinusoidal Excitation

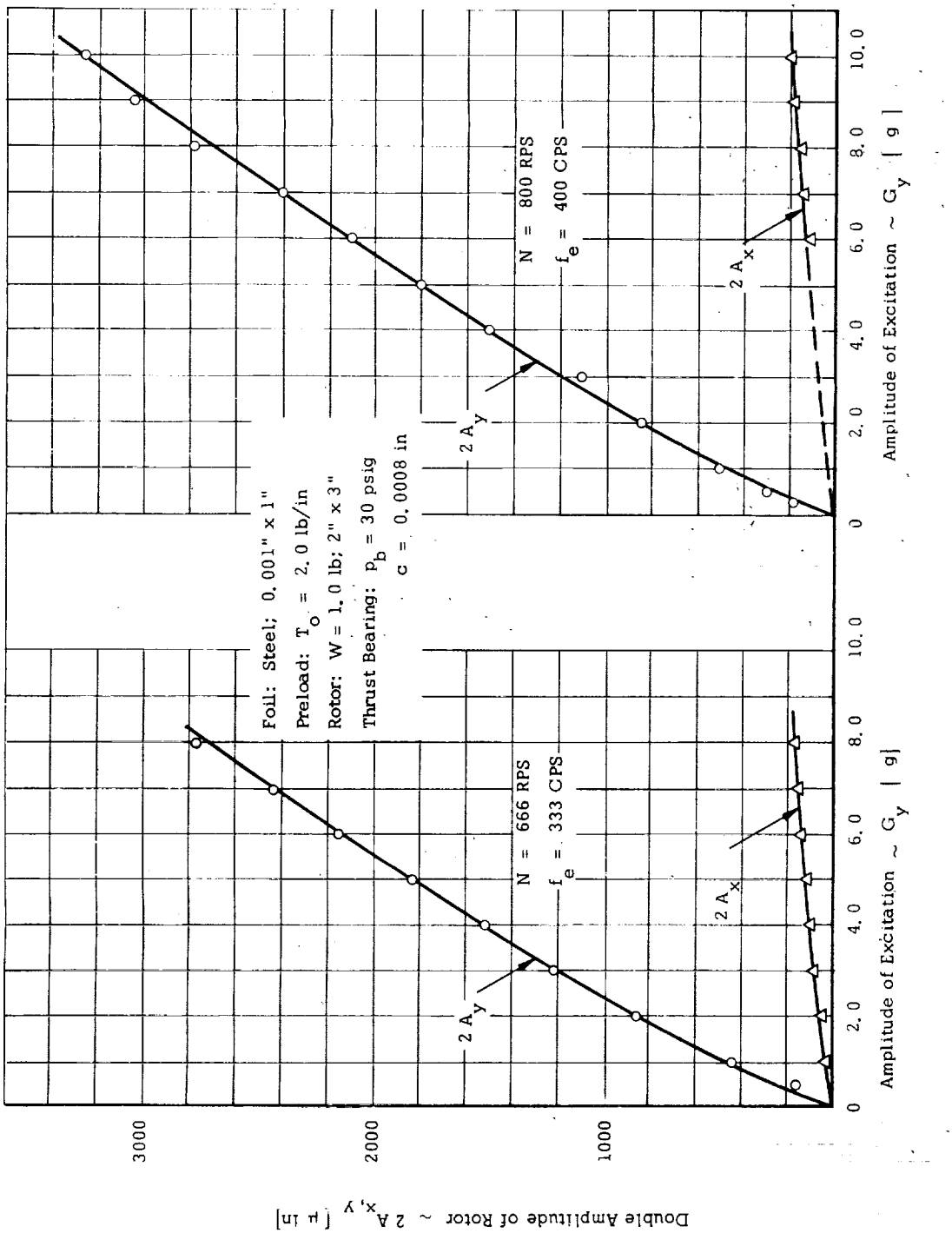

Fig. 4.55 Response of 1.0 lb Rotor to Sinusoidal Excitation of Variable Amplitude and Frequency Equal Half the Rotational Speed

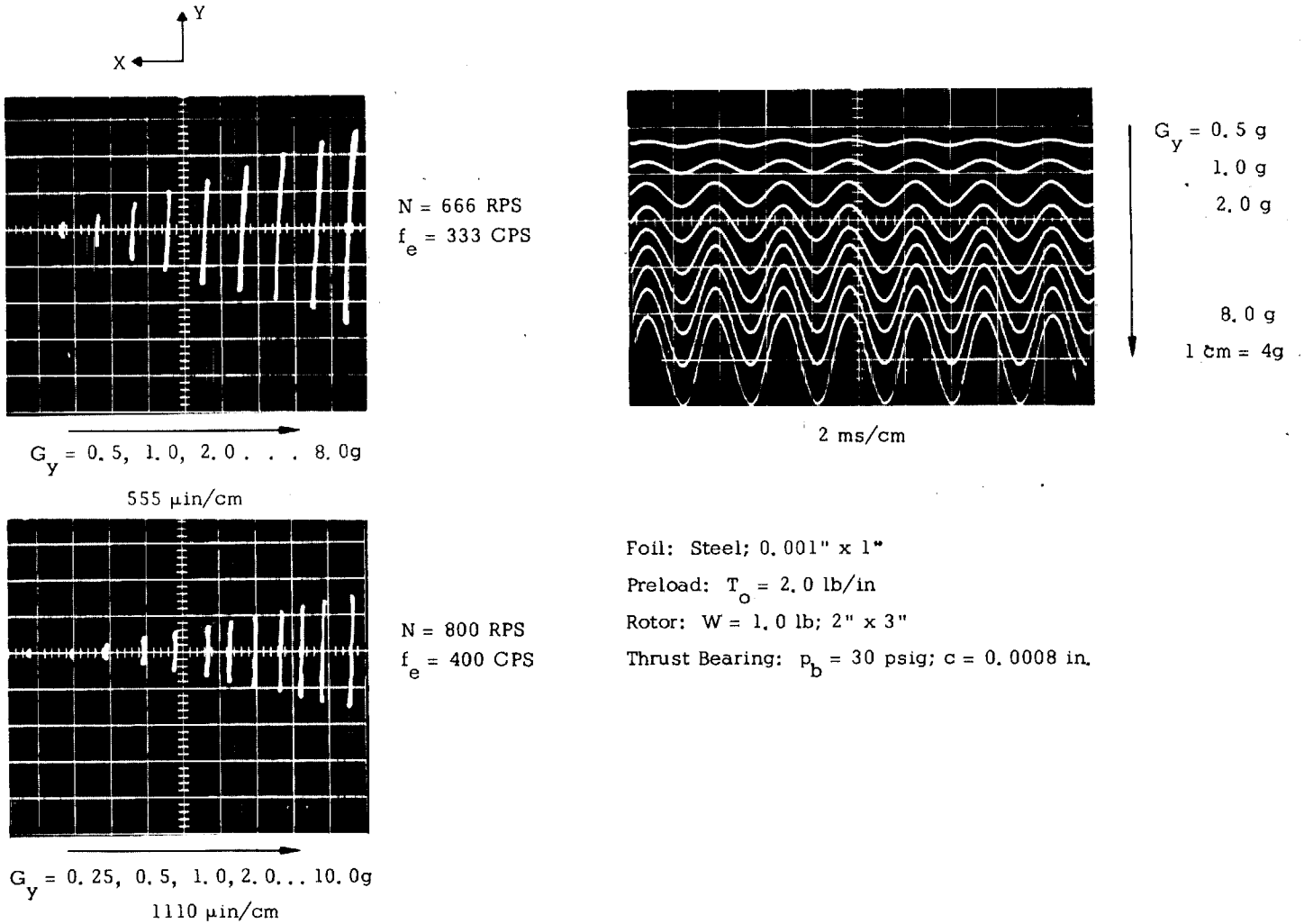

Response of Foil-Bearing Supported Rotor to Variable Excitation at f_e = N/2

Fig. 4.56 Motion of 1.0 lb Rotor Induced by Sinusoidal Excitation of Variable Amplitude and Frequency Equal Half the Rotational Speed

Table 4. 17 Response of 1. 0 lb Rotor to Sinusoidal Excitation of Variable Amplitude and Frequency Equal Half the Rotational Speed

N = 666 RPS

f_e = 333 CPS

G_y	$2A_x$	$2A_y$
g	μin	μin
0. 5	0^+	165
1. 0	30	445
2. 0	55	860
3. 0	80	1220
4. 0	95	1520
5. 0	110	1830
6. 0	140	2160
7. 0	150	2440
8. 0	165	2770

N = 800 RPS

f_e = 400 CPS

G_y	$2A_x$	$2A_y$
g	μin	μin
0. 25	0^+	180
0. 50	0^+	300
1. 0	0^+	500
2. 0	0^+	840
3. 0	0^+	1100
4. 0	0^+	1500
5. 0	0^+	1880
6. 0	100	2100
7. 0	130	2400
8. 0	140	2780
9. 0	160	3040
10. 0	180	3260

Foil: Steel; 0. 001" x 1"

Preload: T_o = 2. 0 lb/in

Rotor: W = 1. 0 lb; 2" x 3"

Thrust Bearing:

p_b = 30 psig

C = 0. 0008 in

N = Rotational Speed

f_e = Frequency of Excitation

G_y = Amplitude of Excitation

A_x = Transverse Amplitude of Rotor Response

A_y = In-Line Amplitude of Rotor Response

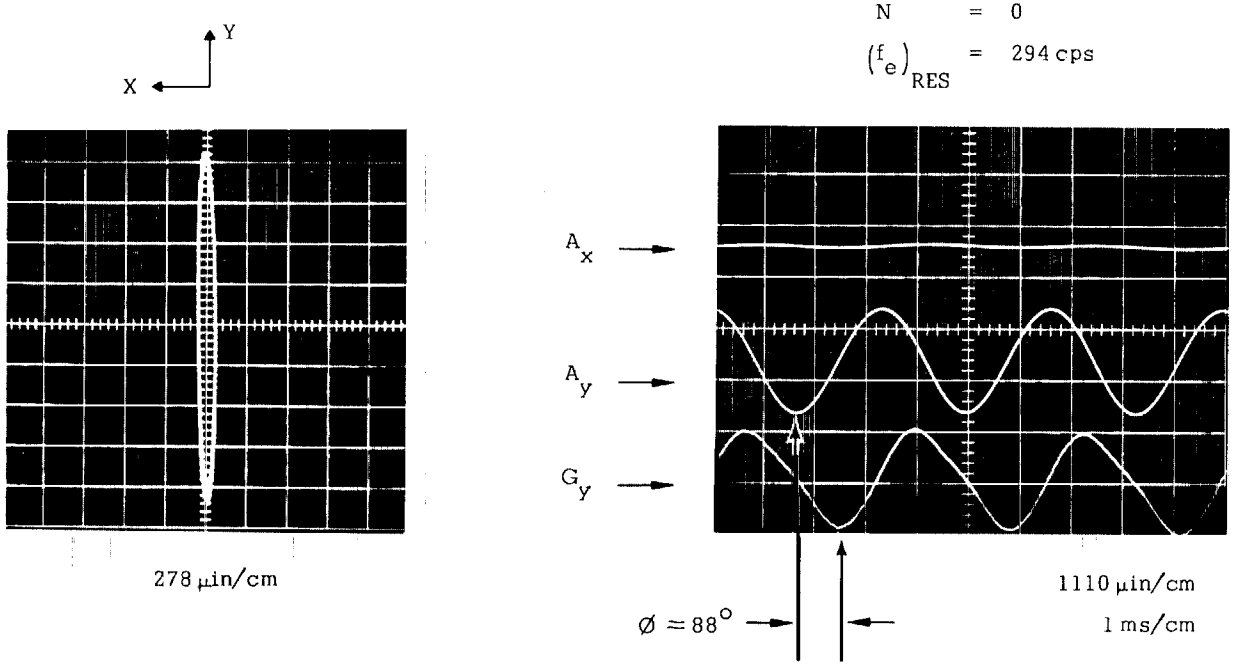

Foil: Steel; 0.001" x 1"

Preload: T_o = 2.0 lb/in

Foil Supply Pressure: p_ℓ = 24 psig

Rotor: W = 1.0 lb; 2" x 3"

Thrust Bearing: p_b = 30 psig ,
c = 0.0008 in

G_y = 0.5g

Note: The total angle of wrap of the 3 foil segments is 180°. There are 2 rows of 24, 0.020" x 0.125" supply orifices, each row at 0.125" from the edge of the foil.

Resonance of Rotor Supported by Pressurized Foil-Bearing

Fig. 4.57 Resonance of Stationary 1.0 lb Rotor Supported in Pressurized Foil Bearing

N = 1000 RPS

Scanning time = 250 sec.

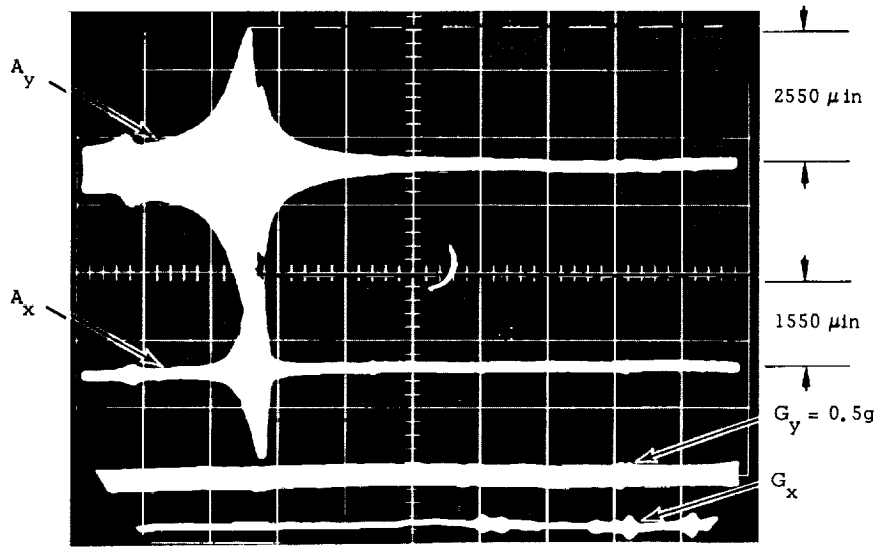

50 72 105 150 218 310 450 650 950 1380 2000

f_e (CPS)

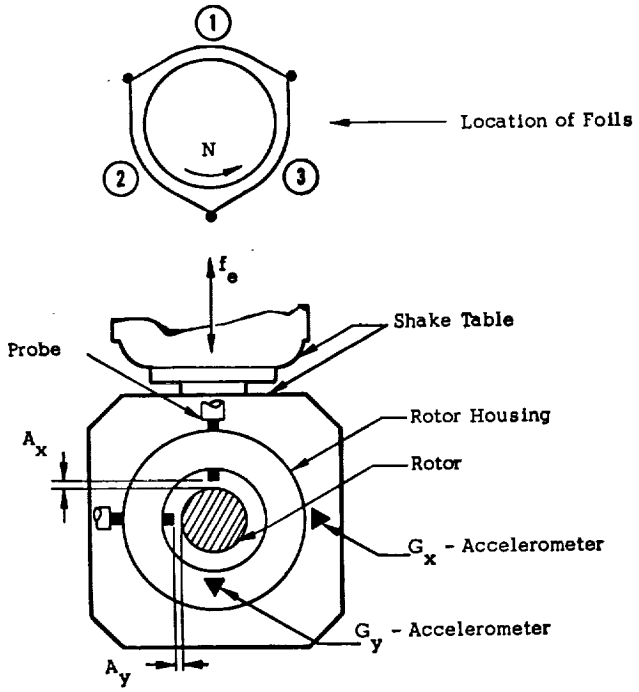

f_e = Frequency excitation

A_x = Amplitude of transverse response

A_y = Amplitude of in-line response

G_x = Amplitude of transverse input to housing

G_y = Amplitude of in-line input to housing

Note: In-line input maintained at $G_y = 0.5g$. For $f_e < 425$ cps, $G_x \approx 0$. For $f_e > 425$ cps, transverse motion excited, but $G_x < 0.2G_y$ Filtered accelerometer output, low-pass bandwidth 6000 cps.

Foil: Steel; 0.001" x 1"

Preload: T_o = 2.0 lb/in

Rotor: W = 2.390 lb; 2" x 3"

Thrust Bearing:

p_b = 45 psig

c = 0.0008"

4.60 In-line and Transverse Response of 2.390 lb Rotor to Sinusoidal Excitation (250 sec Scan 50 - 2000 cps, at N = 1000 rps and G_y = 0.5 g)

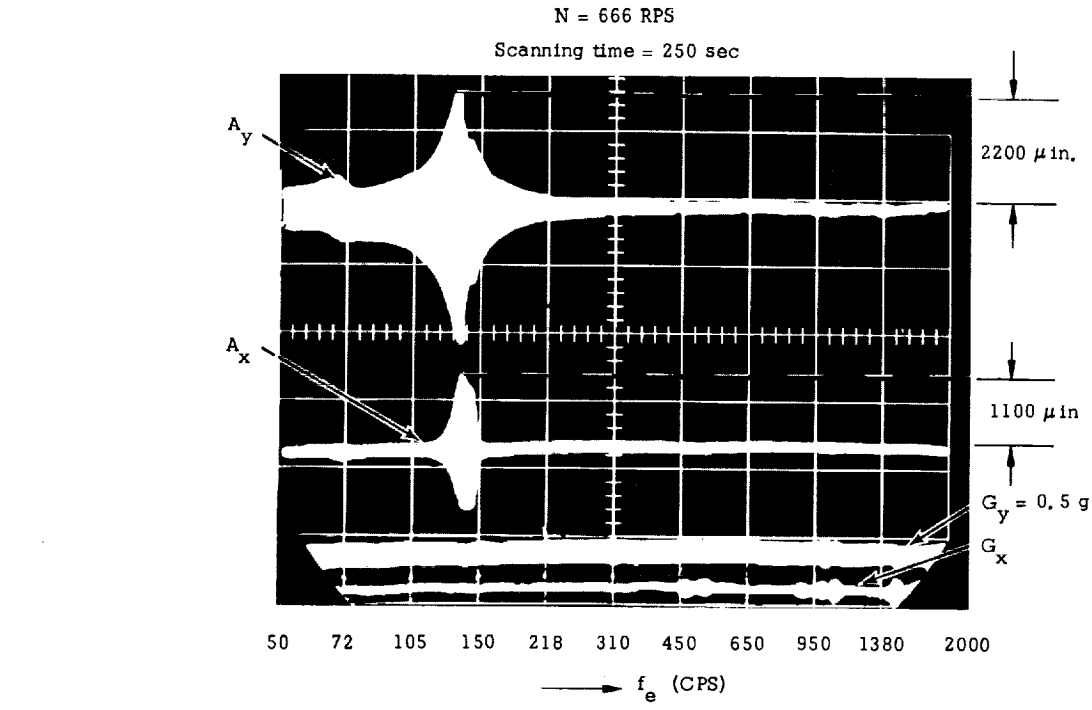

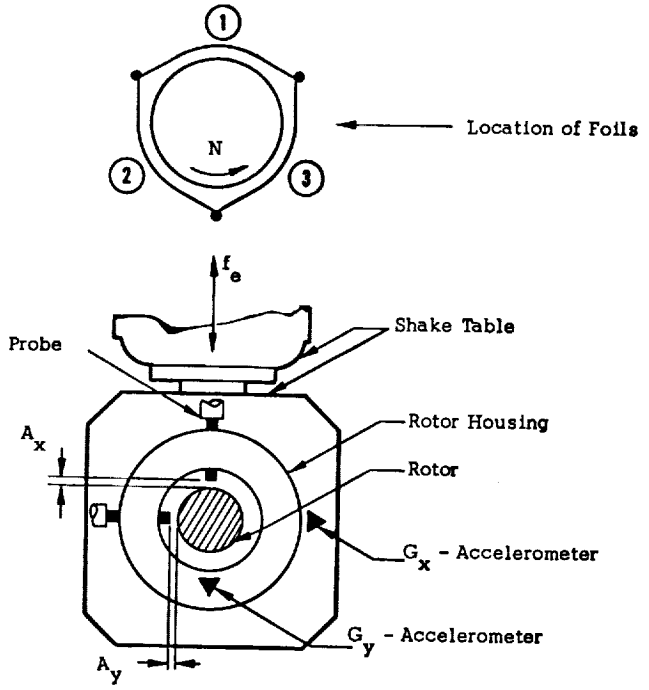

f_e = Frequency of excitation
A_x = Amplitude of transverse response
A_y = Amplitude of in-line response
G_x = Amplitude of transverse input to housing
G_y = Amplitude of in-line input to housing

Note: In-line input maintained at G_y = 0.5 g
For f_e < 425 cps, $G_x \approx 0$. For f_e > 425 cps, transverse motion excited, but $G_x < 0.2 G_y$.
Filtered accelerometer output, low-pass band width 6000 cps.

Foil: Steel; 0.001" x 1"
Preload: T_o = 2.0 lb/in
Rotor: W = 2.390 lb; 2" x 3"
Thrust Bearing:
p_b = 45 psig
c = 0.0008"

Fig. 4.61 In-line and Transverse Response of 2.390 lb Rotor to Sinusoidal Excitation (250 sec Scan 50 - 2000 cps, at N = 666 rps and G_y = 0.5g)

Externally pressurized foil bearing; p_ℓ = 24 psig

$N = 0^+$; G_y = 0.5 g; Scanning time = 250 sec

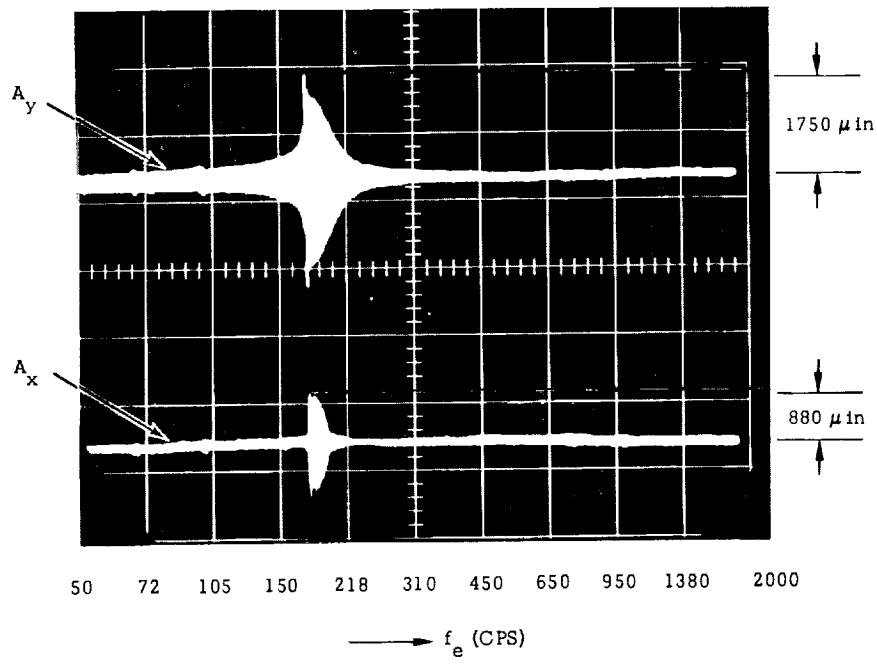

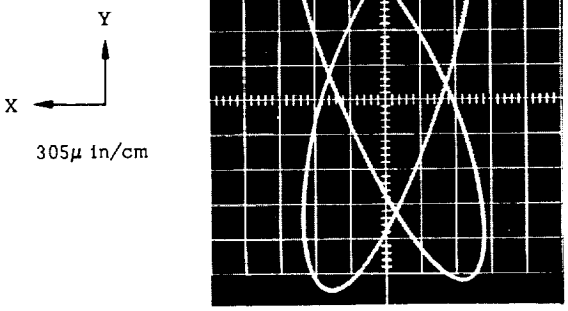

f_e = Frequency of excitation

A_x = Amplitude of transverse response

A_y = Amplitude of in-line response

G_x = Amplitude of transverse input to housing

G_y = Amplitude of in-line input to housing

Note: In-line input maintained at G_y = 0.5g
For f_e < 425 cps, $G_x \approx 0$. For f_e > 425 cps, transverse motion is excited, but $G_x < 0.2G_y$. Filtered accelerometer output, low-pass band width 6000 cps.

$f_{e\ Res}$ = 178 cps

At resonance the orbits oscillate slowly (~1 cps) between the extreme position shown above

Foil: Steel; 0.001" x 1"

Preload: T_o = 2.0 lb/in

Rotor: W = 2.390 lb; 2" x 3"

Thrust Bearing:

p_b = 70 psig;

c = 0.0008"

Fig. 4.62 In-line and Transverse Response of 2.390 lb Rotor to Sinusoidal Excitation (250 sec Scan 50 - 2000 cps, Externally Pressurized, $N = 0^+$ and G_y = 0.5g)

Foil in contact with rotor; T_o = 2.0 lb/in

N = 0; G_y = 0.5g; Scanning time = 250 sec.

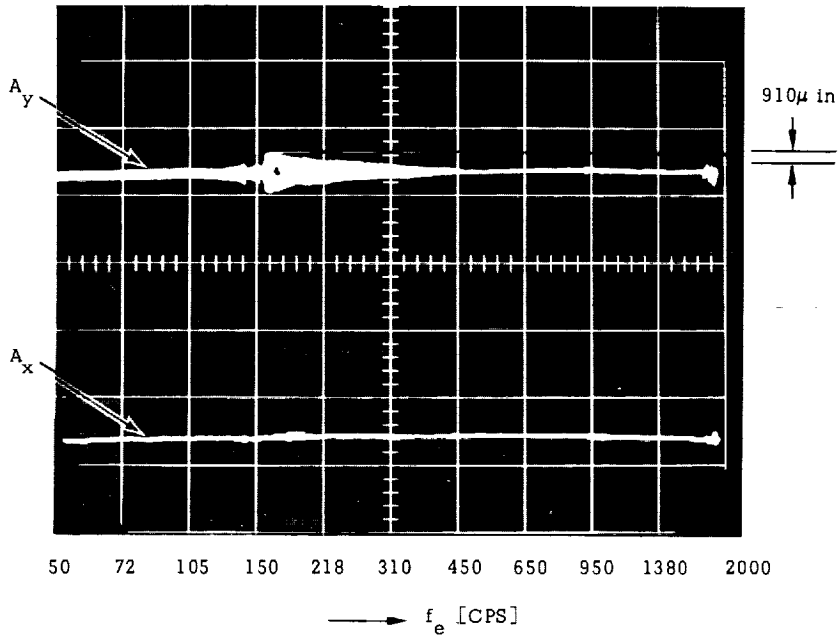

f_e = Frequency of excitation

A_x = Amplitude of transverse response

A_y = Amplitude of in-line response

G_x = Amplitude of transverse input to housing

G_y = Amplitude of in-line input to housing

Note: In-line input maintained at G_y = 0.5g
For f_e < 425 cps, $G_x \approx 0$. For f_e > 425 cps, transverse motion excited, but $G_x < 0.2G_y$. Filtered accelerometer output, low-pass band width 6000 cps

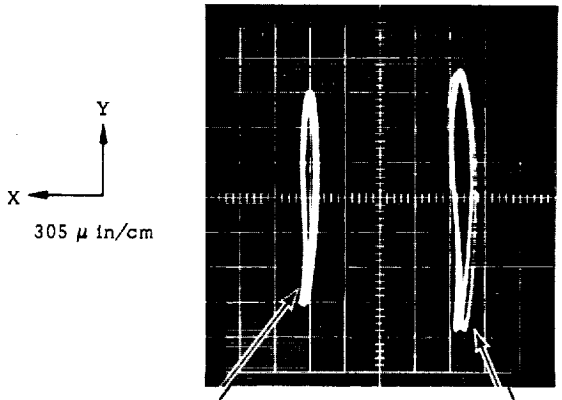

Foil: Steel; 0.001" x 1"

Preload: T_o = 2.0 lb/in

Rotor: W = 2.390 lb; 2" x 3"

Thrust Bearing:

p_b = 70 psig

c = 0.0008"

Fig. 4.63 In-line and Transverse Response of 2.390 lb Rotor to Sinusoidal Excitation (250 sec Scan 50 - 2000 cps, Foil and Rotor in Contact, T_o = 2.0 lb/in and G_y = 0.5g)

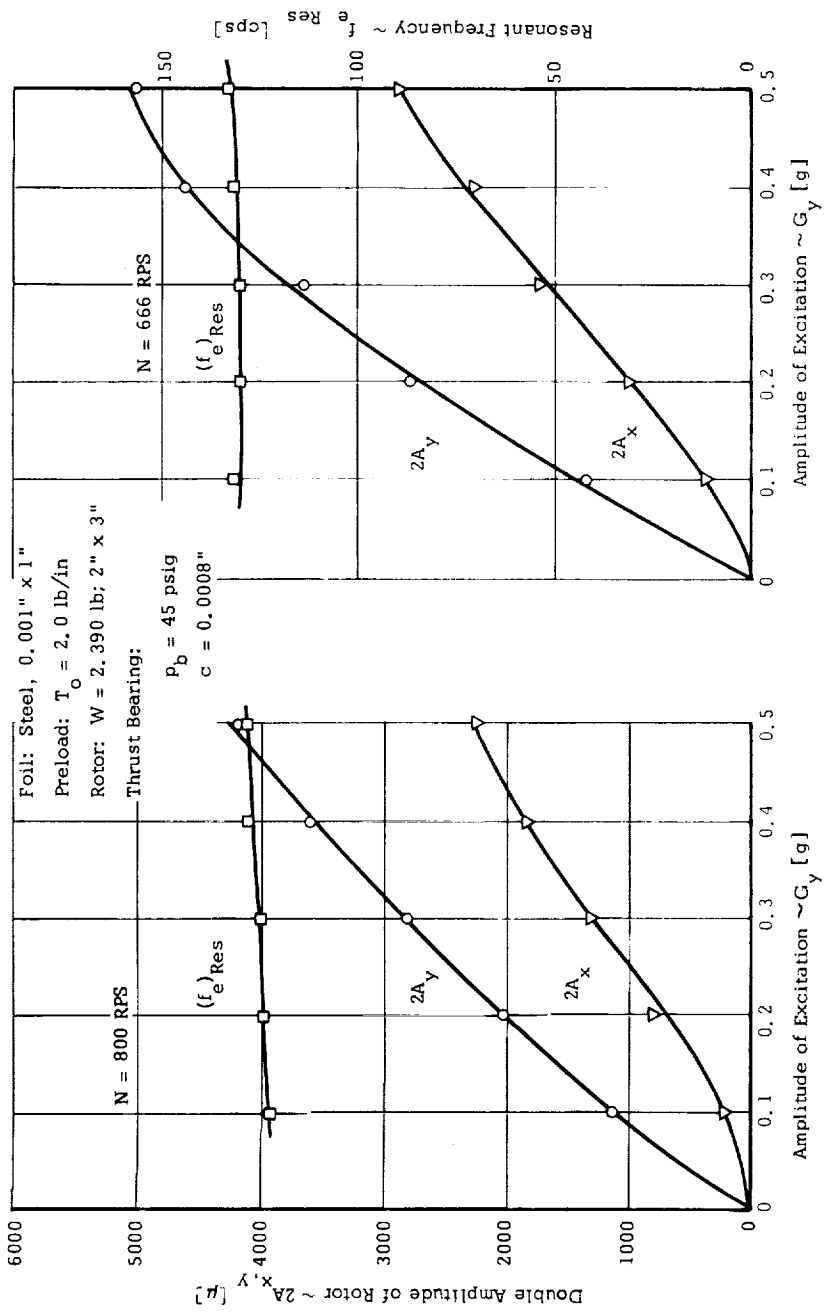

Fig. 4.64 Response of 2.390 lb Rotor to Sinusoidal Excitation of Variable Amplitude at Resonance

Table 4. 19 Response of 2. 390 lb Rotor to Sinusoidal Excitation of Variable Amplitude at Resonance

N = 800 RPS

G_y	$(f_e)_{Res}$	$2A_x$	$2A_y$
g	CPS	μ in	μ in
0.1	122	210	1130
0.2	123	800	2020
0.3	125	1310	2800
0.4	127	1830	3600
0.5	129	2250	4150

N = 666 RPS

G_y	$(f_e)_{Res}$	$2A_x$	$2A_y$
g	CPS	μ in	μ in
0.1	131	370	1370
0.2	130	1000	2780
0.3	130	1730	3650
0.4	131	2250	4600
0.5	132	2860	5000

Foil: Steel; 0.001" x 1"

Preload: T_o = 2.0 lb/in

Rotor: W = 2.390 lb; 2" x 3"

Thrust Bearing:

p_b = 45 psig

C = 0.0008"

N = Rotational speed

G_y = In-line amplitude of excitation

$(f_e)_{Res}$ = Resonant frequency of excitation

A_x = Transverse amplitude of rotor response

A_y = In-line amplitude of rotor response

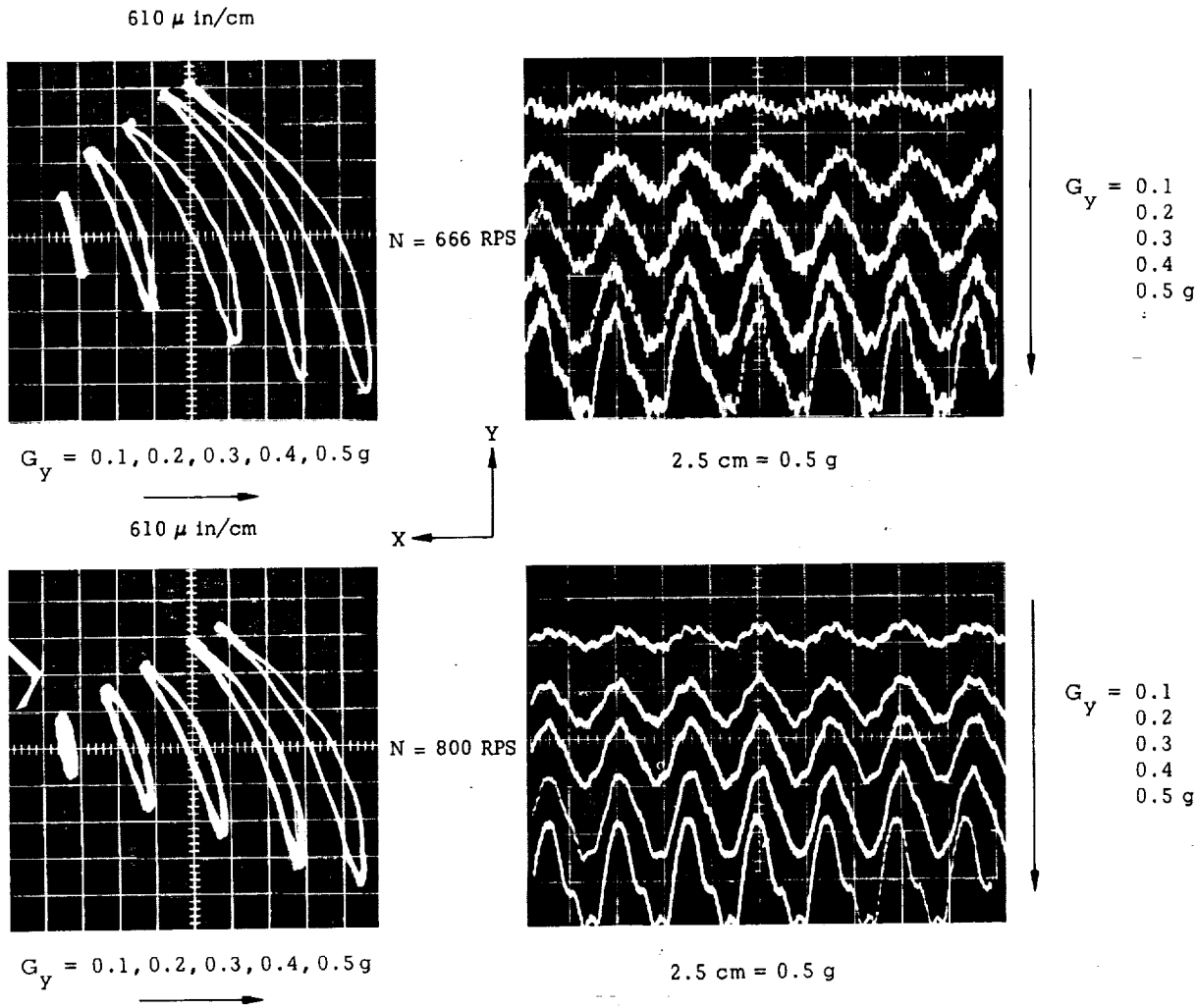

Foil: Steel; 0.001" x 1"

Preload: T_o = 2.0 lb/in

Rotor: W = 2.390 lb; 2" x 3"

Thrust Bearing:

p_b = 45 psig;

c = 0.0008"

Fig. 4.65 Motion of 2.390 lb Rotor at Resonance and Variable Amplitude of Sinusoidal Excitation

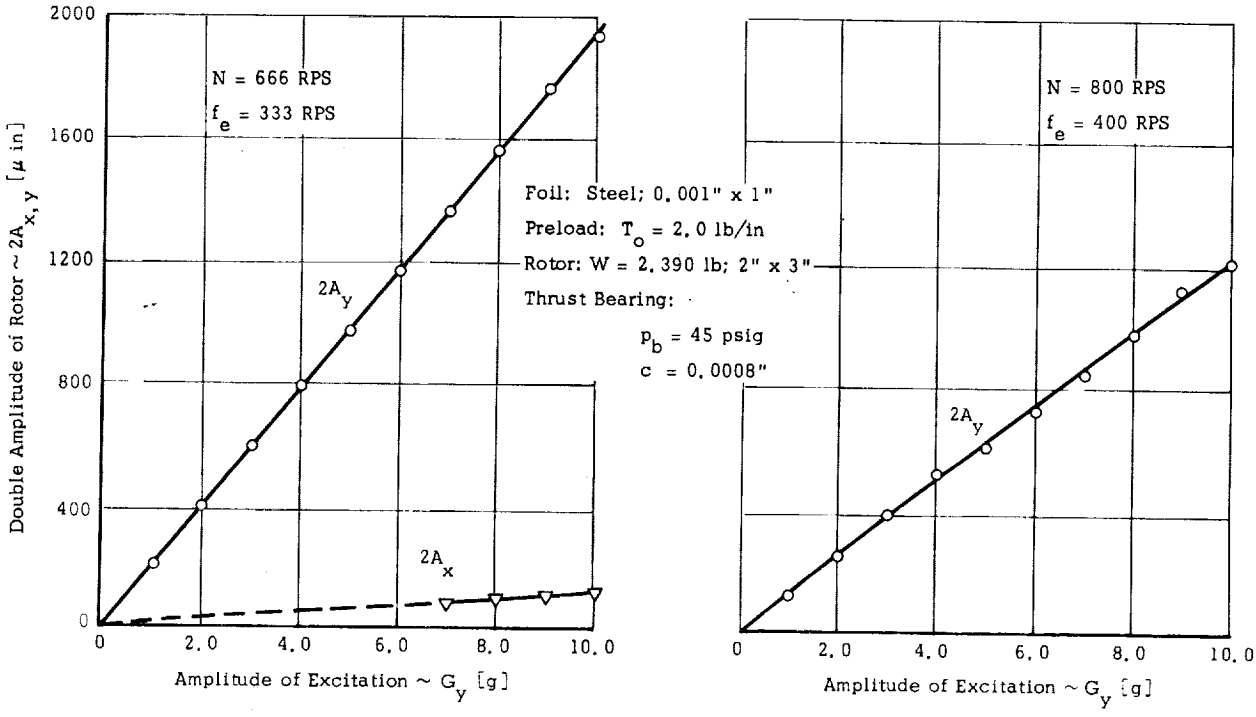

Fig. 4.66 Response of 2.390 lb Rotor to Sinusoidal Excitation of Variable Amplitude and Frequency Equal Half the the Rotational Speed

Table 4. 20 Response of 2. 390 lb Rotor to Sinusoidal Excitation of Variable Amplitude and Frequency Equal Half the Rotational Speed

N = 666 RPS

f_e = 333 CPS

G_y	$2A_x$	$2A_y$
g	μin	μin
1.0	-	210
2.0	-	400
3.0	-	600
4.0	-	790
5.0	-	980
6.0	-	1170
7.0	80	1370
8.0	90	1580
9.0	110	1770
10.0	130	1930

N = 800 RPS

f_e = 400 CPS

G_y	$2A_x$	$2A_y$
g	μin	μin
1.0	-	120
2.0	-	260
3.0	-	380
4.0	-	520
5.0	-	610
6.0	-	730
7.0	-	850
8.0	-	980
9.0	-	1130
10.0	-	1220

Foil: Steel; 0.001" x 1"

Preload: T_o = 2.0 lb/in

Rotor: W = 2.390 lb/in; 2" x 3"

Thrust Bearing:

p_b = 45 psig

C = 0.0008 in

N = Rotational speed

f_e = Frequency of excitation

G_y = In-line amplitude of excitation

A_x = Transverse amplitude of rotor response

A_y = In-line amplitude of rotor response

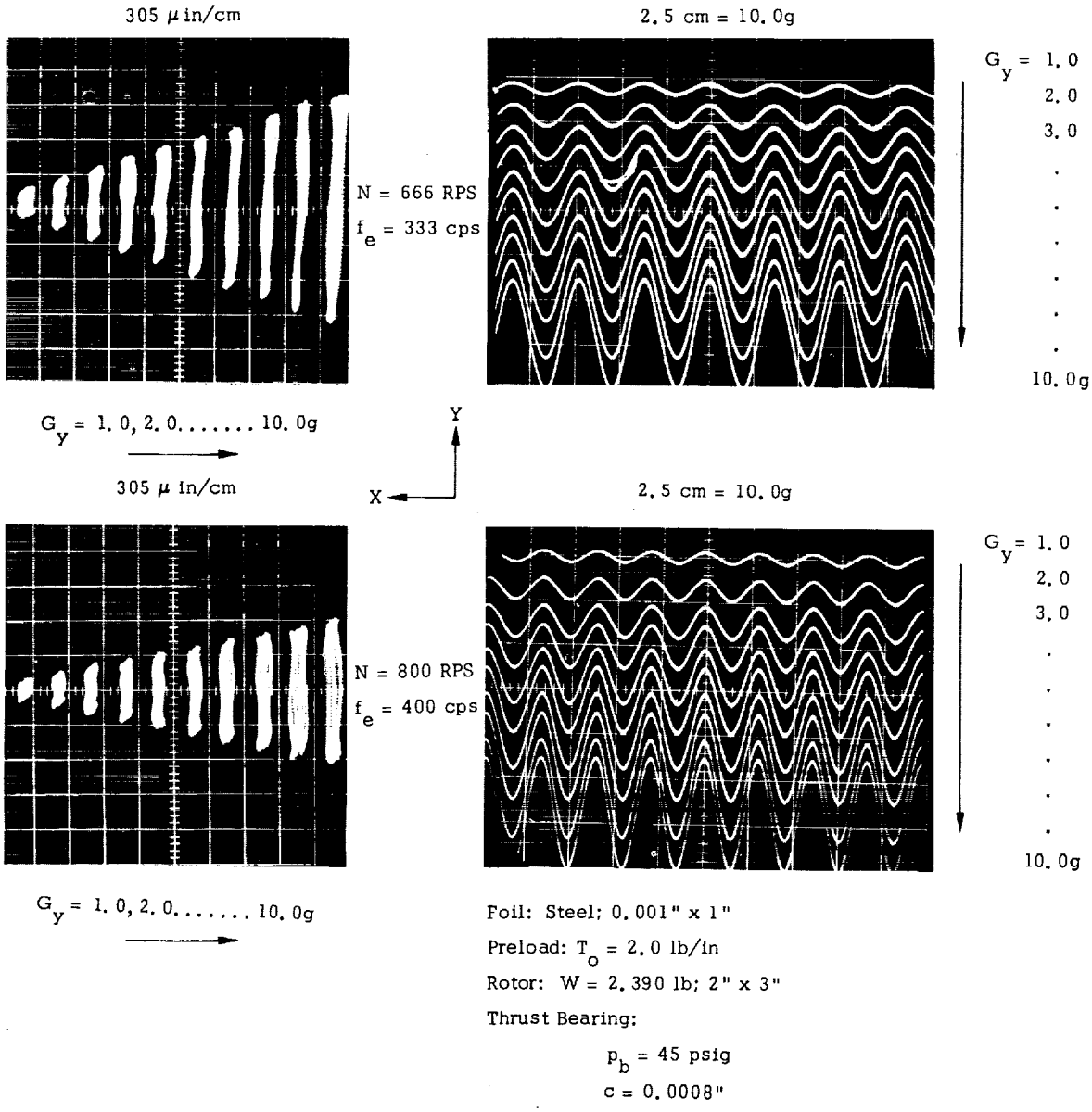

Fig. 4.67 Motion of 2.390 lb Rotor Induced by Sinusoidal Excitation of Variable Amplitude and Frequency Equal Half the Rotational Speed

In a recent paper by Eshel and Wildmann [17], it has been shown that, for the case of a flexible foil and an incompressible fluid, small disturbances propagate along the foil at a speed $V = U/2$, in which U is the surface velocity of the rotor. It has subsequently been shown by Eshel [18] that the relation $V = U/2$ is nearly true for various forms of large disturbances and that it remains insensitive to the rigidity of the foil and the compressibility of the fluid.

The theoretical prediction of the foregoing phenomenon has been verified experimentally in the course of the present investigation and is substantiated by the results presented in Fig. 4.47. The method of initiating a disturbance is illustrated in the schematic diagram appended in the foregoing figure. A narrow, one-inch wide strip of balsa wood was cemented to the foil in the span between the entrance region of a foil sector and an adjacent foil guide. A relatively short wire, terminating in a small anvil, was attached to the balsa strip at a point corresponding to the centerline of the foil. The anvil could be impacted my means of a small hammer attached to the free end of a cantilever spring. In addition to the small hammer, the cantilever spring carried a contactor for the purpose of triggering the oscilloscope sweep. The strength of impact and the sweep delay-time could be controlled by the initial offsets of the anvil and of the contactors, and by the relative deflection of the spring. Two capacitance probes, mounted in an auxiliary fixture opposite the region of wrap, spanned an arc length of 0.873 inch and a corresponding angle of 50° (as compared with the 60° angle of wrap).

The photographs in Fig. 4.47 contain oscilloscope traces of outputs of the two probes following impact. The irregular shape of the ensuing disturbance facilitated the identification of corresponding points in each oscilloscope trace. It can be seen that the disturbance decays and spreads as it is carried downstream in the direction of the exit region.

The correlation of corresponding peaks and valleys is, nevertheless, quite easy. The photographs on the left hand side of Fig. 4.47 correspond to three surface velocities of the rotor. The lateral displacements of corresponding peaks P_1 and P_2 in the foregoing photographs, when interpreted in terms of the appended time-scale factors, give the following ratios of the velocity of propagation and the surface velocity of the rotor:

$$\frac{V}{U} = \begin{cases} 0.48 \\ 0.48 \\ 0.46 \end{cases}$$

The foregoing results are in very good agreement with the predicted order of magnitude of $V/U \approx 0.5$.

Although the position of the rotor is not fixed, it cannot respond instantaneously to a fast tension pulse because of relatively high inertia. The motion of the rotor in the time interval of transit of the decaying disturbance is very small. The photograph in the right hand side of Fig. 4.47 shows the displacement of the foil following a relatively slow pulse, which may be accompanied by a commensurate displacement of the rotor. In the latter photograph, each of the small undulations superposed on the traces corresponds to one revolution of the rotor and reflects the orbital motion due to remanent unbalance.

I. Motion of Rotor Foil in Response to Sinusoidal Excitation

In analogy with the experiment described in the preceding section, the motion of a foil segment has been determined in parallel with the motion of the rotor, under conditions of unidirectional excitation by means of a vibrator.

The probe monitoring the motion of the rotor was in-line with the direction of excitation, that is, along the bisector of foil arc No. 1.

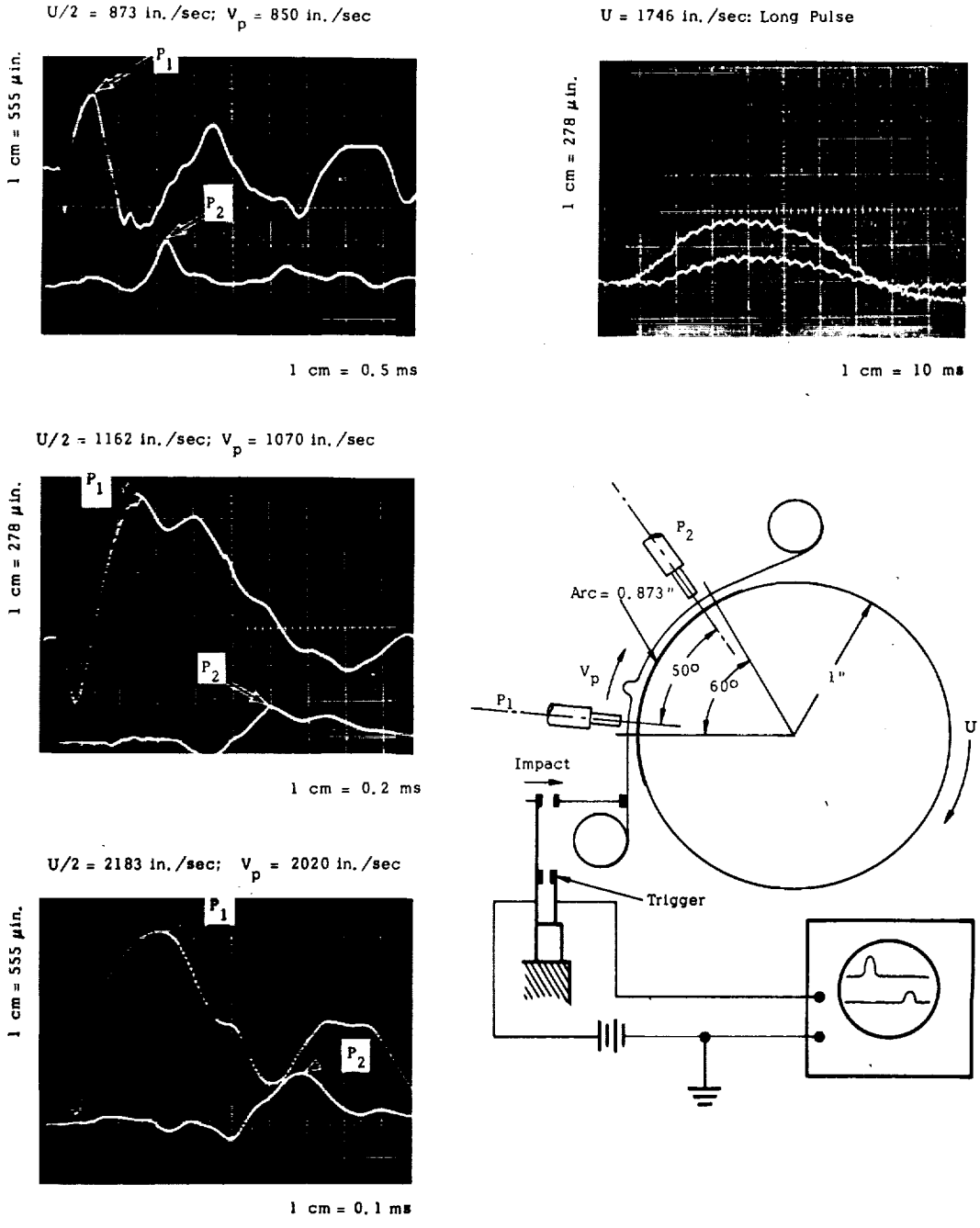

Velocity of Propagation of Disturbance Along a Foil

Fig. 4. 47 Velocity of Propagation of Disturbance along a Foil

The probes monitoring the motion of the foil were spaced symmetrically about the bisector, spanning a 45^{o} arc of the 60^{o} region of wrap. An attempt has been made to maintain nearly equal peak-to-peak excursions of the rotor at all frequencies of excitation by varying the g-level of input to the housing. This objective has been thwarted in part by the presence of varying amounts of "distortion" in the response of the rotor. At one frequency also, it has not been possible to attain the desired amplitude of motion of the rotor without resorting to very high g-levels of excitation.

The excursions of the foil and the displacement of the rotor from their respective equilibrium positions are presented in two sets of six oscilloscope photographs in Fig. 4.59. The experimental runs corresponded to rotational speeds N = 280 rps and N = 560 rps. The upper and middle traces depict the motion of the foil at points adjoining respectively the entrance and exit regions. The lowermost trace represents the motion of the rotor, maintained at approximately $2A_y = 1100\ \mu$ in $\pm 5\%$, except at $f_e = 563$ cps. At $f_e = 563$ cps, it has not been possible to maintain an excursion of $2A_y \approx 1100\ \mu$ in without exceeding a 10-g level of excitation. The data obtained from photographs in Fig. 4.59 is presented graphically in Fig. 4.58 and numerically in Table 4.18. The table lists also the magnitudes of excitation required to maintain the given rotor amplitude at each frequency.

It has been convenient to normalize the displacements of the foil with respect to the displacement of the rotor. The results should be interpreted with caution, since the waveforms of rotor motion at various requencies have not been exactly equal and alike, and because the displacement at $f_e = 563$ cps has been considerably smaller than at other frequencies of excitation. The foregoing remarks are intended to emphasize that the motion of the foil depends on both the frequency and amplitude of rotor excursion. The terms "frequency" and "amplitude" are not

used here in a strict sense, since the ensuing motion of the rotor was not sinusoidal.

Referring to Fig. 4.58 and (preferably) to the oscilloscope records presented in Fig. 4.59, the following observations can be made:

(a) The excursions of the foil at the lowest three frequencies of excitation have been sensibly equal at both probe locations and approximately 50% to 60% smaller than the excursions of the rotor.

(b) The apparent maxima of the peak-to-peak amplitude ratio at f_e = 563 cps should be interpreted in the light of the previous introductory remarks. Note also that the frequency of excitation 563 cps is either equal to, or one-half the rotational speed. Observe that the reduced motion of the rotor is nearly sinusoidal at f_e = 563 cps.

(c) A very pronounced reduction of foil motion occurs at the highest frequency of excitation f_e = 948 cps.

(d) No pronounced or consistent lag-lead relation can be observed between the motion of the foil at the leading and trailing probe locations and between the motion of the rotor. At f_e = 948 cps and N = 380 rps, the order in which maximum excursions occur is: rotor, leading probe, trailing probe. At f_e = 948 cps and N = 560 rps, the order becomes: rotor, trailing probe, leading probe. The rotor time-lead is appreciable at both speeds of rotation, but the order in which maxima occur at the monitoring stations of the foil is reversed.

The foregoing observations reflect the complexity of the motion, which does not lend itself to a simple interpretation.

The gap width at foil sector No. 1, determined under steady-state conditions (Fig. 4.27) was 560 μin at N = 560 rps, and 350 μin at N = 280 rps. On the other hand, the excursion of the rotor from the equilibrium position was in the order of 550 μin, that is, at least as large, or 27% larger, than the steady-state gap width. The corresponding foil excursions were appreciably smaller, especially at f_e = 948 cps. It is reasonable to infer that the minimum gap widths under dynamic conditions may have been but a fraction of the steady-state clearance. Also, since no catastrophic, or even perceptible deceleration due to frictional contact has been observed, one must assume that the oscillations of the foil occurred about a mean position other than that corresponding to the steady-state clearance. If so, the "squeeze-film" effect must have been significant in augmenting the time-average pressure of the air film. The mere facts that no failure occurred, that no decrease in speed has been observed, and that no galling or excessive wear has been noted after approximately two hours of intensive excitation, point up one of the many attractive attributes of the foil bearing.

J. Surface Compatibility of Foil and Rotor; Wipe-Wear Effects

The nature of wear of a journal and of a flexible metal foil is radically different from that which takes place in a bearing, the mating members of which are sensibly rigid. Although the wear characteristics of any bearing can always be improved through judicious choice of materials, it is the flexibility of the foil which is believed to play by far the most important role in the "forgiving" character of the foil bearing.

It is not proposed at this point to engage in a discussion of microscopic and macroscopic phenomena which may distinguish the nature

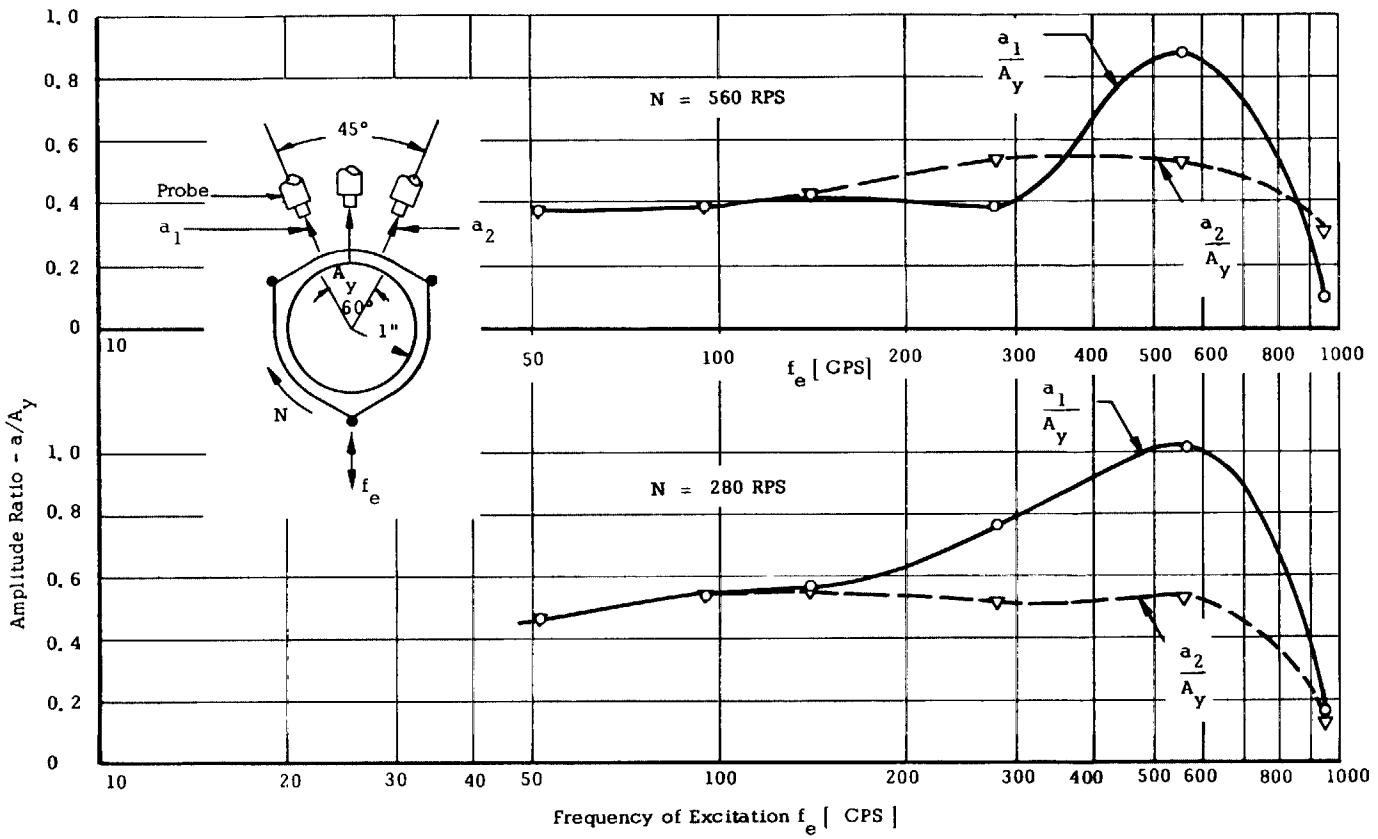

Fig. 4.58 Comparison of Rotor and Foil Excursions Induced by Sinusoidal Excitation

Table 4. 18 Comparison of Foil and Rotor Excursions Induced by Sinusoidal Excitation

	N = 280 RPS						N = 560 RPS					
f_e	$2A_y$	$2a_1$	$2a_2$	a_1/A_y	a_2/A_y	G_y	$2A_y$	$2a_1$	$2a_2$	a_1/A_y	a_2/A_y	G
CPS	μin	μin	μin	-	-	g	μin	μin	μin	-	-	g
53	1080	500	500	0.46	0.46	2.0	1060	390	390	0.37	0.37	2.0
95	1060	560	560	0.53	0.53	1.5	1170	450	450	0.38	0.38	1.8
140	1080	610	590	0.56	0.54	1.3	1060	450	450	0.42	0.42	1.4
280	1110	840	560	0.75	0.50	1.0	1110	420	590	0.38	0.53	1.0
563	750*	750	390	1.00	0.52	10.0	640*	560	330	0.87	0.52	10.0
948	920*	140	110	0.15	0.12	10.0	1140	110	330	0.10	0.29	10.0

*Note: Amplitude of rotor maintained at $2A_y \approx 1110\ \mu$in ± 5% except where indicated by asterisk.

N = Rotor speed

f_e = Excitation frequency

A_y = Amplitude of rotor in direction of excitation

$a_{1,2}$ = Amplitudes of foil at leading and trailing probes

G_y = Amplitude of excitation

Foil: Steel, 0.001" x 1"; angle of wrap = 60^o

Preload: T_o = 2.0 lb/in

Rotor: W = 1.0 lb; 2" x 3"

Probes - Rotor: In-line with direction of excitation, bisecting angle of wrap

- Foil: At 22.5^o, symmetrically spaced about bisector of angle of wrap

Thrust Bearing: p_b = 30 psig; C = 0.0008 in

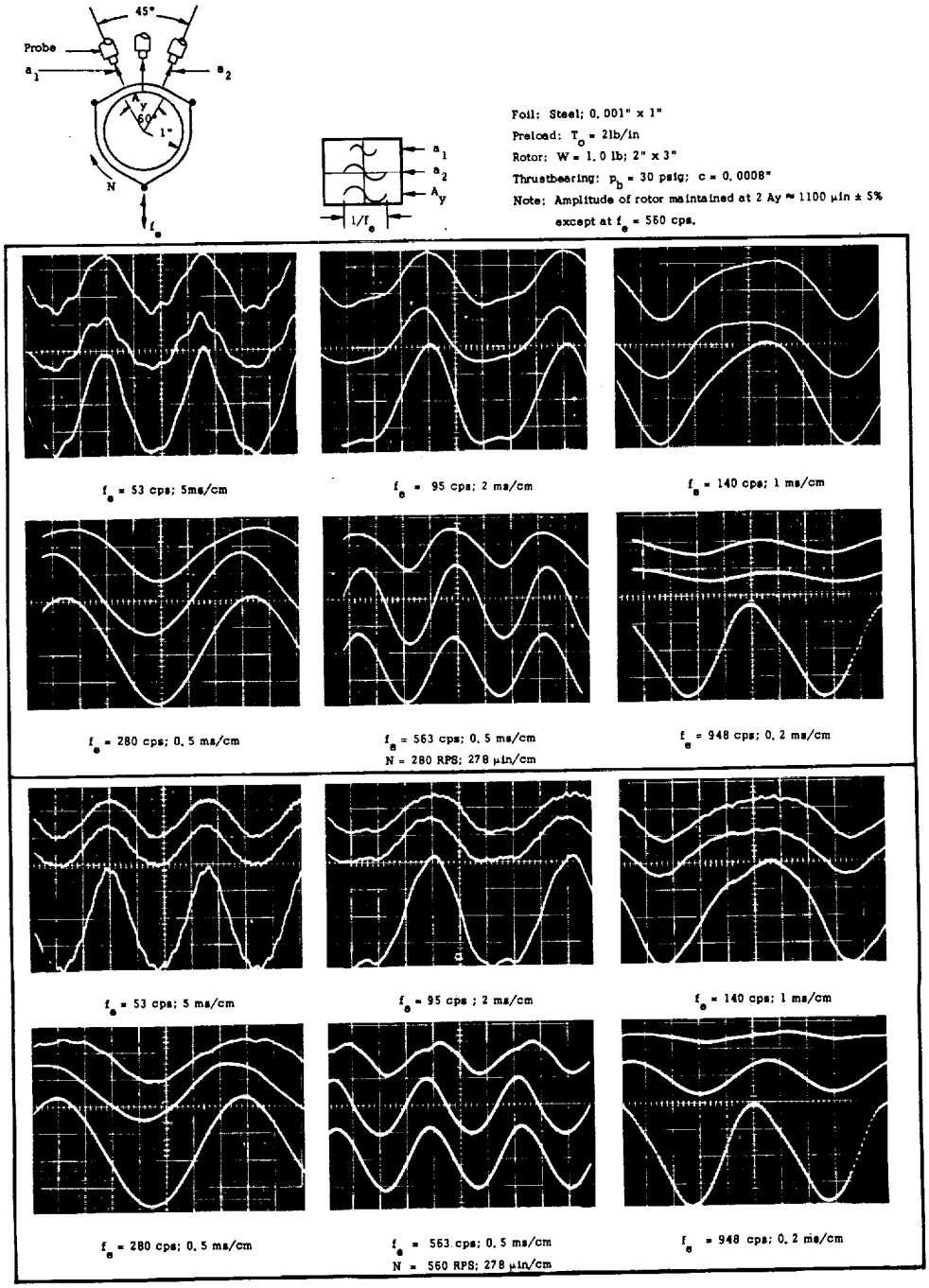

Amplitudes of Foil and Rotor at Constant Speed and Variable Excitation Frequency

Fig. 4.59 Motion of Rotor and Foil Induced by Sinusoidal Excitation

of wear between bounding surfaces of structurally rigid members and surfaces of elements, of which one is extremely compliant. It is self-evident that, if a rigid journal is pressed against a rigid bearing, the entire load will be concentrated in a narrow zone adjacent to the geometrical line of contact. The situation is very different when the journal is pressed against a foil segment, secured at both ends, and the load is distributed over an "effective area" corresponding to the region of wrap. Furthermore, the passage of foreign particles and of debris through the bearing film is facilitated by the ability of the foil to extend and to deflect locally, so that the danger of ploughing and scoring is diminished. In addition, since the foil can conform and deflect locally much more readily than the surface of a massive solid, the stress concentrations are fewer and the load is more evenly distributed. In a conventional gas-lubricated journal bearing, the transition from "no contact" to "contact" is generally a sudden, sharply defined and dangerous event. In the foil bearing, a decrease in clearance involves a surface, rather than a line, and contact occurs progressively at a multiplicity of points, and not as a sequence of concentrated impacts.

With regard to foil-bearing materials, the choice is rather wide and the considerations are probably analogous to those governing the selection of compatible metals in general. In addition to a large variety of commercially available ferrous and nonferrous foils, the selection can be supplemented by clad, bonded, plated and other multilayer products.

The qualitative study of wear characteristics accompanied each phase of the present investigation. The foil materials were stainless steel, beryllium-copper, and brass. The nonferrous materials displayed, of course, the best compatibility with stainless-steel rotors. On two occasions, for example, the rotors have been inadvertently decelerated in the self-acting mode, the brass and beryllium-copper foils playing the role of "friction brakes." In both instances, the rotor was operated again

without replacing the foils. When the latter were finally removed, the "damage" was very slight and both foil and rotor displayed a number of burnished, superficial tracks, rather than scoring marks. No galling or ploughing occurred, and the depth of the tracks could hardly be distinguished from roughness in the profilometer traces.

Steel foils and rotors have been used in the majority of experiments,* but even this adverse combination of materials resulted in a very slight and tolerable degree of wear. Wiping and burnishing, rather than ploughing and scoring, appeared to be the rule. In a number of tests, pressurization of the foil bearing was prolonged and gradually diminished with increasing speed, in order to insure a sensibly large gap width in the entire operating speed range. The reverse procedure has been followed in decelerating the rotor. After a number of starts and stops, varying between 10 and 20, the foils have been removed and examined. Whenever the rotor has been carefully accelerated and decelerated in the foregoing manner, the wear marks have been hardly noticeable.

On the other hand, despite prolonged periods of operation under the most adverse kind of conditions, such as subjecting the housing to appreciable impact, exciting the system at resonance, or inducing large excursions of the rotor at high levels of excitation and low rotational speeds, the amount of wear has remained within very acceptable limits.

Figures 4.68 and 4.69 contain composite photographs of rotors, of foil segments adjacent to the three regions of wrap, and of profilometer traces obtained in traversing the deepest wear tracks on the surface of the rotor. Fig. 4.68 corresponds to the 2.414 lb rotor and a 0.001" steel foil, preloaded to 2.0 lb/in. The rotor has been operated for several

*302 stainless-steel foil and Carpenter, type 416, stainless-steel rotors.

hours, in both the vertical and horizontal attitudes, in the course of determination of the response to residual unbalance at various speeds. Following the conclusion of these tests, the same rotor and foil have been used in the study of response to impact. The photograph illustrates the condition of both rotor and foil at the conclusion of the foregoing experiments. The depth of the most conspicuous wear track was 50 μin

Figure 4.69 contains analogous data for the 1.0 lb rotor, supported by a 0.001" steel foil, preloaded to 2.0 lb/in, and illustrates the state of the rotor and of the foil following the conclusion of vibration experiments described in section G of this chapter. The reader will recall that the foregoing experiments involved intensive excitation and excursions of the rotor greatly exceeding the magnitude of the steady-state gap width. The total running time in this series of experiments, under a variety of operating conditions, has been estimated at between 30 to 40 hours. The profilometer traces taken across the deepest wear tracks indicate maxima of approximately 50 μin and 85 μin, as shown in Fig. 4.69.

Maximum wear occurs along the "anticlastic ridges" in the immediate vicinity and along the edges of the foil. This phenomenon is characteristic of foil bearings and has been the subject of several theoretical and experimental investigations [13, 23]. The gap width in the region of wrap is sensibly uniform, except along the edges of the foil and in the entrance and exit regions. The anticlastic effect and the decrease of pressure in the edge zone of the foil combine in closing the gap along the edges. Although the resistance to closure along the edges increases with foil thickness, the increase of thickness amplifies the anticlastic undulation and increases its wavelength. The latter effect is dominant, and the net result is a decrease of minimum clearance along the edges. In addition, an increase of foil thickness translates the minimum gap width toward the centerline of the foil.

The wear tracks along the anticlastic ridges have, indeed, been more pronounced when a 0.002" steel foil was used in a number of the experiments, but the amount of wear has been tolerable* and, after an initial period of wear-in, the track depth remained nearly constant.

In addition to decrease of clearance along the edges of the foil, a minimum occurs also in the vicinity of the trailing end of the region of wrap [10, 13, 21, 22, 23]. The minimum gap width is approximately 30% less than the clearance in the region of uniformity. A similar situation may also arise in the entrance zone, but only in the case of relatively rigid foils [11].** In the course of the present experiments, contact in the vicinity of the exit zone has been negligible. On the other hand, a characteristic and reproducible wear pattern could invariably be observed in the region of wrap adjoining the entrance zone. It consisted of a series of tracks, regularly spaced at approximately 1/16 in. The tracks originated at the leading edge of the region of wrap and terminated at relatively short, but unequal, distances in the interior. The wear pattern along the anticlastic ridges and in the entrance zone is illustrated in the appended schematic diagram. Two minor wear tracks, colinear with the rows of pressurization orifices, are also indicated in the diagram.

---

*The anticlastic edge effect can be partly suppressed by bevelling the foil along the edges. The use of thicker foils may be advantageous, and the bevelling technique may prove to be useful.

**The effect of fluid inertia and compressibility and the displacement of the foil in the entrance zone is not yet fully understood.

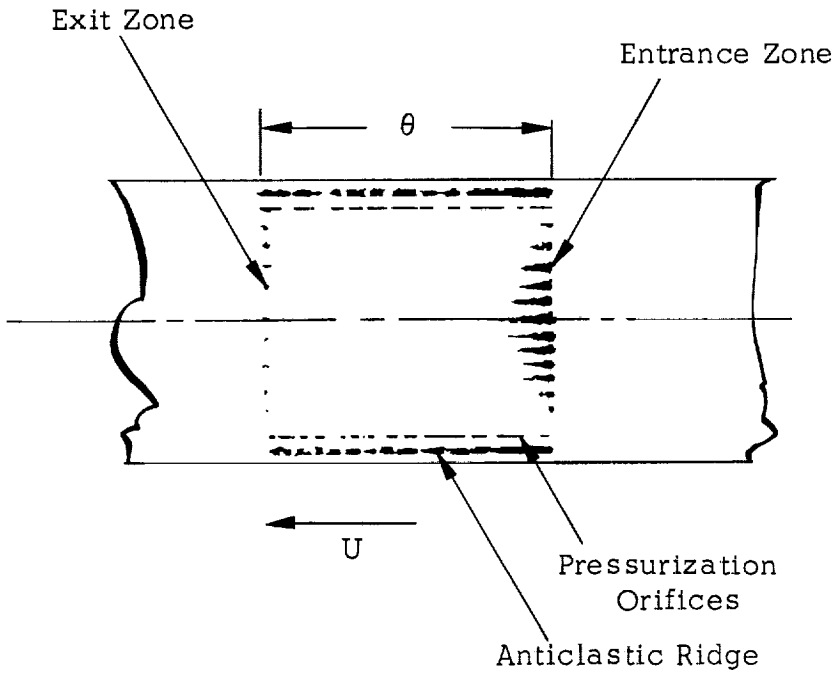

The wear pattern in the entrance zone could not be attributed to the entry of foreign particles. The latter produced fine serations, as opposed to the burnished, or someitmes oxide-coated wipe-wear tracks along the edges and in the entrance region. The regular spacing of the latter ($\sim 0.065"$) appears to have been of the same order of magnitude as the half-wavelength of the inwardly decaying, anticlastic undulation ($\sim 0.075"$). The possibility of a standing wave, with contact occurring at its alternating crests and troughs, must not be excluded. It is also possible that the phenomenon may be related to elasto-hydrodynamic interactions in the entrance zone, which are difficult to predict. The wear pattern in the entrance zone is clearly discernible in the photograph of foil sectors in Fig. 4.69, and the corresponding wear marks on the rotor surface can be easily identified. The depth of these wear marks has been appreciably smaller than the track depth along the edges of the foil and could hardly be distinguished in profilometer records. The slight

dissymmetry of the overall wear pattern with regard to the centerline of the foil reflects deviations from geometrically perfect alignment.

In consideration of severity of dynamic loads applied to the foil-rotor system in the course of the present experiments, and in view of the fact that no attempt has been made to enhance surface compatibility by deposition of suitable metals on the foil, or on the rotor, the foil bearing appears to be endowed with very superior wear characteristics.

Fig. 4. 68 Wipe-Wear Traces on Rotor and Foil

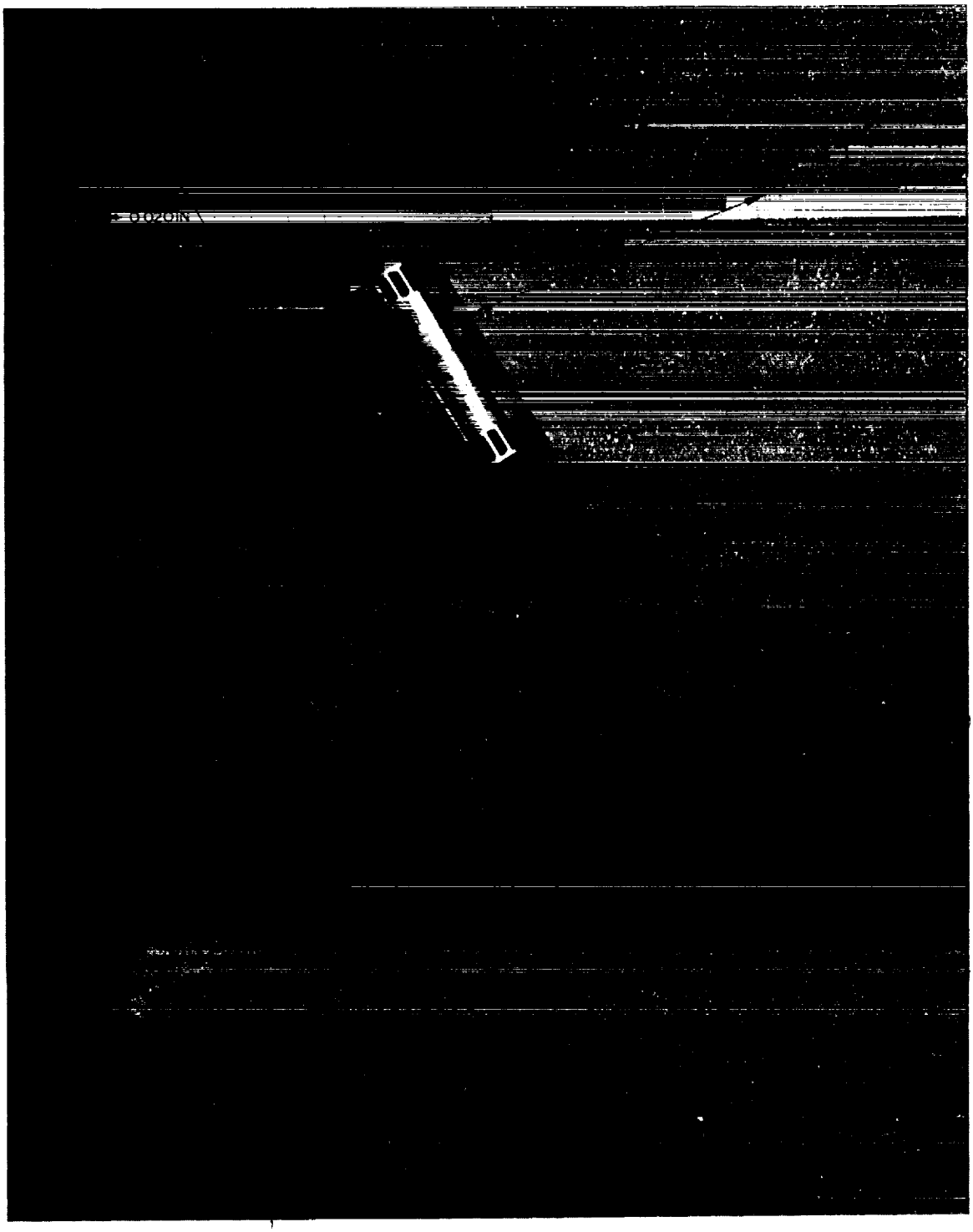

Fig. 4.69 Wipe-Wear Traces on Rotor and Foil

5. THEORY

A. Introduction

The analysis of foil rotor supports involves a number of complexities which are not present in solid-surface bearings. Difficulties are introduced not only because the compliance of the bearing surface must be taken into consideration, but also because the compliance is coupled with the dynamics of the rotor, with thermal effects, with the method of foil support, as well as with fluid inertia and compressibility, especially at high speeds of rotation and frequencies of excitation.

It thus becomes necessary to solve simultaneously the equations of fluid mechanics, of elasticity, and of geometric compatibility. The problem is too complicated to be solved in its entirety and one must resort to an approximate treatment, in which it is reasonable to retain equal orders of approximation.

Three levels of approximation are illustrated in Fig. 5.1. The first level is the most rigorous one. It involves the Navier-Stokes equations, possibly a nonlinear theory of elasticity, and an exact formulation of geometric compatibility. Commensurate with the simplification of the Navier-Stokes equations, by virtue of the fact that $h/r_o \ll 1$, is the linearization of the geometry, as a consequence of the condition that $x/r_o \ll 1$ (in which x is the shaft excursion). This simplification still permits the excursions of the shaft to be "large"; i.e. of the order of the clearance, $x \sim O(h)$. The excursions of tension are also allowed

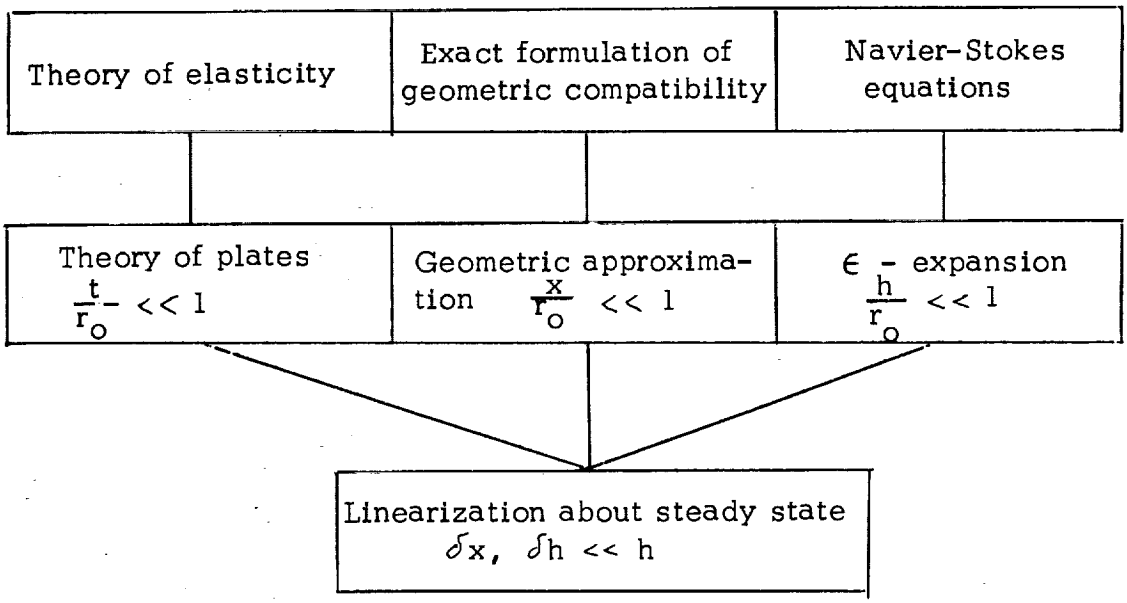

Fig. 5.1 Plan of Theoretical Approximations for Foil Bearing Problem

to be large, of order $\delta T \sim O(T_o)$. Nevertheless, only small strains appear in the foil. In the third level of approximation, only small perturbations from the steady state are allowed, so that $\delta T \ll T_o$, δx, $\delta h \ll h_o$.

In addition to these approximations, which are geometric in nature, further simplification may be considered. For example, the assumptions of incompressibility and negligible inertia effects are usually made in the study of foil bearings. They appear, however, to be invalid in the present application since the parameters $1/2\ \rho_a U^2/(T/r_o)$ and $T/p_a r_o$ are not small compared to unity. In problems of rotor dynamics, which involve solid-surface gas bearings, the time-dependent Reynolds equation is generally used and fluid inertia is neglected. Due to the importance of inertia in the present application, however, it appears reasonable to consider the behavior of the film as quasi-static, at least as a first approach, while retaining the effects of inertia. A study which includes both inertia and time-dependent film effects must follow, in order to establish their relative importance.

The plan of this chapter, therefore, is the following: First, a formulation of the "exact" geometric relations will be presented. These relations will then be simplified, taking advantage of the fact that $x/r_o \ll 1$. At this stage, the assumption of quasi-static film behavior, including, however, inertia and compressibility effects, will be made. The calculation of tensions and of gap widths will be based on this assumption. Finally, the equations will be linearized in terms of small perturbations about the steady state and the natural frequency will be obtained.

B. "Exact" Formulation

The treatment is based on the following assumptions:

1. The problem is planar;
2. The tension is a function of time but is spatially uniform in each foil bearing sector.

Consider n "infinitely wide" foil sectors spaced at equal angular intervals and supporting a shaft. (Fig. 5.2) In the absence of gravity and of a fluid-film, and with zero tension, the shaft center will be located at O (Fig. 5.2). If tension T_o is now introduced, the position of the shaft will remain unchanged because of symmetry. The foil length between the supports at this tension is denoted ℓ_o. Let x, y be fixed coordinates through O, defining the position of the shaft. In addition, consider a set of n auxiliary coordinate systems x_k, y_k through O, such that y_k is along bisector of the k^{th} foil arc and x_k is normal to it, as shown in Fig. 5.2 and 5.3.

Since the angle between the k^{th} support and the first support is

$$\gamma_k = \frac{2\pi}{n}(k-1) \tag{5.1}$$

the coordinates x_k, y_k can be expressed in terms of x, y by the relations

$$x_k = x \cos\gamma_k + y \sin\gamma_k \tag{5.2a}$$

$$y_k = -x \sin\gamma_k + y \cos\gamma_k \tag{5.2b}$$

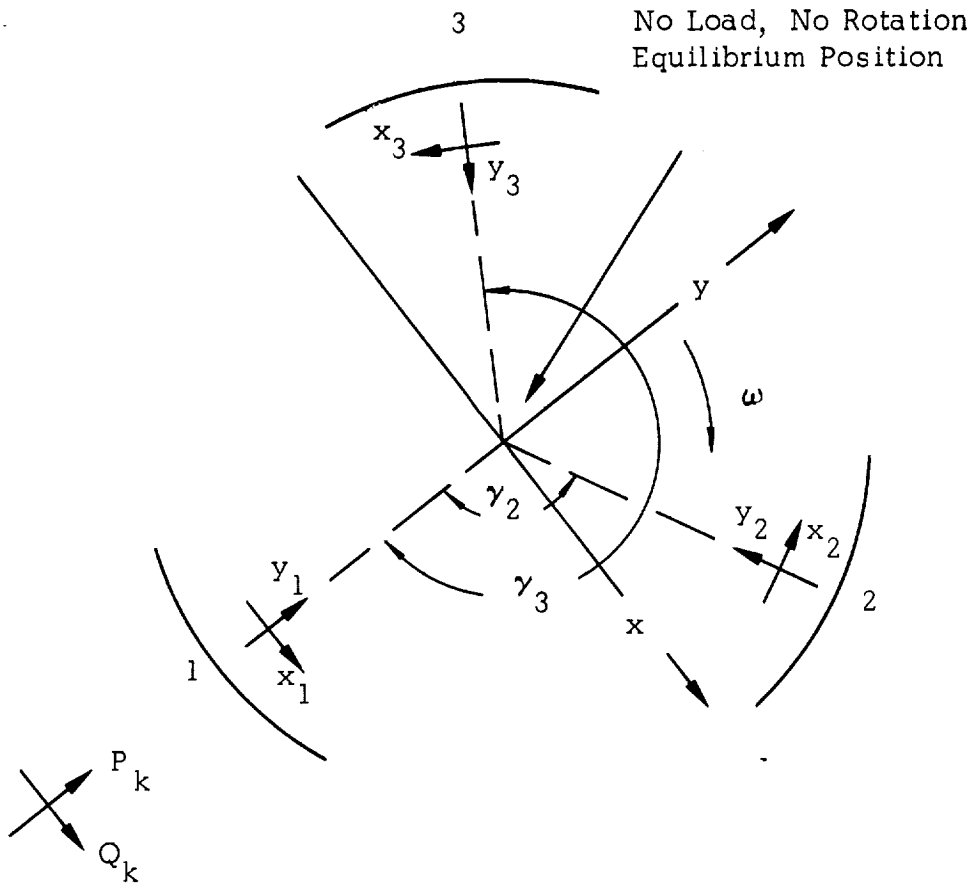

Fig. 5.2 Schematic Diagram of Foil Bearing Configuration

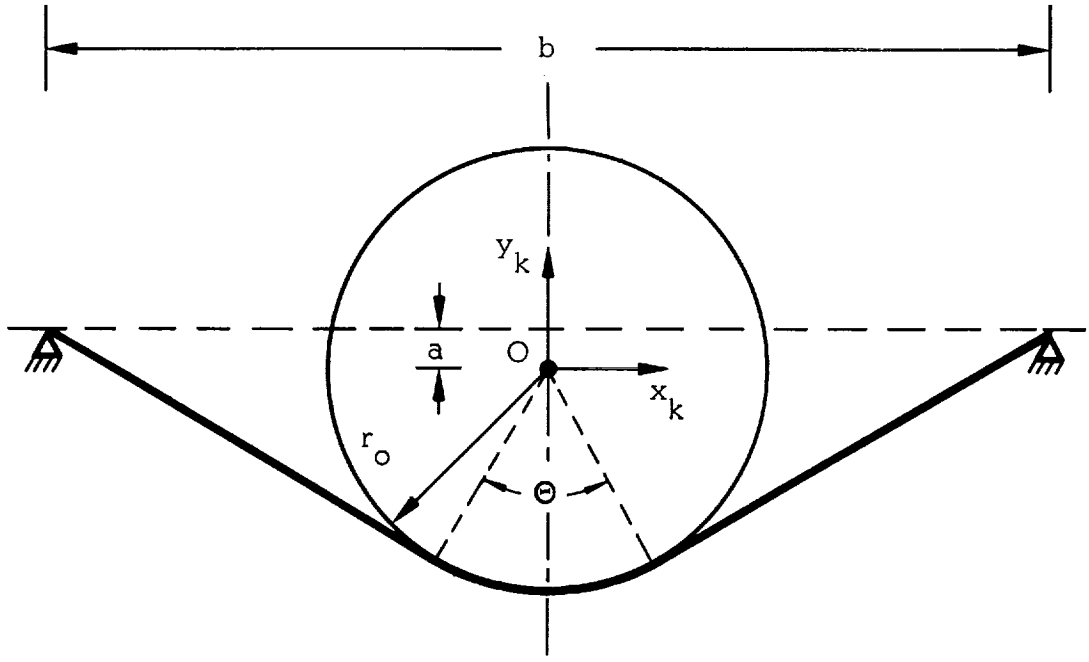

Shaft at Origin - No Rotation Condition

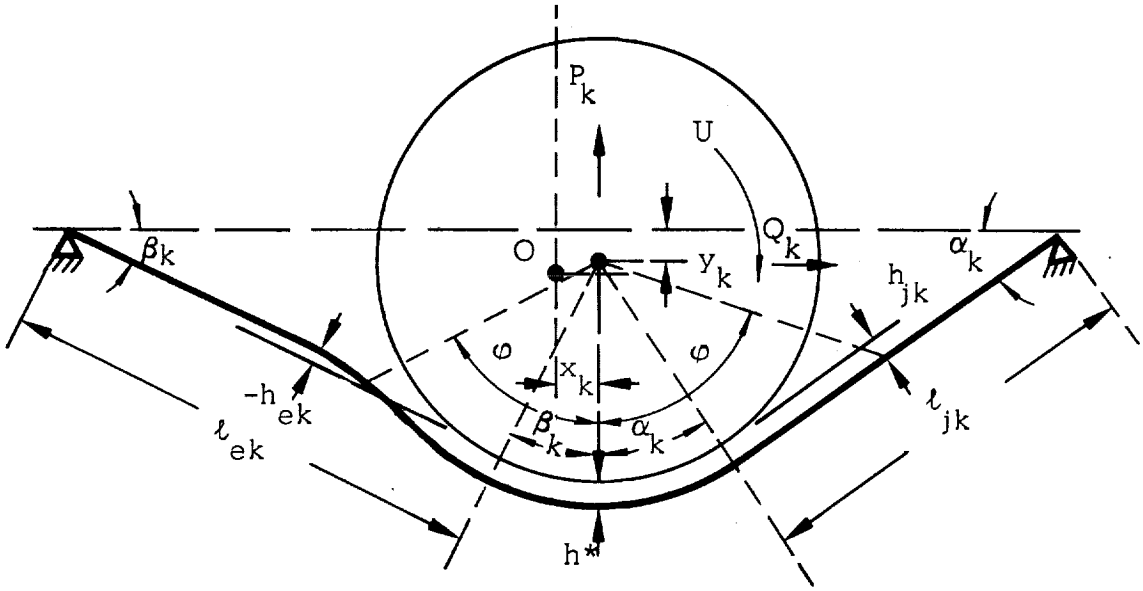

Shaft Displaced to (x, y)

Fig. 5.3 Schematic Diagram of a Single Foil Sector

The resultant force of the k^{th} foil arc on the shaft may be resolved into two components; P_k in the radial direction and Q_k in the trangential direction. These forces will be evaluated later. The resultant force of the whole system on the shaft can be expressed in terms of the individual foil forces as follows

$$F_y = \sum_{k=1}^{n} P_k \cos\gamma_k + \sum_{k=1}^{n} Q_k \sin\gamma_k \tag{5.3a}$$

$$F_x = -\sum_{k=1}^{n} P_k \sin\gamma_k + \sum_{k=1}^{n} Q_k \cos\gamma_k \tag{5.3b}$$

Supposing that at some instant τ the shaft position, in terms of the coordinates of the k^{th} foil segment, is (x_k, y_k), and the clearance distribution is $h_k(\theta, \tau)$, the length of the foil is given by:

$$\ell_k = \int_{-\frac{\pi}{2}-\operatorname{arctg}\frac{a-y_k}{\frac{b}{2}-x_k}}^{\frac{\pi}{2}+\operatorname{arctg}\frac{a-y_k}{\frac{b}{2}+x_k}} \left[(r_o + h_k)^2 + \left(\frac{\partial h_k}{\partial \theta}\right)^2 \right]^{1/2} d\theta \tag{5.4}$$

From the length ℓ_k and the initial length ℓ_o, one may find the tension in the k^{th} foil arc, using the equations of elasticity. The combination of the Navier-Stokes equations, the equations of elasticity, and Eq. (5.4) constitutes the formulation of the problem.

C. Approximations Consistent with the ϵ-Expansion of Foil Bearing Theory

The film forces acting on the shaft are restricted to narrow transition zones in the inlet and exit regions and to the central, or uniformity region. Beyond these regions, the foil bearing equations do not apply. The reason for this limitation is that these equations are based on an approximate expression of the radius of curvature and on Reynolds' equation, both of which do not apply in regions where the clearance is large. Let the region of applicability of the fluid equations be restricted to $-\varphi < \theta < \varphi$ (Fig. 5.3). Beyond this range the foil is assumed to be straight. The asymptotic distances of the foil are h_{ik}, h_{ek}, as given by the solutions of the foil bearing equations [6]. For a given rotor position (x_k, y_k) and clearance $h_k(\theta, \tau)$ obtained by solving the foil-bearing equation, the following geometric relations apply:

$$\frac{b}{2} - x_k = \ell_{ik} \cos \alpha_k + (r_o + h_{ik}) \sin \alpha_k \tag{5.5a}$$

$$\frac{b}{2} + x_k = \ell_{ek} \cos \beta_k + (r_o + h_{ek}) \sin \beta_k \tag{5.5b}$$

$$\frac{b}{2} = \frac{\ell_o - r_o \Theta}{2} \cos \frac{\Theta}{2} + r_o \sin \frac{\Theta}{2} \tag{5.5c}$$

$$\ell_{ik} \sin \alpha_k = (r_o + h_{ik}) \cos \alpha_k + a - y_k \tag{5.5d}$$

$$\ell_{ek} \sin\beta_k = (r_o + h_{ek}) \cos\beta_k + a - y_k \tag{5.5e}$$

$$\frac{\ell_o - r_o\Theta}{2} \sin\frac{\Theta}{2} = r_o \cos\frac{\Theta}{2} + a \tag{5.5f}$$

$$\ell_k = \ell_{ek} - (r_o + h_{ek})\, tg\,(\varphi - \beta_k) + \ell_{ik} - (r_o + h_{ik})\, tg\,(\varphi - \alpha_k) + \\ + r_o \int_{-\varphi}^{\varphi} \left\{ \left(1 + \frac{h_k}{r_o}\right)^2 + \left(\frac{\partial h_k}{r_o \partial\theta}\right)^2 \right\}^{1/2} d\theta \tag{5.5g}$$

$$\ell_o = b\cos\frac{\Theta}{2} + 2a\sin\frac{\Theta}{2} + r_o\Theta \tag{5.5h}$$

The stress-strain relation* for the foil is

$$\frac{T_k - T_o}{Et} = \frac{\ell_k - \ell_o - \delta\ell_p}{\ell_o} \tag{5.5i}$$

where $\delta\ell_p$ is the increase in ℓ_k caused by effects other than tension, such as the thermal elongation or the additional foil length supplied from regions beyond the points of support. This quantity is evaluated in Sec. F.

---

* A more accurate version of Eq. (5.5i) may be obtained by considering a spatially variable tension $T_k(\theta)$, generated by fluid shear:

$$\ell_k - \ell_o - \delta\ell_p = \frac{T_k - T_o}{Et}\left(\ell_{ek} - (r_o + h_{ek})\, tg\,(\varphi - \beta_k)\right) + \\ + \int_{-\varphi}^{\varphi} \frac{T_k(\theta) - T_o}{Et}\, r_o\, d\theta + \frac{T_k + \Delta T_k - T_o}{Et}\left(\ell_{ik} + (r_o + h_{ik})\, tg\,(\varphi - \alpha_k)\right)$$

The small improvement in accuracy does not warrant the added complexity.

The resultant radial force exerted on the shaft by the k^{th} foil sector is*:

$$P_k = T_k(\sin\alpha_k + \sin\beta_k) \tag{5.6a}$$

The resultant tangential force exerted on the shaft is:

$$Q_k = T_k(\cos\alpha_k - \cos\beta_k) \tag{5.6b}$$

The radial and tangential forces at zero speed and at the initial tension are:

$$P_o = 2T_o \sin\frac{\Theta}{2} \tag{5.6c}$$

$$Q_o = 0 \tag{5.6d}$$

Since the fluid mechanical problem is not solved on the basis of the Navier-Stokes equations, but rather on the basis of approximations due to $h/r_o << 1$, no accuracy is lost by using a simplified geometric relation based on $x/r_o << 1$. It is convenient to introduce the notation:

$$\alpha_k = \frac{\Theta}{2} + \delta\alpha_k \qquad \left(\delta\alpha_k \ll \frac{\Theta}{2} \sim O(1)\right) \tag{5.7a}$$

$$\beta_k = \frac{\Theta}{2} + \delta\beta_k \qquad \left(\delta\beta_k \ll \frac{\Theta}{2} \sim O(1)\right) \tag{5.7b}$$

---

* When fluid shear is included, Eq. (5.6a) becomes

$$P_k = (T_k + \Delta T_k)\sin\alpha_k + T_k \sin\beta_k$$

$$l_{ik} = \frac{l_o - r_o\Theta}{2}\delta l_{ik} \qquad (\delta l_{ik} \ll l_{ik}) \tag{5.7c}$$

$$l_{ek} = \frac{l_o - r_o\Theta}{2}\delta l_{ek} \qquad (\delta l_{ek} \ll l_{ek}) \tag{5.7d}$$

The simplified equations to be derived here are justified only when $\Theta \sim O(1)$. Expanding Eqs. (5.5) and using the perturbations (5.7), one finds

$$\delta\alpha_k = \frac{x_k \sin\frac{\Theta}{2} - y_k \cos\frac{\Theta}{2} + h_{ik}}{\frac{l_o - r_o\Theta}{2}} \tag{5.8a}$$

$$\delta\beta_k = \frac{-x_k \sin\frac{\Theta}{2} - y_k \cos\frac{\Theta}{2} + h_{ek}}{\frac{l_o - r_o\Theta}{2}} \tag{5.8b}$$

$$\delta l_{ik} = -x_k \cos\frac{\Theta}{2} - y_k \sin\frac{\Theta}{2} - r_o\delta\alpha_k \tag{5.8c}$$

$$\delta l_{ek} = x_k \cos\frac{\Theta}{2} - y_k \sin\frac{\Theta}{2} - r_o\delta\beta_k \tag{5.8d}$$

$$\delta\alpha_k + \delta\beta_k = \frac{-2y_k \cos\frac{\Theta}{2} + h_{ik} + h_{ek}}{\frac{l_o - r_o\Theta}{2}} \tag{5.8e}$$

$$\delta l_{ik} + \delta l_{ek} = -2y_k \sin\frac{\Theta}{2} - r_o(\delta\alpha_k + \delta\beta_k) \tag{5.8f}$$

Expanding Eq. (5.5g), using the relations (5.7), and subtracting Eq. (5.5h) from Eq. (5.5g), one finds that the elongation to order x/r_o is:

$$\delta\ell_k = -\delta\ell_p + \delta\ell_{ek} + \delta\ell_{ik} + \frac{r_o(\delta\alpha_k + \delta\beta_k)}{\cos^2(\varphi - \frac{\Theta}{2})} - \tag{5.8g}$$

$$-(h_{ek} + h_{ik})\, tg\,(\varphi - \tfrac{\Theta}{2}) + r_o\epsilon \int_{-\varphi/\epsilon^{1/3}}^{\varphi/\epsilon^{1/3}} \left[H_k + \tfrac{1}{2}\left(\frac{\partial H_k}{\partial \xi}\right)^2\right] d\xi$$

where

$$H_k(\xi, \tau) = \frac{h_k(\theta, \tau)}{r_o}\left(\frac{6\mu U}{T_{REF}}\right)^{-2/3} \tag{5.8h}$$

and where

$$d\xi = d\theta \left(\frac{6\mu U}{T_{REF}}\right)^{-1/3} \tag{5.8i}$$

The radial force component of the k^{th} foil arc on the shaft (including the effect of fluid shear) is:

$$P_k = (T_k + \Delta T_k)\sin\left(\frac{\Theta}{2} + \delta\alpha_k\right) + T_k \sin\left(\frac{\Theta}{2} + \delta\beta_k\right) \tag{5.9a}$$

$$P_k = 2T_k \sin\frac{\Theta}{2} + T_k \cos\frac{\Theta}{2}(\delta\alpha_k + \delta\beta_k) + \Delta T_k \sin\frac{\Theta}{2} \tag{5.9b}*$$

$$= 2T_k \sin\frac{\Theta}{2} + T_k \cos\frac{\Theta}{2}\,\frac{-\dot{y}_k \cos\frac{\Theta}{2} + h_{ik} + h_{ek}}{\frac{\ell_o - r_o\Theta}{2}} + \Delta T_k \sin\frac{\Theta}{2}$$

---

* $\dfrac{\Delta T_k}{T_k} \sim \dfrac{1}{T_k}\dfrac{\mu U}{h^*} r_o\Theta = \dfrac{\Theta}{6H^*}\left(\dfrac{6\mu U}{T_k}\right)^{1/3}$

When the shaft is displaced towards a foil sector, the radial force is increased due to three factors. The first term in Eq. (5.9b) represents the contribution of increased tension. The second term is due to changes of the angles α_k, β_k. The third term is due to fluid friction. When $\Theta \sim O(1)$, the second term is negligible compared to the first. The third term is generally small, since $\Delta T_k/T_k << 1$. Hence

$$P_k = 2T_k \sin \frac{\Theta}{2} \tag{5.10}$$

On the other hand, when $\Theta << 1$, the angular changes dominate the radial stiffness.

The tangential component of the force is:

$$Q_k = (T_k + \Delta T_k) \cos\left(\frac{\Theta}{2} + \delta\alpha_k\right) - T_k \cos\left(\frac{\Theta}{2} + \delta\beta_k\right) \tag{5.11a}$$

$$Q_k = \Delta T_k \cos\frac{\Theta}{2} + T_k \sin\frac{\Theta}{2}\left(\delta\beta_k - \delta\alpha_k\right) \tag{5.11b}$$

$$= \Delta T_k \cos\frac{\Theta}{2} + T_k \sin\frac{\Theta}{2} \frac{-2x_k \sin\frac{\Theta}{2} + h_{ek} - h_{ik}}{\frac{l_o - r_o\Theta}{2}}$$

For $\Theta << 1$, the frictional term dominates; $P \sim O(Q)$

for $\Theta \to \pi$, the second term dominates;

for $\Theta \sim O(1)$, $P >> Q$;

D. The Quasi-Static, Simplified Analysis of a Three-Foil Rotor Support

In this section, a simplified analysis is made for the case of $n = 3$. It is assumed that:

1) The film behavior is quasi-static; i.e. the steady-state film thickness distribution applies;

2) $\varphi = \Theta/2$ so that in the central region

$$H(\bar{s}) \equiv H^* = \frac{h^*}{r_o} \epsilon^{-2/3} \quad ; \quad \frac{\partial H}{\partial \bar{s}} = 0$$

in which h^* is the constant, nominal clearance derived from the steady state foil-bearing analysis;

3) The Q-forces are neglected, since their contribution is expected to be of order equal to, or smaller than the neglected dynamic effects.

With the above assumptions, Eq. (5.8g) becomes:

$$\delta \ell_k = -\delta \ell_p - 2 y_k \sin \frac{\Theta}{2} + h_k^* \Theta \tag{5.12}$$

so that Eq. (5.5i) becomes:

$$\frac{T_k - T_o}{\epsilon t} = \frac{-\delta \ell_p - 2 y_k \sin \frac{\Theta}{2} + \Theta h_k^*}{\ell_o} \tag{5.13}$$

in which:

$$h_k^* = r_o H_k^* \left(\frac{6 \mu U}{T_k} \right)^{2/3} \tag{5.14}$$

$$H_k^* = 0.643 + 0.286\, I_k + 1.905\, I_k^2 - \frac{0.183}{C_k} \qquad (5.14a)^*$$

$$I_k = \frac{\frac{1}{2}\rho_a U^2}{T_k / r_o} \qquad \text{(inertia parameter)} \qquad (5.14b)$$

$$C_k = \frac{p_a}{T_k / r_o} \qquad \text{(compressibility parameter)} \qquad (5.14c)$$

For a specified shaft position y_k, given speed, dimensions, and physical properties, the transcendental Eqs. (5.13) and (5.14) are to be solved for the unknowns h_k^* and T_k.

E. Determination of the Bearing Stiffness by Linearization About the Steady State

In order to evaluate the "equivalent spring constant" of the system, it is necessary to obtain expressions of $\partial T_k/\partial x, \partial T_k/\partial y$. Differentiating Eq. (5.13) and collecting terms,

$$\frac{\partial T_k}{\partial x} = \frac{-2 \sin \frac{\Theta}{2} \frac{\partial y_k}{\partial x}}{\frac{l_o}{Et} + \frac{\partial \delta l_p}{\partial T_k} - \frac{r_o \Theta}{T_k}\left(\frac{6\mu U}{T_k}\right)^{2/3}\left[\frac{\partial H^*}{\partial T_k} T_k - \frac{2}{3} H_k^*\right]} \qquad (5.15)$$

---

* The formula for H_k^* is a curve-fit obtained in [20]. The limit of accuracy of this approximate formula is estimated as $\pm 0.1\%$ for $I_k = 0$, increasing nearly linearly to $\pm 20\%$ at $I_k = 0.6$. This estimate of accuracy is uniformly valid for $1 < C_k < \infty$. For $C_k < 1$, the formula underestimates the clearance.

or more specifically:

$$\frac{\partial T_k}{\partial x} = -A_k \frac{\partial \gamma_k}{\partial x} = A_k \sin\gamma_k \qquad \begin{cases} \sin\gamma_1 = 0 \\ \sin\gamma_2 = \sqrt{3}/2 \\ \sin\gamma_3 = -\sqrt{3}/2 \end{cases} \tag{5.16a}$$

$$\frac{\partial T_k}{\partial y} = -A_k \frac{\partial \gamma_k}{\partial y} = -A_k \cos\gamma_k \qquad \begin{cases} \cos\gamma_1 = 1 \\ \cos\gamma_2 = -\frac{1}{2} \\ \cos\gamma_3 = -\frac{1}{2} \end{cases} \tag{5.16b}$$

in which

$$A_k = \frac{2\sin\frac{\omega}{2}}{\frac{\ell_0}{Et} + \frac{\partial \Delta\ell_p}{\partial T_k} + \frac{r_0\omega}{T_k}\left(\frac{6\mu U}{T_k}\right)^{2/3}\left[\frac{2}{3}H_k^* - \frac{\partial H^*}{\partial T_k}T_k\right]} \tag{5.16c}$$

and

$$T_k \frac{\partial H^*}{\partial T_k} = -0.286\, I_k - 3.81\, I_k^2 - \frac{0.183}{C_k} \tag{5.17}$$

Eqs. (5.3) become:

$$F_y = P_1 - \frac{P_2}{2} - \frac{P_3}{2} = 2\sin\frac{\omega}{2}\left(T_1 - \frac{T_2}{2} - \frac{T_3}{2}\right) \tag{5.18a}$$

$$F_x = -P_2\frac{\sqrt{3}}{2} + P_3\frac{\sqrt{3}}{2} = \sqrt{3}\sin\frac{\omega}{2}\left(T_3 - T_2\right) \tag{5.18b}$$

Hence,

$$k_{yy} = -\frac{\partial F_y}{\partial y} = 2\sin\frac{\omega}{2}\left(A_1 + \frac{A_2}{4} + \frac{A_3}{4}\right) \tag{5.19a}$$

$$k_{xx} = -\frac{\partial F_x}{\partial x} = \frac{3}{2}\sin\frac{\omega}{2}\left(A_3 + A_2\right) \tag{5.19b}$$

$$k_{xy} = -\frac{\partial F_x}{\partial y} = \frac{\sqrt{3}}{2} \sin\frac{\Theta}{2}\left(A_2 - A_3\right) \qquad (5.19c)$$

$$k_{yx} = -\frac{\partial F_y}{\partial x} = \frac{\sqrt{3}}{2} \sin\frac{\Theta}{2}\left(A_3 - A_2\right) \qquad (5.19d)$$

For the particular case of no static load, the equilibrium position is $x = y = 0$ and consequently: $T_1 = T_2 = T_3 = T$ and $A_1 = A_2 = A_3 = A$. The expressions for t he stiffness then become:

$$k_{xx} = k_{yy} = 3\sin\frac{\Theta}{2} A = \frac{Et}{r_o} \frac{6\sin^2\frac{\Theta}{2}}{\frac{l_o}{r_o} + \frac{Et}{r_o}\frac{\partial \Delta l_p}{\partial T} + \frac{\Theta}{T/Et}\left(\frac{6\mu U}{T}\right)^{2/3}\left(\frac{2}{3}H^* - \frac{\partial H^*}{\partial T}T\right)} \qquad (5.20a)$$

$$k_{xy} = k_{yx} = 0 \qquad (5.20b)$$

Thus, in the absence of load, the cross-coupling stiffness terms cancel to the first order of approximation. The magnitude of the cross-coupling terms must, therefore, be evaluated from the higher order terms hitherto neglected, such as the frictional terms (Eqs. 5.9, 5.11). On the other hand, in the presence of radial load the cross-coupling stiffness arises from dissymmetry. One may expect, therefore, a qualitative difference between the response under load and under no-load conditions. The bearing-stiffness curves presented in this report apply only to the case, in which no radial load is applied to the rotor.

F. Estimate of $\delta \ell_p = \delta \ell_s + \delta \ell_t$

The quantity $\delta \ell_p$ can be regarded as the sum of $\delta \ell_s$, the additional length of foil supplied across the lines of tangency with the guides, and $\delta \ell_t$, the thermal extension of the foil. The quantity $\delta \ell_p$ is largely a function of specific design. In the present report, this quantity has been evaluated with regard to the specific geometry and the constraints of the experimental foil bearing.

Estimate of Length $\delta \ell_s$ Supplied Across Lines of Tangency of the Foil Guides

In the case of the foil mounting illustrated in Fig. 5.4, a variation of tension T will cause an elongation of the foil length wrapped around $\Theta_{g1} + \Theta_{g2} = \Theta_g$. At any angular position θ, the tension is given by:

$$T(\theta) = T e^{-f\theta} \tag{5.21}$$

and the elongation can be expressed by the integral:

$$\delta \ell_s = \int_0^{\Theta_g} \frac{T - T_o}{Et} e^{-f\theta} r_g \, d\theta = \frac{(T - T_o) r_g}{Et \cdot f} \left(1 - e^{-f\Theta_g}\right) \tag{5.22}$$

$$\frac{\partial \delta \ell_s}{\partial T} = \frac{r_g}{Etf} \left(1 - e^{-f\Theta_g}\right) \tag{5.23}$$

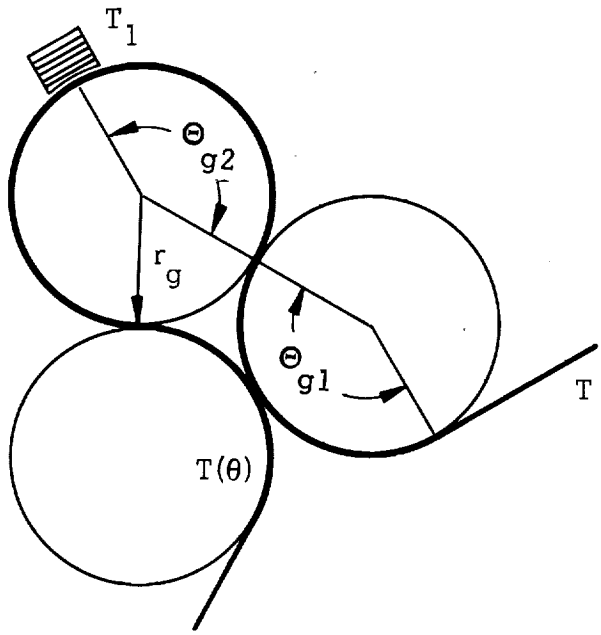

Fig. 5.4 Notation Applicable to Foil-Bearing Problem

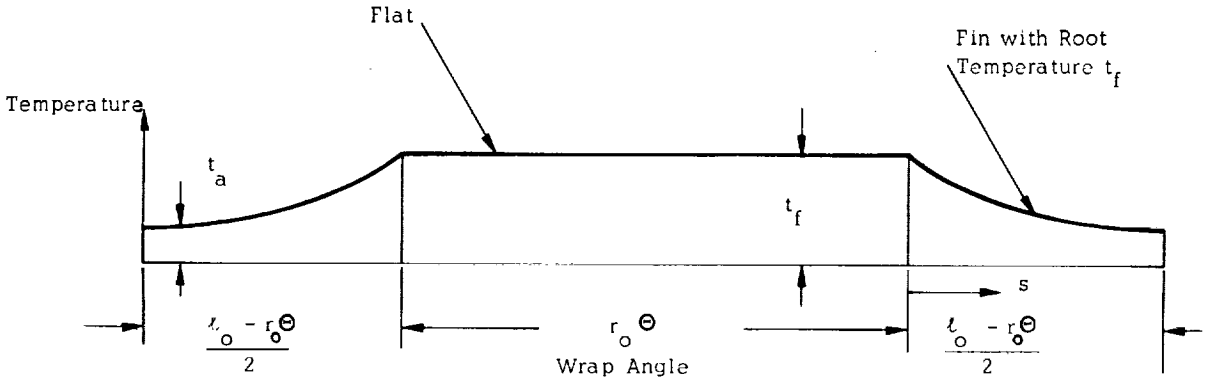

Fig. 5.5 Schematic Representation of Foil Temperature Distribution

The last formula can be used for an approximate study of the foil bearing under time-dependent conditions, only when the tension variations are large enough for slip to occur continuously throughout the entire angle Θ_g* . This applies when $\delta T/T > 2f\Theta_g$. An extension $\delta \ell_s$ at each terminal of a single foil-bearing sector has been taken into account in the numerical calculations.

The Effect of Temperature

An approximate model has been adopted for estimating the foil temperature distribution. (Fig. 5.5)

Assuming that the heat generated per unit area and unit time in the central region is convected from the surface of the foil and that the transfer is characterized by an average value of the film coefficient $\bar{h}$, the process can be described by the simple relationship:

$$\frac{\mu U}{h^*} \cdot U = \bar{h} \left(t_f - t_a\right) \tag{5.24}$$

The inlet and exit branches of the foil can be looked upon as fins, with root temperature t_f. The foil temperature at a distance s from the line of tangency with the shaft is then given by:

$$t(s) - t_a = \left(t_f - t_a\right) \frac{\cosh m\left(\frac{\ell_o - r_o\Theta}{2} - s\right)}{\cosh m\left(\frac{\ell_o - r_o\Theta}{2}\right)} \tag{5.25}$$

* A value of 0.08 of the coefficient of friction at the guides was determined experimentally, so that the foregoing assumption was justified for the present case.

in which

$$m = \sqrt{\frac{2\bar{h}}{kt}} \tag{5.26}$$

($\bar{h}$ film coefficient; k conductivity; t foil thickness)

The average temperature rise in the inlet or in the exit branch can, therefore, be expressed as follows:

$$t_{av} - t_a = \frac{t_f - t_a}{\frac{l_o - r_o\Theta}{2}} \int_0^{\frac{l_o - r_o\Theta}{2}} \frac{\cosh m\left(\frac{l_o - r_o\Theta}{2} - s\right)}{\cosh m\left(\frac{l_o - r_o\Theta}{2}\right)} ds$$

$$= \frac{\mu U^2}{h^* \bar{h}} \frac{\tanh m\left(\frac{l_o - r_o\Theta}{2}\right)}{m\left(\frac{l_o - r_o\Theta}{2}\right)} \tag{5.27}$$

The thermal elongation of the foil is thus estimated as

$$\delta l_t = \frac{\alpha \mu U^2}{h^* \bar{h}} \left(r_o \Theta + \frac{2 \tanh m\left(\frac{l_o - r_o\Theta}{2}\right)}{m} \right) \tag{5.28}$$

In the foregoing equations, h* is regarded as constant under dynamic conditions, on the premise that the time constant of the temperature variation is much longer than the period of motion of the shaft.

G. Dimensionless Representation of the Results

The functional equations for the tension, the clearance, and the stiffness in the absence of gravity load are the following:

$$\frac{T-T_o}{Et} = f\left[\frac{U^2\alpha\mu}{h^* l_o k}\left(r_o\Theta + \frac{2\,tgh\; m\frac{l_o - r_o\Theta}{2}}{m}\right), \frac{r_g}{r_o f}\left(1-e^{-f\Theta_g}\right), \Theta, \frac{r_o}{l_o}, \frac{h^*}{r_o}\right] \tag{5.13}$$

$$\frac{h^*}{r_o} = f\left(\frac{6\mu U}{T}, \frac{\frac{1}{2}\rho_a U^2}{T/r_o}, \frac{p_a}{T/r_o}\right) \tag{5.14}$$

$$\frac{k r_o}{Et} = f\left(\frac{r_o}{l_o}, \frac{r_g}{r_o f}\left(1-e^{-f\Theta_g}\right), \Theta, \frac{T}{Et}, \frac{6\mu U}{T}, \frac{p_a}{T/r_o}, \frac{\frac{1}{2}\rho_a U^2}{T/r_o}\right) \tag{5.15}$$

Because of the large number of parameters involved, the presentation of a complete parametric map is not feasible. More limited objectives have, therefore, been set in planning the graphical presentation.

The effects of varying the speed, the radius, the initial tension and the extension characteristics appear to be the most important variables for geometrically similar foil bearings. On the other hand, the ratio r_o/l_o, the angle of wrap Θ, the thermal characteristics, and the relative effect of added supply of foil across the supports are not likely to differ greatly in many foil-bearing designs. The foregoing consideration is reflected in the choice of dimensionless variables used in presenting numerical data. The following design parameters have been obtained as a result of regrouping of dimensionless quantities occurring "naturally" in the equations:

Speed parameter.: $$P_u = \sqrt{\frac{2I}{C}} = \sqrt{2\,\frac{\frac{1}{2}\rho_a U^2}{T/r_o}\Big/\frac{p_a}{T/r_o}} = \frac{U}{\sqrt{p_a/\rho_a}} \tag{5.29a}$$

Radius parameter: $$P_r = \sqrt{\frac{72IC}{\epsilon^2}} = \sqrt{\frac{72\,\frac{1}{2}\rho_a U^2\,\frac{\rho_a}{T/r_o}\,\frac{1}{T/r_o}}{\left(\frac{6\mu U}{T}\right)^2}} = \frac{r_o}{\mu/\sqrt{\rho_a p_a}} \qquad (5.29b)$$

Extension parameter: $$P_e = \frac{1}{\left(\frac{T}{Et}\right)\epsilon}\sqrt{\frac{72I}{C}} = \frac{\sqrt{\frac{\frac{1}{2}\rho_a U^2}{T/r_o}\cdot 72\cdot\Big/\frac{\rho_a}{T/r_o}}}{\frac{T}{Et}\cdot\frac{6\mu U}{T}} = \frac{Et}{\sqrt{\mu^2\rho_a/\rho_a}} \qquad (5.29c)$$

Initial tension parameter: $$P_{T_o} = \frac{T_o}{Et}P_e = \frac{T_o}{\sqrt{\frac{\mu^2\rho_a}{\rho_a}}} \qquad (5.29d)$$

Thermal expansion parameter: $$P_t = \frac{\alpha\rho_a\sqrt{\frac{\rho_a}{\rho_a}}}{\bar{h}}\left(\Theta + \frac{2\,\mathrm{tgh}\,m\left(\frac{l_o - r_o\Theta}{2}\right)}{m r_o}\right) \qquad (5.29e)$$

Slack parameter: $$P_s = \frac{\delta l_s}{r_o}\frac{Et}{T-T_o} = \frac{2r_g}{r_o f}\left(1 - e^{-f\Theta_g}\right) \qquad (5.29f)$$

Dimensionless gap: $$P_h = \frac{h^*}{r_o}P_r = \frac{h^*}{\mu/\sqrt{\rho_a p_a}} \qquad (5.29g)$$

Dimensionless stiffness: (per unit width) $$P_k = \frac{k r_o}{Et}\frac{P_e}{P_r} = \frac{k}{p_a} \qquad (5.29h)$$

The functional relations (5.13), (5.14) and (5.20), when expressed in terms of the design parameters, become:

$$\frac{T-T_o}{Et} = f\left(P_u, P_r, \frac{h^*}{\mu/\sqrt{p_o p_a}}, P_t, P_s, \Theta, \frac{r_o}{l_o}\right) \tag{5.30a}$$

$$\frac{h^*}{\mu/\sqrt{p_o p_a}} = f\left(P_u, P_r, P_e \cdot \frac{T}{Et}\right) = f\left(P_u, P_r, P_e, P_{T_o}, P_t, P_s, \Theta, \frac{r_o}{l_o}\right) \tag{5.30b}$$

$$\frac{k}{p_a} = f\left(P_u, P_r, P_e, P_{T_o}, P_t, P_s, \Theta, \frac{r_o}{l_o}\right) \tag{5.30c}$$

The parameters r_o/l_o, Θ, P_s, P_t are expected to remain sensibly invariant for geometrically similar designs. The latter have been assigned constant values in the charts contained in this report. These values correspond to the experimental foil bearing used in the course of the present study. Given the parameters P_u, P_r, P_e, P_{T_o}, for example, the dimensionless clearance and the dimensionless stiffness, as well as the value of $(T-T_o)/Et$ can be found with the aid of the appended design charts.

Each curve in Figs. 5.6 through 5.9 has been assigned a value of the pertinent dimensionless parameter and a sample-value of the characteristic physical variable. This dual notation has been intended to facilitate the physical interpretation of the results. In selecting the sample values, the following magnitudes of physical parameters have been used:

p_a = 14.7 psi

ρ_a = 0.075 Lbm/ft^3

μ = 0.265×10^{-8} Lbf-sec/in^2

E = 30×10^6 Lbf/in^2

α = 9×10^{-6} in/in

$\bar{h}$ = 230 BTU/hr ^{o}F ft^{2}

k = 26.3 BTU/hr ^{o}F ft

Θ = 60^{o} = 1.05 rad

f = 0.08

Θ_g = 240^{o} = 4.19 rad

r_g/r_o = 0.375

ℓ_o/r_o = 1.985

The curves are intended for design purposes within limits of the representative parametric variations which have been included.

H. Sample Calculation

It is required to find the nominal clearance and the bearing stiffness and tension per unit width for a design geometrically similar to that shown in Figs. 2.1 and 2.2 . The following conditions will be considered in addition to the data given in the previous section:

W = 0 (No radial load)

r_o = 1 in

ℓ_o = 1.985 in

t = 1 mil

T_o = 2 Lb/in

N = 36,000 RPM = 600 RPS

$\frac{\ell_o}{r_o}$ = 1.985

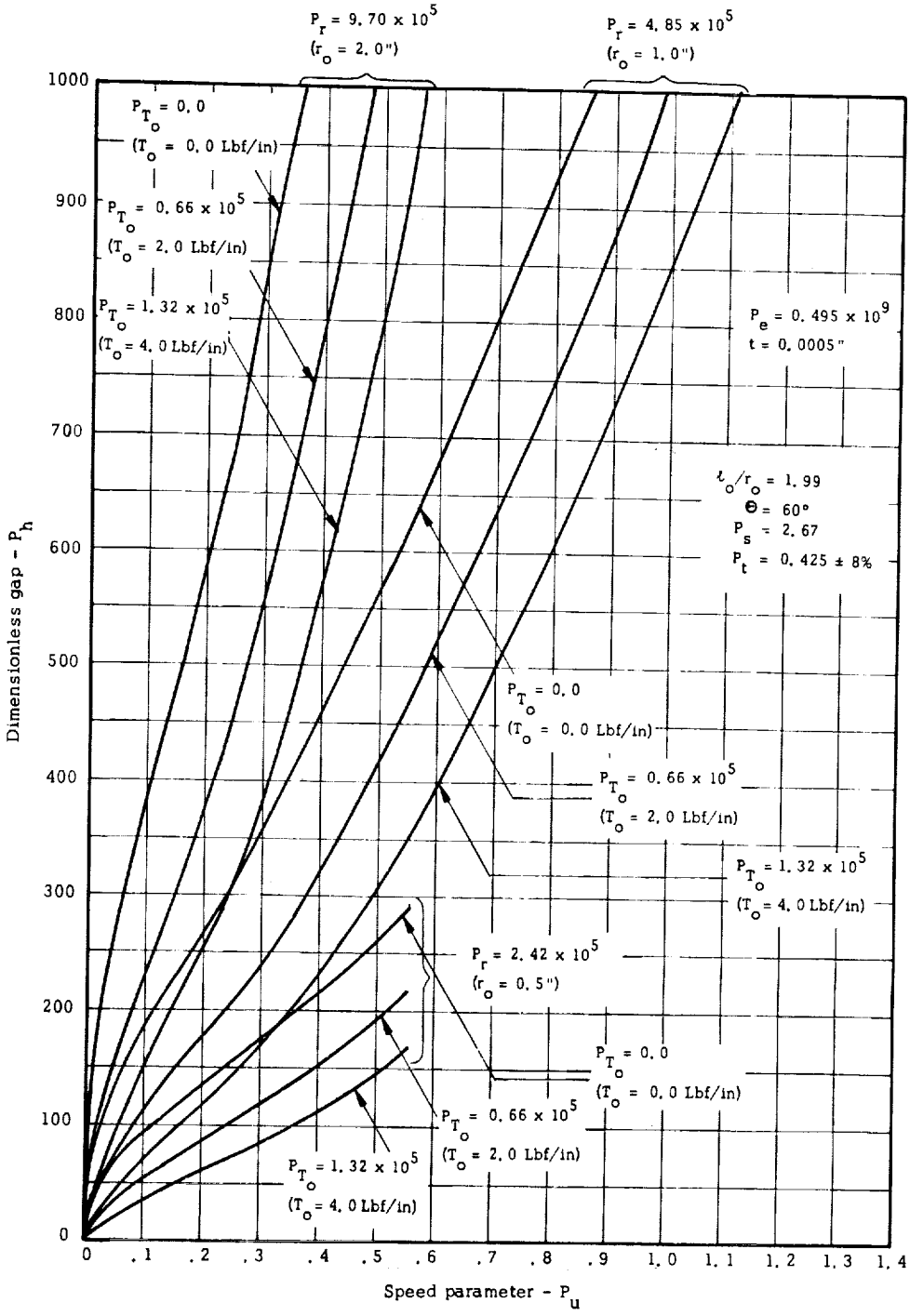

Fig. 5.6a Dimensionless Gap versus Speed Parameter ($P_e = 4.95 \times 10^8$)

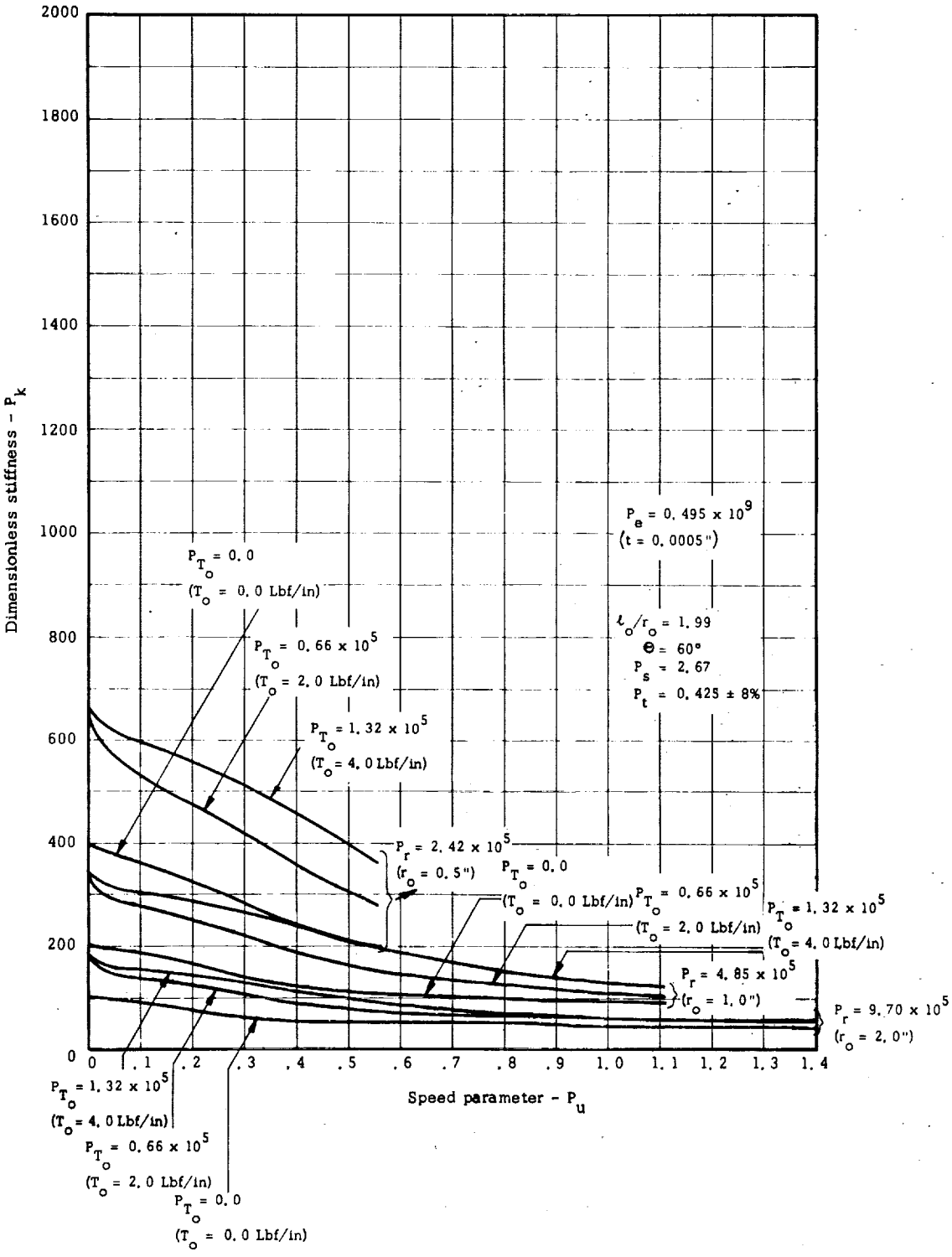

Fig. 5.6b Dimensionless Stiffness versus Speed Parameter ($P_e = 4.95 \times 10^8$)

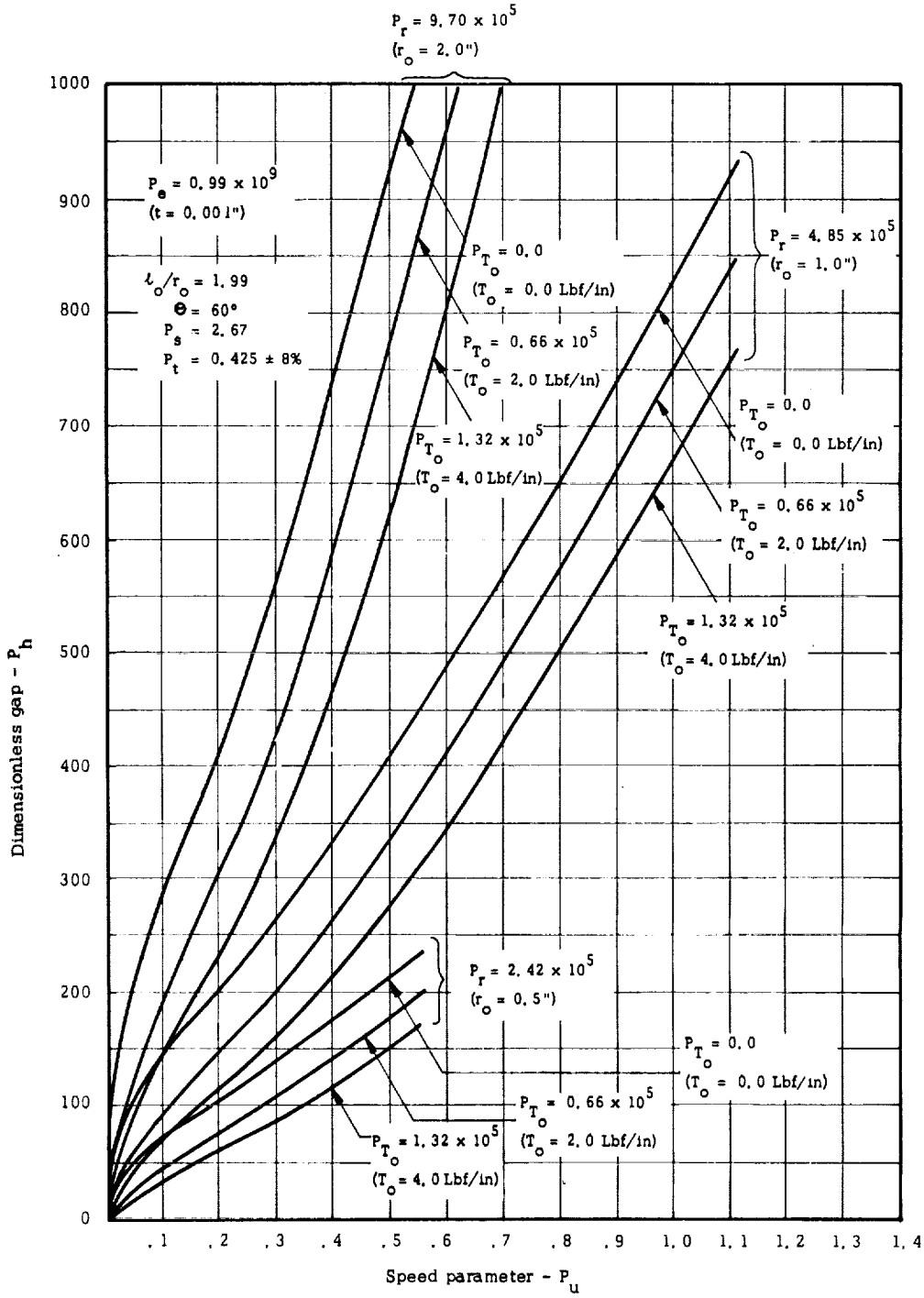

Fig. 5.7a Dimensionless Gap versus Speed Parameter ($P_e = 9.90 \times 10^8$)

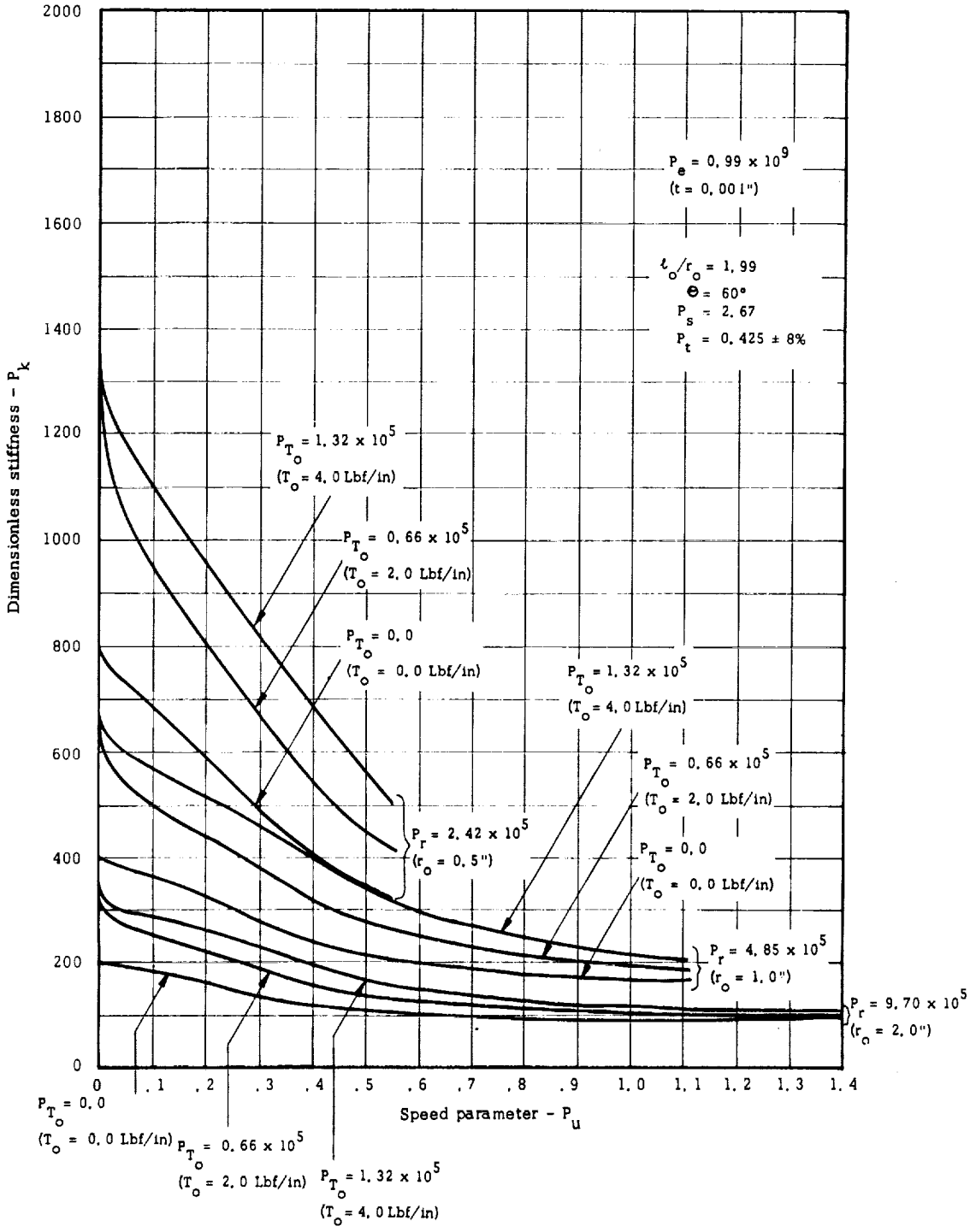

Fig. 5.7b Dimensionless Stiffness versus Speed Parameter ($P_e = 9.90 \times 10^8$)

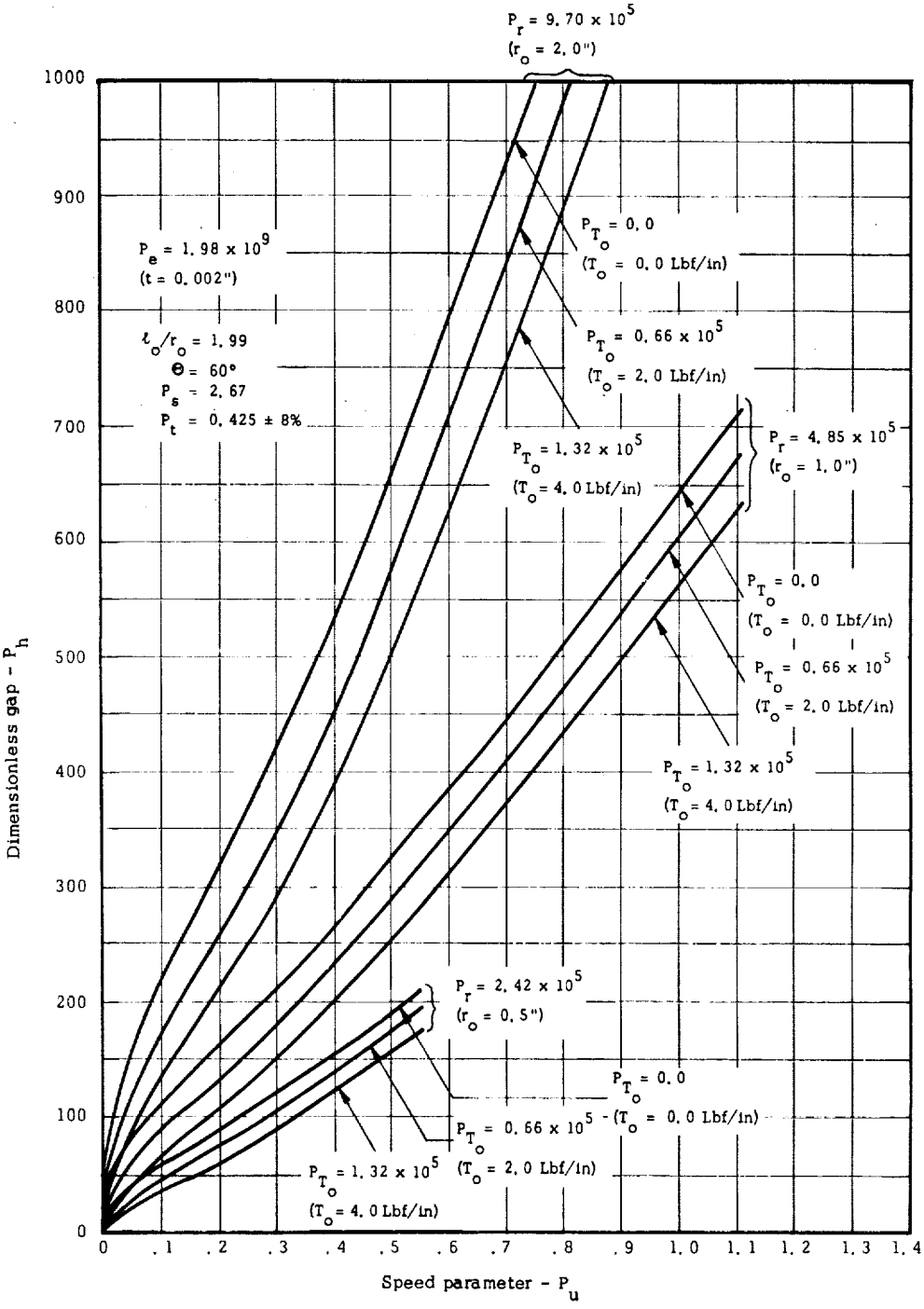

Fig. 5.8a Dimensionless Gap versus Speed Parameter
($P_e = 19.8 \times 10^8$)

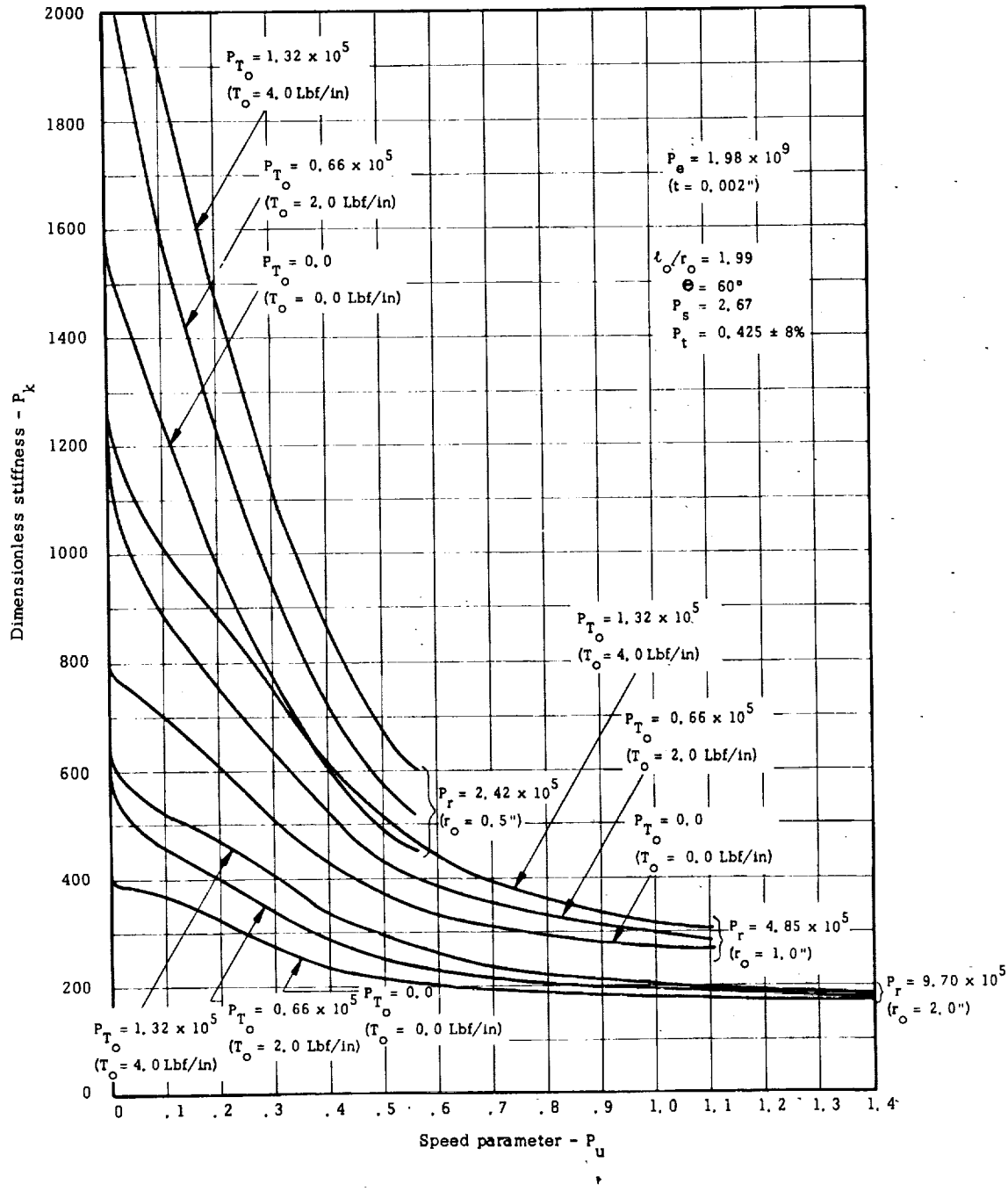

Fig. 5.8b Dimensionless Stiffness versus Speed Parameter ($P_e = 19.8 \times 10^8$)

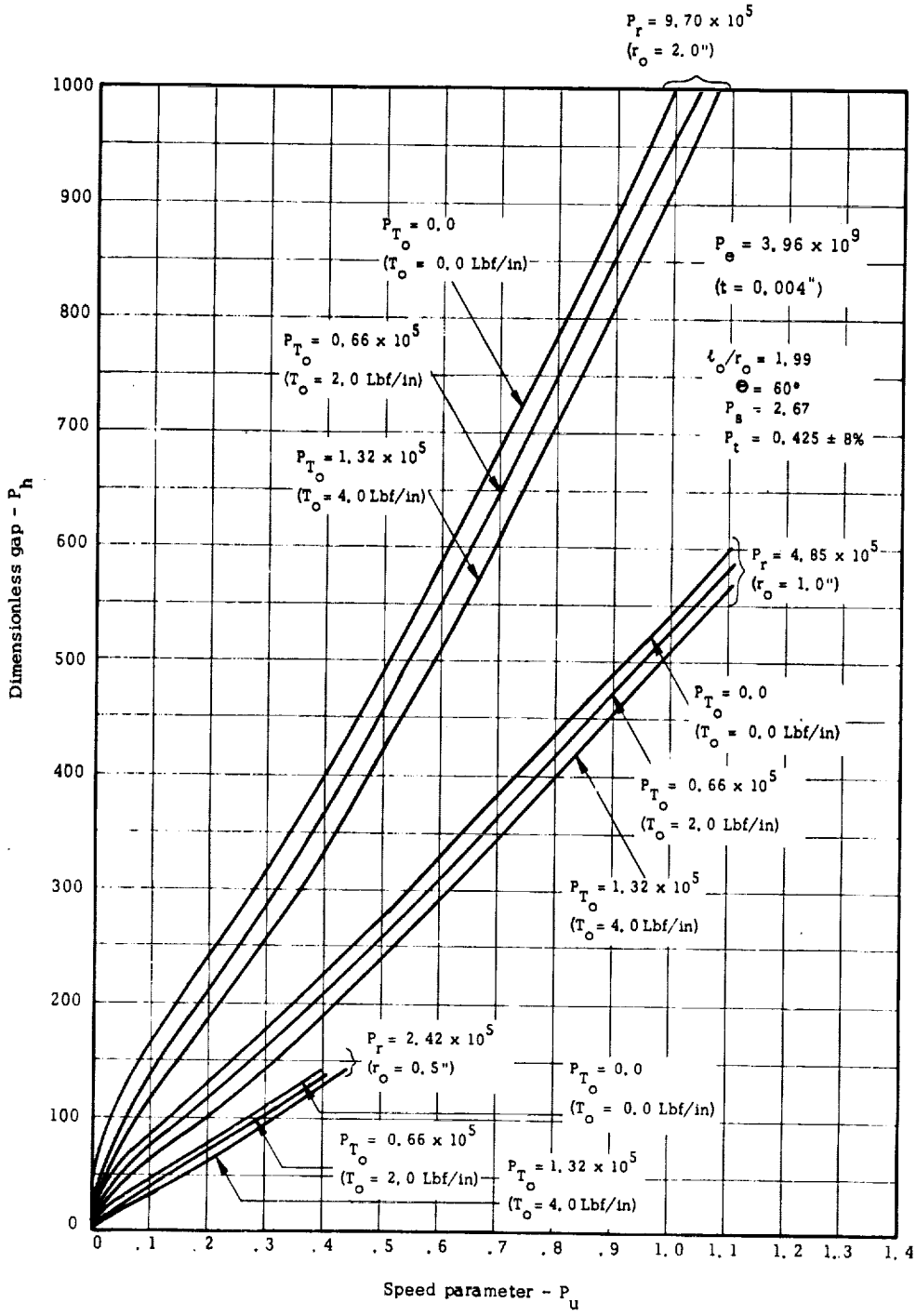

Fig. 5.9a Dimensionless Gap versus Speed Parameter ($P_e = 39.6 \times 10^8$)

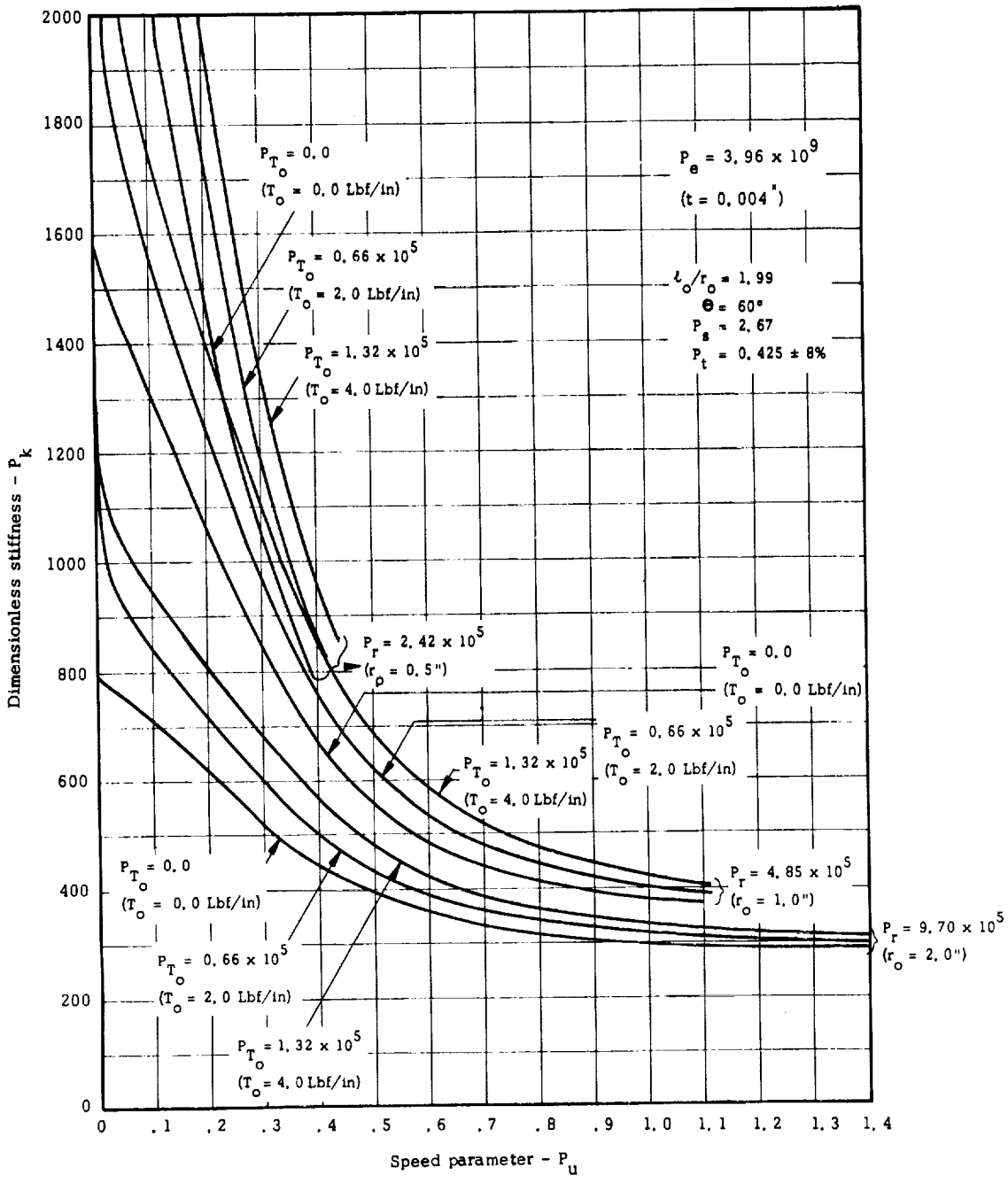

Fig. 5.9b Dimensionless Stiffness versus Speed Parameters ($P_e = 39.6 \times 10^8$)

$$P_u = \frac{U}{\sqrt{p_a/\rho_a}} = \frac{2\pi \times 600 \times 1}{\sqrt{14.7 \times 386 \times 12^3 / 0.075}} = 0.33$$

$$P_r = \frac{r_o}{\mu / \sqrt{p_a \rho_a}} = \frac{1}{0.265 \times 10^{-8} / \sqrt{\frac{0.075}{12^3 \times 386} \times 14.7}} = 4.85 \times 10^5$$

$$P_e = \frac{Et}{\sqrt{\mu^2 p_a / \rho_a}} = \frac{30 \times 10^6 \times 1 \times 10^{-3}}{\sqrt{(0.265 \times 10^{-8})^2 \times 14.7 / \frac{0075}{12^3 \times 386}}} = 9.9 \times 10^8$$

$$P_{T_o} = \frac{T_o}{Et} P_e = \frac{2}{30 \times 10^6 \times 1 \times 10^{-3}} \times 9901 \times 10^8 = 6.60 \times 10^4$$

$$m = \sqrt{\frac{2\bar{h}}{k t}} = \sqrt{\frac{2 \times 230}{26.3 \times 10^{-3} \times 12}} = 38.2 \quad 1/in$$

$$P_t = \frac{\alpha p_a \sqrt{\frac{p_a}{\rho_a}}}{\bar{h}} \left(\Theta + \frac{2 \operatorname{tgh} m \cdot \frac{l_o - r_o \theta}{2}}{m r_o} \right) =$$

$$= \frac{9 \times 10^{-6} \times 14.7 \sqrt{\frac{14.7 \times 386 \times 12^3}{0.075}}}{\frac{230}{0001285 \times 3600 \times 12}} \left(1.05 + \frac{2 \operatorname{tgh} 38.2 \left(\frac{1.985 - 1.05 \times 1}{2} \right)}{38.2 \times 1} \right) = 0.40$$

$$P_s = \frac{2 r_g}{r_{of}} \left(1 - e^{-f \Theta_g} \right) = \frac{2 \times 0.375}{0.08} \left(1 - e^{-0.08 \times 4.19} \right) = 2.670$$

From Fig. 5.7a it is found that the dimensionless gap is $P_h = 223.$ Using Eq. (5.29g) one obtains

$$h^* = P_h \frac{\mu}{\sqrt{p_a \rho_a}} = 223. \frac{0.265 \times 10^{-8}}{\sqrt{\frac{0.075}{12^3 \times 386} \times 14.7}} = 460 \times 10^{-6} \text{ inch}$$

From Fig. 5.7b, the dimensionless stiffness is found to be $P_k = 392$ and, hence, the stiffness per unit width becomes:

$$k = p_a \cdot P_k = 14.7 \times 360. = 5290 \ (\text{Lbf/in})/\text{in}$$

From Fig. 5.10 one finds that

$$\frac{T - T_0}{Et} = 0.62 \times 10^{-4}$$

and hence the tension per unit width

$$T = Et\left(\frac{T - T_0}{Et}\right) + T_0 = 30 \times 10^6 \times 1 \times 10^{-3} \times 062 \times 10^{-4} + 2 = 3.86 \text{ Lbf/in}$$

The foregoing results can now be used to perform an approximate calculation for a typical application.

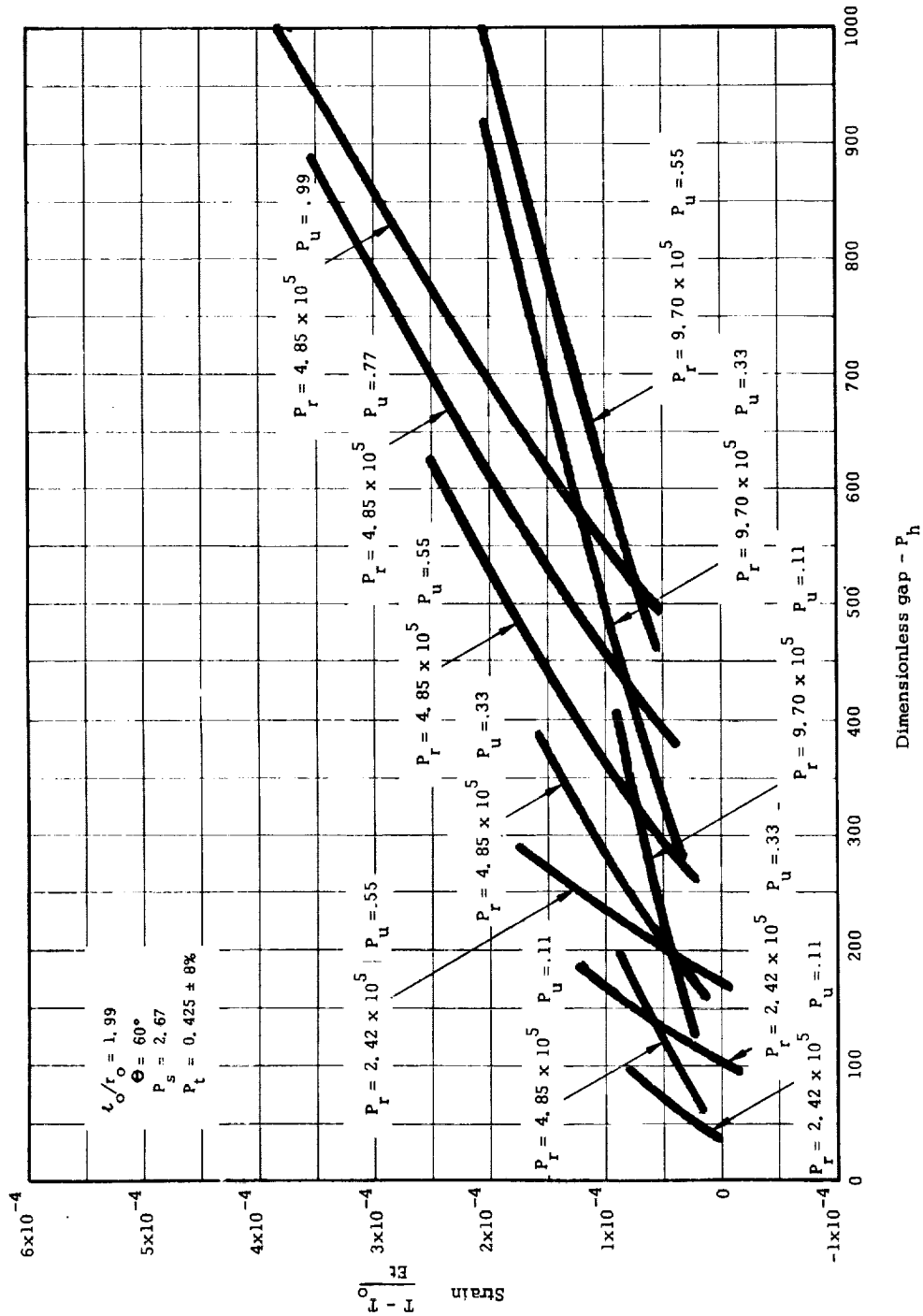

Fig. 5.10 Foil-Strain versus Dimensionless Gap

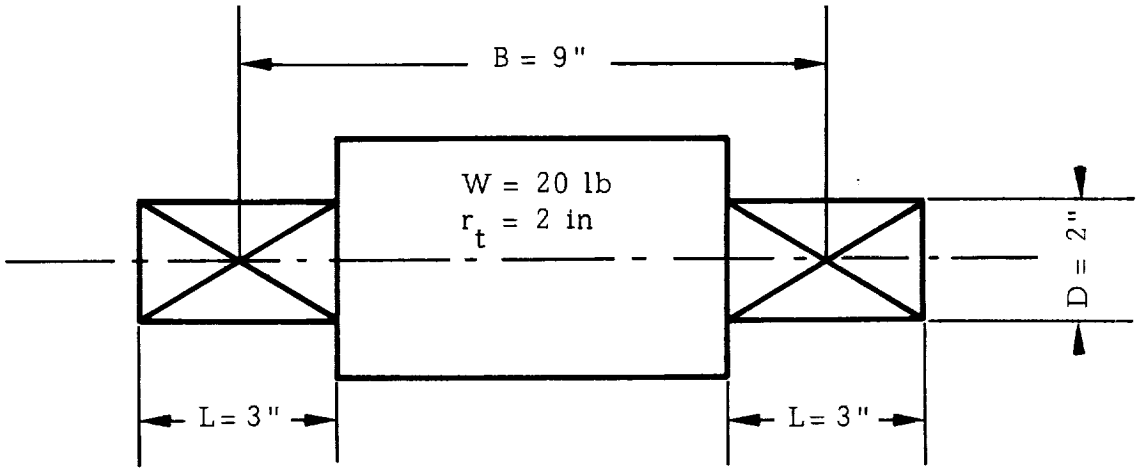

Fig. 5.11 Schematic Diagram of Rotor Supported in Two Foil Bearings

Figure 5.11 shows schematically a rotor supported on two foil bearings. For the specified data, the natural frequency in the cylindrical and conical modes are given by

$$f_{cyl} = \frac{1}{2\pi}\sqrt{\frac{k \cdot 2L}{W} g} = \frac{1}{2\pi}\sqrt{\frac{529_0 \times 2 \times 3 \times 386}{20}} = 127 \text{ cps}$$

and

$$f_{con} = \frac{1}{2\pi}\sqrt{\frac{(k \cdot 2L)\left(\frac{B}{2}\right)^2 g}{W \cdot r_t^2}} = \frac{1}{2\pi}\sqrt{\frac{529_0 \times 2 \times 3 \times 4.5^2 \times 386}{20 \times 2^2}} = 285 \text{ cps}$$

The gyroscopic effects have not been included in the foregoing calculation and a bearing stiffness corresponding to N = 600 rps has been used. It could be anticipated, therefore, that external excitation at above frequencies would result in large amplitudes. Note that the resonant frequencies are functions of the rotational speed and that additional calculation would have to be made to determine the frequencies of synchronous resonance.

An estimate of the displacement of the rotor under gravity may be obtained by using the above value of bearing stiffness, i.e. on the assumption that the stiffness remains sensibly constant for displacements about the central position.

For a load W = 20 Lb the displacement is:

$$y = \frac{W}{k \cdot 2b} = \frac{20}{5290 \times 2 \times 3} = 0.00063 \text{ inch}$$

The corresponding displacement of the rotor, in contact with a preloaded foil at zero speed is smaller in magnitude because of increased stiffness. Finally, the frictional horsepower can be estimated by assuming Couette flow in the bearing clearance .

$$\text{POWER} = \frac{\mu U^2}{h^*} \times 2L \times 3r_0 \textcircled{\sim} = \frac{0.265 \times 10^{-8} \times (2\pi \times 600 \times 1)^2 \times 2 \times 3 \times 3 \times 1 \times \frac{\pi}{3}}{460 \times 10^{-6} \times 550 \times 12} = 0.23 \text{ HP}$$

It should be noted that inertia effects may distort the velocity profile considerably and therefore the above estimate gives an order of magnitude only.

6. CONCLUSIONS

It has been demonstrated that the foil bearing possesses many attractive characteristics in comparison with rigid-surface fluid-flim bearings. Among the advantages which have been demonstrated in the course of the present investigation are the following:

A. Stability

The phenomena of "half-frequency" or "fractional-frequency" whirl, invariably associated with most fluid-film bearings has not been observed in the case of the foil bearing, regardless of whether a radial load has been applied or not.

B. Resonance

An inherent characteristic of self-acting, fluid-film bearings is that the ability of the film to resist the motion of the rotor is greatly impaired when the latter is excited at a frequency equal to half the rotational speed. Whenever the latter condition arises, the excitation produces large amplitudes of motion.* The response of a foil-bearing supported rotor is quite immune to an excitation $f_e = N/2$, as demonstrated by the results of vibration tests. Furthermore, the gross behavior in the self-acting mode appears to be characterized by only one resonant bandwidth in the low-frequency range.

*The term "resonance" should, therefore not be interpreted here in the sense of a simple, second-order system.

C. Constraint of Clearance

In conventional bearings, the maximum excursion of the journal is limited to the bearing clearance. This constraint imposes particularly severe limitations with regard to gas bearings, expecially if the anticipated excursions of the rotor and thermal distortions are commensurate with the nominal clearance. The foil bearing imposes no such limitations and the rotor is not constrained to move within narrowly circumscribed dimensions of the clearance circle of a rigid-surface bearing. Moreover, the gap width of the foil bearing does not play an analogous role to eccentricity, since excursions of the rotor are accompanied by both displacement and extension of the foil. It has been demonstrated that rotation was not impaired by relatively large amplitudes of rotor displacement.

D. Tolerance of Misalignment and Distortion

The foil is flexible and conforms readily with the surface of the journal. It offers at the same time negligible resistance in torsion, so that the foil-bearing is capable of tolerating an appreciable degree of misalignment. It is reasonable to assume that the foil bearing is also capable of accommodating variations of journal diameter resulting from temperature gradients in the axial direction. Furthermore, it appears that operational characteristics of the foil-bearing supported rotor may be quite insensitive to fairly large variations of tension.

E. Wear Characteristics

The response to contact is benign, and tolerance of foreign particles and debris is enhanced through the ability of the foil to deform locally and to deflect. Contact stresses are distributed, rather than concentrated. Wear is characterized by burnishing and progressive polishing of asperities, rather than by ploughing and galling. The wear tracks along

the anticlastic ridges are tolerable and diminish rapidly after a period of initial wear-in.

F. Simplicity

The construction is relatively simple and does not require the degree of precision involved in the manufacture of rigid-surface gas bearings. It is also less complex in comparison with herringbone-grooved and and pivoted-pad types of bearings. The essential elements are strips of foil, foil guides, and anchoring (locking) posts.

It would be unreasonable to expect so many basic benefits ensuing from the foregoing advantages without proper consideration of problems which may arise in the application of foil bearings to rotating machinery. In gaining freedom from the constraint of clearance circles of inflexible bearings, one must consider the limits imposed by other surfaces concentric with the axis of rotation. It may be necessary, in the case of seals for example, to resort to a flexible, or bellows-mounted seal, or achieve sealing by annuli between discs, rather than between cylindrical surfaces.

Typical values of foil-bearing "stiffness" are expected to fall within the range 5,000 to 10,000 lb/in, so that resonances are likely to occur at low speeds and frequencies of excitation. This may be advantageous under conditions of synchronous excitation by residual unbalance in acceleration to rated speed, but poses problems with regard to the level of impact and to external excitations which could be tolerated.

REFERENCES

1. H. Blok and J. J. Van Rossum, "The Foil Bearing - A New Departure in Hydrodynamic Lubrication," Lub Eng., Vol. 9, No. 6, Dec. 1953, 316-320.

2. B. J. Patel and A. Cameron, "The Foil Bearing," Proc., Conf. on Lub. and Wear, London, Oct. 1957, Paper No. 63, 219-223.

3. H. K. Baumeister, "Nominal Clearance of Foil Bearings," IBM J. of Res. and Dev., Vol. 7, No. 2, April 1963, 153-154.

4. W. A. Gross, Gas Lubrication, John Wiley and Sons, New York, 1962, 138-141.

5. W. E. Langlois, "The Lightly Loaded Foil Bearing at Zero Angle of Wrap," IBM J. of Res. and Dev., Vol. 7, No. 2, April 1963, 112-116.

6. A. Eshel and H. G. Elrod, Jr., "The Theory of the Infinitely Wide, Perfectly Flexible, Self-Acting Foil Bearing," J. of Basic Eng., Trans. ASME, Vol. 87, Ser. D, No. 4, Dec. 1965, 831-836.

7. I. Pelech and A. H. Shapiro, "Flexible Disc Rotating on a Gas Film Next to a Wall," J. of Applied Mechanics, Trans. ASME, Vol. 31, Ser. E., No. 4, Dec. 1964, 557-58.

8. R. T. Pearson, "The Development of the Flexible Disc Magnetic Recorder," Proc. IRE, Vol. 49, Jan. 1961, 164-174.

9. L. Licht and B. H. Indergard, "Flexible-Hoop Transport and Storage Device," IBM Research Report No. RC-1215, June 1964.

10. E. J. Barlow, "Self-Acting Foil Bearings of Infinite Width," J. of Lub. Tech., Trans. ASME, Vol. 85, Ser. F, No. 3, July 1967, 341-345.

11. A. Eshel and H. G. Elrod, Jr., "Stiffness Effects on the Infinitely Wide Foil Bearing," J. of Lub. Tech., Trans. ASME, Vol. 89, Ser. F, No. 1, Jan. 1967, 92-97.

12. A. Eshel, "Compressibility Effects on the Infinitely Wide, Perfectly Flexible Foil Bearing," J. of Lub. Tech., Trans. ASME, Vol. 90, Ser. F, No. 1, Jan. 1968, 221-225.

13. A. Eshel, "Analytical Study of the Self-Acting Foil Bearing," Doctoral Dissertation, Department of Mechanical Engineering, Columbia University, May 1966.

14. E. J. Barlow, "Derivation of Governing Equations for Self-Acting Foil Bearings," J. of Lub. Tech., Trans. ASME, Vol. 89, Ser. F, No. 3, July 1967, 334-340.

15. E. J. Barlow, "Externally Pressurized Foil Bearings," J. of Basic Eng. Trans. ASME, Vol. 87, Ser. D, No. 4, Dec. 1965, 968-990.

16. M. Wildmann and A. Wright, "The Effect of External Pressurization of Self-Acting Foil Bearings," J. of Basic Eng., Trans. ASME, Vol. 87, Ser. D, No. 3, Sept. 1965, 631-640.

17. A. Eshel and M. Wildmann, "Dynamic Behavior of a Foil in the Presence of a Lubricating Film, ASME Paper 68-APM-9, to be published in J. of Applied Mechanics, Trans. ASME.

18. A. Eshel, "The Propagation of Disturbances in the Infinitely Wide Foil Bearing," Ampex Corporation report No. RR-67-13, May 1967, to be presented at the International Gas Bearing Symposium, Las Vegas, Nevada, June 1968.

19. E. J. Barlow and M. Wildmann, "The Axisymmetric, Perfectly Flexible Foil Bearing with Porous Inlet Restrictor," J. of Lub. Tech., Trans. ASME, Vol. 90, Ser. F, Jan. 1968, 145-152.

20. A. Eshel, "On Fluid Inertia Effects in Infinitely Wide Foil Bearings," Ampex Corporation report (to be published).

21. J. T. S. Ma, "An Investigation of Self-Acting Foil Bearings," J. of Basic Eng., Trans. ASME, Vol. 87, Ser. D, No. 4, Dec. 1965, 837-846.

22. L. Licht, "Preliminary Experiments with Foil Bearings," J. of Basic Eng., Trans. ASME, Vol. 88, Ser. D, No. 1, March 1966, 1-3.

23. L. Licht, "An Experimental Study of Elasto-Hydrodynamic Lubrication of Foil Bearings," J. of Lub. Tech., Trans. ASME, Vol. 90, Ser. F, No. 1, Jan. 1968, 199-220.

24 V. Nejezchleb, "Pressure Distribution in a Magnetic Tape Foil Bearing," M.S. Thesis, Syracuse University, 1966.

25. D. D. Fuller, Columbia University, Department of Mechanical Engineering, Private Communication.

26. A. F. Stahler and A. Huckabay, "Analyzation, Design, Fabrication, and Testing of a Foil Bearing Rotor Support System," Ampex Corporation report, No. RR 68-21, June 1966.